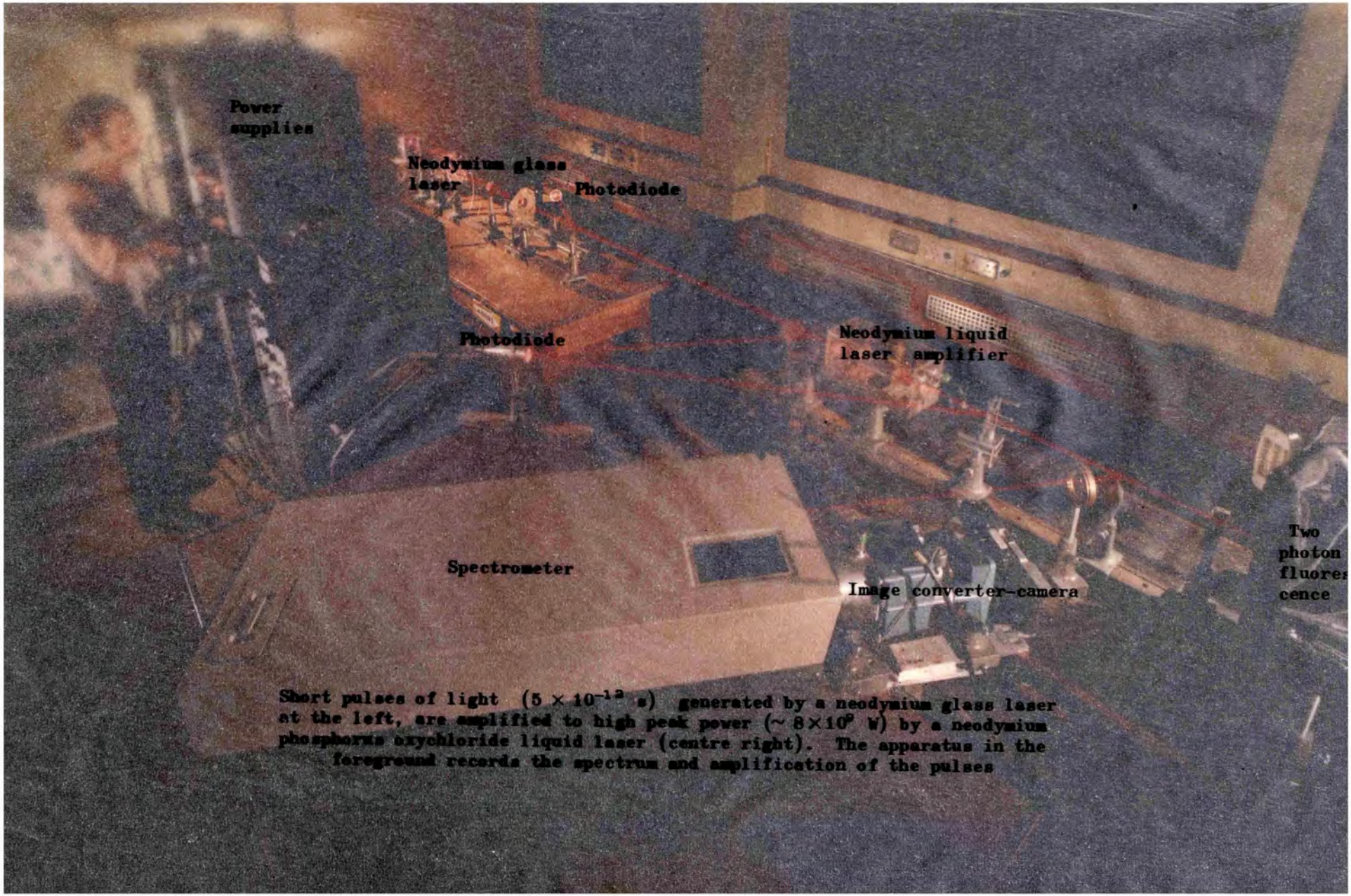

Short pulses of light (5×10^{-12} s) generated by a neodymium glass laser at the left, are amplified to high peak power ($\sim 8 \times 10^{9}$ W) by a neodymium phosphorus oxychloride liquid laser (centre right). The apparatus in the foreground records the spectrum and amplification of the pulses

AMPLIFICATION OF LIGHT PULSES IN A LIQUID LASER

by

DOROS ANDREOU

Thesis submitted for the
Degree of Doctor of Philosophy
at the University of London
January, 1973

ABSTRACT

A study of the performance of the $Nd^{+3} : POCl_3 : ZrCl_4$ liquid laser system is presented. Its properties are described and compared with those of other neodymium lasers. An evaluation of the potentialities of this system as an actively Q-switched oscillator and as a high power amplifier is made. The generation and amplification of picosecond pulses in neodymium laser systems are reviewed. Frequency shifts in broad band amplifiers have been observed and their effect on the power gain has been investigated.

PREFACE

The object of the present work is to provide a coherent account on the properties and capabilities of inorganic liquid lasers, particular attention being paid to the field of high power generation and amplification. The growing interest in the development of liquid lasers is due mainly to their obvious inherent advantages over solid state lasers, namely that the liquid can be circulated and cooled in heat exchangers and thus their average output power does not depend on heat dissipation by thermal conductivity; their preparation cost is low and is only a small fraction of the cost of solid state materials; they are easy to prepare in quantity and the components are readily recoverable by standard chemical techniques; they cannot be permanently damaged (provided they are photochemically stable). This is a very important advantage in view of the fact that solid-state materials are susceptible to damage in high power and high energy devices. Thus in the course of this investigation the areas of the generation and amplification of picosecond pulses have been reviewed and the development of nanosecond pulses in the liquid laser has been investigated. The recent application of short pulses in the production of very hot dense plasmas for use in thermonuclear fusion experiments, make the neodymium liquid laser an attractive device in view of its inherent properties mentioned above.

Two solutions, $SeOCl_2$ and $POCl_3$ are mainly used as host materials for the neodymium ion, the latter being the more attractive one because it is less toxic and less corrosive, and thus provides fewer engineering problems. The number of acids used in conjunction with the

above solutions in order to provide chemical stability is continually increasing. The general problems associated with the solutions are described in the relevant chapter on liquid lasers. From the performance of the laser solutions examined, it is widely believed that the $Nd^{+3} : POCl_3 : ZrCl_4$ system is the best performing one, and most suitable in laser applications, and this is the system which was mainly investigated in this work.

Since in this research project, certain modes of operation of the liquid laser were performed for the first time (active Q-switching, amplification of picosecond pulses) the results of these experiments are described in separate sections, and have been arranged so as to provide a direct reference to the performance of the liquid laser. Thus a comprehensive account of the characteristics of laser pulses is given in the first three chapters where the subjects of the generation and amplification of nanosecond and picosecond pulses and their effects in liquids have been reviewed. Their object is to provide a direct reference to the experimental results described in the following chapters. The observations made are compared and explained using the information contained in these chapters, the relevant areas being presented in detail.

In Chapter IV the development and the spectroscopic properties of the liquid laser systems are described and are compared with those of glass lasers. Certain aspects of the engineering problems in the construction of circulating lasers are included but a complete account is outside the scope of this thesis. Chapter V contains information on the construction and performance of apparatus used in the experiments. The following four chapters describe the performance of the liquid laser as an oscillator and as a high power amplifier. The problems in the generation and amplification of picosecond pulses described in the early chapters are also tackled experimentally. Several parameters of the liquid laser system such as the

passive loss, the efficiency and the stimulated cross-section are measured directly.

Finally the ability of trivalent neodymium to serve as the active ion in different host materials with slightly different spectroscopic properties has provided the necessary conditions for the direct observation of several effects occurring during the amplification process. These are described in Chapter X, where frequency shifts occurring during the amplification of light signals and their effect on the power gain of the amplifier are investigated.

The symbols used in formulae are explained in the text. However to avoid the confusion which may occur when the same symbol is used in different sections with different meanings, lists of symbols used in each section can be found at the back of the thesis (Appendix).

The scientific information presented in this thesis is already being used in the construction of a 10 pps Q-switched $Nd^{+3} : POCl_3 : ZrCl_4$ liquid laser at Culham Laboratory. The results are very encouraging and a report on the construction and performance of this system can be found at the back of this thesis. I hope that it will also prove useful to other laser engineers and designers.

The results obtained hitherto suggest that the liquid laser is more suitable than glass lasers for high power amplification, and this is the natural domain for future scientific investigations. A general assessment of the results and comparison with other systems is given in the conclusions, where future experimental work is also discussed.

All nature is but art unknown to thee,
All chance, direction which thou canst not see;
All discord, harmony not understood;
All partial evil, universal good;
And, spite of pride, in erring reason's spite,
One truth is clear, Whatever is, is right.

Alexander Pope

C O N T E N T S

CONTENTS
(continued)

C O N T E N T S
(continued)

C O N T E N T S
(continued)

CHAPTER I

LASER SYSTEMS

1.1 INTRODUCTION - THE BASIC PROPERTIES OF LIGHT IN RELATION TO THE LASER

A laser is a device for the generation and amplification of light by stimulated emission of radiation. It consists of an optical resonator containing an amplifying medium, the purpose of which is to replenish the losses of the electromagnetic field configuration inside the resonator through stimulated emission of radiation. The above description suggests that the properties of the active medium as well as the properties of the electromagnetic field inside the cavity are of great importance in laser operation and design. The object of this chapter is to provide a summary of the concepts of stimulated and spontaneous emission, and the properties of materials in the inverted state.

Most of the fundamental properties of the electromagnetic field inside a laser cavity are described in the original paper of Schalow and Townes[1] in their attempt to investigate the possibility of maser action at optical frequencies. Ever since - with the achievement of laser action - the behaviour of the electromagnetic field in a laser cavity has been extensively studied[2-4]. A special feature associated with a laser is that it is an open cavity and this has the consequence that the vast majority of the modes have a very high loss. Relatively very few of them are low loss modes and their development depends on the cavity parameters and the properties of the active medium which needs to be excited in such a way as to supply energy to those cavity modes whose frequencies lie under the line profile of the laser transition. Since the very concept of a mode involves the degree of monochromaticity, the polarization and diffraction limitations, the coherence of the output beam depends on the particular

laser system and its mode of operation, where by coherence we mean the phase relation between any two points (space or time) in the beam. Coherence is usually described by correlation functions which are intensity like quantities describing the average fluctuation of two signals[24]

$$\Gamma_{12}(\tau) = \langle I_1(t+\tau)\ I_2^*(t)\rangle$$

where τ is the coherence time.

For $\tau = 0$ and $I_1 = I_2$ this reduces to

$$\Gamma_{11}(0) = \langle I_1(t)\ I_1^*(t)\rangle = \langle I_1(t)^2\rangle = \langle \mathfrak{I}\rangle$$

where $I(\vec{r},t)$ is a complex, random and analytic function defined by

$$I(\vec{r},t) = X(\vec{r},t) + iY(\vec{r},t)$$

where X and Y are related to Hilbert transforms (which makes this description very useful as it is easy to be treated mathematically) and are the real and imaginary parts of $I(\vec{r},t)$ respectively. The brackets denote the ensemble average.

Assuming that the light is quasimonochromatic, i.e. $\frac{\Delta\nu}{\nu} \ll 1$, $I(\vec{r},t)$ can be represented by

$$I(\vec{r},t) = I_0(\vec{r},t)\ \exp(2\pi i\nu t)$$

where the envelope of the quasimonochromatic signal varies slowly in time $\tau < \frac{1}{\Delta\nu}$, i.e. $I_0(t) \simeq I_0(t+\tau)$.

We distinguish between two kinds of coherence:

(a) The temporal coherence in which we consider the electromagnetic field at a certain point in the beam at two different times separated by a time interval τ and is described by the auto-correlation function

$$\Gamma_{11}(\tau) = \langle I_1(t+\tau) I_1^*(t)\rangle \ .$$

In general we say that the beam is coherent at a particular point, over a time τ such that the number of maxima (or minima) passing through that

point with frequency ν, is not greater than the number of maxima passing with frequency $\nu + \Delta\nu$, by more than one, i.e. $(\Delta\nu + \nu)\,\tau - \nu\tau \leq 1$ or $\Delta\nu\tau \leq 1$ where τ is the coherence time.

(b) The spatial coherence in which we are sampling the radiation at two different points in space at the same instant, and is described by the spatial correlation function

$$\Gamma_{12}(0) = \Gamma(\vec{r}_1, \vec{r}_2, 0) = \langle I_1(\vec{r}_1, t)\; I_2^*(\vec{r}_2, t)\rangle \ .$$

Spatial coherence can be measured with a simple Young's double slit experiment, the coherence area being the area over which interference fringes can be observed.

The basic properties of coherence mentioned above are closely related to the uncertainty principle which infers that two points in the beam (space or time) are coherent only if a particular photon cannot be localized at one point as opposed to the other[24].

The coherence properties of a laser beam are very important in laser applications such as holography, measurement of distances and communications[25]. As pointed out above these are dependent on the particular laser system and its mode of operation. In practice, the spatial coherence of a laser is found to depend on the number of transverse modes over which the oscillator energy is distributed[5,6]. Giant pulse lasers show improved spatial coherence because there is no time for many transverse modes to develop due to non-uniform density or temperature shifts[7]. The importance of the number of transverse modes, the back mirror, the short build-up time and the active medium has been shown experimentally[5].

As the effect of the variation of the refractive index in liquid lasers is greater than in other laser materials [16], the liquid laser designer is confronted with a variety of problems in the production of

coherent output beams. These range from the instantaneous local variation of the refractive index producing pure transverse modes[8], to thermal motions occurring in the liquid due to heating by the pumping radiation[9]. The problems arising from refractive gradient effects are described in the relevant section on liquid lasers.

As with every system sustaining electromagnetic radiation, a laser is characterized by its diffraction losses. These depend on the size of the limiting apertures of the resonator, the distance between the two reflectors and the number of ways in which radiation can be scattered into off axial modes. With regard to diffraction phenomena an open plane resonator is analogous to a transmission system, comprising a series of equally spaced collinear apertures, with diameter equal to those of the resonator mirrors (or of any other limiting apertures), the separation between successive apertures being equal to the resonator length. The losses of the system are allowed for by assuming an absorption filter at each aperture[10]. The changes occurring during the passage of the wave diminish with increasing number of apertures. After a sufficiently large number of diffractions, an amplitude and phase distribution results which is reproduced at every subsequent period to within a constant factor (quasimodes of the resonator). If the radiation in the resonator is considered to be limited by an aperture of diameter 2d, then the diffraction angle can be approximated to $\theta \simeq \frac{\lambda}{2d}$. After traversing one resonator length L the fraction of the diffracted energy lost is $\frac{2L\theta}{d}$, giving a relative diffraction loss proportional to $\frac{L\lambda}{d^2}$, or

$$N = \frac{d^2}{L\lambda} \qquad \ldots (1.1)$$

N is called the Fresnel number and is a parameter characterizing the diffraction losses. The smaller the value of N the higher the diffraction losses. The development of the mode configuration in a resonator

has been investigated in detail by Fox and Li[10] who assumed a uniform plane wave excitation across one of the mirrors and calculated the field at the other mirror as the superposition of spherical waves from the individual surface elements of the first mirror. This analysis has shown certain important characteristics of the modes of an optical resonator. For large values of $\frac{d^2}{L\lambda}$ the diffraction losses are independent of the shape of the limiting aperture. During the first few passages the amplitude and phase show pronounced diffraction peaks at the mirror. These peaks are real and correspond to the number of Fresnel zones at one mirror when looking at the opposite mirror[11]. This field distribution represents the dominant mode of the interferometer and is called the fundamental mode. After a few hundred reflections the distribution is stationary and quite smooth with a strong concentration in the centre. In addition to the fundamental transverse modes can occur due to the superposition of two or more plane waves. The number of transverse modes corresponds to the number of minima at the mirror. The results of Fox and Li show that for a small number of transits the amplitude variations were large and extremely complex, indicating the presence of many higher order modes which were damped out more rapidly. For $\frac{d^2}{L\lambda} \gg 1$ the curves for diffraction losses and phase differences for the fundamental mode in a log-plot give almost straight lines. The losses increase with increasing mode order and in every case the fundamental has the lowest diffraction losses. Since diffraction losses differ in magnitude for the different modes, a competition of modes results.

In a resonator containing an active medium, the distribution and development of the modes as described above is greatly affected by the physical and spectral properties of the system. These problems are discussed later, and the production of transverse modes is investigated experimentally for mode-locked neodymium systems.

Since the transverse components of the modes lying perpendicular to the resonator axis are very much larger compared with the longitudinal components they are classified - by analogy with the modes of hollow waveguides - as transverse electromagnetic. They are denoted as TEM_{mnq}, where m and n denote the number of zeros in the x and y directions on the mirror respectively. The parameter q denotes a set of longitudinal modes of the same transverse type.

1.2 LIGHT AMPLIFICATION BY A MATERIAL IN AN INVERTED STATE

The basic properties of the radiation field are described in most laser text-books[12,24], and the concepts of stimulated and spontaneous emission from atoms and molecules in the excited state are explained in numerous papers[1,14]. Some of the basic characteristics of stimulated emission which will be of use later are mentioned below.

The total induced transition rate $W(\nu)$ due to a monochromatic signal of frequency ν, is[14]

$$W(\nu) = \frac{c^2}{8\pi h\nu^3 \tau} g(\nu) I_\nu \qquad \ldots (1.2)$$

where

τ = $1/A$ where A is the spontaneous transition rate

$I_\nu d\nu$ = energy flux (watts/cm^2) due to frequencies between ν and $\nu + d\nu$

$g(\nu)d\nu$ = the probability that a given transition will result in an emission or absorption of a photon with energy between $h\nu$ and $h(\nu + d\nu)$.

The atomic line shape function $g(\nu)$ takes account of any variation of the radiation density per unit frequency interval $p(\nu)$ which occurs over the frequency range in which the atomic system can interact with the radiation field. The shape of $g(\nu)$ is identical with the normalized absorption (or emission) intensity against frequency ν. This distribution

can have its origins in a spread in the Doppler shifts as in the case of gases or to an actual spread in the position of the energy levels as in glasses and liquids. In wide band lasers such as neodymium in glasses and liquids the frequency range over which radiation can interact with the atomic system is very important in operations such as mode-locking and pulse sharpening in travelling wave amplifiers, (see later chapters). The line shape function is usually approximated to two distributions,

(a) $g(\nu)$ is Lorentzian with full width at half the maximum $\Delta\nu$ and the normalized distribution $\left(\int_0^\infty g(\nu)\,d\nu = 1\right)$ is

$$g(\nu) = \frac{2}{\pi\Delta\nu} \quad \frac{1}{1+\left(\frac{\nu-\nu_0}{\frac{\Delta\nu}{2}}\right)^2}$$

where ν_0 is the frequency at the centre of the distribution.

(b) $g(\nu)$ is Gaussian and the normalized distribution is given by

$$g(\nu) = \frac{2\sqrt{\ell n\, 2}}{\sqrt{\pi}\,\Delta\nu} \exp\left\{-\left(\frac{\nu-\nu_0}{\frac{\Delta\nu}{2}}\right)^2 \ell n\, 2\right\}.$$

Considering the amplification process by a material in an inverted state a light signal of frequency ν and intensity $I_0(\nu)$, will be amplified to a value $I(\nu,x)$ at a distance x inside the medium given by[13]

$$\frac{I(\nu,x)}{I_0(\nu)} = \exp\,[k(\nu)x] \qquad \ldots (1.3)$$

where $k(\nu)$ is the absorption coefficient of the medium and is given by

$$k(\nu) = \left(N_2 - N_1 \frac{\mathcal{J}_2}{\mathcal{J}_1}\right)\sigma(\nu) = \Delta N\,\sigma(\nu) \qquad \ldots (1.4)$$

$\sigma(\nu)$ being the stimulated atomic cross-section of the medium and is given by $\sigma(\nu) = g(\nu)\, B\, \frac{h\nu_0}{c}$.

In the relations above

N_1, N_2 are the population densities of levels 1 and 2 in ions/cm^3,
$\mathcal{J}_1, \mathcal{J}_2$ are the multiplicities of levels 1 and 2, and
B is the Einstein stimulated emission coefficient.

The stimulated emission cross-section as described by equation (1.4) is a measure of the probability that stimulated emission will occur. In terms of equation (1.4) it can be thought of as the 'area of an atom' which when multiplied by the number of atoms in a particular volume is responsible for the amount of stimulated emission occurring during the passage of radiation through that volume. The stimulated cross-section of a particular ion or molecule depends greatly on the properties of the host material.

1.3 THE THRESHOLD CONDITION. THREE AND FOUR LEVEL SYSTEMS

In a laser oscillator a standing wave is formed and can be thought of as being generated mainly by a plane wave bouncing back and forth between the two mirrors. The threshold or start oscillation condition is reached when the induced power is equal to that lost by the resonator, i.e.

$$\left(\frac{dI}{dt}\right)_{induced} + \left(\frac{dI}{dt}\right)_{lost} \geq 0 \ .$$

Now

$$\left(\frac{dI}{dt}\right)_{induced} = h\nu \left(N_2 - N_1 \frac{\mathcal{J}_2}{\mathcal{J}_1}\right) c W$$

where the symbols have the same meanings as for equation (1.2),

$$\left(\frac{dI}{dt}\right)_{lost} = - \frac{I}{t_p}$$

where t_p is a parameter characterizing the loss of photons from the cavity. It is related to the total loss per pass γ by

$$t_p = \frac{L}{\gamma c} = \frac{Q}{2\pi\nu}$$

Q being defined as the quality factor of the resonator. Rearranging the above relations and using equation (1.2), the threshold of oscillation condition for a laser is

$$\left(N_2 - N_1 \frac{\mathcal{J}_2}{\mathcal{J}_1}\right)_{threshold} = \Delta N_T = \frac{8\pi\nu^2}{c^3 g(\nu_0)} \frac{\tau}{t_p} \qquad \ldots (1.5)$$

where ΔN_T is referred to as the critical population inversion. Two

important observations can be made from equation (1.5):

(a) The population inversion depends on the spectral quality factor $g(\nu_o)$ and thus the spectroscopic properties of the material are important in laser operation.

(b) ΔN_T depends only on a single resonator parameter t_p which depends on the properties of the active medium and the structure of the optical resonator.

For either a Gaussian or a Lorentzian line, equation (1.5) becomes

$$N_2 - N_1 \frac{g_2}{g_1} = \text{constant} \times \frac{2\pi\tau\Delta\nu}{t_p} .$$

Thus in order to achieve a low threshold inversion a material with very small line broadening $2\pi\tau\Delta\nu$ should be used. The quality factor Q of the cavity must be kept high.

In the discussion of the threshold condition above, an ideal laser transition from level 2 to level 1 was considered. Laser systems have more complicated configurations than that, and in considering pumping power requirements it is useful to divide them into two categories[28].

(a) Four level systems. The terminal level of a four level system is far enough above the ground state so that $E_1 \gg kT$ (Fig. 1.1). The population N_1 of level 1 is small compared with the critical inversion ΔN_T, and from equation (1.5) $N_2 \simeq \Delta N_T$. Since ΔN_T atoms must be maintained in level 2, the minimum power which must be expended is

$$P_{min} = \frac{h\nu}{\tau} V \Delta N_T$$

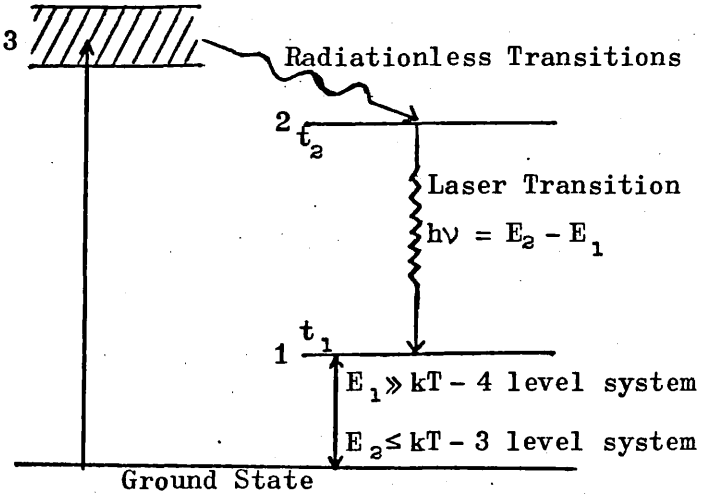

Fig.1.1
Energy level diagram for three and four level systems

where V is the volume of the active material, and τ is the spontaneous emission time of level 2.

Using equation (1.5) for a Lorentzian line

$$P_{min} = \frac{4\pi^2 h\nu^3 V}{\tau} \Delta\nu$$

from which we see that the atomic linewidth should be as small as possible for minimum pumping power. In solid state lasers the separation of level 1 from the ground state must be greater than 10 kT for a four level system.

(b) Three level systems. In this case the population of level 1 is much greater than the population inversion ($N_1 \gg \Delta N_T$) and it is of the order $N_1 \sim N_2$ since the separation of this level from the ground state is of the order of kT. Comparing the three- and four-level systems, we see that the pumping requirements for a four level laser are smaller than those for a three level laser by a factor of $\Delta N_T/N_2$. For typical solid state materials $\Delta N_T \sim 10^{17}$ and $N_2 \sim 10^{19}$, therefore the pump power needed for three level operation is approximately 100 times that needed for four level operation. Since the present work is concerned with four level systems, subsequent discussion will be restricted to those systems.

1.4 LASER MEDIA

Since much of this work is concerned with the development of a neodymium liquid laser it would be appropriate to compare the properties of the active ions in different host materials and the different excitation methods.

Optical pumping is the most efficient pumping for dielectric crystals and liquids because this is the only way of introducing sufficient energy into the laser medium. The active ions should therefore possess broad band resonance absorption transitions. The sharp fluorescence lines of such materials result from the shielding of the optical electrons

by the outer shells from the surrounding crystal lattice, enabling the transitions to be similar with those of the free ions. The effect of the external field is dependent on the degree of shielding. This means that an ion which exhibits laser action in one crystal should not necessarily exhibit laser action in another crystal. For elements of the iron group the optical 3d electrons are shielded only by one outer shell. The effect of the crystal field is so large that an ion may not even exhibit laser action in another crystal. Thus ruby is the only crystal in which chromium exhibits laser action ($Al_2O_3\,Cr^{+3}$). In rare-earth elements the optical 4f-electrons are surrounded by two outer shells and thus their spectral behaviour in the host medium resembles the spectral behaviour of the free ions. Thus Nd^{+3} is used as the active ion in several crystals, in glasses and in liquids. The problems associated with the formation of the ion environment in liquids are described in the relevant section on liquid lasers[17].

With gas lasers optical pumping is limited because all transitions are narrow band transitions and a pump source should have a frequency sufficiently close to the frequency of a pump transition in a gas. Several other methods are used for excitation in gas lasers. In the helium-neon laser, helium atoms are excited into higher states by an electric discharge and on their way down many of these collect into a metastable state where they exchange energy by collision with unexcited neon atoms which are pumped to higher levels. This process of excitation is called excitation by exchange of energy. Excitation in Ar, Kr and Xe lasers is believed to take place via inelastic collisions with the discharge electrons. Population inversions can also be achieved by combining various excitation processes, as in a molecular gas laser, for example CO_2. Finally, semiconductor lasers are excited by direct electric current injection[13].

1.5 THE FABRY-PEROT RESONATOR — OUTPUT CHARACTERISTICS OF LASERS

The properties of the Fabry-Perot resonator as described in section 1.1 combine with the spectral properties of the active medium to produce the output characteristics of the laser oscillator. A material in a state of negative absorption has a certain thermal linewidth. This constitutes the frequency region over which radiation can interact with matter. It can be considered as originating from the superposition of all the linewidths of the individual atoms. When a strong monochromatic signal with frequency ν_s interacts with the atoms of a thermal linewidth centred at ν_o with full width at half the maximum $\Delta\nu$ we can distinguish between two cases of interaction:

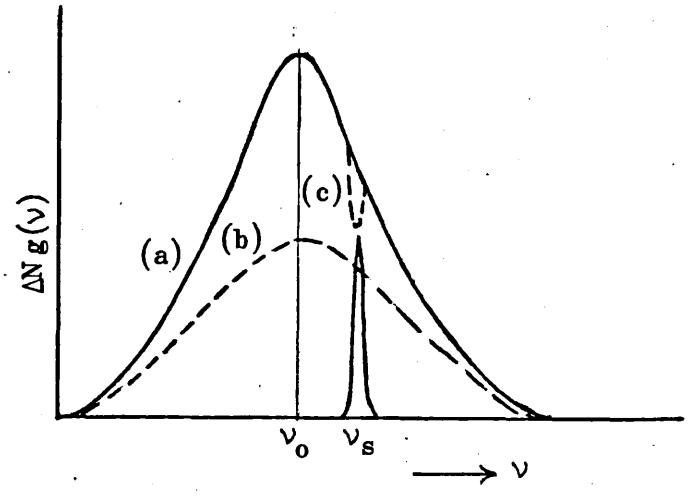

Fig.1.2
Homogeneous and inhomogeneous broadening of an amplifying linewidth

(i) If the interaction is long compared with the thermal relaxation, atoms from other regions will diffuse into the vicinity of ν_s and interact with the signal. The whole linewidth will decrease uniformly and its shape will be preserved. It will acquire the shape and height of the line **b** in Fig.1.2. This process is called homogeneous broadening of the line. (ii) If the interaction time is short compared with the thermal relaxation, only atoms in the vicinity of ν_s will interact with the signal and thus a selective spectral depopulation of the line will occur in the region of frequency ν_s. The line will preserve its shape and its height, but a 'spectral hole' (c) will be burnt (see Fig.1.2) in the vicinity of ν_s. Such a line is said to be inhomogeneously broadened. The

cross-relaxation rate to the region of ν_s can be assumed to be directly proportional to the departure of the population inversion distribution from equilibrium[15].

The gain of the oscillator as a function of frequency peaks at the line centre. Therefore the first longitudinal mode to oscillate is that nearest to the line centre and the gain is expected to saturate at a value not much greater than the threshold value. With higher pump powers, more modes which have the same cavity Q as that of the threshold mode but lower gain, can be made to oscillate[28]. Multimode oscillation can then occur in an inhomogeneously broadened line. These modes can be made to interfere and produce beats. The appearance of new modes affects the modes which are already oscillating because of the frequency dependence of the dispersion line in the active medium. This tends to shift the emission frequency to the line centre. Inhomogeneous broadening occurs in solid state lasers, depending on the variation of the crystal field from ion to ion. In liquids it occurs because of the slightly different fields in which the ions exist inside the clusters (see Chapter IV).

Multimode oscillation also occurs in homogeneously broadened lines because of the spatial variation of the inversion. In a cavity we get stationary waves. The probability of stimulated emission at each point is proportional to the field intensity at that point, i.e. to the energy density of radiation at that point. Therefore stimulated emission will be minimum at the nodes and maximum at the antinodes, a spatial periodic saturation occurring for each mode. At high energies the spatial variation in the field intensity of the various modes produces a non-uniform distribution of the inversion[3]. It is possible, but highly unlikely, especially with solid state materials, that these distributions would smooth out by spatial cross-relaxations since cross-relaxation times are

very large in solids. It is therefore very difficult to obtain single mode operation at high pumping powers. With higher pumping powers, more modes can oscillate whose antinodes coincide with the nodes of the first mode.

Thermal gradient effects occurring in the active medium during pumping can cause a frequency shift in the output spectrum [29]. The cavity resonance is much narrower than the atomic resonance and therefore the frequency of oscillation depends on the cavity length. The cavity length varies because of vibration and also refractive gradient effects. If ℓ is the length of the active medium, the optical length is $n\ell$ where n is the refractive index of the laser material. A variation of $\frac{\lambda}{2\ell}$ in the refractive index will cause a change in the optical length of $\lambda/2$. This causes a frequency shift of $\frac{c}{2\ell}$.

As pointed out in section 1.1, the different diffraction losses for the different transverse modes are responsible for the preferential selection towards lower order modes. With an amplifying medium inside the Fabry-Perot resonator the gain peaks at the centre of the amplifying line and the fundamental saturates the inversion there first as described above. The difference in the diffraction losses is the factor determining the time before the fundamental becomes dominant over other modes.

Resonator perturbations can affect the growth and distribution of modes. These must therefore be small and preferably have slow growth for single mode operation in order to allow time for the fundamental to establish itself over other modes.

In liquid lasers the output characteristics described above are greatly affected by the nature of the medium. The pumping radiation can cause changes in the refractive index which are much more serious than in solids. The local refractive index is a function of the local temperature

introduced into that area of the medium by the pumping radiation[16]. The light rays will be deflected according to the distribution of the refractive index in the liquid, and transverse modes will establish themselves as a function of that distribution[8]. In addition, if the change in temperature is high, the change in density occurring can cause thermal motions in the laser medium[9] (see Chapter IX).

In considering the properties of linewidths, liquids differ from glasses in that the ions are free to move in an environment which is no longer rigid. Owing to this mobility of the ions, the spatial variation of the inversion as described above, has a better chance of smoothing out. However problems of this nature which can occur in liquid lasers have not yet been investigated[17].

Liquids in general are known to exhibit a large number of interactions with intense radiation[18,19]. Several non-linear effects (see Chapter II) occur as a result of these interactions. When liquids are placed in laser cavities they can influence the time emission[18,20], as well as the spectral emission[21] of the laser. In liquid lasers the active medium itself experiences these interactions in the cavity. These can influence the output characteristics of the liquid laser[22] (see Chapter VI).

The Fabry-Perot resonator with plane mirrors, is one of many different arrangements used to sustain the electromagnetic field. Curved mirrors are often used in different configurations in order to provide a more stable system for the electromagnetic field[13]. A resonator is stable if the condition[23]

$$0 < \left(\frac{L}{L_1'} - 1\right)\left(\frac{L}{L_2'} - 1\right) < 1 \qquad \ldots (1.6)$$

is satisfied, where L_1', L_2' are the radii of the two mirrors. The stability condition means that a beam of light is refocused whenever it traverses the resonator. If the condition is not satisfied, then the beam is

dispersed every time it is reflected between the mirrors. Examining the stability condition at the boundary between stability and instability, we get $\frac{L}{L_1'} = 1$, $\frac{L}{L_2'} = 1$ and the hyperbola $L = L_1' + L_2'$. A stability-instability diagram can be drawn showing the regions separating stable from unstable resonators[13,23]. Lenses can be used inside a resonator to produce the same effect as concave mirrors, The lens-mirror combination leads to the concept of the image mirror whose relation to the original mirror is governed by the rules of geometrical optics[23]. Resonator arrangements are important where the changes in refractive index occurring in the active material due to pumping are significant. Lenses are usually used inside cavities to counteract the effect of the thick lens formed by the active medium due to heating by the pumping radiation.

CHAPTER II

DESCRIPTION OF LASER PULSES

This chapter is intended to provide the background to the experimental work of this thesis.

2.1 POWER OUTPUT CHARACTERISTICS IN LASER OSCILLATORS

Before deriving the equations for the power output of laser oscillators it seems appropriate to describe some of the characteristics of the relaxation oscillations in neodymium glass lasers under different conditions of operation. Relaxation oscillations are the transient oscillatory processes which arise at the onset of stimulated emission in a laser oscillator. The temporal and spectral characteristics of these oscillations are dependent on thermal processes taking part in the active medium due to pumping, and are different for clad and unclad laser rods. Cladding the rod with a material having lower index of refraction than the core and a good interface between core and cladding, provides a large number of modes of equal Q by total internal reflection. The Q's can be made relatively low by using a low end mirror reflectivity. Relaxation oscillations from neodymium glass lasers can be classified in three main categories[28]. (a) Oscillations showing random spiking behaviour from either clad or unclad rods which have narrow beam spreads. These are described by well defined standing waves, but because of thermal effects and microphonics, the conditions for high Q modes are erratically established, resulting in multimoding and random spiking behaviour. (b) Damped oscillations from clad rods which show large beam spreads. Their spectrum consists of bands a few angstroms wide instead of sharp lines characteristic of the random spiking behaviour. Here there are sufficient changes in the active medium to scramble the modes with the result that the system responds as a single unit, without the establishment of discrete standing

waves in the cavity. (c) Finally undamped oscillations or limit cycles can occur in clad rods. These are due to saturated absorption in the glass at the laser wavelength due to several kinds of inclusions (e.g. UO_2^{2+} ions)[30]. The processes leading to this behaviour are similar to those of saturable absorption by liquids placed in the laser cavity[31].

The rate equations used by Statz and deMars[2] to explain the relaxation oscillations in masers have been modified to include the effect of cladding the rod, the neodymium ion concentration and its effect on quenching and cross-relaxation[31,32]. These can be written as (with reference to Fig.1.1)

$$\frac{d\Phi}{dt} = -\frac{\Phi}{t_p} + (Af + B'\Phi)\, N_2 \qquad \ldots (2.1)$$

$$\frac{dN_2}{dt} = P_i - (A\mu + B'\Phi)N_2 + F(N_2' - N_2) \qquad \ldots (2.2)$$

where Φ is the number of photons per unit volume in the cavity

N_2 = the inverted population per unit volume

$t_p = Q/2\pi\nu$ = lifetime of a photon in the cavity

$A\mu = 1/\tau$, τ being the measured lifetime of level 2, the factor μ taking account of other processes depleting the population inversion such as spontaneous emission in other lines and non-radiative transitions.

$f = n_1 - n_c/n_c$ = fraction of spontaneously emitted light coupled into the aperture of the clad rod; n_1, n_c are the refractive indices of core and cladding respectively.

P_i = Pumping power

$N_2' = P_i/A\mu$ = inversion that would exist had there been no laser radiation in the cavity.

$B' = 1/\tau\, p_m$ where p_m is the density of modes.

The cross-relaxation rate F is considered to be proportional to the departure of the inversion from equilibrium[15]. This can be incorporated into the other terms by defining the coefficients P_i' and μ' by

$$P_i' = P_i\left(1 + \frac{F}{A\mu}\right) \qquad \text{and} \qquad \mu' = \left(\mu + \frac{F}{A}\right) .$$

The resulting equations can easily be solved for small oscillations about the steady state values N_o and Φ_o obtained for $\frac{d\Phi}{dt} = \frac{dN_2}{dt} = 0$, by substituting $\Phi = \Phi_o + i(t)$ and $N_2 = N_o + n'(t)$. A single second order differential equation in i can be obtained which is characterized by the frequency and damping of the relaxation oscillations. The results of this analysis indicated certain interesting points:

(a) For a certain inversion there is more radiation in the cavity for $f \neq 0$, as expected.

(b) The damping of the relaxation oscillations increases with increasing concentration of the neodymium ions.

(c) The damping of the relaxation oscillations is greater for $f \neq 0$.

(d) The damping time can be shown to be long enough so that microphonics and thermal distortions interrupts the train of pulses[31].

(e) Limit cycles can be shown to occur by assuming a change in the inverse of the photon lifetime $1/t_p$ proportional to the light intensity in the cavity[32].

A different approach which includes the effects of inhomogeneous broadening on the relaxation oscillations has recently been published by Casperson and Yariv[4] who incorporated the frequency dependence of the quantities $I(\nu)$, $N_2(\nu)$ and $P(\nu)$ in equations (2.1) and (2.2), and have solved them accordingly. For neodymium lasers however, homogeneous broadening is assumed to occur since the cross-relaxation rate is comparable to the time duration of the relaxation oscillations. The relaxation oscillations are discussed further in Chapter VI, where a comparison between glass and liquid systems is made. Other effects arising in the free running operation of liquid lasers, such as self-Q-switching, are also described.

Cladding a laser rod also reduces the threshold pumping power and increases the available output[33]. This happens because rays striking the side surface of a dielectric cylinder are refracted towards the normal as shown in Fig.2.1. All rays striking the surface of the sheath at a point, at angles of incidence between the tangent and the normal will pass the axis of the cylinder with a minimum distance $r = \frac{r_2}{n_c}$ where r_2 is the radius of the cylinder and n_c is the refractive index of the cylinder material. Therefore all the light that enters the cylinder eventually passes through a smaller internal cylinder of radius $\frac{r_2}{n_c}$. Thus cladding a rod increases the pumping efficiency of the laser. We can look at the situation from a different point of view. When the laser rod is viewed from the outside it appears to have a bigger diameter when it is clad. Thus it subtends a larger angle at a point on the pumping lamp, and therefore receives a larger fraction of the emitted light. With a liquid laser the cladding is automatically provided by the thickness of the tube containing the active medium.

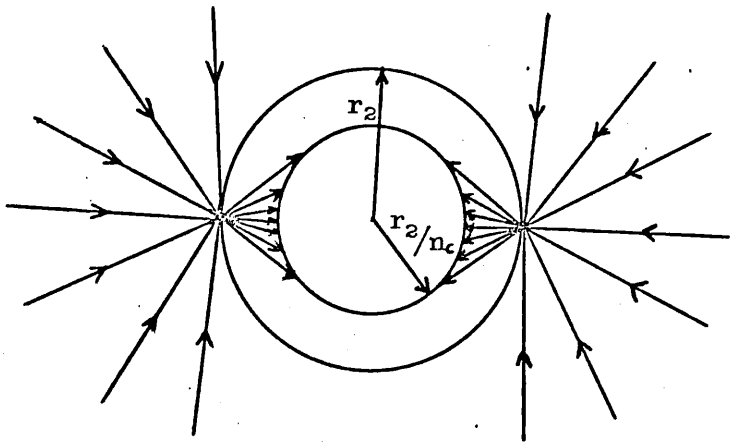

Fig.2.1
Rays incident on the surface of a dielectric cylinder are refracted towards the axis

A pair of linear equations which can serve to characterize the laser can be derived from the rate equations[26,34]. These are only valid for pumping pulses which are comparable or longer than the fluorescence decay time and thus a steady state approximation can be assumed[35]. The kinetic equations for a four level system can be written as

$$\frac{dN_2}{dt} = -\frac{N_2}{t_2} - W(N_2 - N_1) + \mathcal{R}_2 \qquad \ldots (2.3)$$

$$\frac{dN_1}{dt} = -\frac{N_1}{t_1} + \frac{N_2}{t_2} + W(N_2 - N_1) + \mathcal{R}_1 \qquad \ldots (2.4)$$

where

N_1, N_2 are the populations of levels 1 and 2 respectively per unit volume.

W = induced transition rate

t_1 = lifetime of atoms in level 1

t_2 = spontaneous lifetime of level 2 for a $2 \rightarrow 1$ transition

$\mathcal{R}_1, \mathcal{R}_2$ represent the number of atoms per unit volume per second pumped into the levels 1 and 2 respectively.

Assuming a steady state $\left(\frac{d}{dt} = 0\right)$

$$N_2 - N_1 = \frac{\mathcal{R}_2' t_2}{Wt_2 + 1} \qquad \ldots (2.5)$$

where

$\mathcal{R}_2' = \mathcal{R}_2\left[1 - \frac{t_1}{t_2}\left(1 + \frac{\mathcal{R}_1}{\mathcal{R}_2}\right)\right]$ = effective pumping rate of level 2.

The rate of stimulated emission into the cavity P_c is

P_c = $W \Delta N_T h\nu V$

where

V = volume of the active medium

ν = frequency of oscillation

ΔN_T = $N_2 - N_1$ at threshold.

Using equation (2.5)

$$P_c = (\mathcal{R}_2' t_2 - \Delta N_T)\frac{h\nu V}{t_2} \qquad \ldots (2.6)$$

where the quantity $\mathcal{R}_2' t_2$ represents the population that would be achieved had there been no stimulated emission. If P is the electrical power input to the lamp then the rate at which photons are coupled into the active medium per unit volume is

$$\mathcal{R}_2' = \frac{Pq}{h\nu V} \qquad \left(\frac{\text{ions}}{\text{cm}^3\,\text{sec}}\right)$$

where $q = \epsilon_1 \epsilon_2 \epsilon_3 \frac{\nu}{\nu_p}$

ϵ_1 being the conversion efficiency of the electrical power into useful light in the pump bands

$\epsilon_2 \frac{\nu_p}{\nu}$ the efficiency with which photons are coupled into the active medium, $h\nu_p$ being the average energy per photon in the absorption bands.

ϵ_3 the quantum efficiency with which the medium utilizes the photons.

Substituting into equation (2.6)

$$P_c = (P - P_T)q \ .$$

The output power P_{out} is then

$$P_{out} = (P - P_T)q \frac{T}{T + 1 + e^{-\alpha \ell}} \frac{r_1}{r_2/n_c}$$

where P_T = power at threshold

T = transmission of the output mirror

α = passive loss per cm

ℓ = length of the active medium

r_1 = radius of the active medium

r_2 = outer radius of the cell (cladding)

n_c = refractive index of the cell material.

If we assume that the pumping pulse is a square pulse then the equation above can be turned into an energy equation. This is the least reliable of the assumptions made. Thus

$$E_{out} = (E - E_T)q \frac{T}{T + 1 + e^{-\alpha \ell}} \frac{r_1}{r_2/n_c} \ . \qquad \ldots (2.7)$$

The extent to which the assumptions made in the above derivations are applicable, are described in detail in reference 35.

The threshold condition for oscillation can be written in terms of the output mirror reflectivity R (the other mirror is assumed to be opaque) as[32]

$$R \exp \left[\sigma \Delta N_T - \alpha\right] 2\ell = 1 \qquad \ldots (2.8)$$

where the symbols have the same meanings as above. Note that equation (1.5) is directly derivable from equation (2.8) where the quality factor is written as

$$\frac{1}{Q} = \frac{c}{2\pi\nu}\left(\frac{1}{2\ell} \ell n \frac{1}{R} + \alpha\right) . \qquad \ldots (2.9)$$

Assuming the steady state approximation the threshold energy E_T is

$$E_T = \frac{\Delta N_T \, h\nu \, V}{q \, t_2} t_{laser} = \frac{1}{\zeta} \Delta N_T \qquad \ldots (2.10)$$

where t_{laser} is the time during which the laser is operating $\left(P_T = \frac{E_T}{t_{laser}}\right)$ and equation (2.8) becomes

$$E_T = \frac{\alpha}{\zeta\sigma} - \frac{\ell nR}{2\zeta\ell\sigma} \qquad \ldots (2.11)$$

The threshold energy is thus linear in ℓnR.

Equations (2.7) and (2.11) are useful in evaluating the parameters of a laser system to the extent that the steady state and square pulse approximations are valid[35].

2.2 THE Q-SWITCHING OF LASERS

2.2.1 Generation Dynamics of the Giant Pulse

Most of the laser applications require single high power pulses. A laser can be made to emit such pulses by the introduction of an optical shutter inside the cavity[36]. The production of a giant pulse is accomlished by pumping the active medium until the population inversion reaches a value far above threshold. The shutter is then opened and the radiation builds up rapidly in the cavity. The excess excitation is then discharged in a very short time. The parameters characterizing the giant pulse are the energy and peak power radiated, the rise and decay times of the pulse and the build-up time between switching and the evolution of the pulse. The switching off time of the shutter also affects the evolution

of the pulse. For a fast switch the giant pulse will build-up exponentially, the rise time depending on the gain per unit length of the active medium at the time of switching, and the losses per unit length of the laser cavity.

A number of optical shutters are available[13] and they are usually divided into two broad categories: Active shutters which can be opened at any prescribed moment in time, and passive shutters which are opened by the laser radiation itself, the respective operations being called active and passive Q-switching.

Several papers have been devoted to the investigation of the Q-switching of lasers. The case of a fast switch (switching-off time less than 50 ns) has the most practical importance and in this case a simple theory suffices to explain most of the experimental results. In this thesis the experiments on Q-switching (Chapter VII) were performed with a fast switch (Pockels cell) and a simplified theory[37] which can account for most of the experimental results is given below.

2.2.2 Simple Theory of Q-Switching

In the theory below fast switching is assumed, i.e. the shutter is switched in a time so short that no significant change in the population inversion takes place during the switching process. Two simple differential equations describing the variation of the photon density Φ and population inversion ΔN with time can be written[37]

$$\frac{d\Phi}{dt} = \left(\frac{k\ell}{L/c} - \frac{1}{t_p}\right)\Phi \qquad \ldots (2.12)$$

$$\frac{d\Delta N}{dt} = -\frac{2k\ell}{L/c}\Phi \qquad \ldots (2.13)$$

where k is the amplification coefficient and is proportional to the population inversion ΔN. It can be written as $k = k_o \frac{\Delta N}{N_o}$ where k_o is the absorption coefficient of the unexcited material; N_o is the

number of active ions per unit volume, ℓ is the length of the laser material, and L is the optical distance between the reflectors.

Equations (2.12) and (2.13) are special cases of the Statz and deMars rate equations (2.1) and (2.2), where the effect of pumping, spontaneous emission and cross-relaxation have been omitted.

By introducing the normalized variables $n = \frac{\Delta N}{N_o}$ and $\varphi = \frac{\Phi}{N_o}$ and changing the timescale to make the photon lifetime $t_p = \frac{L}{\gamma c}$ the unit of time, equations (2.12) and (2.13) are readily reduced to[12]

$$\frac{d\varphi}{dt} = \left(\frac{n}{n_m} - 1\right)\varphi \qquad \ldots (2.14)$$

$$\frac{dn}{dt} = -\frac{2\,n\varphi}{n_m} \qquad \ldots (2.15)$$

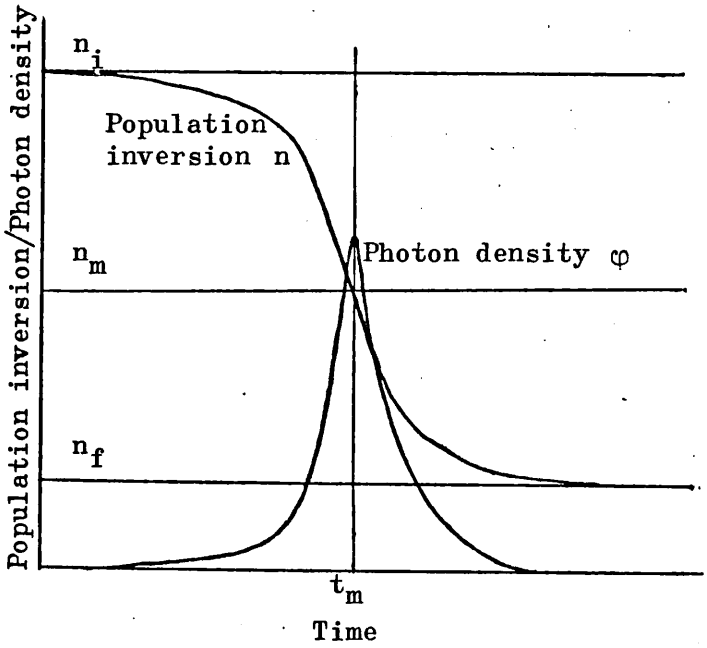

Fig.2.2
Variation of the inversion and the photon density in the evolution of the giant pulse

where $n_m k_o \ell = \gamma$ and n_m is the inversion at the peak of the pulse, and this is the only remaining parameter characteristic of the laser. The procedure is illustrated in Fig.2.2. The photon density φ rises from a low value φ_i to a value φ many orders of magnitude higher, and then decays to zero, while the population inversion is a monotonically decreasing function of time with an initial value n_i and a final value n_f. From equation (2.14) we also see that the initial rise of φ is exponential as pointed out in the giant pulse dynamics above (time constant $\sim \frac{n_m\, t_p}{n_i - n_m}$).

From equations (2.14) and (2.15) it follows that

$$\varphi = \varphi_i + \frac{1}{2}\left[n_m \ell n \frac{n}{n_i} - (n - n_i)\right] \qquad \ldots (2.16)$$

and noting that φ_i and φ_f are negligibly small

$$\frac{n_f}{n_i} = \exp\left\{\frac{n_i}{n_m}\left[\frac{n_f}{n_i} - 1\right]\right\} \qquad \ldots (2.17)$$

which shows the relation between n_f/n_i and n_i/n_m. The total energy radiated is

$$E_{out} = \frac{1}{2}\left(n_i - n_f\right) V N_o \, h\nu \, \frac{\gamma_c}{\gamma} \qquad \ldots (2.18)$$

where $k_o \ell n_m = \gamma = \gamma_c + \gamma_i$, γ_c representing the radiation loss due to coupling to the output and γ_i all the other losses. The peak power radiated is

$$P_{out} = \frac{\varphi_m N_o V h\nu}{t_p} \frac{\gamma_c}{\gamma} . \qquad \ldots (2.19)$$

We notice that n_m and n_f are independent of the cavity length. Hence from equation (2.18) it is obvious that the output energy does not depend on the cavity length. On the contrary the output power decreases with increasing cavity length because of its dependence on the photon lifetime $t_p = \frac{L}{\gamma c}$ as can be seen from equation (2.19). Equation (2.19) also shows that the output power is dependent both on n_m and γ_c and thus for a specific laser system there is a specific value of γ_c which maximizes the output power[38]. γ_c is largely controlled by the output mirror reflectivity.

The equations (2.16), (2.17) and (2.18) have been analysed in detail by Wagner and Lengyel[37,12] who have also considered the evolution of the pulse in time, by dividing the procedure into three regions, the central region B where φ is large and the regions A and C preceding and following it respectively, and the dependence of the pulse shape on the ratio n_i/n_m has been demonstrated.

Vuylsteke[39] has examined the giant pulse problem from a more general point of view and derived two coupled rate equations which have been numerically analysed by Midwinter[40]. The results have shown the dependence of the formative time and the shape of the pulse on the ratio n_i/n_m at the time of switching. The build-up time was also shown to depend on the output mirror reflectivity. For $R > 0.5$ the pulse builds up very rapidly giving a very high field in the cavity. This field however is not efficiently coupled out and most of the energy is lost in scattering. The output mirror reflectivity was found to be optimum in the region 20% to 35% for maximum output power. These predictions are discussed from the experimental point of view later (also in reference 41).

A complete theoretical account on the generation of the giant pulse has recently been given by Ratner and Chernov[42], who, in the case of fast switching, have shown that the maximum power and the total energy generated in the peaks, increase as n_i/n_m increases; the width of the pulse decreases as n_i/n_m increases.

The evolution of the giant pulse is greatly affected by the space-time development of the generated field and the initial spatial distribution of the population inversion[43]. In cases where these factors are dominant, the emitted pulse is due to the superposition of a series of closely spaced pulses generated by neighbouring regions of the laser. These propblems have to be considered in laser applications such as communications where the structure of the giant pulse is of great importance.

2.2.3 Methods of Q-Switching

There is a large number of Q-switching methods[12,13], each one having its own particular characteristics. The main ones are briefly mentioned below.

Passive Q-switching provides the simplest method of laser Q-switching. In this case saturable absorbers are introduced into the laser cavity. These are materials whose absorption properties change rapidly with strong illumination[44]. In order to prevent the shutter (absorber) from being too inert, i.e. does not open rapidly and completely, the number of absorbing centres must be much smaller than the number of excited active luminenscence centres. This implies that the oscillator force must be much greater for the absorbing centres than for the active centres. Thus the density as well as the molecular structure of the absorbers are vital in the Q-switching operation. This introduces the concept of thin and thick saturable absorbers, i.e. whether the photon irradiance should be regarded as a function of position within the absorbing medium or not[45]. The absorption band of the shutter must also be broad enough to overlap the spectral line of the laser. If the absorbing centres have a metastable level to which they transfer after excitation, then the shutter has a low inertia, i.e. it opens rapidly and completely. However in the majority of cases no such level exists and it is necessary to excite them repeatedly as they return to the ground state, in order to maintain them in the excited state. This leads to an increase in the inertia of the shutter. Since the probability of de-activation of the centres in the saturable absorber is inversely proportional to the fluorescence lifetime, the latter plays an important role in the switching process. This greatly affects the evolution of the pulse[46]. In order to explain the dynamics of the passive Q-switching, complicated theoretical considerations are needed and even these can only roughly be approximated to experimental results.

Active Q-switching can be performed with mechanical shutters, rotating prisms, ultrasonic cells, Kerr cells and other electro-optic devices[12,13]. The latter provide shutters which can be switched off very fast and they are of great practical importance. In this thesis

studies on the Q-switching of the liquid laser were made using a Pockels cell as the optical shutter, and its operation is described in the relevant section (Chapter VII).

Many laser applications, particularly in the field of plasma diagnostics, require a short pulse with a sharp leading edge. This can be achieved with an electro-optic switch by performing a second switching operation, after the first, to close the shutter when the photon density in the cavity has a high value. The existing energy in the resonator is then emitted in a lateral direction, usually from the polarizing prism[47].

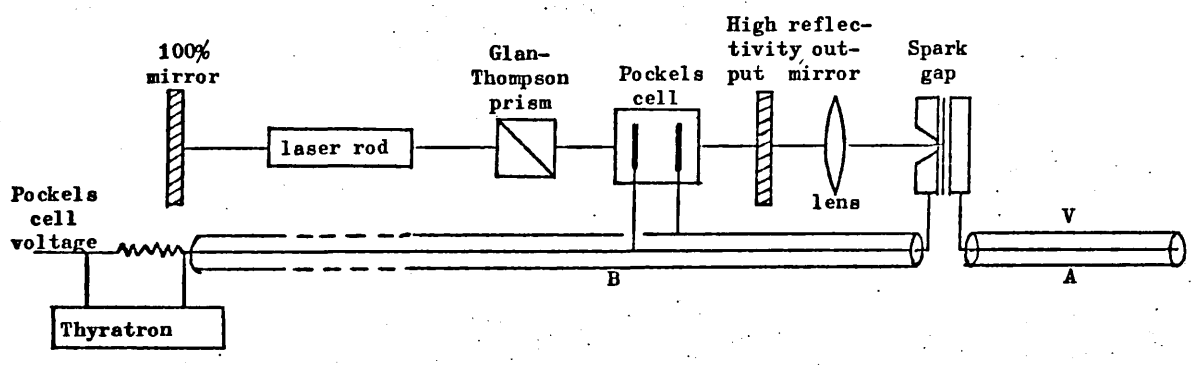

Fig.2.3
Schematic diagram demonstrating the generation of PTM

The procedure is illustrated schematically in Fig.2.3. The Pockels cell acting as a birifringent element in conjunction with the Glan-Thomspon prism provide the dominant loss mechanism for ordinary Q-switching (see Chapter VII). The Pockels cell is switched off using the thyratron, the giant pulse begins to evolve (see Chapter VII) and is emitted through the high reflectivity output mirror. It is focused into the spark gap shown and when it reaches a certain level it breaks the spark gap and discharges the voltage V from cable A to cable B in a time equal to the double transit time of cable B. The Pockels cell is thus closed again for a period equal to the double transit time of cable B. The existing energy in the resonator is discharged through the Glan-Thompson prism and it is

usually of a square pulse form[48]. The rise and fall times of the pulse depend on the speed with which the Pockels cell is switched off and on. This is very fast, and rise times of approximately 1 ns are easily obtainable. A number of other methods for producing PTM are now available.

2.3 THEORY OF MODE-LOCKING AND THE GENERATION OF ULTRA-SHORT PULSES

The generation of ultra-short pulses (mode-locking) has recently become one of the most important areas of laser physics. The interaction of such extremely short (10^{-12} s), high power pulses with matter has stimulated great interest in scientific and industrial laboratories. The possible applications of these pulses include the rapidly developing subject of non-linear optics, the production of high temperature plasmas, investigations into the spectroscopic properties of liquids, solids and gases, high speed photography, holography and many others.

The theories on the generation and properties of these pulses vary widely. Different approaches have been employed by several workers and in several cases they are in conflict. In the following, a comprehensive account will be given but only areas which are of interest in the present work will be stressed.

2.3.1 Definition and Properties of Mode-Locking

Mode-locking occurs when a large number of modes are oscillating together with similar amplitude and fixed phase relations. This results in an exchange of power between modes, i.e. they are coupled together. Let us consider the interaction of a large number of modes having a fixed phase difference φ. From the Fourier theorem the time dependent electric field $E(t)$ at any point can be written as

$$E(t) = \sum_{m=-N}^{m=N} E_o \exp i\left[\left(\omega_o + m\Delta\omega\right)t + m\varphi\right] \qquad \ldots (2.20)$$

where ω_o is the centre frequency and $\Delta\omega$ the frequency difference between two successive resonances,

$$\Delta\omega = \frac{\pi c}{L} = 2\pi\Delta f \ . \qquad \ldots (2.21)$$

A straight forward evaluation of the summation (2.20) gives

$$E(t) = A(t) \exp i\,\omega_o t \qquad \ldots (2.22)$$

where

$$A(t) = \frac{E_o \sin\left[(2N+1)\,\frac{(\Delta\omega t + \varphi)}{2}\right]}{\sin\left[\frac{(\Delta\omega t + \varphi)}{2}\right]} \ . \qquad \ldots (2.23)$$

Equations (2.22) and (2.23) characterize the behaviour of the time dependent electric field resulting from the interaction of modes with fixed phase difference φ. The output power is proportional to $A^2(t)$ where $A(t)$ changes with time as in equation (2.23). A graph showing the variation of $A^2(t)$ with time for seven coupled modes, is shown in Fig.2.4. The basic characteristics of the output power follow directly from (2.22) and (2.23). The pulse maxima occur when the denominator of (2.23) is zero; two successive maxima are therefore separated by

$$T = \frac{2\pi}{\Delta\omega} = \frac{2L}{c} \qquad \ldots (2.24)$$

where T is the round trip time of the cavity. The time difference $\Delta\tau$ between the peak of the pulse and its first zero is

$$\Delta\tau = \frac{2\pi}{\Delta\omega}\ \frac{1}{(2N+1)} = \frac{1}{\Delta\nu} \qquad \ldots (2.25)$$

where $\Delta\nu$ is the total oscillating bandwidth. Equation (2.25) shows that the larger the number of modes the sharper the resulting pulses. Equation (2.24) suggests that the oscillation in the cavity consists of a pulse propagating back and forth between the reflectors. It is interesting to note in equation (2.23) that as $\frac{\Delta\omega t + \varphi}{2} \to 0$, $A(t) \to (2N+1)E_o$ and therefore the peak power radiated becomes

$$I_p \sim (2N+1)^2\ E_o^2 \ , \qquad \ldots (2.26)$$

which is the DiDominico[49] result derived before mode-locking has been achieved when considering coupling of modes within a resonant cavity.

The simple mathematical explanation above showed how the modes of a resonant cavity with fixed phase differences, interfere to produce sharp pulses of light. To achieve this in practice, we introduce an externally driven modulator inside the cavity which produces a sinusoidally time varying loss of frequency equal to $\Delta\omega$. In this case each mode will be coupled to its two adjacent ones by the superposition of side bands of the amplitude modulated beam on it. In this way the modes are locked together with a fixed phase difference φ. The process is illustrated in Fig.2.5 where the gain curve of the laser is superimposed on the cavity modes. The effect of the gain of the laser on the coupling of the modes will be discussed later.

There is a number of ways of introducing a loss modulation at the mode-frequency difference, and they are classified into two broad categories. Active modulators[66] which are driven by an external signal, and passive modulators which are opened by the action of the laser radiation and are usually saturable absorbers introduced inside the cavity. For a general account on the subject, reference is made to two recent review articles by P.W. Smith[50] and M.A. Duguay et al[51]. In this thesis however, we will deal exclusively with passive mode-locking and this is what will be considered below.

2.3.2 Passive Mode-Locking

This method of mode-locking consists of introducing a saturable absorber into the laser cavity. Let us first consider the dynamics of the situation with the aid of Fig.2.6. The laser emission will be initiated by random intensity fluctuations which exist in the cavity due to spontaneous emission and noise in the direction of the laser axis. At some

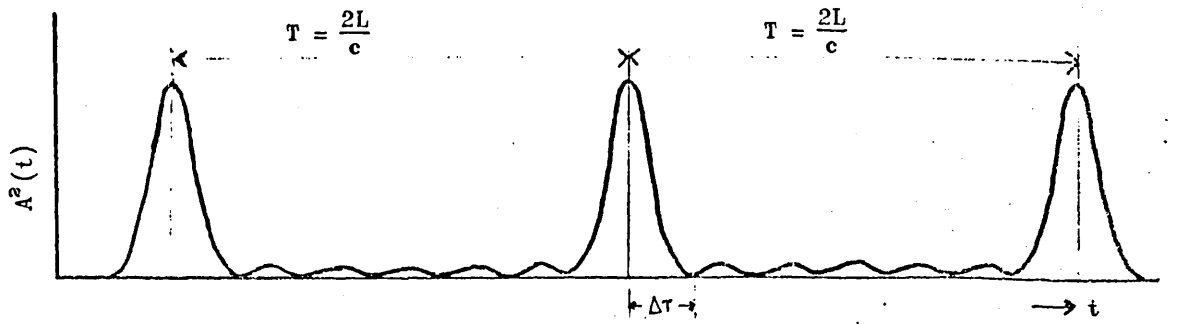

Fig.2.4 The light intensity for seven oscillating modes of equal amplitude and locked phases

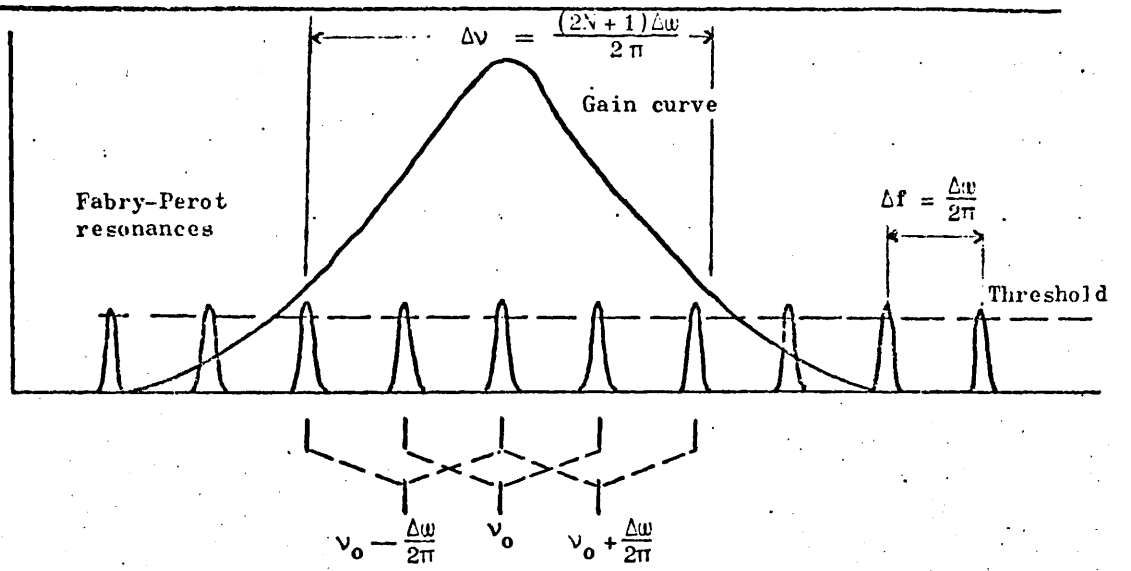

Fig.2.5
The gain curve of the laser superimposed on the cavity modes

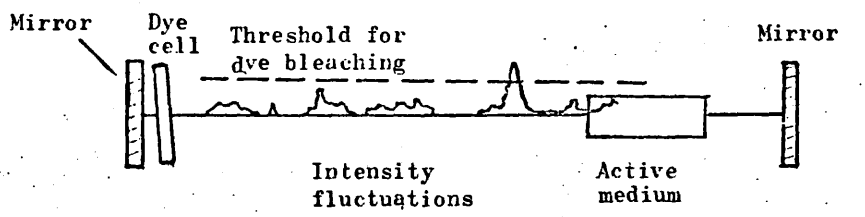

Fig.2.6 Visual representation of the initiation of mode-locking by random intensity fluctuations

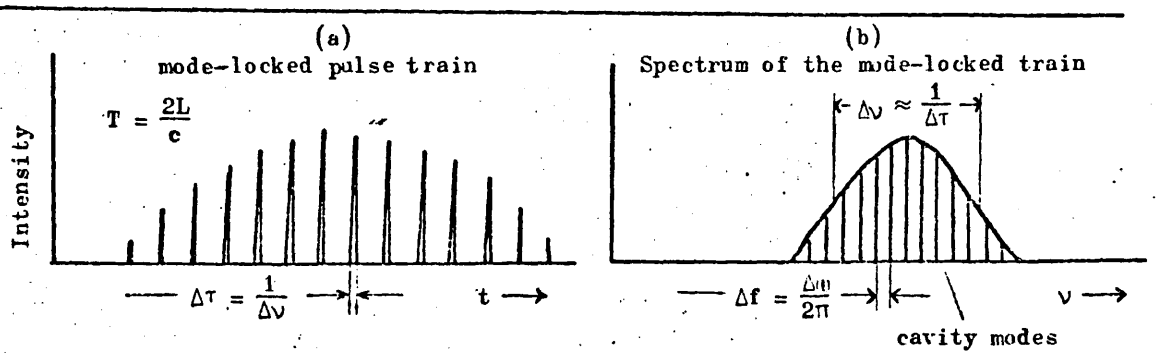

Fig.2.7 Time and spectral variation of the output of a mode-locked laser

instant in time one of the more intense fluctuations will induce a non-linear polarization in the absorber of the form $P = \chi_1 E + \chi_3 E^3$ (see section 2.4), where χ_1 and χ_3 are the first and third order polarizabilities. The third order term is the one responsible for the bleaching of the dye. It is obvious that if we express the electric field as a cosine function and consider the sum of two modes differing in frequency by $\Delta\omega$, the third order term will produce terms containing $\omega + \Delta\omega$ and $\omega - \Delta\omega$, i.e. the adjacent modes will be coupled together. The pulse will continue to grow inside the cavity due to the gain of the active medium, whilst at the same time more and more modes will be coupled together. The situation of the interaction of any two adjacent modes with the absorber can be visualized if we consider that the interaction leads to a difference in population between the lower and the upper state of the absorber, which contains a term oscillating at the difference frequency of the two modes. This oscillating term acts as the time varying loss within the cavity and it couples each mode to its neighbouring ones. Since each mode has a well defined standing wave pattern within the cavity, and the bleaching of the absorber will be according to these standing wave patterns, the position of the dye cell within the cavity is of importance[67] (see later). The decay time of the upper state of the absorber must be much shorter than the period of the difference frequency between two adjacent modes if a time varying loss of the saturable absorber is to be produced.

Two important points which will be discussed experimentally later need to be pointed out here. The gain of the active medium at the time of bleaching must not be too high, otherwise the mode lying near the centre of the amplifying linewidth (Fig.2.5), will grow very fast and deplete the inversion before sufficient modes are oscillating. On the other hand it should not be too low so that a large number of modes will be oscillating. Thus there should be an optimum gain for achieving best mode-locking.

Many authors have produced different interpretations of mode-locking and have derived theories using different approaches. The results of the analysis of Sacchi et al[52] will be summarized below, with due relevance to the work of this thesis. The approach considers, for simplicity, the interaction of three modes under the following three assumptions: (i) Rate-equation approximation, (ii) The non-linear polarization terms are retained up to third order, and (iii) All modes have equal amplitude ($A_m(t) = A(t)$). Under these assumptions the rate equations for the interaction of electromagnetic radiation with a saturable absorber have been solved by writing the field of the m^{th} cavity mode as

$$E_m(\vec{r},t) = A_m(t)U_m(\vec{r}) \exp\,(i\omega_m t + \theta_m(t)) + \text{complex conjugate}\ ,$$

where $A_m(t)$ describes the time evolution of the amplitude, and $\theta_m(t)$ describes the time evolution of the phase of the field. $U_m(\vec{r})$ are the space dependent parts of the mode-functions and form a normalized orthogonal set. Two differential equations describing the variation of the amplitude and phase in time have been derived:

$$2\dot{A} = -\,(\Delta + \Delta_a)A + \left[C_1 + \xi\, C_2 \cos\,(\theta_{m-1} - 2\,\theta_m + \theta_{m+1})\right] A^3 \qquad \ldots\ (2.27)$$

$$\dot{\theta}_m = \left(\frac{\mu}{\hbar}\right)^2 \frac{\Delta_a\, T_1}{1 + (\Delta\omega\, T_1)^2}\, A^2\, \xi \sin(\theta_{m-1} - 2\theta_m + \theta_{m+1}) \qquad \ldots\ (2.28)$$

where Δ takes into account the gain of the active material and the losses of the cavity, but not the loss of the saturable absorber, and Δ_a takes account of the losses due to the absorber. They can both be expressed as the inverse of the respective rise and decay times; μ is the electric dipole moment of the absorber, T_1 its relaxation time, and $\Delta\omega$ the difference frequency between adjacent modes. C_1 and C_2 are constants and ξ is a parameter describing the mode overlap in the dye cell and is given by

$$\xi = \int_{\text{cell}} U_{m-1}\, U_m^2\, U_{m+1}\, dV \Big/ \int_{\text{cell}} U_m^2\, dV\ .$$

In equation (2.27) the bleaching of the saturable absorber is described by the second term. Once the gain of the active material exceeds the losses of the cavity (first term in (2.27)), the field amplitude A starts from noise level and then increases faster and faster due to the bleaching of the absorber described by the second term in (2.27).

It is easily seen that the rate equation for the phase θ_m has two stationary values

$$\theta_{m-1} - 2\theta_m + \theta_{m+1} = 2n\pi \qquad \ldots (2.29)$$

$$\theta_{m-1} - 2\theta_m + \theta_{m+1} = (2n+1)\pi \; . \qquad \ldots (2.30)$$

By considering small deviations of the phase θ about a central value θ_o corresponding to the solutions (2.29) and (2.30), it can be shown[52] that the sign of ξ determines which of the two conditions (2.29), (2.30) is applicable. For a plane resonator $U_m(\vec{r})$ can be written as

$$U_m = \sqrt{\frac{2}{V}} \sin\left(\frac{m\pi x}{L}\right)$$

where V is the volume of the resonator and x is the distance along the resonator axis. Then, evaluating ξ from its definition above, we get

$$\xi = \frac{1}{2V}\left[2\cos\frac{2\pi x_o}{L} + 1\right] \qquad \ldots (2.31)$$

where x_o is the coordinate of the centre of the dye cell. Equation (2.31) is fundamental in describing the effect of the positioning of the saturable absorber in the cavity. It is obvious that if the cell is placed near either $x_o = 0$ or $x_o = L$, $\xi > 0$ and (2.29) applies. The pulse period is then $\frac{2L}{c}$ as described in (2.24). If the dye cell is placed in the centre of the cavity $\left(x_o = \frac{L}{2}\right)$, $\xi < 0$ and equation (2.30) applies. In this case it can be shown that the pulse period is L/c, i.e. equal to the single transit time of the cavity. For $x_o = \frac{L}{3}$ and $x_o = \frac{2L}{3}$ equation (2.31) gives $\xi = 0$ and no mode-locking is expected.

However this is not true in practice and if the interaction of many modes is considered[53] it can be shown that three pulses exist in the cavity and the period of the pulses in the emitted train is $\frac{2L}{3c}$ [67]. These effects will be considered experimentally later.

The output of the mode-locked laser will consist of a series of pulses as shown in Fig.2.7a. The pulses are sharper the broader the oscillating spectrum. Since the Fourier transform of a series of delta functions in time, is a series of delta functions in frequency, the spectrum of the output train has the form of Fig.2.7b. The spectrum of each individual pulse in Fig.2.7a corresponds to the envelope of the modes shown in Fig.2.7b.

2.3.3 Two Photon Fluorescence Measurements

The determination of the temporal behaviour of laser emission on a picosecond scale has become a subject of increasing importance in recent years. Intensity correlation measurements provide much information about the structure of light pulses on this timescale, and the two photon fluorescence (TPF) technique has been widely used in determining the duration of the mode-locked pulses generated by laser systems[51]. The recent invention of a picosecond streak camera for direct linear measurement of ultrashort light pulses will certainly provide more insight into the structure of light on the picosecond scale[54].

Two principal methods exist for determining the width of the picosecond pulses by TPF. The triangular method in which the main beam is split in two beams which then meet in the dye cell travelling in opposite directions. The other method, which has been used in the work of this thesis, consists of reflecting the pulses back on themselves with the aid of a mirror placed at the back of the TPF cell. Fluorescence is excited in the dye solution at the points where the forward and backward travelling

pulses meet. The fluorescence intensity is proportional to the square of the incident intensity. In this case the overlapping pulses are sub-structures introduced into each mode-locked pulse by having a parallel faced output mirror[55]. The Fabry-Perot resonances of the output mirror modulate the pulses, with peaks spaced at twice the double transit time of the width of the mirror[68]. The fluorescence picture will therefore contain pulses spaced at intervals equal to the width of the output mirror. The stationary overlap regions of locally high intensity excite TPF in the dye more strongly than in the intervening spaces. These regions can be described by intensity correlation functions[51] (similar to those mentioned in section 1.1). The fluorescence density $F(\tau)$ as a function of position from the reflecting mirror is given by[56]

$$F(\tau) = \Gamma^{(2)}(0) + 2\,\Gamma^{(2)}(\tau) \qquad \ldots (2.32)$$

where $\Gamma^{(2)}(\tau)$ is the second order correlation function defined by

$$\Gamma^{(2)}(\tau) = \int I(t)\, I(t+\tau)\, dt \qquad \ldots (2.33)$$

where τ is twice the light transit time from the mirror to the point under consideration. $\Gamma^{(2)}(\tau)$ characterizes the overlapping of the pulses.

The analysis of TPF intensity records is complicated because the phase modulation of light can produce different patterns. For perfectly mode-locked light the ratio of the intensity peaks to the background fluorescence should be 3, whilst for randomly phased modes it is 1.5[51]. The whole range of intermediate values can exist. In the case of reflecting the pulses back on themselves the ratio has been shown to be much less than 3, and this has been attributed to random fluctuations within the pulses on a picosecond time scale[130]. Sub-picosecond structure in mode-locked pulses from Nd^{+3} lasers has been the subject of recent controversy[57]. The recent work of Von der Linde et al[58,59] on single picosecond pulses has shown that no such structure exists. Bradley et al[130] however, have shown that sub-picosecond structure in mode-locked pulses occurs under certain conditions. The work of Von der Linde et al has also shown

that the spectrum of each pulse fits very closely to a Lorentzian curve.

It has been observed that when a parallel faced output mirror is used, a variety of periodic structures on the TPF recordings occur. Satellite pulses are usually observed at equal intervals on either side of the main TPF profile[9,55]. The intensity distribution of the pulses depends on the initial fluctuations at the instant of generation. A simple theoretical explanation is given below which accounts for the existence of these pulses. It can be shown by Fourier analysis that if a frequency spectrum $F(\omega)$ is amplitude modulated by a cosine function $a\cos\omega\tau'$ in the form of

$$H(\omega) = F(\omega)\ (1 + a\cos\omega\tau') \qquad \ldots (2.34)$$

the waveform $G'(t)$ of the time dependent amplitude[60,61] is

$$G'(t) = G(t) + \tfrac{1}{2}a\,G(t-\tau') + \tfrac{1}{2}a\,G(t+\tau') \qquad \ldots (2.35)$$

where $G(t)$ is the Fourier transform of the unmodulated spectrum $F(\omega)$. Equation (2.35) shows that the original waveform is accompanied by two equally spaced subsidiary waveforms (*) displaced by $\pm\tau'$. The intensity structure of the waveform is then

$$\begin{aligned} I(t) &= |G'(t)|^2 \\ &= G^2(t) + a\left[G(t)\ G(t+\tau') + G(t)\ G(t-\tau')\right] \\ &\qquad + \tfrac{1}{4}a^2\left[G^2(t+\tau') + 2G(t+\tau')\ G(t-\tau') + G^2(t-\tau')\right] \\ &= I_1(t) + \tfrac{1}{4}a^2\left[I_1(t+\tau') + I_1(t-\tau')\right] \qquad \ldots (2.36) \end{aligned}$$

The cross terms in (2.36) have been omitted since they vanish for pulses of width less than τ'. Putting $p = \frac{1}{4}a^2$ and substituting (2.36) in (2.33)

$$\Gamma^{(2)}(\tau) = \int I(t)\ I(t+\tau)\,dt$$

(*) The existence of the pair of satellite waveforms was pointed out to me by A.C. Selden.

$$= \int I_1(t)\ I_1(t+\tau)$$

$$+ p\left\{I_1(t+\tau)\ I_1(t+\frac{\tau'}{2}) + I_1(t+\tau)\ I_1(t-\frac{\tau'}{2}) + I_1(t)\ I_1(t+\frac{\tau'}{2}+\tau) + I_1(t) I_1(t-\frac{\tau'}{2}+\tau)\right\}$$

$$+ p^2\left\{I_1(t+\frac{\tau'}{2}) I_1(t+\frac{\tau'}{2}+\tau) + I_1(t+\frac{\tau'}{2})\ I_1(t-\frac{\tau'}{2}+\tau) + I_1(t-\frac{\tau'}{2})\ I_1(t+\frac{\tau'}{2}+\tau)\right.$$

$$\left. + I_1(t-\frac{\tau'}{2})\ I_1(t-\frac{\tau'}{2}+\tau)\right\} \qquad \ldots (2.37)$$

TPF will be recorded at the values of τ which produce an intensity square term. At these points the expression (2.37) becomes the integral of delta functions and the integral sign is dropped.

$$= I_1^2(0)$$

$$+ p\left\{I_1^2\left(\frac{\tau'}{2}\right) + I_1^2\left(-\frac{\tau'}{2}\right) + I_1^2\left(-\frac{\tau'}{2}\right) + I_1^2\left(\frac{\tau'}{2}\right)\right\}$$

$$+ p^2\left\{I_1^2(0) + I_1^2(\tau') + I_1^2(-\tau') + I_1^2(0)\right\} \qquad \ldots (2.38)$$

Equation (2.38) shows that the resulting TPF picture will consist of five fluorescent lines at the points $0, \pm\frac{\tau'}{2}, \pm\tau'$ whose normalized intensities will be in the ratio $1 + 2p^2 / 2p / p^2$. The situation is drawn schematically in Fig.2.8. Since p corresponds to the amplitude of the

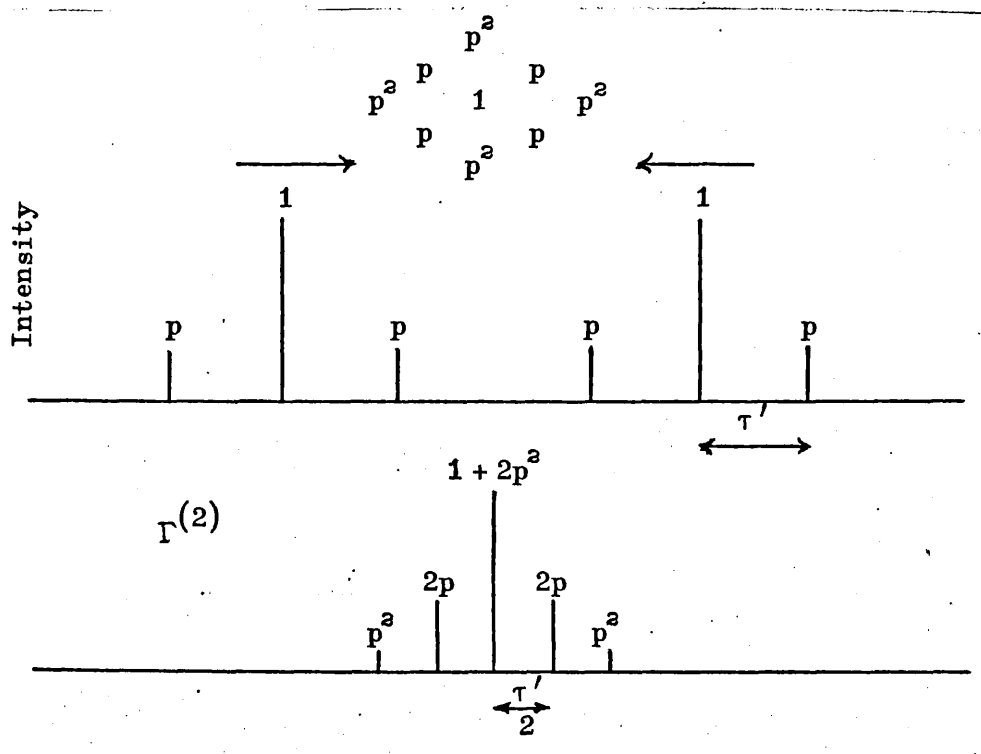

Fig.2.8
A pair of satellite waveforms at $\pm\tau'$ is responsible for the observation of satellite pulses on either side of the main TPF pulse

modulation of the frequency spectrum the brightness of the satellite pulses depends on the depth of modulation in the frequency spectrum described by equation (2.34) For an amplitude modulation $a=\frac{1}{2}$, of the frequency spectrum the ratio of the main pulse to the first pair of satellite pulses is 8 : 1. Pulses of this kind have been observed experimentally, and are described later (see Chapter IX). Other kinds of modulation can produce other more complicated TPF patterns which usually occur for imperfect mode-locking[69,70].

The two photon fluorescence method provides a high resolution measurement of the pulse width, but it is not representative of the pulse shape. In fact the third order correlation function reflects an asymmetry present in the pulse[51,59]. All intensity correlation methods are therefore inferential in determining pulse widths and provide little information on the pulse shape.

2.3.4 Cavity Modulations

The interference of several random phased modes can produce short intensity fluctuations. The interaction can take place through several processes and the fluctuations are periodic with cavity or sub-cavity modulation, precisely because it is the cavity length which determines the mode-frequency spacing as it was shown above. Sub-cavities inside the main laser cavity greatly affect the mode-locking because they provide a frequency selective filter for certain modes, and not for others[66,71]. Brewster-ended rods are to be preferred from plane parallel rods for mode-locking because of this reason.

Optical inhomogeneities present in the laser cavity can induce phase-locking. These inhomogeneities can occur due to spatial variations in the excitation density, discontinuity in the amplifying medium (change in the active atom density) and self-modulation. Self-modulation has been shown

to play an important part in the emission of a mode-locked laser[62]. The phase self-modulation accounts to a considerable degree for the spectral structure of the mode-locked laser and the discrepancy between the experimental and theoretical results for the duration of the ultra-short pulses[63,65]. During the first stage of generation the pulses are shortened as a result of the increased number of locked modes and during the second stage, the pulses are broadened as a result of the dispersion of the medium inside the resonator[64]. The main contribution to the phase modulation is made by the change in refractive index of the active element. Many other non-linear mechanisms can affect mode-locking and some of the effects which can occur in liquids are described in the next section.

2.4 NON-LINEAR EFFECTS IN LIQUIDS

Liquids are known to exhibit a large number of interactions with light, most of which are either inherently non-linear or become so through stimulated processes[73]. The interaction takes place through the scattering of light from various fluctuations in the liquid, through field effects which distort the liquid from its equilibrium state (electrostriction), and through molecular scattering[72]. These processes are induced in the liquid medium by the non-linear polarization given by

$$P = \chi_1 E + \chi_2 E^2 + \chi_3 E^3 + \ldots \quad \ldots (2.39)$$

where E is the electric field and the constants $\chi_1, \chi_2, \chi_3 \ldots$ are the first, second, third ... order polarizabilities. For high electric fields, such as those produced by high power lasers, the second and third order terms give rise to many non-linear optical phenomena. The second order term gives rise to frequency doubling and parametric amplification, and exists in non-centrommetric media only, whilst it is zero in centro-symmetric media. Thus for liquids, equations (2.39) becomes

$$P = (\chi_1 + \chi_3 E^2) E \quad \ldots (2.40)$$

We can see from equation (2.40) that the third order term which is responsible for the non-linear effects, is equivalent to a change of polarizability proportional to E^2. This is the result of the effect of temperature, density, molecular orientation and molecular polarizability on the dielectric constant. These changes give rise to the various processes leading to the scattering of light by the irradiated liquid. In what follows a description of the main effects which occur in liquids under the action of radiation will be given.

The Rayleigh scattering, whose frequency is essentially unchanged from that of the incident radiation is due to thermal and molecular fluctuations in the liquid[74] (strictly speaking there are two kinds of this scattering: Rayleigh scattering in which a change in entropy occurs at constant pressure and thermal scattering in which a change of pressure occurs at constant entropy). The resulting emission line is symmetric about zero frequency shift and two Rayleigh wings are observed on either side (Fig.2.9a). The width of the line is determined by the decay of entropy fluctuations due to thermal diffusion in the fluid and the extent of the wings by the damping of molecular anisotropy fluctuations.

Two equally shifted lines occur on either side of the Rayleigh line and they are known as the Brillouin doublet (Fig.2.9a). These result from the scattering of light by density fluctuations propagating in the fluid with the velocity of sound. In common liquids the amount of shift in the backward direction is generally in the range 0.1 to 0.5 cm^{-1} [75].

Finally Raman scattering is due to molecular vibrations in the liquid[73]. The incident light is inelastically scattered by a liquid molecule and gains or loses according to whether it causes the molecule to make a transition to a lower or a higher energy level. The frequency shift corresponds to the frequency of the vibration of the molecule and is

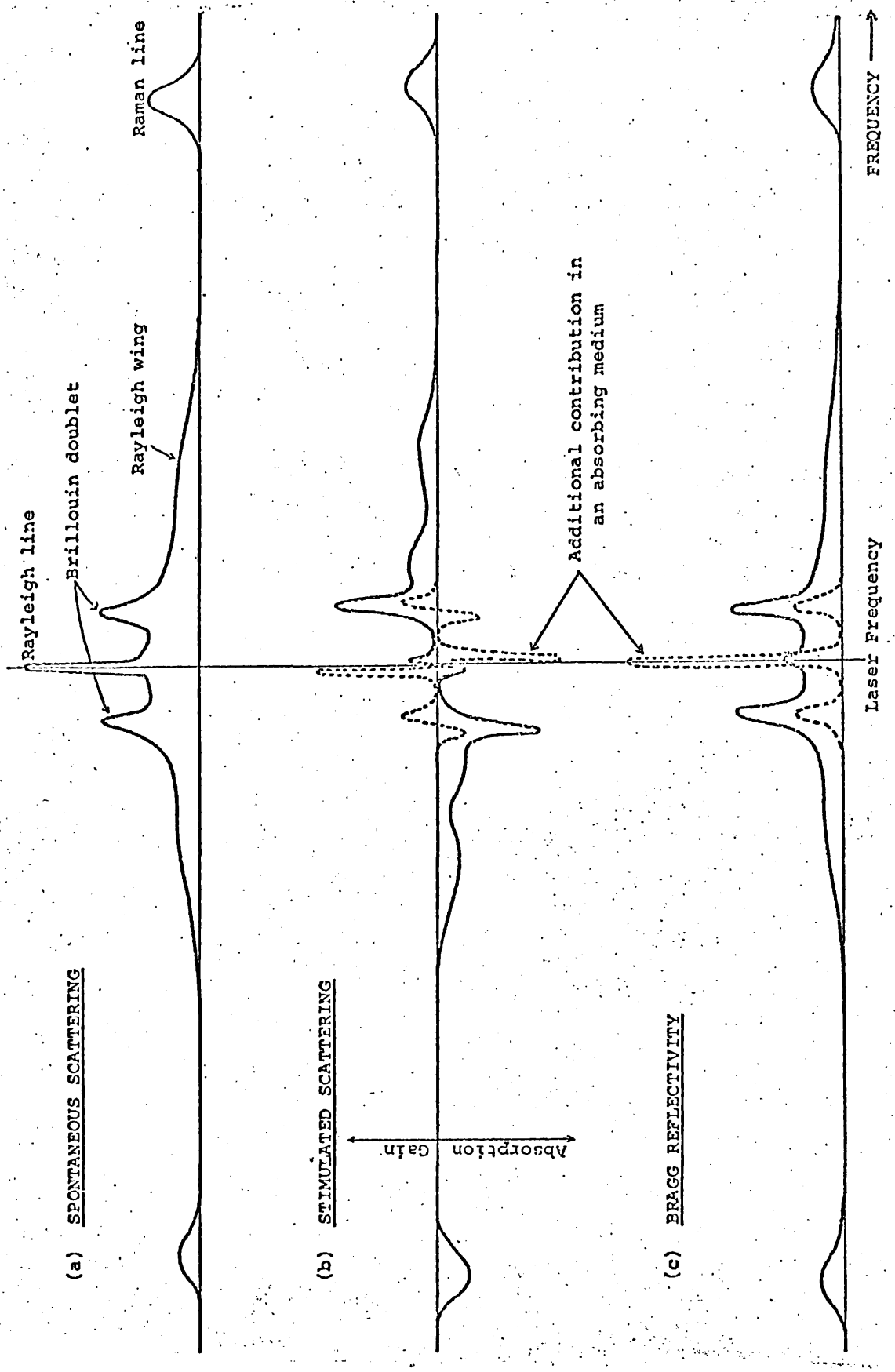

Fig.2.9
Scattering of light in liquids(76)

independent of the incident light. The shift usually ranges from 200 to 3000 cm^{-1}. Since in thermal equilibrium there is a larger number of molecules in the ground state the intensity of the up-shifted in frequency light is stronger than the down-shifted one. All the spontaneous processes described above occurring when the liquid is irradiated with light from conventional sources are shown in Fig.2.9a.

Under laser irradiation the magnitude of these effects is greatly increased and for sufficiently intense coherent light stimulated processes are generated[72]. Fig.2.9b shows the spectrum for the stimulated scattering of light. The dotted line represents an additional term to the spectrum for an absorbing medium. This arises from direct thermal absorption of energy from the incident light and the resulting increase in local temperature and density[76]. The stimulated scattering of light has different characteristics from the spontaneous scattering, and the scattered intensity can assume large values under stimulated emission approaching that of the incident intensity.

Stimulated scattering processes are usually investigated using giant pulse lasers, which provide high light intensities. Several parameters characteristic of the liquid medium have been determined by stimulated scattering. The molecular re-orientation times in benzene derivatives have been measured using stimulated Raman wing scattering[77]. The velocity of hypersound in liquids and glasses has been measured from observations on stimulated Brillouin scattering[75]. Finally, in laser systems which contain liquids emitting at the Raman line, it was found that a high percentage of the total laser energy is shifted to the Raman wavelength.

Several of the non-linear effects described above can occur together and they can produce a combined effect which results in the formation of a phase grating in the liquid[18]. When the liquid is in the laser cavity

the grating acquires a periodic structure, the amplitude of which depends on the field intensity in the liquid. Light can be reflected off the phase grating at the Bragg angle[19]. The reflectivity of the phase grating is shown in Fig.2.9c where again the dotted line shows an additional term which has to be introduced when an absorbing liquid is used[76].

Each of the non-linear effects described above has a characteristic response and decay time. These relaxation times have the following orders of magnitude:

Thermal effect	$10^{-7} - 10^{-8}$ second
Raman	$10^{-11} - 10^{-12}$ second
Electrostriction	$10^{-9} - 10^{-10}$ second ,

Thus the duration of the high power pulse used in the investigation of these effects is important. For picosecond pulses for example, we can only expect Raman scattering to occur since the duration of these pulses is too short for the other effects to develop. For pulses on the nanosecond scale however, several effects can occur and these have been extensively investigated[73].

Non-linear effects occurring in lasers with liquid active media can lead to power limitations of the output[78]. These will be dealt with in later sections.

CHAPTER III

LIGHT AMPLIFIERS

3.1 TRAVELLING WAVE AMPLIFIERS. THE AMPLIFIER EQUATION

Certain laser applications require high power pulses of specific shape, rise and fall times. Exponential amplification by a material in an inverted state, as described in section 1.2, only occurs at low powers when it can be assumed that the population inversion remains uniform throughout the length of the amplifier during the passage of the pulse. The characteristics of a high power light pulse, however, change during its propagation through an amplifier due to pulse sharpening, saturation and spectral cross-relaxation effects. The amplification of a pulse when cross-relaxation effects are not important will first be considered.

Consider the propagation of a light pulse of duration τ and energy $E(x)$ ($J\ cm^{-2}$) through an amplifier of length ℓ, the photon flux $(\frac{\text{photons}}{\text{sec cm}^2})$ at a point x along the amplifier and at time t being $I(x,t)$. Consider the processes occurring in a slab of thickness δx at a distance x along the amplifying medium. Two differential equations characterising the conservation of energy and conservation of ions can be written[79,80]

$$\frac{1}{c}\frac{\partial I(x,t)}{\partial t} = \sigma\, \Delta N(x,t)\, I(x,t) - \alpha\, I(x,t) - \frac{\partial I(x,t)}{\partial x} \qquad \ldots (3.1)$$

$$\frac{\partial \Delta N(x,t)}{\partial t} = -\sigma\, \Delta N(x,t)\, I(x,t) \qquad \ldots (3.2)$$

where $\Delta N(x,t)$ is the population inversion per cm^3, σ is the stimulated emission cross-section, and α represents the lumped losses per cm. The time dependency can be eliminated by integrating the time resolved photon pulse over its entire length at a given position x:

$$I(x) = \int_0^{\tau} I(x,t)dt \qquad (\frac{\text{photons}}{\text{cm}^2}) \,. \qquad \ldots (3.3)$$

Substituting equations (3.3) and (3.2) in equation (3.1) and rearranging

$$\frac{d}{dx}\int_0^\tau I(x,t)dt = -\int_{\Delta N}^{\Delta N(x,t)} \frac{\partial \Delta N(x,t)}{\partial t}\,dt - \frac{1}{c}\frac{d}{dt}\int_0^\tau I(x,t)\,dt - \alpha\int_0^\tau I(x,t)\,dt$$

$$\frac{dI(x)}{dx} = -\left[\Delta N(x,t) - \Delta N\right] - \alpha\, I(x) \qquad \ldots (3.4)$$

where ΔN is the population inversion per cm^3 before any stimulated emission occurs. From equation (3.2)

$$\left.\begin{aligned} \int_{\Delta N}^{\Delta N(x,t)} \frac{d\Delta N(x,t)}{\Delta N(x,t)} &= -\sigma\int_0^\tau I(x,t)dt \\ \Delta N(x,t) &= \Delta N\exp(-\sigma I(x)) \end{aligned}\right\} \qquad \ldots (3.5)$$

Substituting in (3.4)

$$\frac{dI(x)}{dx} = \Delta N\left\{1 - \exp\left(-\sigma I(x)\right)\right\} - \alpha I(x) \qquad \ldots (3.6a)$$

or putting $E(x) = h\nu I(x)$ $\quad (J\ cm^{-2})$

$$\frac{dE(x)}{dx} = h\nu\,\Delta N\left\{1 - \exp\left(-\frac{\sigma E(x)}{h\nu}\right)\right\} - \alpha E(x) \qquad \ldots (3.6b)$$

Equation (3.6) is the amplifier equation describing the amplification of a light signal with energy E passing through an amplifier of length x. A dimensionless plot of the quantities in equation (3.6b) has recently been given from which the amplification can be calculated for arbitrary numerical solutions for a wide range of numerical conditions[81].

3.2 SIMPLIFIED THEORY OF GAIN SATURATION IN TRAVELLING WAVE AMPLIFIERS

Equation (3.6) above has been derived under the assumption that the boundary condition (3.3) is valid. Let us consider the distribution of light energy and population inversion analytically, assuming that the lumped losses $\alpha I(x,t)$ are small and can be neglected. We calculate the distribution $I(x,t)$ at a particular point x at time t for a square input pulse $I_o = \int_0^t I(t)dt = I(t)dt$. Under these assumptions, integrating equation (3.6a)

$$\int_{I_o}^{I(x)} \frac{dI(x)}{1 - e^{-\sigma I(x)}} = \int_{o}^{x} \Delta N(x)dx$$

$$I(x) = \frac{1}{\sigma}\left\{\log_e\left[e^{\sigma I(t)t} + e^{-\sigma \Delta N(x)x} - 1\right] + \sigma\, \Delta N(x)x\right\} \qquad \ldots (3.7)$$

where $\Delta N(x)$ represents the number of available ions per unit amplifier length within the cross-section occupied by the signal transmission mode. Differentiating and using equation (3.3)

$$\frac{\partial}{\partial t}\int_{o}^{t} I(x,t)dt = \frac{1}{\sigma}\frac{\partial}{\partial t}\left\{\log_e\left[e^{\sigma I(t)t} + e^{-\sigma \Delta N(x)x} - 1\right] + \sigma \Delta N(x)x\right\}$$

$$I(x,t) = \frac{I(t)\exp(\sigma I(t)t)}{e^{\sigma I(t)t} + e^{-\sigma \Delta N(x)x} - 1} \; . \qquad \ldots (3.8)$$

Equation (3.8) gives the number of photons per unit time which pass the amplifier cross-section at a point x along its length at time t. In order to find the number of available ions per unit amplifier length $\Delta N(x,t)$ within the cross-section occupied by the signal transmission mode we use equation (3.5) in (3.7)

$$-\frac{1}{\sigma}\int_{\Delta N(x)}^{\Delta N(x,t)} \frac{d\Delta N(x,t)}{\Delta N(x,t)} = \frac{1}{\sigma}\left\{\log_e\left[e^{\sigma I(t)t} + e^{-\sigma \Delta N(x)x} - 1\right] + \sigma \Delta N(x)x\right\}$$

$$\Delta N(x,t) = \frac{\Delta N(x)\exp(-\sigma\, \Delta N(x)x)}{e^{\sigma I(t)t} + e^{-\sigma \Delta N(x)x} - 1} \; . \qquad \ldots (3.9)$$

Equations (3.8) and (3.9) give the variation of the photon flux and active ions along the amplifier length for a square pulse input signal $\left(\int_{o}^{t} I(t)dt = I(t)t\right)$ and uniform distribution of the population inversion along the amplifier axis $\left(\int_{o}^{x} \Delta N(x)dx = \Delta N(x)x\right)$. They were first derived in a different way by Schulz-Dubois[82] and show a number of mathematical properties characteristic of the physical situation. Let us examine equations (3.8) and (3.9) using the general definitions for gain

$$G(x,t) = \frac{I(x,t)}{I(t)}$$

and saturation

$$S(x,t) = \frac{\Delta N(x,t)}{\Delta N(x)} .$$

From equation (3.8) we see that the gain $G(x,t)$ decreases monotonically with time from an initial value $G(x,o) = \exp \sigma \Delta N(x)x$ down to unity. The gain is greater for larger values of x. From equation (3.9) the saturation parameter $S(x,t)$ decreases monotonically from unity to zero. It drops faster for larger values of x. Consider the case when the original gain is large and the degree of saturation at the input is small, i.e.

$$G(x,o) = e^{\sigma \Delta N(x)x} \gg 1 \qquad \sigma I(t)t \ll 1$$

both conditions being very good approximations to many physical situations. Then from equation (3.8) the variation of the relative instantaneous gain

$$\frac{G(x,t)}{G(x,o)} = \frac{\frac{I(x,t)}{I(t)}}{e^{\sigma \Delta N(x)x}} = \frac{1}{1 + \sigma\, G(x,o) I(t)t} \qquad \ldots (3.10a)$$

Also from (3.9)

$$\frac{\Delta N(x,t)}{\Delta N(x)} = \frac{1}{1 + \sigma\, G(x,o)\; I(t)t} . \qquad \ldots (3.10b)$$

Equations (3.10a,b) describe a hyperbola. The curve describes directly the shape of the output signal. It can be seen from equation (3.10a) that the drop in the output signal occurs faster when the input signal and the initial gain are higher. This was to be expected from the conservation of energy law. Directly at the input the stored energy decays according to an exponential law, whilst further along the x-axis it follows a hyperbolic law.

3.3 NON-LINEAR AMPLIFICATION OF LIGHT PULSES

It is obvious from the above discussion that for a pulse of certain length passing through an amplifier, the first portion of the pulse will be amplified more than the rear portion since the gain of the amplifier will be less for the latest parts of the pulse. This non-linear interaction will distort the shape of the pulse, the magnitude of the effect depending on the gain per unit length of the amplifier. The coefficient of amplification K (section 1.2) is determined by two parameters of the radiating particles, namely the cross-section σ of the radiative transition and the inverted population density between the two levels. The non-linearity of the amplification usually results from the change in the population difference of the two levels under the influence of intense radiation as described above[84]. However other non-linearities may occur during the amplification process due to the dependence of the cross-section of the radiative transition on the intensity. This type of non-linearity has hardly been studied due mainly to the lack of sufficient experimental results, although the recent production of powerful ultrashort pulses provides a practical method for investigating this effect[83,140].

The saturation type non-linearity has been investigated most thoroughly and the pulse sharpening occurring during the amplification of a giant pulse has recently become a subject of particular interest[83,84]. Under saturation conditions the pulse peak moves with a velocity which considerably exceeds that of light[85]. Pulse shortening can occur during the process and the effect is greater for larger slopes of the incoming pulse front. This pulse-shaping is of particular interest in applications where powerful pulses with specified rise times are needed, as for example, in the case of the production of hot plasmas.

The propagation of the pulse peak with velocity greater than that of light has produced some controversy. Schulz-Dubois[82] first described

the motion of the peak by considering the power at some point on the rising part of the pulse envelope to be sufficient to saturate the amplifier and thus decreasing the gain thereafter. The result is that the pulse maximum continually moves ahead as successive earlier parts of the profile reach saturation. Letokhov[83,85] has recently produced several analyses of the motion of the crest of the pulse, and the conditions for the existence of stationary states of a pulse are demonstrated. It is important to note that the laws of special relativity are not violated because of the velocity of propagation of the pulse maximum, since information does not travel with velocity greater than light, but only the distortion of the pulse envelope[83,86].

The amplification of square shape pulses (obtained from pulse transmission mode, section 2.2.3) provides a convenient method of investigating the saturation parameters of laser amplifiers since the remaining gain can be measured directly from the shape of the output pulse[87]. Mode-locked trains provide analogous situation, the gain of each pulse depending on the amount of energy removed from the amplifier by the previous pulses[9]. This method is discussed in detail in the latter parts of this thesis.

3.4 CROSS-RELAXATION EFFECTS IN LASER AMPLIFIERS

As pointed out in section 1.5 an amplifying medium possesses a thermal linewidth. The interaction of the input signal with the amplifying medium depends also on the properties of the linewidth as well as the spectrum of the input signal. Thus in equations (3.1) and (3.2) the intensity I of the incident radiation, the cross-section σ and the population inversion ΔN are all functions of frequency[15]. An additional term proportional to the departure of the population inversion from equilibrium should be added in equation (3.2), the constant of proportionality being the cross-relaxation rate into the depleted regions from other parts of the linewidth.

In neodymium systems the amplifying linewidth consists of an inhomogeneous line formed by the superposition of many homogeneously broadened lines. Such a line structure is the result of the superposition of the different spectra of different ions, in different environments[88,89]. The width of the homogeneous line has been found by several workers, to lie between 10 and 25 Å for Nd-glass lasers[88]. The overall inhomogeneous linewidth is approximately 200-250 Å depending mainly on the temperature of the medium. Consider a signal whose spectral width is much narrower than the homogeneous linewidth, interacting with the atomic medium. The cross-relaxation rate for filling the depleted region of the population inversion from other ions within the homogeneous linewidth is very fast ($> 10^{10}\ s^{-1}$). Thus during the amplification of nanosecond pulses it can be assumed that all the atoms within the homogeneous linewidth contribute to laser action[90]. Energy transfer into a depleted region can occur from regions within the inhomogeneous linewidth[15]. The cross-relaxation rate for this process is slow and it has been measured to be of the order of $10^5\ s^{-1}$ [91,92]. This means that much of the energy under the inhomogeneous line remains unused when nanosecond pulses with narrow spectrum (< 10 Å) are amplified. Certain aspects of linewidth problems have been investigated experimentally and are discussed in detail later.

Many other effects occur in laser amplifiers which in general affect their performance. Super-radiance can occur in an amplifier, i.e. spontaneous emission is amplified by stimulated emission. Super-radiance originates in the entire volume of the material and thus in calculating the noise background at the output we must integrate over the amplifier length. It can be shown that the signal-to-noise ratio increases rapidly with increasing amplification and it is also inversely proportional to the number of modes considered. In the optimum case the signal is applied in one mode and measured at the output in this mode[13,24].

The interest in the operation of ring lasers and amplifiers has recently been revived though they have never quite acquired the importance of cavity lasers or travelling wave amplifiers. The operation of ring lasers differs greatly from a normal laser cavity in that it supports two essentially independent travelling waves, one travelling in each direction around the ring. Ring amplifiers however, provide very good means of investigating the saturation parameters of the active medium. For a square pulse, for example, the slope of the output pulse will be different for each pass through the amplifier according to the residual distribution of the population inversion left from the previous pass.

CHAPTER IV
LIQUID LASERS

4.1 HISTORICAL INTRODUCTION

The search for liquid laser materials started immediately after laser action had been achieved in solids and gases, but it did not produce any encouraging results. This initial failure led to the general feeling amongst scientists that laser action in liquids is unlikely to be achieved because the scattering losses which arise from the change of refractive index due to heating by the pumping radiation, are one or two orders of magnitude greater than those in solids[93].

The performance of the first liquid laser reported in 1963 by Lempicki and Samelson[94] was not very encouraging. The laser substance was a solution of trivalent Europium in an organic chelate and the laser was operated at 77°K. The substance was highly viscous and resembled a glass rather than a liquid. The subsequent work on chelates in 1964, though it led to the achievement of room temperature operation, had only produced lasers which were inferior to gas and solid state lasers. It was realized that the inferior performance of the chelate laser was due to intense absorption of the pumping radiation by the chelate which limited the penetration depth of the pumping radiation to a few microns. With the end of the chelate era, liquid laser research came to a standstill.

Revived interest in liquid lasers came in 1966-1967 when two new kinds of liquid lasers were reported[95-97]. This arose from the understanding of the general problems which must be overcome for laser action to occur in liquids.

4.2 GENERAL PROBLEMS IN ACHIEVING LASER ACTION IN LIQUIDS

Liquid laser research was split into two broad categories, the organic liquid laser based on solutions of purely organic compounds and the inorganic liquid laser based on solutions of rare earth ions in aprotic solvents.

The achievement of laser action with organic compounds came when it was realized that the main problem was the accumulation of excited molecules from the first excited level of the singlet state to the triplet state by fast radiationless transitions. Thus the triplet state acts as a sink for the excited molecules. Triplet-triplet transitions may occur in which the fluorescence emission is reabsorbed, thus prohibiting laser action. To overcome this difficulty, organic lasers were first pumped with Q-switched ruby lasers which provided a high intensity in a sufficiently short time, thus overcoming the effects of the fast radiationless relaxation to the triplet state. Flashlamps with sufficiently short rise times have been developed to overcome the effects of the triplet state[98]. More recently quenching of the triplet state has been achieved with the aid of other substances in the laser solution. Reliable dye-lasers have now been constructed. The main advantage of an organic laser as compared to an inorganic laser is its wide range of tunability[99]. Only small powers can be achieved with dye lasers however, and the search for liquids which could dissolve rare-earth elements went on.

It became evident that the poor performance of inorganic liquid lasers was not due to the change of the index of refraction due to pumping because it is known that there exist liquids whose optical performance on heating is as good as with solids. Investigations on the behaviour of trivalent neodymium in aqueous solutions had shown quenching rates of the luminescent level to be $10^8 sec^{-1}$. It is obvious that such a high rate of quenching of the luminescent level would not allow sufficient population

to build up for stimulated emission to occur in solutions containing water. Further studies on the radiationless relaxation rates have shed more light into the problem of the quenching of the fluorescence in liquids. It was already known from the work of Hutchinson and Magnum[100] that replacement of the hydrogen atoms by deuterium in the molecules of naphthalene leads to a decrease in the rate of radiationless relaxation. Subsequent experiments have indicated that the presence of hydrogen atoms was intimately connected with the quenching of fluorescence in the solutions[101]. Finally Heller[102] was able to show that the main factor responsible for the quenching of the fluorescence of rare earth ions in solutions was the hydroxyl group. The experimental work involved had shown that the rate of radiationless relaxation depends strongly on the energy of the acceptor vibrations. This result was to be expected since it is well known that the closer the matching of the energy a donor can donate to the energy an acceptor can accept, the faster the rate of energy transfer becomes. High vibrational energies, therefore, increase the overlap between the vibrational levels and the electronic levels of the excited atoms. Considering that the vibrational energy of the hydroxyl group is 3600 cm^{-1} (energies denoted in this way are in units of hc) and that the separation between the lowest electronically excited level and the highest vibrational level of the ground state of neodymium is 5300 cm^{-1} (Fig.4.1), we see the reason for the fast quenching rate of the neodymium luminescence in aqueous solutions.

Thus solvents with light atoms and consequently high vibrational energies will quench fluorescence and therefore are not suitable for liquid lasers. Solutions with heavy atoms should therefore be used to dissolve the active ions. The other requirement is that a solvent must have a high dielectric constant in order to dissolve ionic compounds. Selenium oxychloride was the first such solvent to the used. Its highest vibrational energy is 955 cm^{-1} which is small compared with 5300 cm^{-1} of the de-excitation energy of trivalent neodymium. Its dielectric constant is 46.

After the problem of radiationless relaxation had been solved, there was only one problem remaining in the achievement of good liquid lasers and this was the problem of self-quenching. This occurs when neodymium ions are very close to each other, then de-excitation of an ion in the metastable level $^4F_{3/2}$ to the ground state $^4I_{15/2}$ may occur, with the simultaneous excitation of a second ion from the ground state $^4I_{9/2}$ to the upper level of the ground multiplet $^4I_{15/2}$ (Fig.4.1). This becomes even more serious in liquids where diffusion takes place. To overcome self-quenching, chemical solutions are used which form a cluster around each ion thus preventing the ions to approach each other within a distance less than 1.5×10^{-7} cm. Each ion is then surrounded by a shell made up by the solvent's molecules. During the formation of the chemical systems it must be made certain that anions which are small and have high charge densities are excluded since they may attract other neodymium ions and bring them within quenching distance. The same effect can result from the presence of anions which coordinate with rare-earth cations. The presence of these ions may well result in precipitation or polymerization[17].

4.3 INORGANIC LIQUID LASER SOLUTIONS

Liquid laser solutions can now be prepared which have all the adequate properties for laser action. At the present time we have two main solutions which serve as host materials for Nd^{+3}. These are the selenium oxychloride ($SeOCl_2$) and the phosphorous oxychloride ($POCl_3$). Chelate lasers using Europium as the active ion, have not produced any practical devices and they are mainly of historical interest. A chelate solution serving as the host medium for neodymium ions was recently reported, which had the advantages of being non-toxic and non-corrosive[103]. However a short investigation which I have carried out on this solution has only produced discouraging results. Also short investigations which I have carried out on perchlorate solutions(*) containing neodymium have produced negative results so far.

(*) These solutions have been prepared by the chemistry group at Harwell after the recent report of Haas and Stein[104] that 95% fluorescent quantum yield can be obtained on substituting an appropriate deuterated solvent in place of hydrogeneous solvents.

The fundamental properties of the best performing solutions so far, $SeOCl_2$ and $POCl_3$, are summarized here: (i) They have no atoms lighter than oxygen and therefore their vibrations do not have sufficient energy to accept the energy corresponding to the gap between the excited and the ground multiplets of neodymium. This prevents radiationless relaxation from taking place. (ii) The highest vibration of $SeOCl_2$ is 955 cm^{-1} compared with the smallest possible gap between the $^4F_{3/2}$ and $^4I_{15/2}$ levels (Fig.4.1), which is 5300 cm^{-1}. (iii) $SeOCl_2$ has a high dielectric constant (46) and dissolves ionic compounds easily. The dielectric constant of $POCl_3$ is 14 and the dissolution of Nd^{+3} ions requires a special process (see below). (iv) The introduction of Nd^{+3} ions into the solutions results from the dissolution of Nd-oxide and Nd-chloride. In order to dissolve substantial amounts of rare-earth oxides, the solutions are acidified with aprotic acids (tin tetrachloride ($SnCl_4$) and antimony pentachloride ($SbCl_5$)). These aprotic acids prevent precipitation of the solution[96,105,106].

The most recently developed and most widely used liquid laser material utilizes $Nd^{+3} : POCl_3 : ZrCl_4$ (Nd^{+3} ions dissolved in phosphorous oxychloride acidified with zirconium tetrachloride). This solution has certain advantages compared with the previous solutions and this is the solution whose laser properties are investigated in the present work. It is less corrosive and less sensitive to atmospheric moisture. It shows unusual spectroscopic behaviour compared to the other solutions, being the only solution which shows a sharp decrease in lifetime and intensity at acid concentrations above stoichiometric (Fig.4.2); the other solutions show such decrease below stoichiometric acid concentrations only[107]. (A stoichiometric solution is one which has resulted from the use of the proper weight relations in the chemical reactions.) At high neodymium concentrations it shows severe quenching of the fluorescence with excess acidity, which indicates that the excess $ZrCl_4$ alters the coordination of the neodymium ions

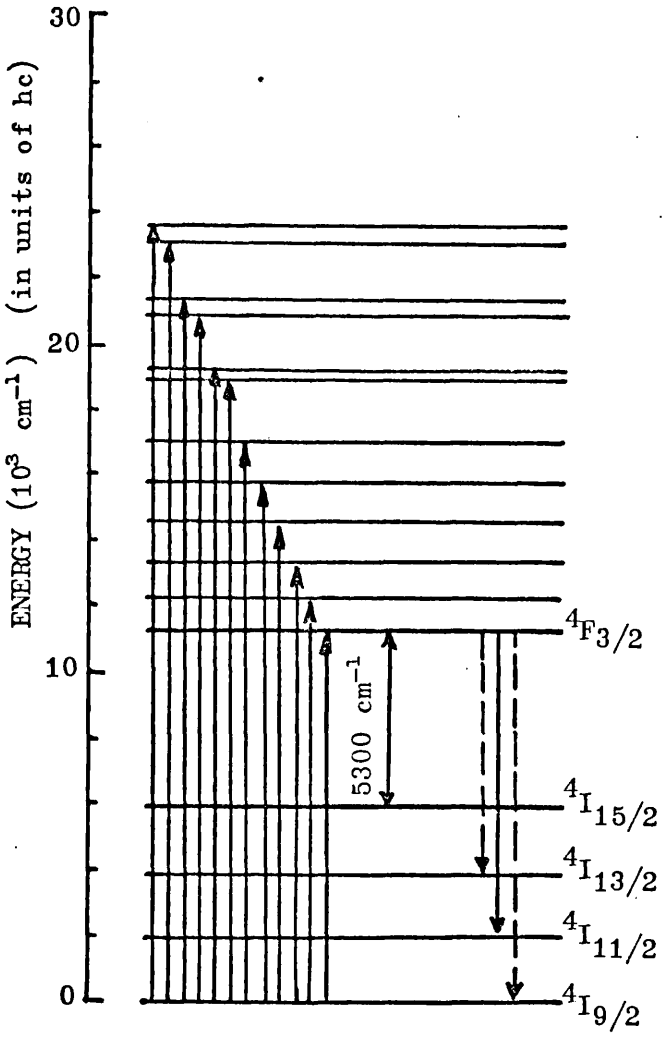

Fig.4.1
Energy level scheme for ionic neodymium[17]

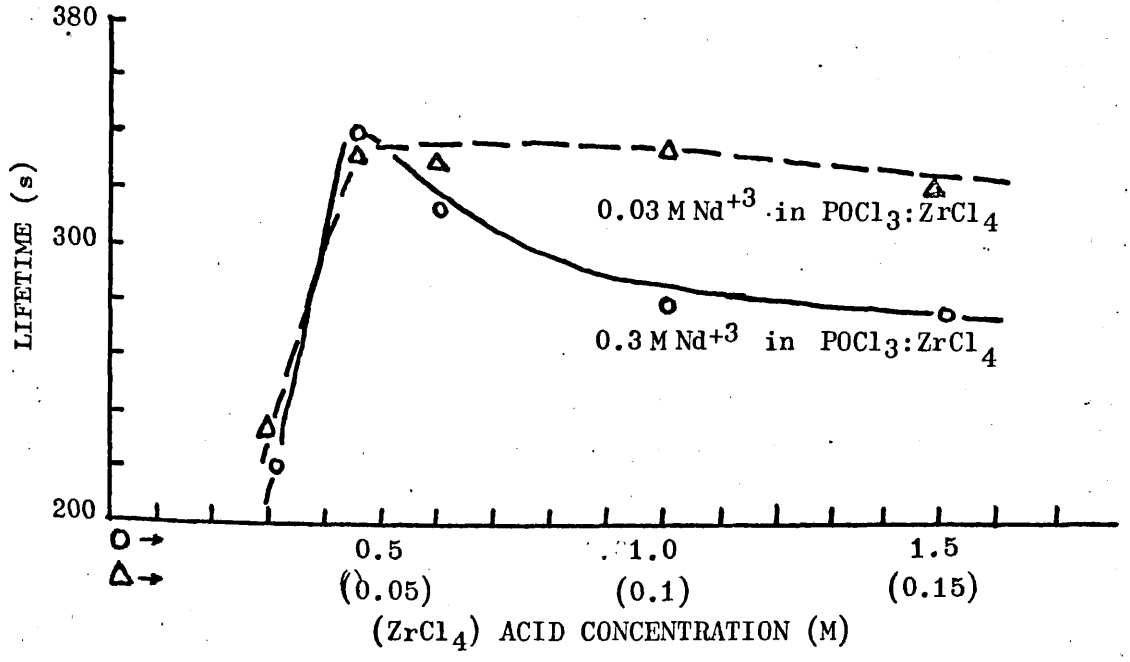

Fig.4.2
Dependence of fluorescence decay time of Nd^{+3} on acidity, in $POCl_3$: $ZrCl_4$ [107]

in such a way as to allow cross-quenching by other Nd^{+3} ions (section 4.2). At stoichiometric concentrations however, this solution is chemically more stable than the others. Its preparation is described in references 96 and 105. The only difficulty present in the formation of this solution is the low dielectric constant (14 compared with 46 of $SeOCl_2$) and thus the solubility of ionic salts is lower. The solubility can be increased and stabilization can be achieved by adding sufficient quantities of other solvents such as polyphosphoryl chloride polymer during the preparation. Degradation of the polymer leads to precipitation of Nd^{+3} out of the solution[105].

In experiments which I have carried out, precipitation occurred after pumping the solutions with xenon flashtubes. These were solutions whose acid concentration was not stoichiometric or that the addition of polymers during the formation was not sufficient. Precipitation occurred in the form of crystals deposited on the bottom of the laser tube.

As with every other laser system, the optical quality of the active medium plays an important part in laser operation. For liquids in particular the chemical properties of the solution may affect the optical quality, and also scattering losses may be significant. Brecher et al[105] have measured the transmission losses of several liquid laser solutions with four different methods: (i) By direct transmission which involves using small signals from an oscillator and recording the relative intensity before and after passing through the solution (see also Andreou et al[9]). (ii) By the laser static loss method which is a very accurate measurement of the optical loss. An anti-reflection coated cell containing the solution is inserted into the cavity of a CW operating Nd-YAG laser. The cell is then removed from the cavity and replaced by a quartz plate which introduces a known reflective loss as a function of the angle of incidence. This angle is varied until the same threshold for laser action is obtained;

from this the optical loss is determined. (iii) By the laser dynamic loss method. This method is described in Chapter VI. (iv) By the right angle scattering method which involves the measurement, with the aid of a photomultiplier, of the light scattered at right angles to the beam from a gas laser. This method provides a measure of the concentration of scattering centres within the solution.

The experiments of Brecher et al have indicated certain important characteristics of the liquid laser solutions. (a) The passive loss for a laser solution was a factor of six to eight times higher than in the pure solvent and appeared to be intrinsic to the material. This high loss was caused by the pyrophosphoryl chloride formed during dissolution of the Nd^{+3} salt which has proven essential to the chemical stability of the laser and hence cannot be removed. Losses of this order of magnitude are comparable to those of glass. (b) Contamination of the solutions by H_2O increased the absorption loss by a significant amount. This was due to the intense absorption of H_2O at 1.06μ. (c) $POCl_3$ solutions which have been contaminated with H_2O show high scattering losses and are quite viscous. Reduction of the viscosity could be achieved by the addition of several other chemicals such as PCl_5. (d) The scattering losses in the best attained solutions so far have a maximum of about 0.3% per cm. Table 4.1 below shows the scattering losses for some of the liquid laser solutions based on $POCl_3$ as reported in the above mentioned paper.

TABLE 4.1

TRANSMISSION LOSS IN VARIOUS LIQUIDS

Material	Transmission loss at 1.06 μ (% per cm) ± 20%	Method of Measurement
(1) $POCl_3$	0.1	Static loss
(2) H_2O + $ZrCl_4$	> 1	Transmission
(3) 0.3 M Nd^{+3} in $POCl_3$-$SnCl_4$ (contaminated with water)	2	Dynamic loss
(4) 0.3 M Nd^{+3} in $POCl_3$-$ZrCl_4$	0.16 0.2 - 0.3	Static loss Transmission
(5) 0.3 M Nd^{+3} in $POCl_3$-$ZrCl_4$ (contaminated with water)	0.6	Static loss

4.4 PROPERTIES OF THE NEODYMIUM ION

A comparison of laser media based on the neodymium ion with other active media was made in section 1.4. From the rare earth elements neodymium has more attractive properties than other elements because (i) it has a four level scheme and at room temperature the final laser level is almost unoccupied (Fig.4.1). (ii) It has many absorption bands in the visible and infra-red regions where powerful radiation sources are available which are strong compared to those of other trivalent elements (Fig.4.3). (iii) The wavelength of emission is in the one micron region where fast detectors exist (Fig.4.4).

The different neodymium systems have different characteristics. As pointed out in section 1.3, the threshold of oscillation population inversion ΔN_T is directly proportional to $2\pi\tau\Delta\nu$ and inversely proportional to the photon lifetime in the cavity t_p. Table 4.2 shows the values of $2\pi\tau\Delta\nu$ for three different neodymium laser systems.

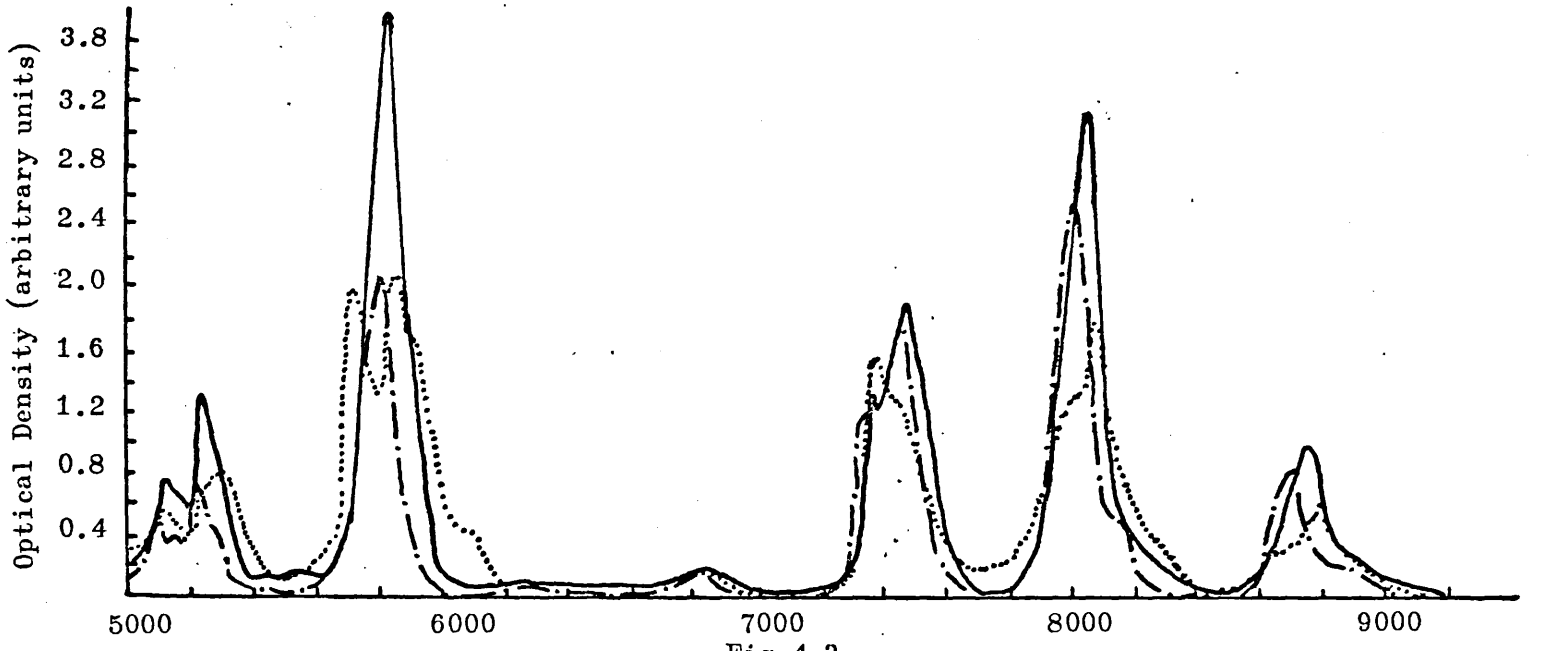

Fig.4.3

Absorption spectra of Nd^{+3} in : ——— $SeOCl_2 : SnCl_4$;
-·-·-·- $POCl_3 : ZrCl_4$; ····· Glass LG 55 (107)

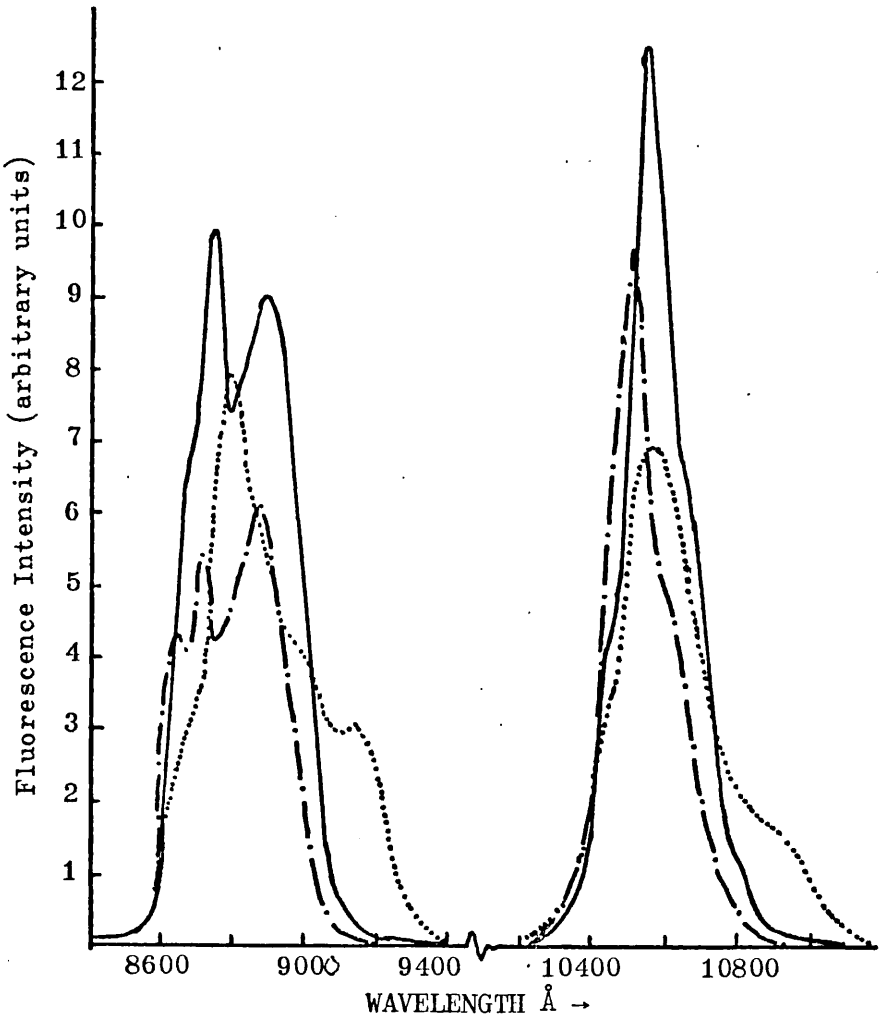

Fig.4.4

Emission spectra of Nd^{+3} in : ——— $SeOCl_2:SnCl_4$; —·—·— $POCl_3:ZrCl_4$ ····· Glass LG 55 . Concentration 1.8×10^{20} cm^{-3} (107)

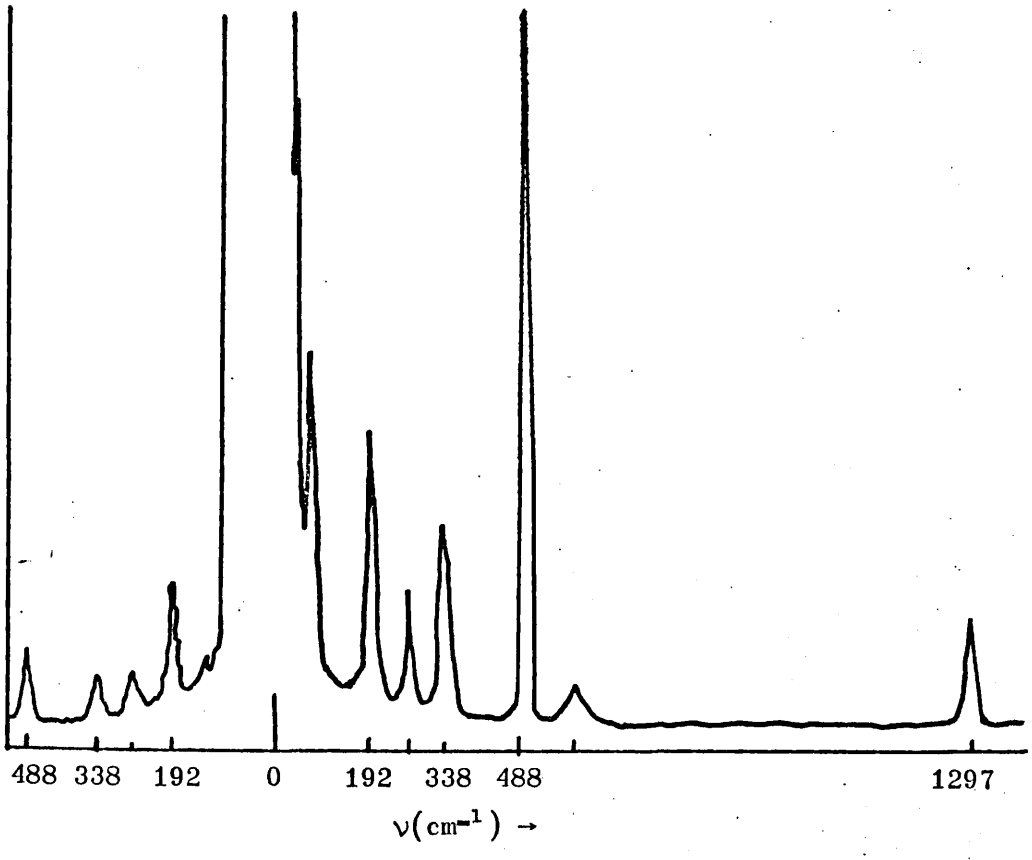

Fig.4.5

Raman spectrum of pure $POCl_3$

TABLE 4.2

	$CaWO : Nd^{+3}$	Nd-glass LG 55	$Nd^{+3} : POCl_3 : ZrCl_4$
$\tau(s)$	0.15×10^{-3}	0.7×10^{-3}	0.33×10^{-3}
$\Delta\nu(s^{-1})$	10^{12}	$\sim 10^{13}$	$\sim 3 \times 10^{12}$
$2\pi\tau\Delta\nu$	10^{9}	$\sim 5 \times 10^{10}$	$\sim 6 \times 10^{9}$

Neodymium in crystal materials such as $CaWO_4$ has a very narrow fluorescent band. This is due to the uniformity of the crystal field surrounding the ions. In liquids the absorption and emission bands are much wider than in crystals, whilst glasses exhibit very broad fluorescent spectra (Fig.4.4). The broad bands are due to the differences in the glass sites and the liquid clusters in which the ions exist. The type of glass used (silica, phosphate, fluoride) determines the width of the fluorescent lines. Silica glass lasers (Schott 55,56) have the ~~most wide~~ widest spectrum and this is why they have high thresholds. Phosphates exhibit sharper lines than silica, whilst fluoride glasses exhibit the best properties for glass lasers. However the preparation of fluoride glasses is very difficult and requires special procedure, and has not yet been commercially manufactured[108]. In general, crystals have the lowest thresholds, glasses the highest thresholds, with those of liquids (see experimental results of Chapter VI) lying in between. This was to be expected according to the values of Table 4.2. From Fig.4.4 we can see that the maxima of the fluorescent lines vary for different host materials. For the $Nd^{+3} : POCl_3 : ZrCl_4$ liquid laser solution the fluorescence of neodymium is found in (Figs.4.1 and 4.4) :

				Energy of terminal level above ground level
(i)	The resonance transition	$^4F_{3/2}$-$^4I_{9/2}$	at ~ 8800 Å	~ 400 cm^{-1}
(ii)	The laser transition	$^4F_{3/2}$-$^4I_{11/2}$	at 10520 Å	~ 2000 cm^{-1}
(iii)	The transition[109]	$^4F_{3/2}$-$^4I_{13/2}$	at 13300 Å	~ 3800 cm^{-1}

Fig.4.3 shows the pumping regions of neodymium. The principal pumping region lies in the 5000 - 6000 Å band.

The gain of a laser system is proportional to the atomic cross-section (section 1.2). Comparing the atomic cross-sections for the dominant fluorescent line of neodymium (in the region of 1.06 μ) for the different host materials from Table 4.3, we see that the cross-sections for liquids are intermediate between those of YAG and glasses. The main factor determining the type of neodymium laser to be used for a specific application depends on the atomic cross-sections of the fluorescent lines. For CW operation the gain must be high because continuously operating excitation lamps have limited brilliance and therefore YAG lasers are superior in this respect. For high energy output crystals fail because of their limited energy storage ability. Glass-lasers can be made to emit kiloJoule pulses and are therefore useful for high output requirements. In systems requiring repetitive operation with average output powers we see that crystal lasers fail because of their limited storage ability and glass lasers because of their high threshold and heat dissipation problems. The intermediate cross-sections of the liquid lasers and the advantage that they have in circulating the active medium provide the natural domain in which liquid lasers could be applicable[107,110].

TABLE 4.3

Medium	Atomic cross-section cm^2	Fluorescence lifetime s	
YAG	$(27\text{-}90)\times10^{-20}$	0.24×10^{-3}	For the
Liquid[9,111,112]	$(6-8)\times10^{-20}$	$(0.25-0.4)\times10^{-3}$	$^4F_{3/2} - {}^4I_{11/2}$
Glass	$(0.3\text{-}3)\times10^{-20}$	$(0.1-1.0)\times10^{-3}$	transition

4.5 NON-LINEAR EFFECTS IN LIQUID LASERS

As pointed out in section 2.4, liquids exhibit a large number of interactions with intense light pulses. In liquid lasers non-linear effects can occur due to the interaction of the active medium with the pulse undergoing amplification. These processes may limit the power capabilities of light amplifiers based on liquid media.

Fig.4.5 shows the spontaneous Raman spectra of pure $POCl_3$ [78]. The most intense line occurs at 488 cm^{-1} away from the centre frequency of the incident radiation. Observation of stimulated Raman spectra from a liquid laser operating under mode-locked conditions was reported by several workers[113,114].

An investigation recently carried out by Alfano et al[78] on the non-linear effects in liquid laser solutions ($SeOCl_2$ and $POCl_3$) has given a fair indication of the extent to which these would affect the laser performance. The experiments were performed by focusing powerful light pulses from a single mode ruby laser into a cell (50 cm long) containing pure $POCl_3$. Stimulated Brillouin scattering was shown to have a threshold of about 35 MW/cm^2, whilst stimulated Raman scattering was shown to have a threshold of 110 MW/cm^2. It was also shown that self-focusing does not play a dominant role at this power level. Large amounts of Raman conversion occurred only at high powers and long cell lengths, typically 140 MW/cm^2 and 50 cm respectively. It is important to point out here that no connection has been found between stimulated Brillouin scattering and the phenomenon of self-Q-switching. This subject will be dealt with in detail later.

4.6 ENGINEERING PROBLEMS IN CONSTRUCTING LIQUID LASERS

The present work is mainly concerned with the evaluation of the potentialities of the best known performing liquid laser system $Nd^{+3}:POCl_3:ZrCl_4$;

subsequent discussion will therefore be restricted to this system. This system is relatively safer and far less corrosive than systems based on $SeOCl_2$ and it is also less sensitive to atmospheric moisture. The less corrosive nature of the $POCl_3$ provides a larger choice of materials available for the construction of circulating systems. The refractive index of $POCl_3$ is 1.47 which is very close to that of silica glass 1.455. This makes the laser operation easier as there will be no reflections from the liquid-glass interface. The problems arising in the construction of static systems will be discussed later, but it would be appropriate here to outline the main engineering problems in constructing circulating systems.

The development of the latter involves the selection of materials compatible with the corrosive solvent $POCl_3 : ZrCl_4$, finding a leakproof mechanical pump for circulating this liquid and constructing a dry sealed flow system of pipes and mechanical joints incorporating a suitable laser cell. The materials which are known to be inert to the $POCl_3 : ZrCl_4$ solvent are glass, alumina ceramic, PTFE, nickel and some stainless steels[107]. A circulating system consists mainly of the laser head, the pipe line, the pump, the heat exchangers, and the drying chambers[115]. The laser head and the drying chamber are usually made of glass, the pipe line of PTFE and the heat exchanger of nickel because of its good thermal conductivity[110]. Most of the engineering problems arise in the construction of the circulating pump. Two pumps have so far been constructed and used in circulating laser systems. The centrifugal-type pump[107], and the bellows-type pump[110]. They have both been operated successfully.

The ability of liquid lasers to be circulated and cooled by flowing the laser medium through a heat exchanger, is an intrinsic advantage over solid lasers for repetitive pulsing, because heat can only be removed from the latter by conduction to the surface and transfer to a coolant flow.

This may result in radial temperature gradients and thermal stresses which affect the quality of the laser beam[32]. Radial temperature gradients can be avoided in circulating liquid laser systems by ensuring turbulent flow[117] and controlling the wall temperature. The distribution of optical pumping which is the only remaining factor affecting the quality of the beam can be controlled independently. The pulse repetition rate is only limited by the flow rate.

A detailed description of circulating systems is outside the scope of this work; a complete account on their construction and performance can be found in a report at the back of this thesis[110].

CHAPTER V

THE DESIGN AND TECHNOLOGY OF APPARATUS USED IN THE EXPERIMENTS

5.1 GENERAL DESCRIPTION OF ELECTRICAL APPARATUS

Two capacitor banks were used. (a) A condenser discharge unit consisting of two 200 μF condensers which could be discharged through two xenon flashtubes via 50 μH inductances. (b) A condenser unit consisting of two 400 μF condensers which could be discharged through two xenon flashtubes via 100 μH inductances. The flashtubes were triggered with a 20 kV pulse from a trigger box unit type 1736 B. The time between triggering the two discharges could be arranged using a delay unit type 1755 A. Power supplies of the type 1617 A were used to provide the EHT for the photodiodes. A variac was used in conjunction with an EHT power unit type 8003 A to provide a variable voltage. This arrangement was used to provide the EHT for the Pockels cell and the image converter (see below).

Detection of time dependent signals was made with two Tektronix oscilloscopes types T 555 and T 519. Two S1 photodiodes were used to collect the signals (see below). Energy measurements were made with a TRG 107 cone calorimeter connected to a microvoltmeter (Keithley instruments model 150 B).

Detailed accounts on the functioning of the apparatus listed above are given in the relevant experimental sections.

5.2 LIQUID LASER CELLS AND MODE-LOCKING DYE CELLS

Fig.5.1 shows the liquid laser cell used in the experiments. It was 155 mm long and 0.75 mm in diameter (internal). The outer diameter was 12.5 mm. The windows were attached to the cell by a quartz sealing technique since no glue resistant to $POCl_3$ was available (very recently a glue called 'Gupalon 20 transparent' was found to be resistant to $POCl_3$). The

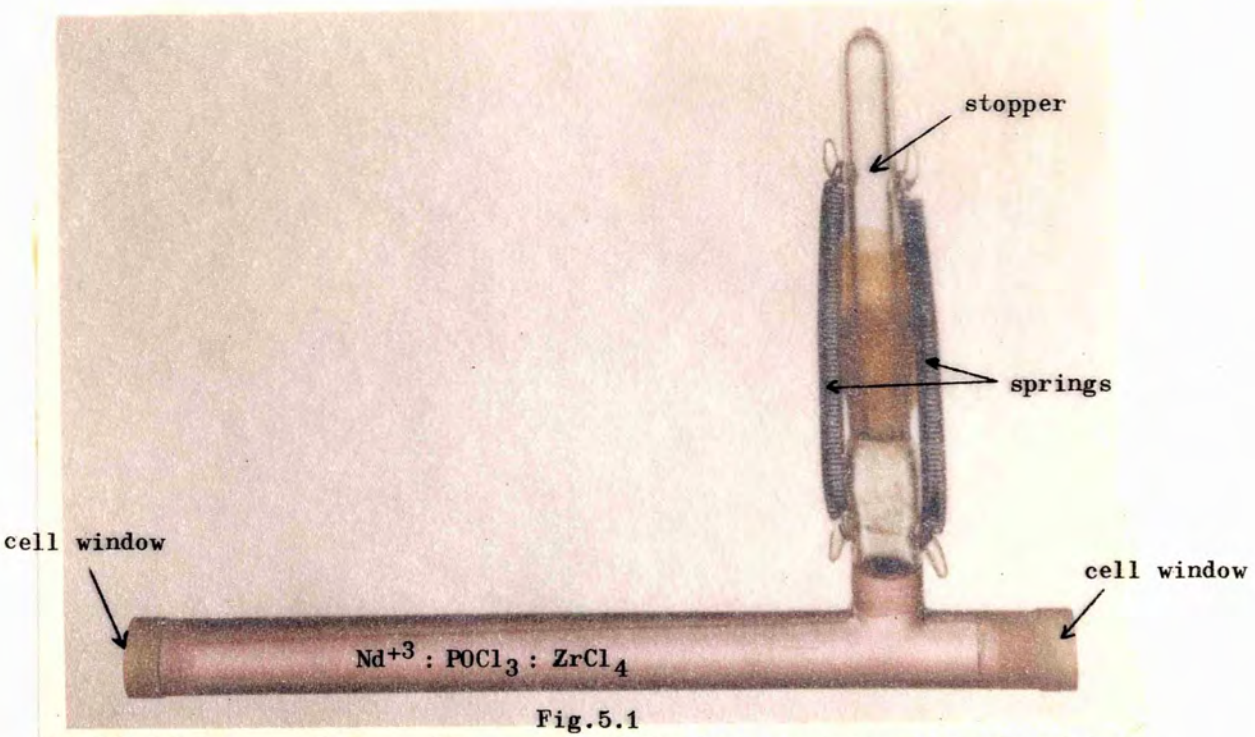

Fig.5.1

The liquid laser column. The colour of the laser solution reproduced here is a fair representation (lilac). The tube above is 0.8 of the actual size

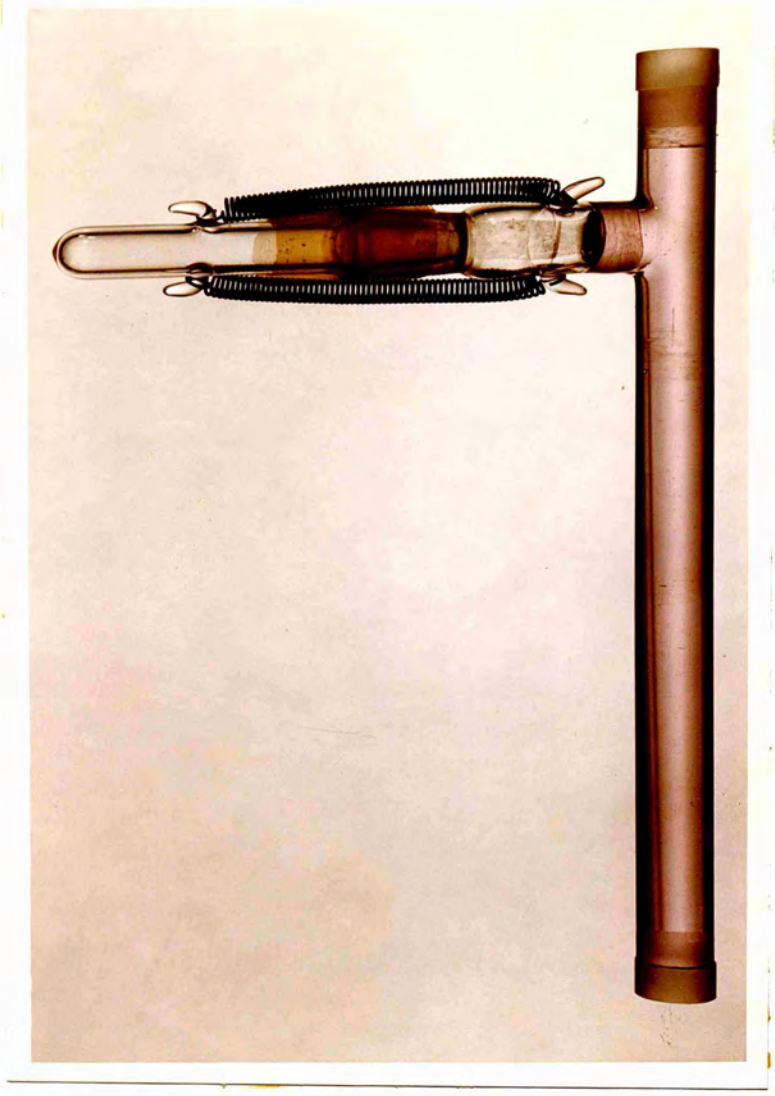

technique consists of careful contacting of two optically flat surfaces and subsequent fusion of the contacted areas. The cell and windows were made of silica and the stopper was firmly held in contact with the walls of the stem using two springs on either side. The tube was well sealed so that no atmospheric moisture could come into contact with the liquid. In Fig.5.1 the colour reproduction of the liquid laser solution is a fair indication. The solution is $Nd^{+3} : POCl_3 : ZrCl_4$, of concentration 1.8×10^{20} cm^{-3} and fluorescence lifetime 330 μs.

Although in the main experiments a commercially manufactured mode-locking dye cell was used (see later chapters), one millimeter path length cells were also constructed using the quartz sealing technique. Two optically flat discs were attached to a thin polished glass ring spacer by careful contacting and fusion of the surfaces. It was found that after about fifty firings of the laser fringes could be observed between the contacted surfaces. These were attributed to shock waves which could occur in the mode-locking dye during operation thus forcing the surfaces apart.

It should be pointed out here that in the construction of cells for use in laser systems, no direct flame heating of the glass should be attempted. Direct heating results in the distortion of its optical qualities.

5.3 THE DOUBLE-FLASHLAMP ARRANGEMENT

The liquid laser head consisted of the cell containing the active medium (Fig.5.1) with two xenon flashlamps placed on either side, the whole arrangement being wrapped with a polished silver reflector. Pyrex tubes were normally used round the flashlamps to filter the UV radiation. It was found in setting up the laser head that a silver reflector was much more efficient for pumping than an aluminium reflector. The laser head was placed in a perspex box for safety against accidental breakage of the laser

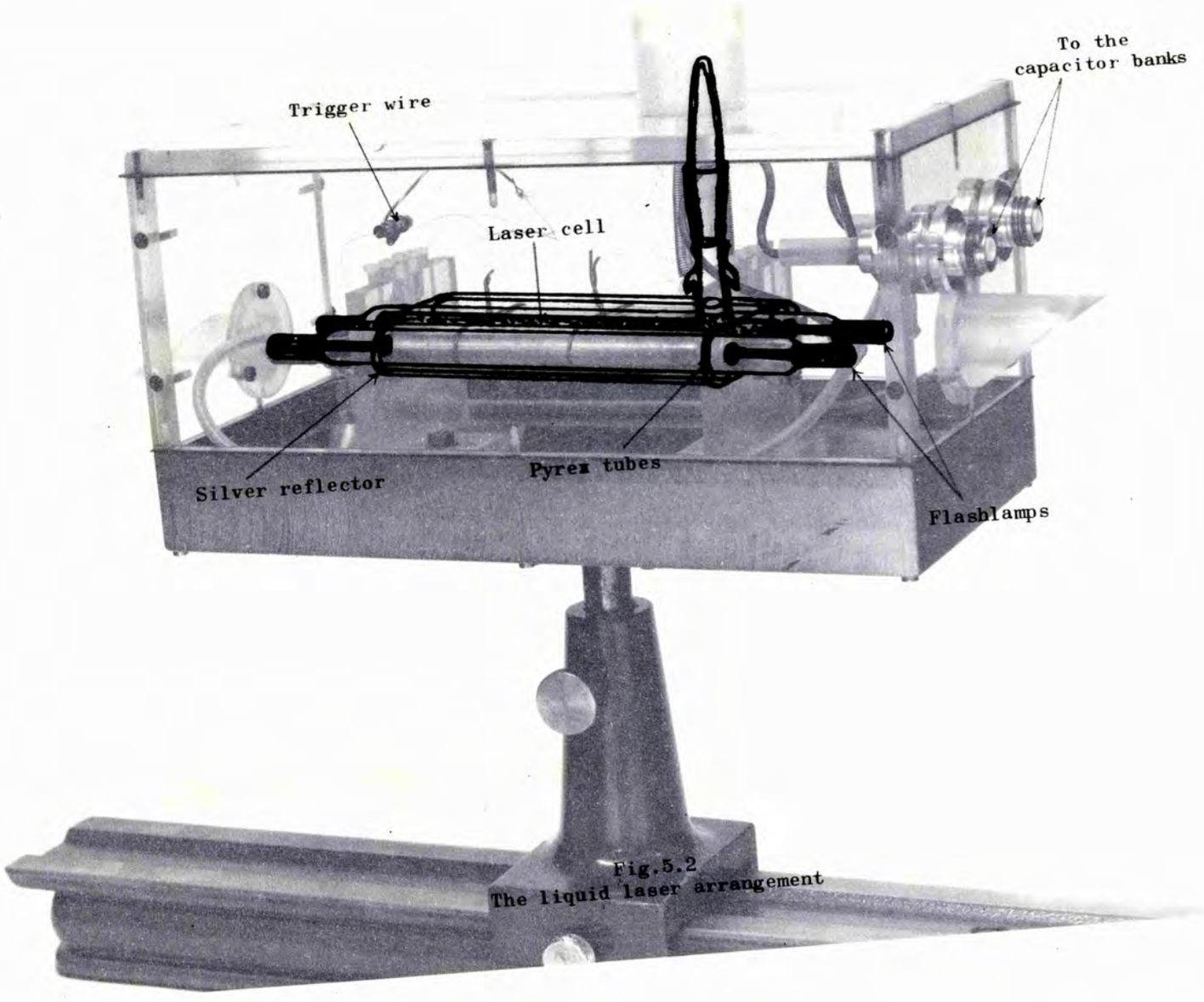

Fig.5.2
The liquid laser arrangement

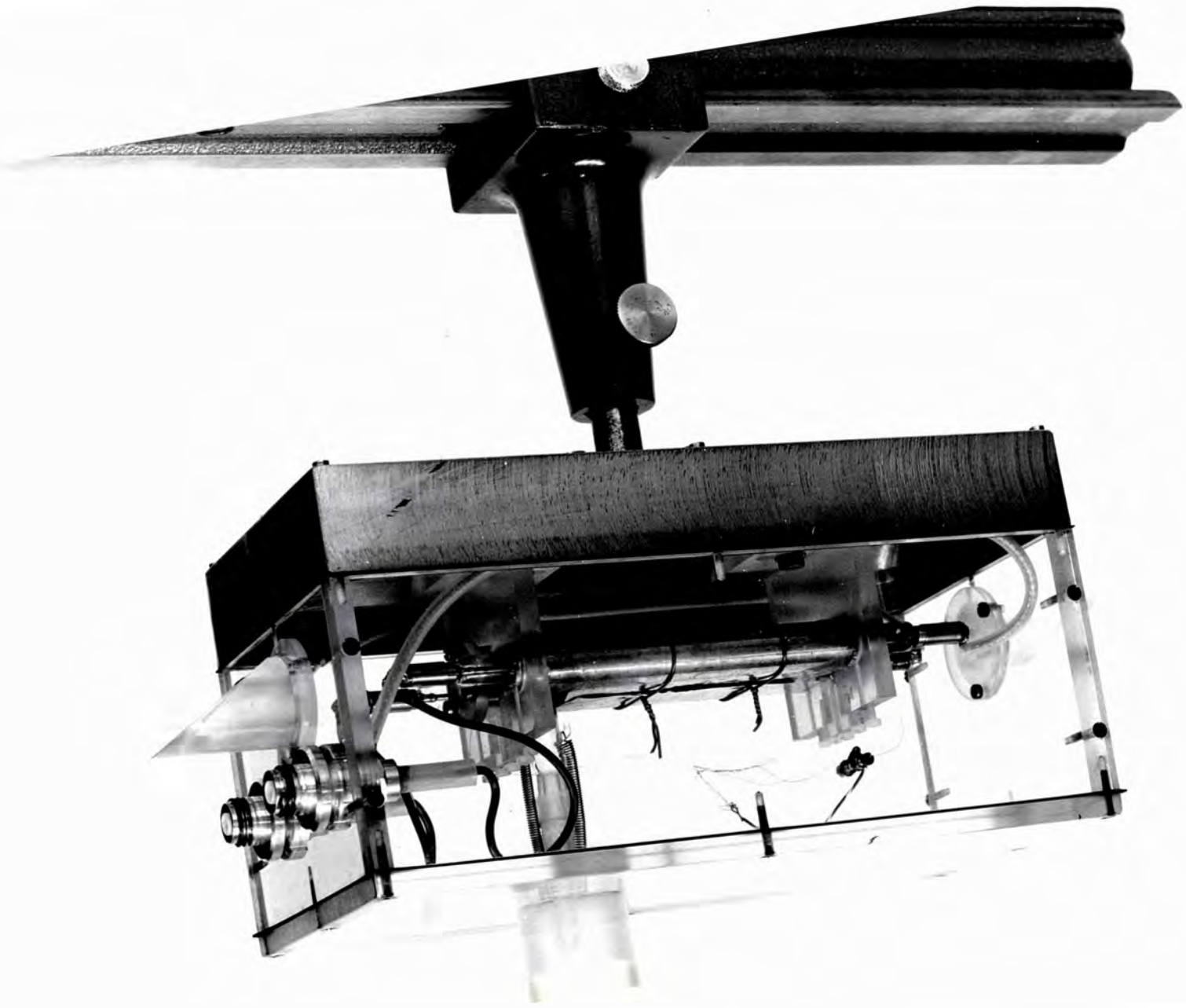

cell. Fig.5.2 shows the whole arrangement.

A similar arrangement was used for the glass laser and is shown in Fig.5.3. The laser rod was clad with a water jacket in order to provide a more uniform illumination (section 2.1). A Brewster-ended rod was used since the glass laser was mainly used for mode-locking. The rod was an LGN 55 Nd-glass with nominal 5% doping, and was 150 mm long and 9.5 mm in diameter. No pyrex tubes were used round the flashlamps since the water jacket consisted of pyrex. The silver reflector needed cleaning approximately every 100 firings because it used to tarnish at the points of contact with the flashlamps.

The double flashlamp arrangements described above were used in order to provide uniform illumination of the laser material. The optimal number of lamps is given by $N \approx D/d$ where D and d are the apparent diameters of the specimen and the luminous element in the lamp respectively. In both the above cases $2 > N > 1$, therefore two flashlamps were used[118]. Finally, filtering of the UV radiation is a necessary precaution for minimizing the optical distortion of the laser medium due to heating by the pumping radiation (chapter IX). From Fig.4.3 it can be seen that the neodymium ion has no absorption bands for $\lambda < 4000$ Å and therefore the efficiency of the laser is not lowered if such radiation is filtered out.

Now let us consider the discharge of the two capacitor banks described in section 5.1 through two linear xenon flashlamps. Fig.5.4 shows the light output from the flashlamps for different arrangements: Comparing (a) and (b) we see the effect of the inductance and capacitance on the pulse shape and pulse duration. Comparing (a) and (c) we see that the length of the xenon discharge is important in the pulse shaping of the light output. This is due to the change in the resistance across the two electrodes. The pictures (a), (b), (c) and (d) show that a matching of the resonance condition for the inductance, capacitance and resistance is vital in the

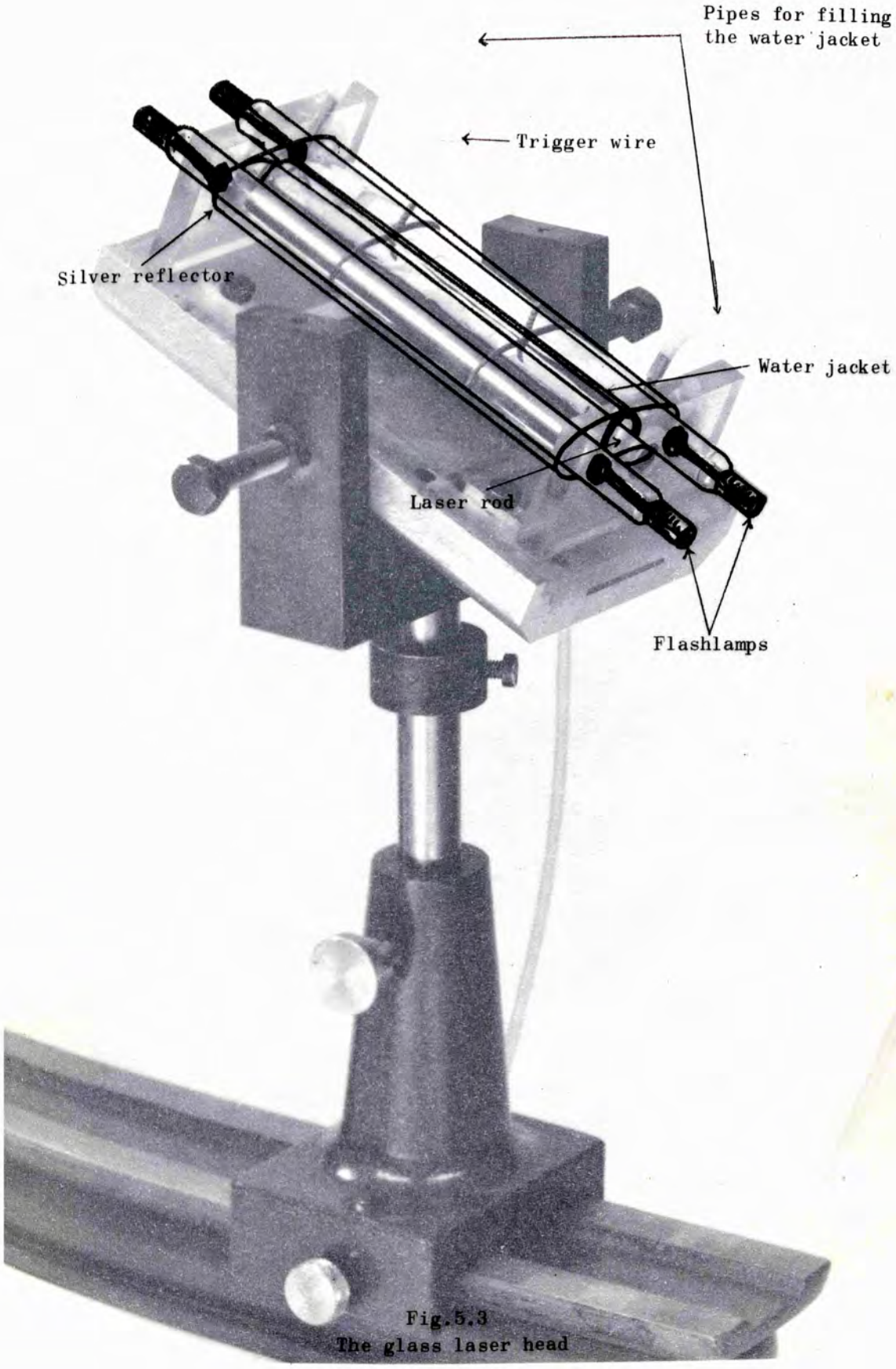

Fig.5.3
The glass laser head

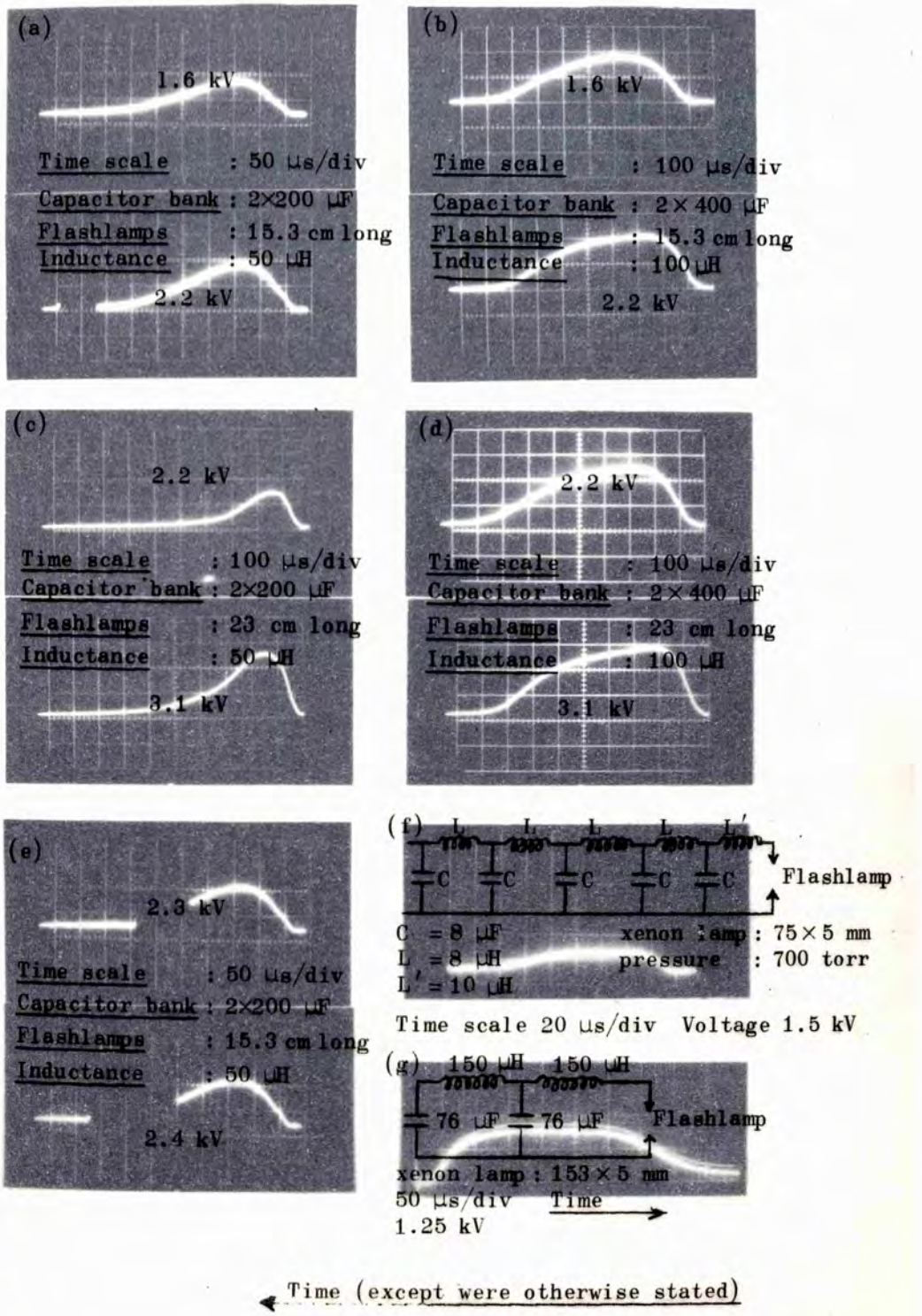

Fig.5.4
The light output pulse from xenon flashlamps for different arrangements

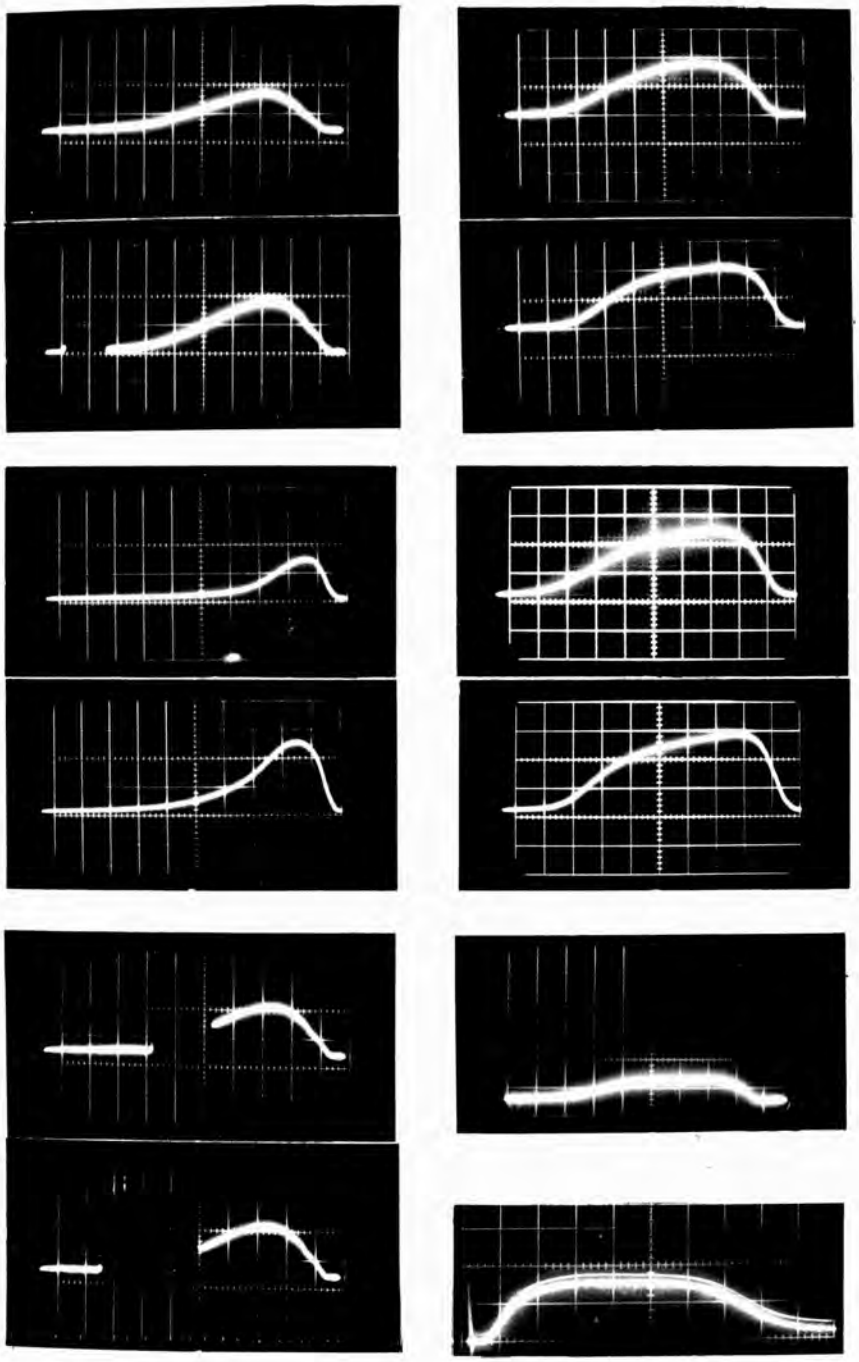

production of the best light output pulse possible. Pictures (f) and (g) show circuits used in the production of short square-shaped light pulses[110].

The production of light from electrical energy is a complicated process and many effects which may disrupt the uniform production of light flux can occur. One of these effects is shown in picture (e) where there is a clear disruption of the light flux when high voltages are applied across the flashtube. This may be due to high electric currents across the electrodes and the production of strong shock waves inside the flashtubes which affect the conversion of electrical energy into light. It may also be due to electrical surges in the circuit affecting the photodiode response. The shock waves inside flashtubes have been shown to have an amplitude directly proportional to the electrical input energy[119]. The conversion efficiency is limited to a maximum depending on the electrical input energy. Beyond this maximum the light output diverges substantially from being directly proportional to the electrical input energy. Another factor which may affect the linearity of conversion of electrical energy into light is the flashlamp 'self-loading' due to the reflective enclosure. This effect leads to saturation of the light intensity with input energy[34].

5.4 THE PHOTODIODE

Since many of the experiments required the recording of two or three interpenetrating mode-locked trains a fast detector was needed. For this purpose an ITT F 4000 (S1) photodiode was mounted in a holder which was specially constructed to give short response time according to the design of Edwards[120]. The whole arrangement is shown in Fig.5.5. It should be noted that there is a small change from the original design in that a cylindrical capacitor is constructed between the holder and the photodiode instead of a disc capacitor. This arrangement has less capacitance, the dielectric medium being melanex wound round the internal wall of the holder.

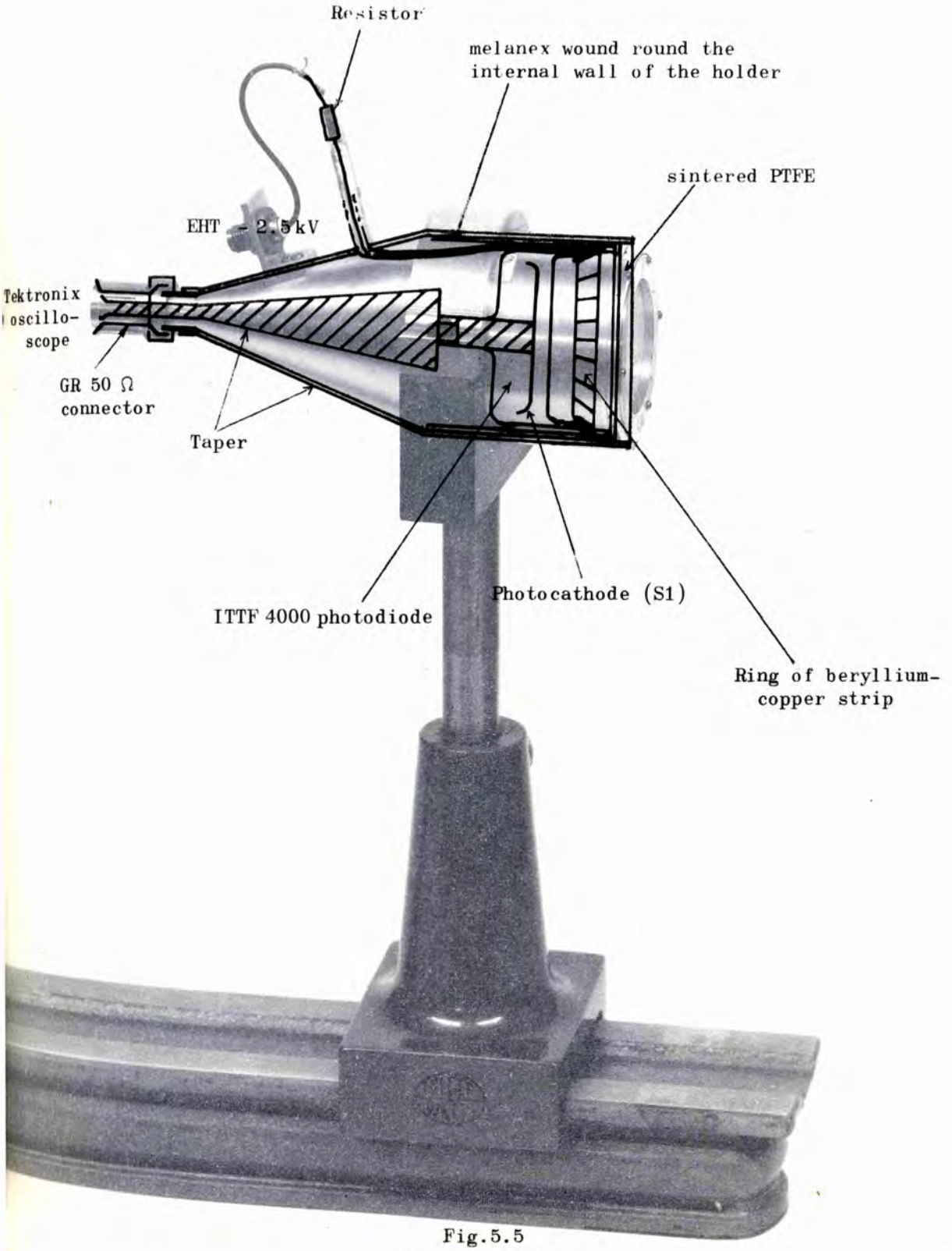

Fig.5.5
The photodiode

The photodiode was connected to a Tektronix 519 oscilloscope and the rise time of the oscilloscope-photodiode arrangement was measured to be 0.4 ns (see Chapter VIII). The geometry is arranged to give a constant sensitivity for all the possible rays between entrance and exit ports. The taper had an impedance of 50 Ω, the outer angle being 19.2° and the inner angle 8.4°. Diffusers consisting of 3 mm thick discs of sintered PTFE, were mounted in front of the attenuating filters on the photodiode to avoid damage to the photocathode, and to avoid any transmission non-linearity caused by fine structure in the laser beam profile. Sintered PTFE is ideal for this purpose because it is granular and is highly transmissive in the near-infrared, out to wavelengths of 3.7 μm. The transmission of the neutral density filters used in attenuating the input signals was measured to have the following values at 1.06 μ: ND1 = 0.29, ND2 = 0.09, ND 0.4 = 0.62, ND 0.33 = 0.66.

5.5 THE CAMERA-IMAGE CONVERTER ARRANGEMENT

The only means at present available of recording light at 1.06 μ directly is a Kodak Z-plate. Unfortunately this requires elaborate preparation before use. In order to overcome this difficulty, an image converter was used in conjunction with a camera operating with ordinary film (see section 10.2 for experimental results taken with this arrangement).

Fig.5.6 shows the complete camera-image converter arrangement. The image converter was a Mullard 6929-1 type which had an S1 photocathode. The response of the photocathode is shown in Fig.5.7. (This is the same as the response of the cathode of the photodiode described in section 5.4.) The anode of the tube required an operating voltage of 16 kV which was supplied from an EHT power unit type 8003 A (section 5.1). The screen phosphor was a P 20 type and the minimum useful cathode diameter was 25.4 mm. The cathode had a curvature of approximately 60 mm. An oscilloscope camera was attached to the system and was focused onto the fluorescent screen.

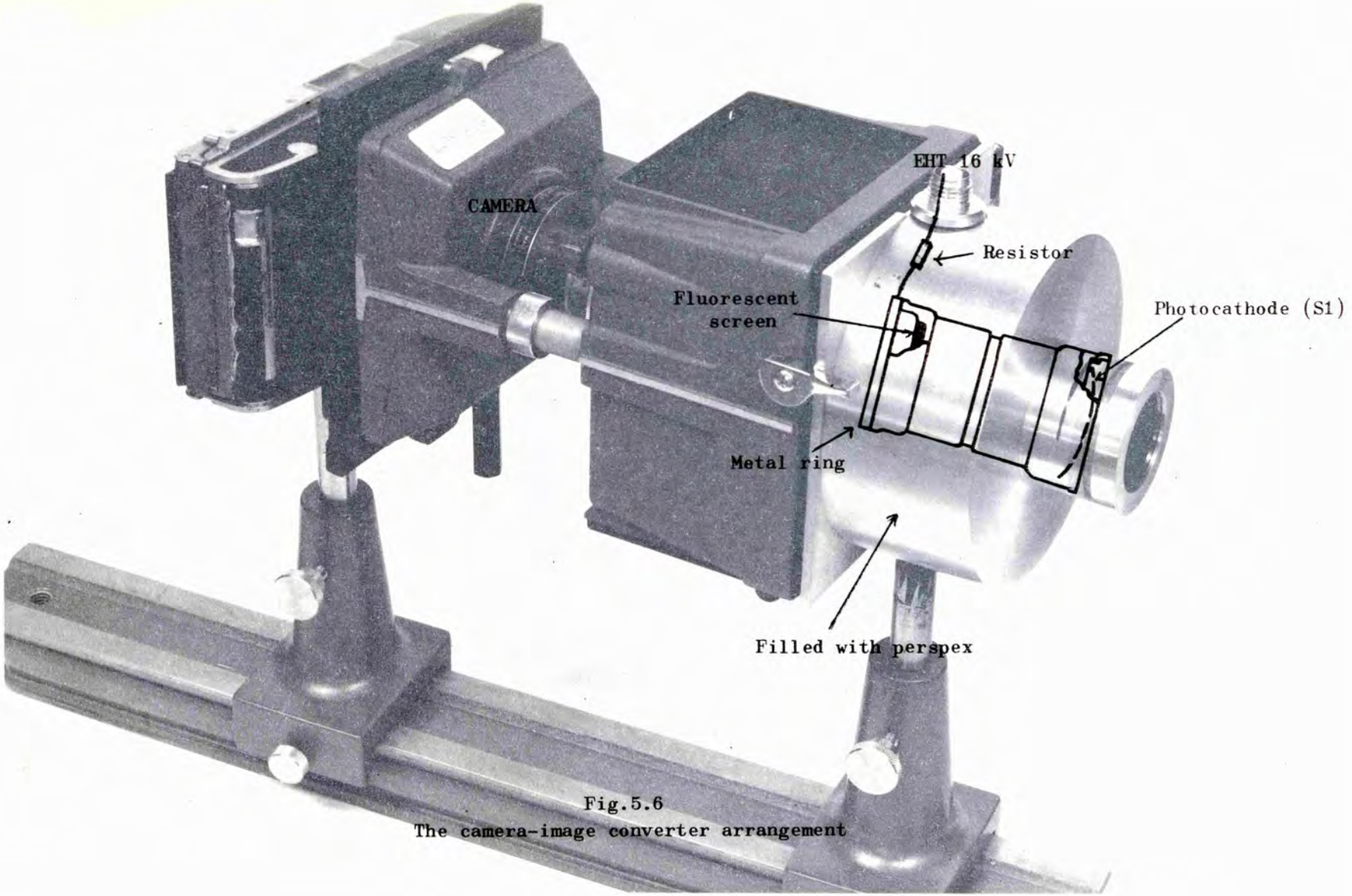

Fig.5.6
The camera-image converter arrangement

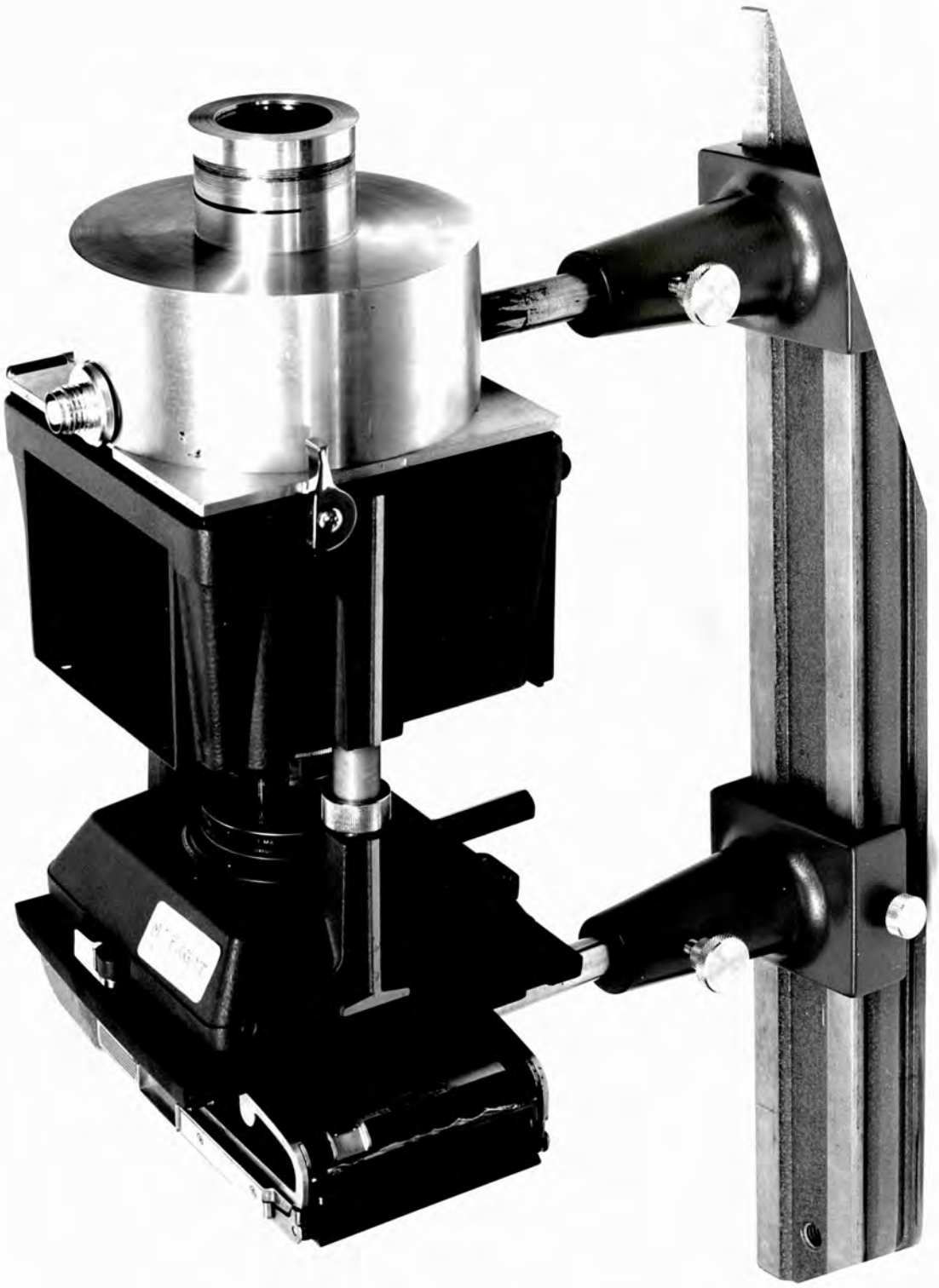

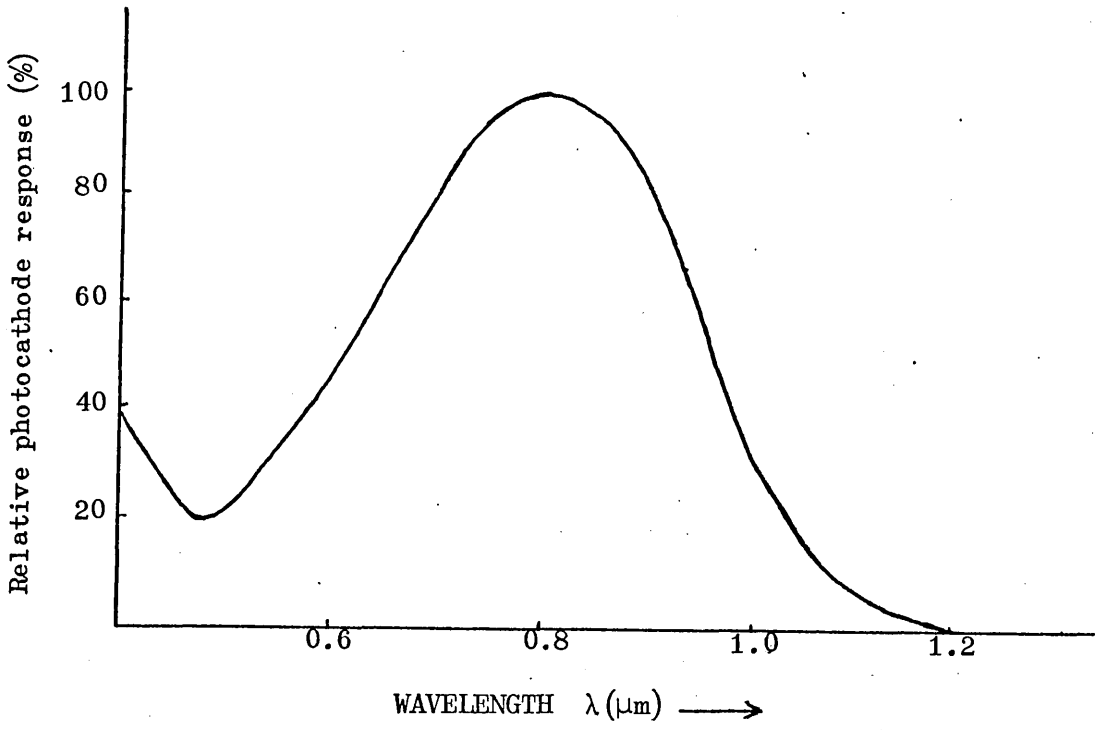

Fig.5.7
The image converter photocathode (S1) relative spectral emissivity curve

Fig.5.8 shows pictures of the laser beam profile taken with the image converter. These are compared with the polaroid beam burn patterns below each picture. It can be seen that polaroid beam burn patterns give a very good indication of the shape of the laser beam but the fine structure of the beam profile is only revealed by the image converter photographs. The pictures in Fig.5.8(a) show uniform beam cross-sections from a neodymium glass laser, whilst those in Fig.5.8(b) show distinct filamentary action.

Recording of the spectra (Chapter X) was made with a Monospek 1000 Grating scanning spectrometer whose exit slit was removed and the photocathode of the image converter was placed in the plane of the slit. A mercury discharge lamp was used to check the accuracy of the recording system. Fig.5.9 shows the second order diffraction of the mercury green line for positions of the grating differing by 30 Å and 10 Å. It was found that the system was accurate to ± 0.5 Å. The curvature of the lines at

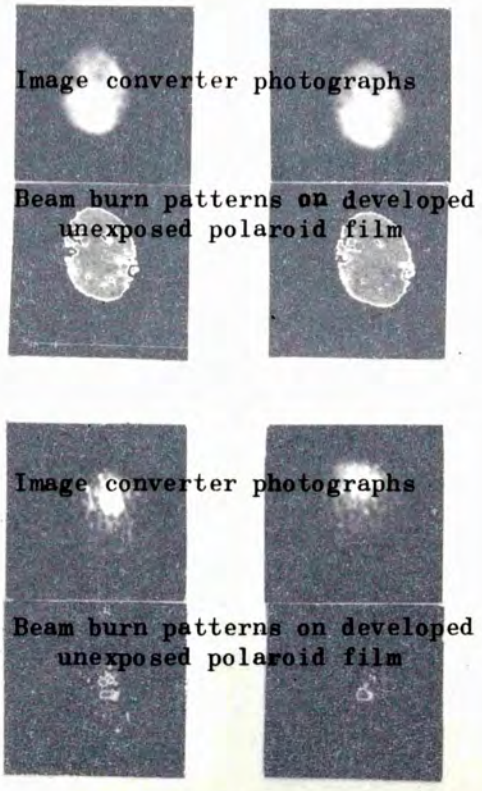

Fig.5.8
The laser beam profile photographed with the image converter and the corresponding beam burn patterns on developed unexposed (polaroid) film

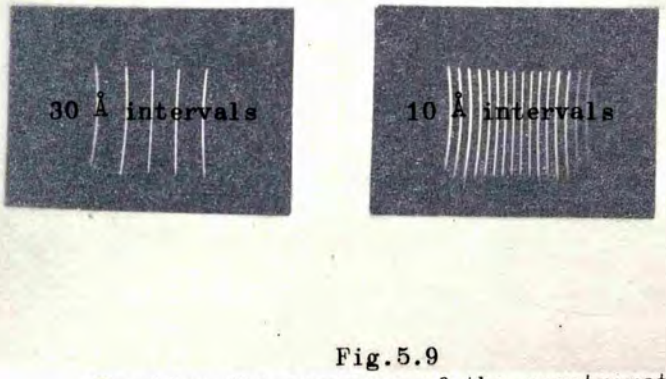

Fig.5.9
Checking the accuracy of the spectrometer-image converter arrangement

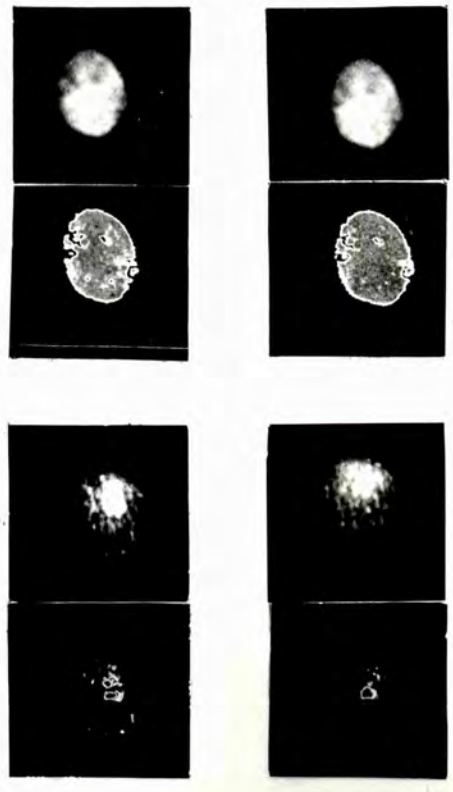

the extreme ends is due to the curved photocathode affecting the optics of the image converter.

5.6 THE POCKELS CELL ARRANGEMENT

Certain crystals exhibit double refraction, i.e. a light beam on entering the crystal splits into two beams which are plane polarized mutually perpendicularly. These crystals are called birefringent and the two beams travel through the crystal with different velocities, and thus they have different phases[121]. Some crystals become birefringent only when a voltage is applied across them, the degree of the birefringence depending on the magnitude of the voltage. The operation of a Pockels cell depends on the properties of such a crystal.

The Pockels cell arrangement used in the Q-switching experiments of this thesis is shown in the photograph of Fig.5.10. The Pockels cell itself consisted of a KD*P (Potassium dihydrogen phosphate) crystal, the voltage being applied through two ring electrodes 1.27 cm in diameter (type P.C.12 KD manufactured by Electro-Optic Developments Ltd.). The field is then parallel to the direction of propagation of the light. The Pockels cell voltage was supplied from a power unit type 8003 A (section 5.1). It could be switched off using a Mullard PL 81 valve operated by a transistor circuit. A prescribed delay time could be introduced between triggering and switching-off time using a delay box unit type 1755 A (section 5.1). The latter was measured to be approximately 40 ns (see Chapter VII).

Let us now consider the way in which a Pockels cell operates, with the aid of the diagram on the transparency of Fig.5.10. The diagrams at the foot of the page show the cross-section of the beam and the directions of polarization at the different stages of propagation. Consider the Pockels cell being placed between two crossed polarizers. A beam of unpolarized light (a) is linearly polarized by the first polarizer. The

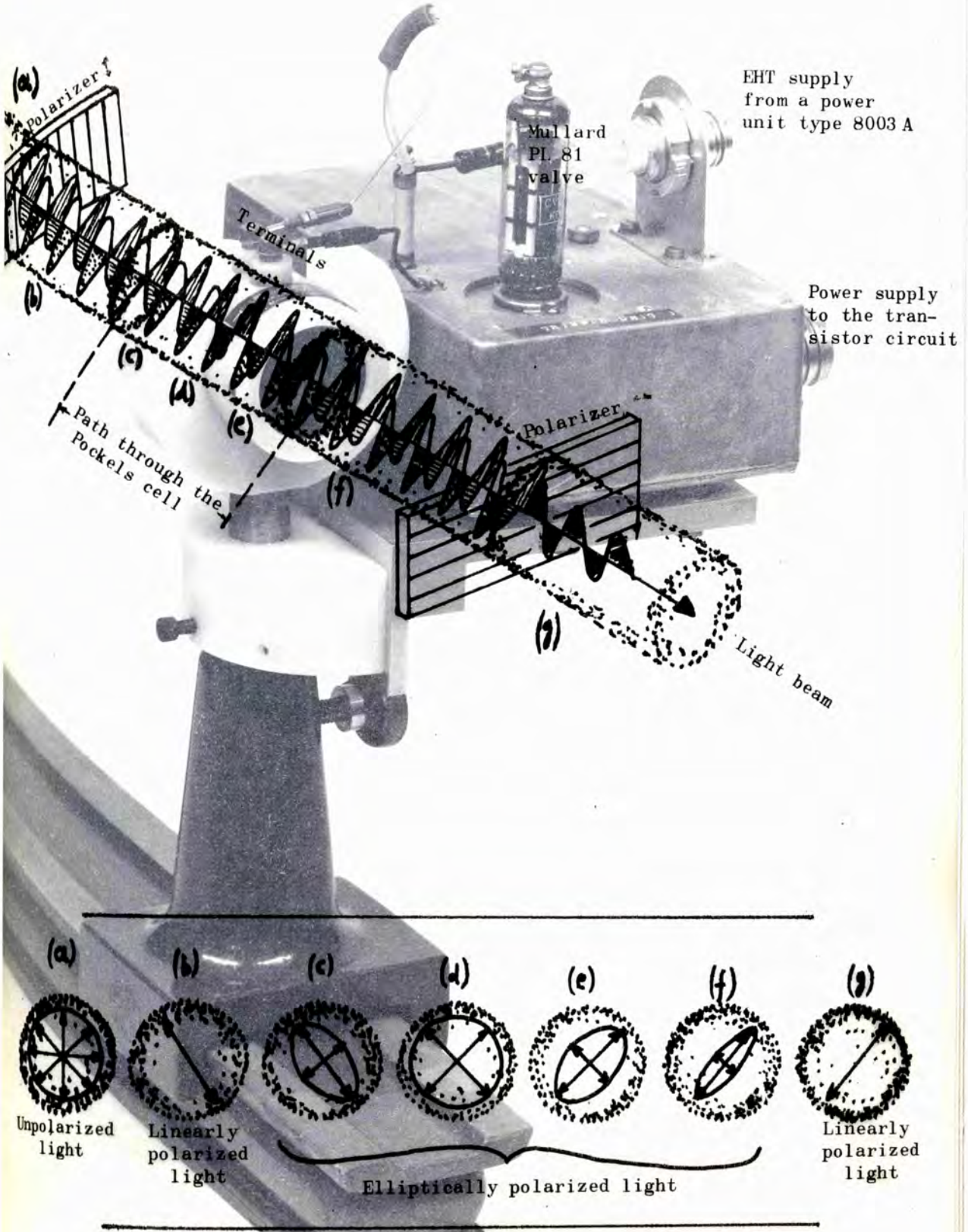

Fig.5.10
Pockels cell arrangement. The illustration on the transparency shows the rotation of polarization through 90° for a half-wave voltage

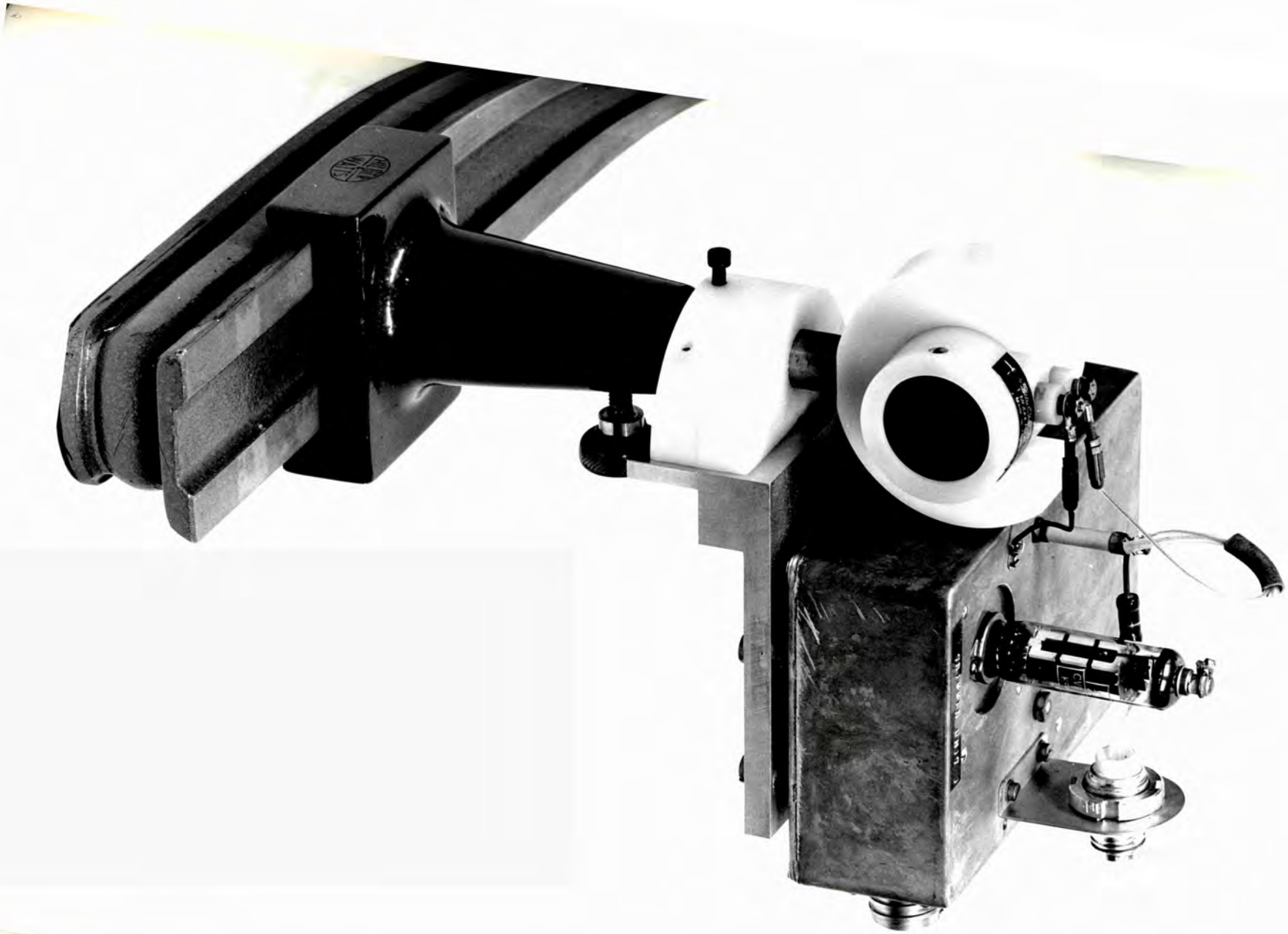

linearly polarized beam can be represented by vertical and horizontal components which are in phase (b). The beams travel through the Pockels cell with different velocities and hence gradually become out of phase. The stages c, d, e and f show the cross-section of the elliptically polarized light as it travels through the Pockels cell. The second polarizer allows only the component which is parallel to its transmission axis to be transmitted (g). The voltage needed in order that the direction of polarization of the beam changes by 90° from (b) to (g) is called the half-wave voltage of the cell. Now if a mirror were placed in the position of the second polarizer and only half of the above voltage were applied to the Pockels cell, stage (f) would have been reached after the beam had traversed the Pockels cell length twice. If the first polarizer were a Glan-Thomson prism one component of (f) would vanish being perpendicular to the polarizing

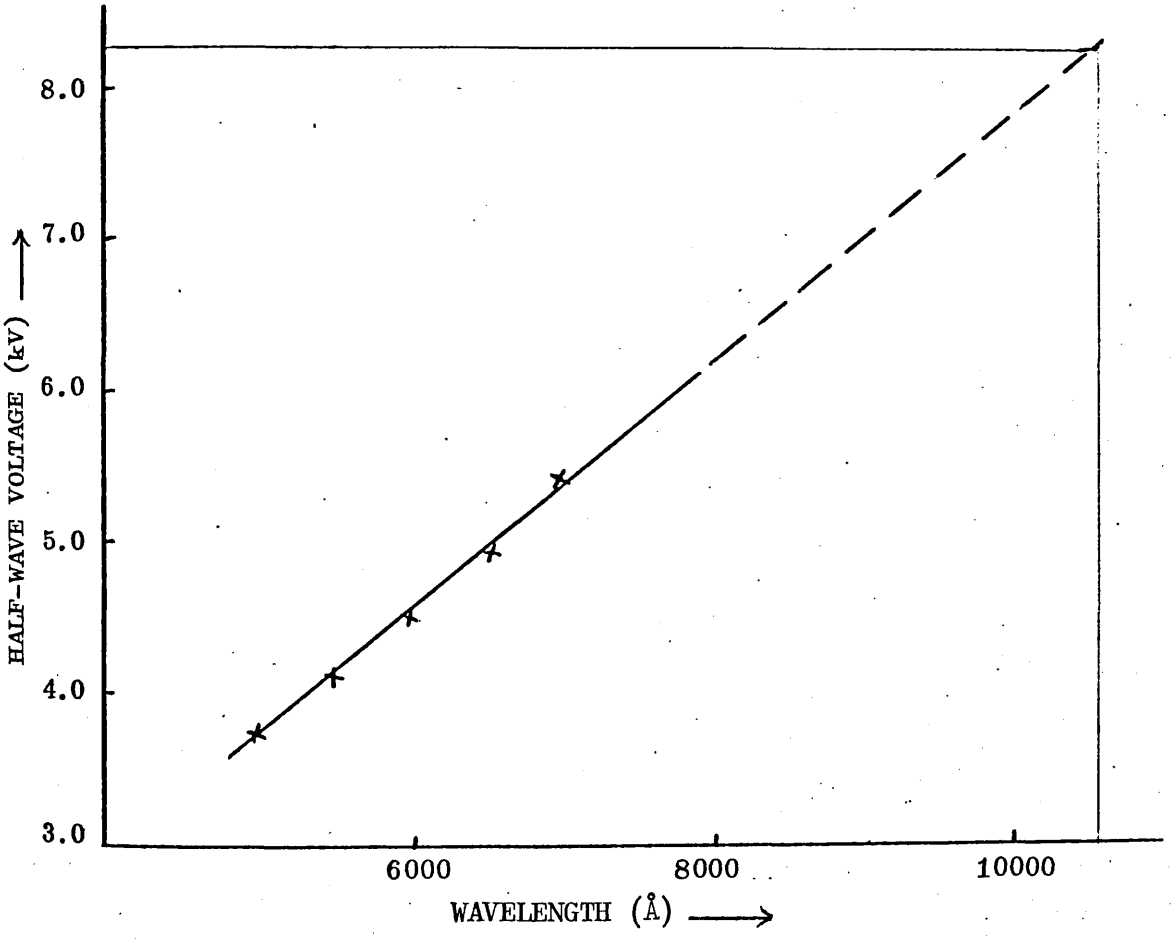

Fig.5.11
Calibration of the Pockels cell. The quarter-wave voltage needed at 1.06 μ is 4.1 kV

axis of the prism, and the other would be reflected in a perpendicular direction, off the interface inside the prism. Thus the Pockels cell in conjunction with the Glan-Thomson prism forms an optical shutter. This is called the quarter-wave mode operation and it has been employed in the experiments of Chapter VII.

A calibration of the Pockels cell voltage against wavelength was made using an incandescent filament and a Monospek 1000 grating scanning spectrometer. The graph of Fig.5.11 shows the half-wave voltage needed for a particular wavelength. Assuming linearity of voltage against wavelength the graph has been extrapolated out to wavelengths of 1.06 μ. It can be seen from the graph that the half-wave voltage needed at this wavelength is 8.2 kV and therefore for quarter-wave operation 4.1 kV should be applied to the cell.

CHAPTER VI

THE OUTPUT CHARACTERISTICS OF THE INORGANIC LIQUID LASER SYSTEM $Nd^{+3} : POCl_3 : ZrCl_4$

6.1 RELAXATION OSCILLATIONS IN NEODYMIUM LASER SYSTEMS

Fig.6.1 shows the relaxation oscillations of a glass laser. The laser head (Fig.5.3) was placed between two plane parallel reflectors with reflectivities of 100% and 66%. The light pumping pulse is shown in Fig.5.4b. Fig.6.1(a) shows the relaxation oscillations obtained from this arrangement for two different input energies, 1024 J and 1936 J. The beam patterns at the right of each picture show the beam shape at a distance of 260 cm from the output mirror. Irregular spiking was observed and the oscillation was sustained for approximately 400 μs. A meniscus lens 200 cm f.l. was then introduced into the cavity at a distance of 2 cm from the 100% mirror and the laser was fired under the previous conditions. The oscillation took the form shown in Fig.6.1(b). The beam burn patterns shown to the right of each picture acquired a more uniform shape. This behaviour is similar to that of damped oscillations described in section 2.1 and in reference 32. This behaviour is attributed to the fact that the introduction of the lens provides a more stable cavity for sustaining the electromagnetic radiation (section 1.5). It is important to point out that no such effect was observed when the same lens was placed in the cavity of a liquid laser. In this case the modes are already scrambled due to the thermal motions taking place in the liquid during operation, (Chapter IX), and the lens no longer serves as a refocusing element. In the case of a glass laser a stationary thermal lens exists which affects the cavity radiation, the effect of the lens being to refocus the radiation every time it traverses the cavity length.

Fig.6.2 shows the relaxation oscillations of three different neodymium laser systems. In (a) the relaxation oscillations of the

Fig.6.1
Relaxation oscillations in a glass laser
Time scale: 100 μs/div
Beam shapes: 260 cm from the output mirror

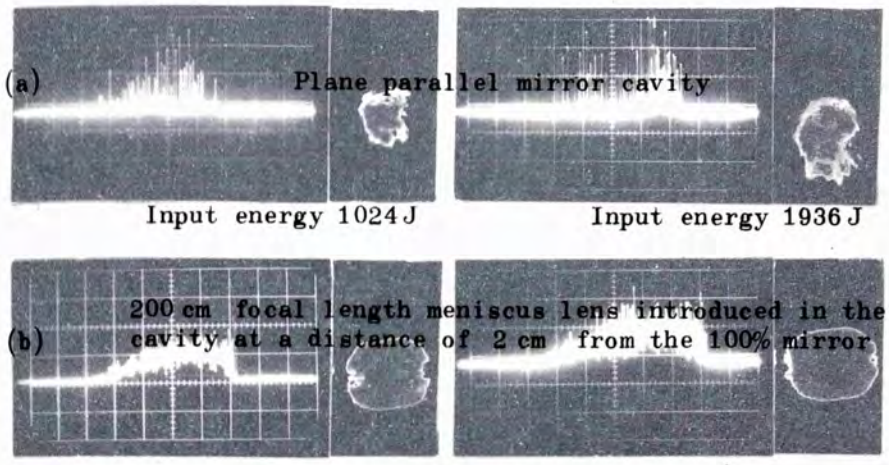

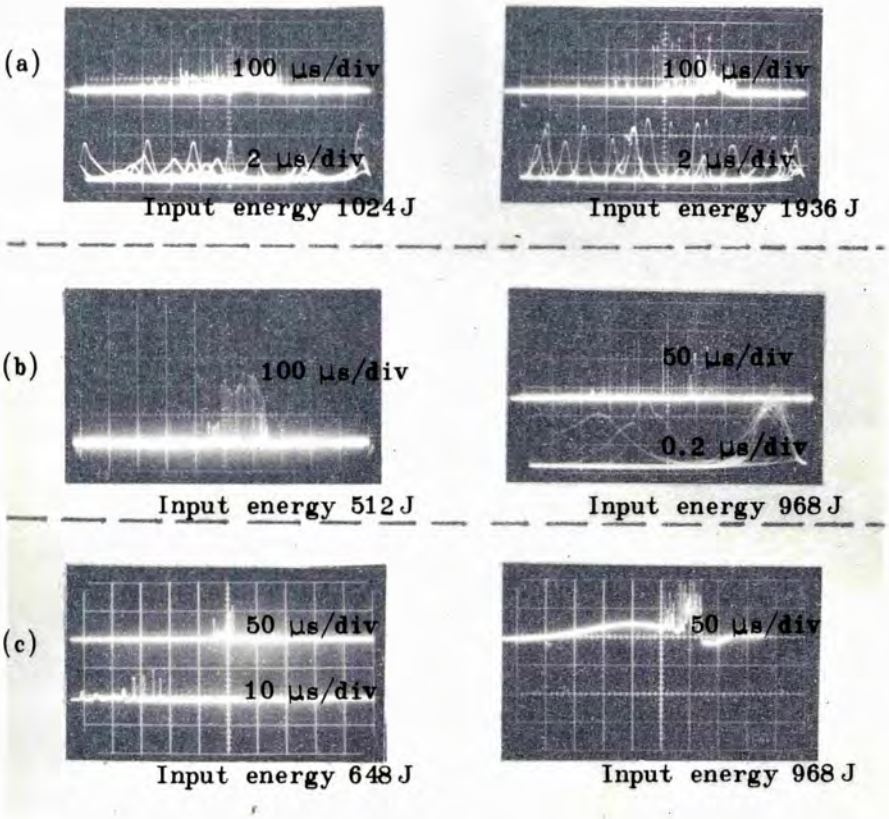

Fig.6.2
The relaxation oscillations in three different laser systems (a) neodymium glass laser
(b) neodymium liquid laser $Nd^{+3} : POCl_3 : ZrCl_4$
(c) neodymium liquid laser $Nd^{+3} : POCl_3 : SnCl_4$

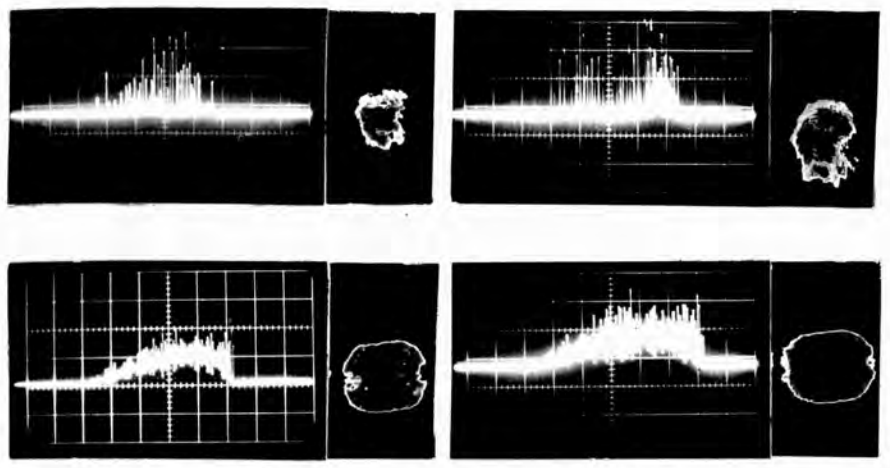

neodymium glass laser system described above, using a cavity with plane parallel reflectors are shown. The lower traces in each picture show parts of the upper traces on an expanded time scale. The spikes are approximately 600-700 ns long. In (b) the relaxation oscillations of the $Nd^{+3} : POCl_3 : ZrCl_4$ liquid laser system are shown. The laser head is shown in Fig.5.2, and the light pumping pulse in Fig.5.4(a). The spiking lasted for approximately 220 μs and had a more regular character than for glass. It is also important to notice that the relaxation oscillations of the liquid laser are approximately 250 ns long compared with 700 ns for the glass laser. In (c) the relaxation oscillations of a slightly different liquid laser system $Nd^{+3} : POCL_3 : SnCl_4$ are shown. When these pictures were taken the solution showed slight precipitation and its optical qualities were poor. This system provides more solubility problems than other liquid lasers[34].

6.2 ENERGY OUTPUT CHARACTERISTICS OF THE LIQUID LASER

The energy output characteristics of the $Nd^{+3} : POCl_3 : ZrCl_4$ will be considered here. Fig.6.3 shows the experimental arrangement used. The laser head (Fig.5.2) was placed between two plane parallel reflectors, one of which had a 100% fixed reflectivity. The energy was measured with a

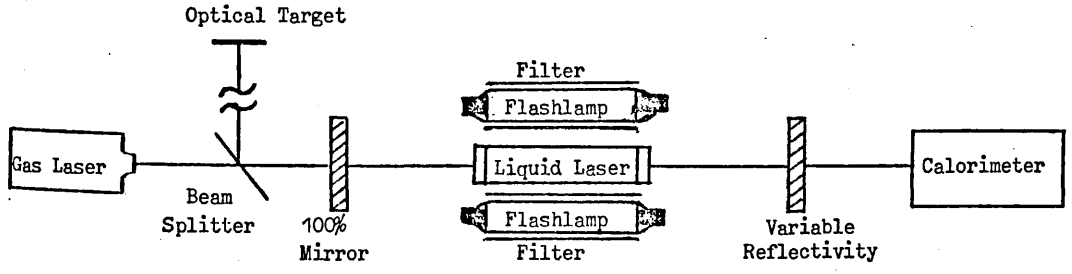

Fig.6.3
Experimental arrangement for the measurement of the output energy as a function of input energy for various output mirror reflectivities

calorimeter placed in front of the output mirror. The cavity length was 74 cm long. The arrangement was aligned with a He-Ne laser placed at the back of the 100% mirror. Fig.6.4 shows the results obtained for the output energy as a function of the input energy for various output mirror reflectivities. The initial parts of the curves are linear, but at high input energies there is a departure from linearity. It can be seen that the points at which the departure from linearity occurs are related to the output mirror reflectivity. They occur at higher input energies for lower mirror reflectivities. Samelson et al[34] have shown that the departure from linearity depends also on the cell diameter and that it occurs at a certain power flux level. This non-linear behaviour is characteristic of the liquid laser since no such effect is observed when glass is used as the active medium. No explanation has been given so far but its dependence on the mirror reflectivity and the power flux suggests that it may be related to the self-Q-switching effect described in the next section.

TABLE 6.1

E_T (J)	R	$-\ell n R$
80	0.83	0.186
100	0.66	0.416
120	0.55	0.598
180	0.28	1.27

Let us now consider the curves of Fig.6.4 in relation to equation (2.11). Table 6.1 shows the threshold values E_T for different mirror reflectivities taken from Fig.6.4. The threshold values E_T are plotted against $-\ell nR$ in Fig.6.5. From the interception of the energy axis and the gradient of the graph, the dynamic loss coefficient (section 4.3) is calculated from equation (2.11) to be 2.1% per cm. This value is in good agreement with that reported by Samelson et al[34] for the phosphorous oxychloride system. It is important to realize that the dynamic loss

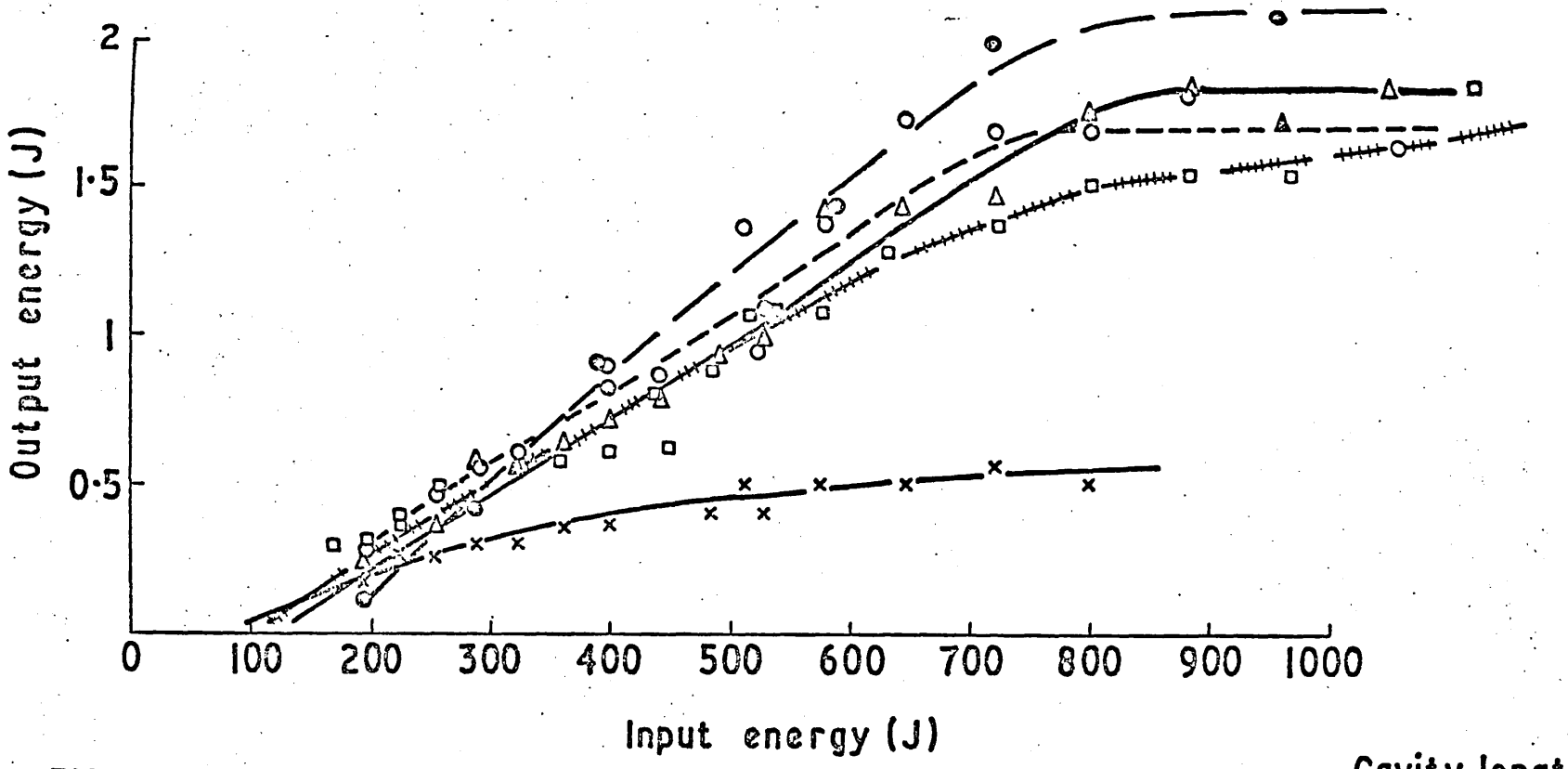

FIG. 6-4 OUTPUT ENERGY AS A FUNCTION OF INPUT ENERGY FOR VARIOUS OUTPUT MIRROR REFLECTIVITIES R

Cavity length 74 cm

×: 83% mirror reflectivity: pump light unfiltered ————

o: 55% mirror reflectivity: pump light unfiltered - - - - - - -

Δ: 55% mirror reflectivity: flashlamps filtered with pyrex tubes ————

o: 28% mirror reflectivity: flashlamps filtered with yellow corning — — —

□: 66% mirror reflectivity: flashlamps filtered with pyrex tubes +++++ +++++ +++++

coefficient is an average value accounting for all the losses occurring during the whole of the laser operation, i.e. approximately 200 μs. The losses change during the laser operation due mainly to thermal effects taking place in the active medium (Chapter IX). The dynamic loss coefficient is thus expected to be much higher than the ordinary transmission coefficient of phosphorous oxychloride (Chapter IX).

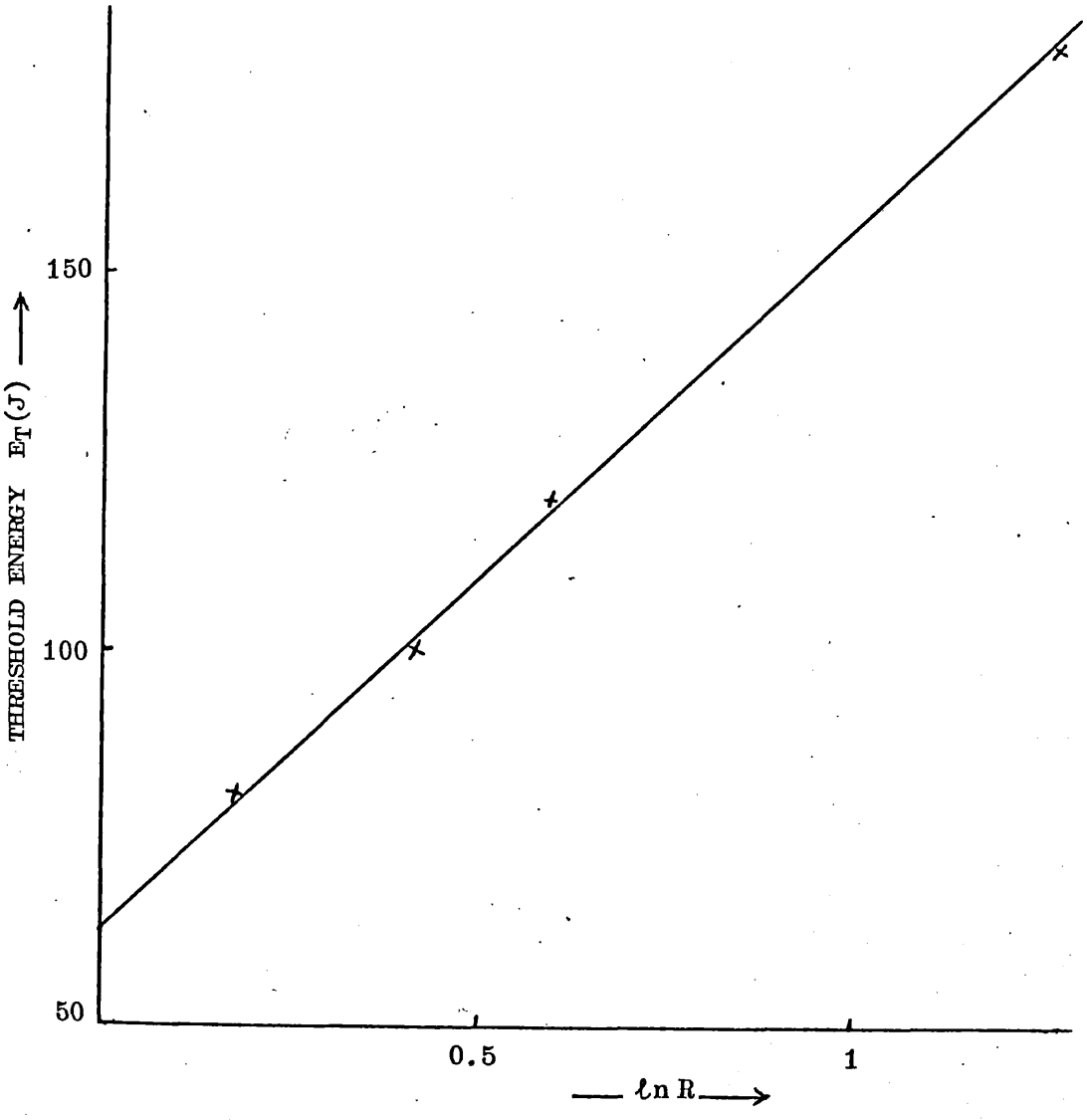

Fig.6.5
Threshold energy as a function of the output mirror reflectivity of the laser cavity

Now let us consider equation (2.7). For the present system $\frac{r_1}{r_2/n_c} = 0.87$ and $1 - e^{-\alpha\ell} \approx 0.26$. From the slope efficiencies of Fig.6.4 and equation (2.7), Table 6.2 is drawn up and the value of q is calculated to ±25%. Thus the material efficiency factor q is approximately 0.45%.

TABLE 6.2

E_{out}(J)	E (J)	E_T (J)	$\frac{E-E_T}{E_{out}}$	T	q
1.8	700	180	288	0.72	0.0055
1.25	600	120	384	0.45	0.0048
0.9	500	100	445	0.34	0.0046
0.25	250	80	682	0.17	0.0042

Now from Fig.6.5, $1/\zeta\sigma \simeq 2890$ J cm. Taking the value $\sigma = 7.5\times10^{-20}$ cm^2 calculated in Chapter IX, $1/\zeta \simeq 21.6\times10^{-17}$ J cm^3. Since the laser energy is emitted within approximately 220 μs (Fig.6.2(b)), and from section 2.1 $1/\zeta = \frac{t_{laser} h\nu V}{q\, t_2}$, we calculate the spontaneous emission lifetime for a $2 \rightarrow 1$ transition to be approximately 240 μs. This value is close enough to the measured fluorescence lifetime (~ 300 μs) of the neodymium in phosphorous oxychloride system. It must be pointed out that the above calculations are only approximate, the main source of error arising from the assumptions made for the light pumping pulse (see section 2.1 and Fig.5.4a).

The results described in this section are in good agreement with those reported by Samelson et al[34] who have also obtained better efficiencies with bigger laser systems. The space angular characteristics of the liquid laser system depend on the size of the active medium and the thermal lens formed in the active medium due to heating by the pumping radiation. These were investigated by Salkova et al[122] for systems having different Fresnel numbers (section 1.1). The correspondence between the space angular characteristics of induced radiation and models of equivalent resonators of liquid lasers was established. The experiments have shown that optical

uniformity and high photo-chemical stability of the liquid are essential in the production of beams with very small divergence.

Having described the free-running operation of the liquid laser, some of its inherent properties will be investigated in the next section and an evaluation of its potentialities as a high power amplifier will be made in subsequent chapters.

6.3 THE SELF-Q-SWITCHING OF THE LIQUID LASER

The liquid laser systems display a rather unusual phenomenon which is described as self-Q-switching[20]. The nature of the spiking of the free-running liquid laser described in section 6.1 changes as the output mirror reflectivity is decreased. Some of the spikes acquire a Q-switched character and the magnitude of the effect depends on the mirror product reflectivity $R_1 R_2$[22].

This self-Q-switching behaviour of the liquid laser has lately been the subject of considerable discussion. One mechanism which has been proposed[22] involved the establishment of a phase grating from backward stimulated Brillouin scattering (SBS) within the liquid column (section 2.4). This would have altered the overall reflectivity of the cavity, and thereby have changed the cavity gain. However, if the mechanism had been due to SBS, there would have been an observable frequency shift in the back-scattered light. Alfano et al[78] were unable to confirm this experimentally, and they concluded that the mechanism proposed by Key et al[19], was therefore more likely to be true. In this mechanism, the phase grating was produced by the forward and backward waves in the cavity. At the maxima of the standing wave, the refractive index of the liquid would be increased by one of a number of possible non-linear optical processes (section 2.4). Two very obvious processes would be electrostriction and heating due to absorption. This kind of phase grating, because of its

stationary nature, would not produce a Doppler shift in the reflected light and would thus account for Samelson's observations.

Very recently, Selden[123] has devised a mechanism to account for the production of a thermal grating which seems to account for most of the observed phenomena. In this mechanism, the fast non-radiative decay to the ground state of the lower level of the laser transition, deposits thermal energy into the liquid.

Since the population of the lower level of the laser transition is determined by the stimulated emission process, the heat flow into the liquid from the fast transmission of this level to the ground state also follows the stimulated emission process. The fast transmissions which populate the upper laser level however are controlled by the pumping, and the heat evolved in this process has no spatial correlation with the heat evolved in the lower transition. The latter heat is spatially deposited in the liquid with maxima corresponding to the maxima of the stimulated optical standing wave. The net effect is a density and hence refractive index variation which gives rise to a phase grating. Selden shows that the reflectivity of this thermal grating is proportional to the cavity gain. Furthermore, he points out that owing to the much greater thermal expansivity of liquids over solids, the effect of this process in liquids is very much greater than the corresponding effect in solids. This accounts very simply for the fact that self-Q-switching phenomena are more readily observed in liquids than in solids.

A number of experiments have been carried out by the author to explore the mechanism of the self-Q-switching behaviour of the liquid laser, namely:

(1) the spiking behaviour of a liquid laser as a function of the output mirror reflectivity;

(2) using a cavity with a fixed reflectivity and a constant length, the spiking behaviour of the glass rod alone;

(3) the spiking behaviour of the glass rod with the liquid laser column in the cavity unpumped

(4) the spiking behaviour of the combined glass and liquid laser.

The last arrangement enabled the overall gain in the cavity to be increased without changing the parameters controlling the state of the liquid. The experimental details and results are described below[124].

First, the spiking behaviour of the $Nd^{+3} : POCl_3 : ZrCl_4$ system was investigated as a function of the reflectivity product $R_1 R_2$. The laser head (Fig.5.2) was placed between two plane parallel reflectors and output energies of 1.7J with input energies of 650J were obtained for a reflectivity product greater than 0.3. Irregular spiking was observed starting 130μs after firing the flashlamps and lasting for 200μs. The spiking had duration of approximately 450ns and power of 10 With a reflectivity product of 0.04 output energies of 0.9J were obtained using input energies of 650J. Fewer spikes were now observed and amongst these were some of duration 100-200ns and peak power of the order of 80kW. A pause in spiking was usually observed following each high power spike. This self-Q-switching behaviour is similar to that originally reported by Samelson et al[22]. The effect however was less marked in the present experiments because of the lower energy and smaller size of the system.

The Nd-glass laser (Fig.5.3) was placed in a cavity 100cm long with fixed reflectivities of 100% and 50%. Output energies of 1.7J and 2.5J were obtained with input energies of 1000J and 1600J respectively. The threshold of the laser was 600J. Spiking started 300μs after firing the flashlamps and lasted for 400μs. The spikes (see Fig.6.7(a)) were approximately 700ns long and had power approximately 5 to 10kW.

The liquid laser was now introduced into the same cavity as the neodymium glass laser (Fig.6.6). With the liquid not pumped, the threshold

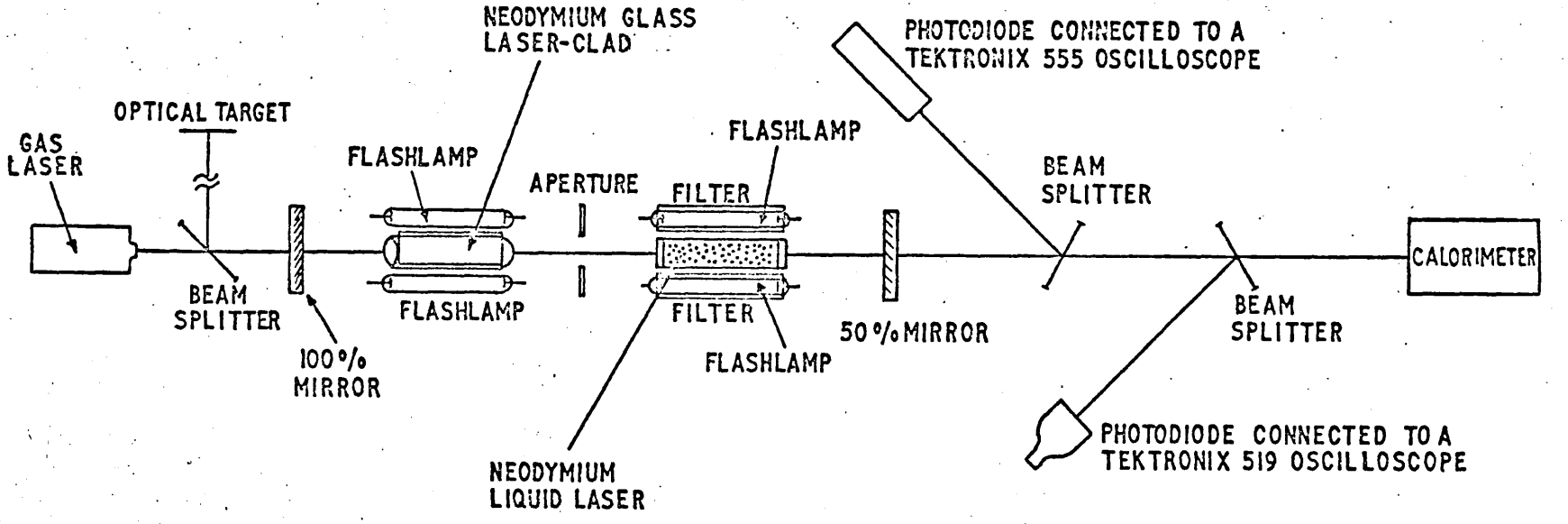

FIG. 6-6 INVESTIGATION OF THE SPIKING BEHAVIOUR OF A LASER WITH COMBINED ACTIVE MEDIA

of the glass laser increased to 900 J , i.e. by a factor $\frac{3}{2}$ of its value without the liquid laser cell in the cavity. This was attributed to the passive loss of the $POCl_3$ and the reflections from the cell windows, a total insertion loss of 30% per double pass. A few spikes with duration 150-250 ns and peak power 60-80 kW were regularly observed when the glass laser was pumped up to 1600 J . Fig.6.7(b) shows the spiking behaviour of the Nd-glass laser with the liquid laser cell placed in the cavity unpumped. Thus the introduction of the Nd-liquid medium into the cavity of the Nd-glass laser produces a small Q-switching effect analogous to Q-switching by organic solvents as reported in reference 18, where it was reported that liquids which had very little absorption at the laser wavelength showed very small Q-switching effects. The $POCl_3$ solution falls into this category and thus behaves as expected.

The most interesting results were obtained when both lasers were simultaneously pumped in the same cavity. Spiking started approximately 90 μs after firing the flashlamps and lasted for 150 μs . The oscillations consisted of powerful uniform pulses of approximately equal height as can be seen from Figs.6.7(c,d). Short pulses of duration 20 ns full width at half the maximum (FWHM) and powers up to 1 MW were observed for every shot. These were recorded on a T 519 oscilloscope. Typical oscillograms are shown in Fig.6.8. Total output energies of 3.5 to 4J were obtained.

Due to the limitations of the flashlamps it was not possible to pump the system harder than the levels reported above. Attention however is drawn to the results of the experiments 3 and 4. When the liquid is not pumped, the glass laser shows some signs of Q-switching. Clearly, the mechanism at work here cannot be that proposed by Selden, because the quantum energy of the stimulated radiation in the cavity is insufficient to raise the liquid laser to its upper laser transition level. Since Alfano et al[78] have shown that SBS is not the operative mechanism either, then this small

Fig.6.7
The top traces in each picture show the spiking behaviour of the arrangement in Fig.6.6. The lower traces in each picture show parts of the top traces on an expanded scale. Read from right to left

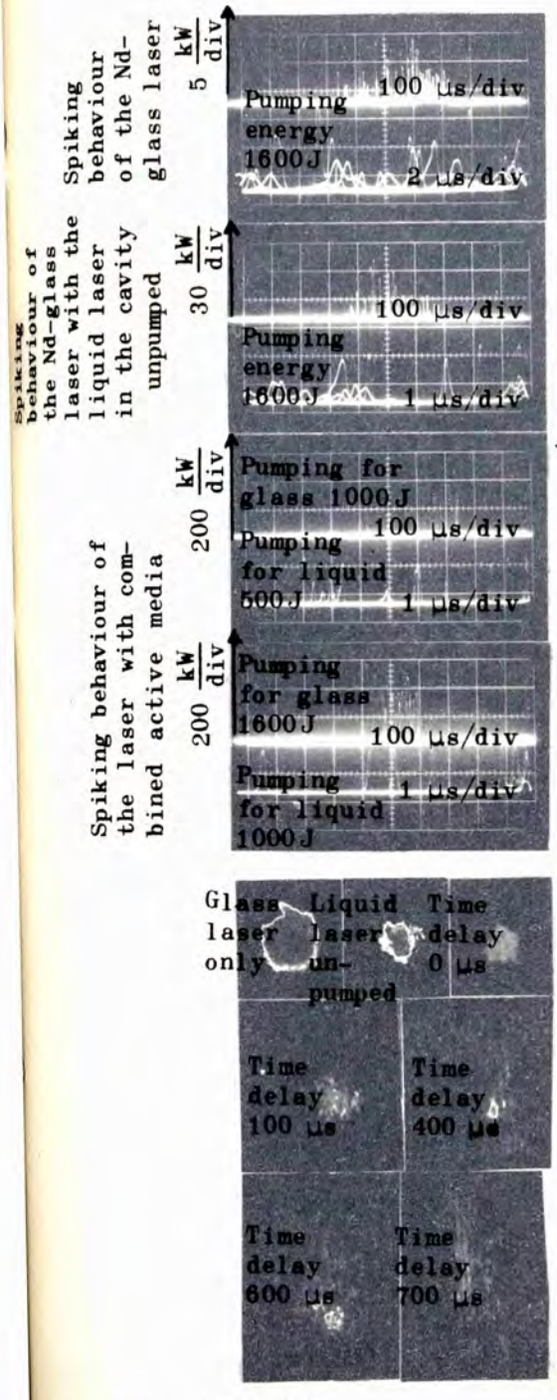

Fig.6.9
Beam burn patterns obtained by firing the glass laser through the liquid laser after the latter had been pumped

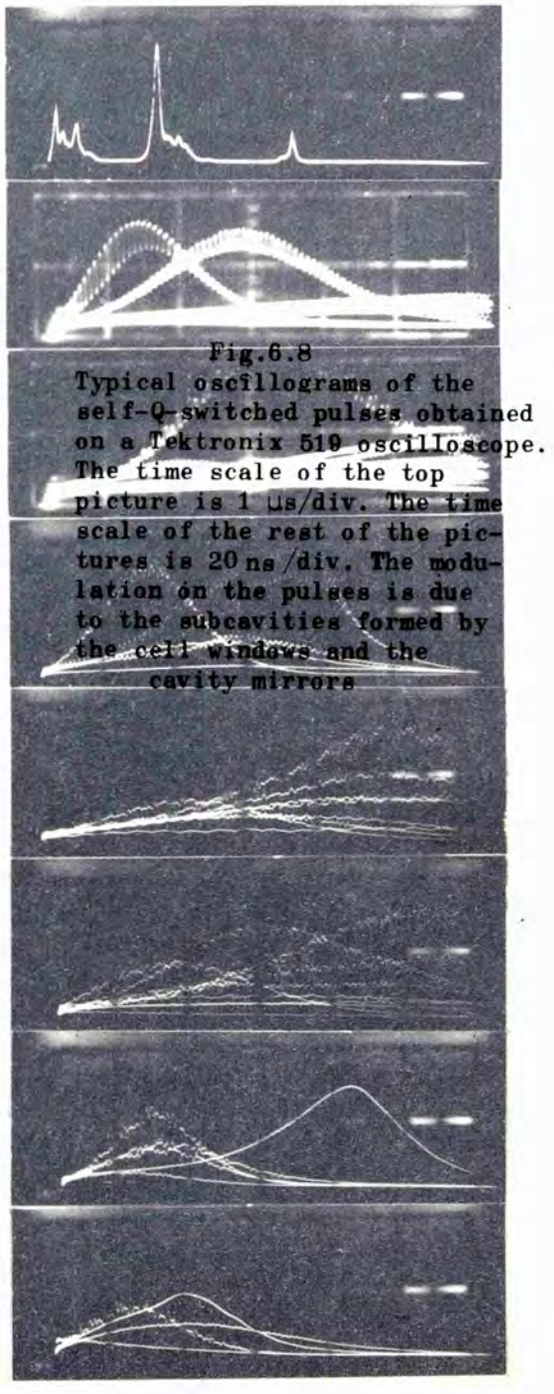

Fig.6.8
Typical oscillograms of the self-Q-switched pulses obtained on a Tektronix 519 oscilloscope. The time scale of the top picture is 1 µs/div. The time scale of the rest of the pictures is 20 ns/div. The modulation on the pulses is due to the subcavities formed by the cell windows and the cavity mirrors

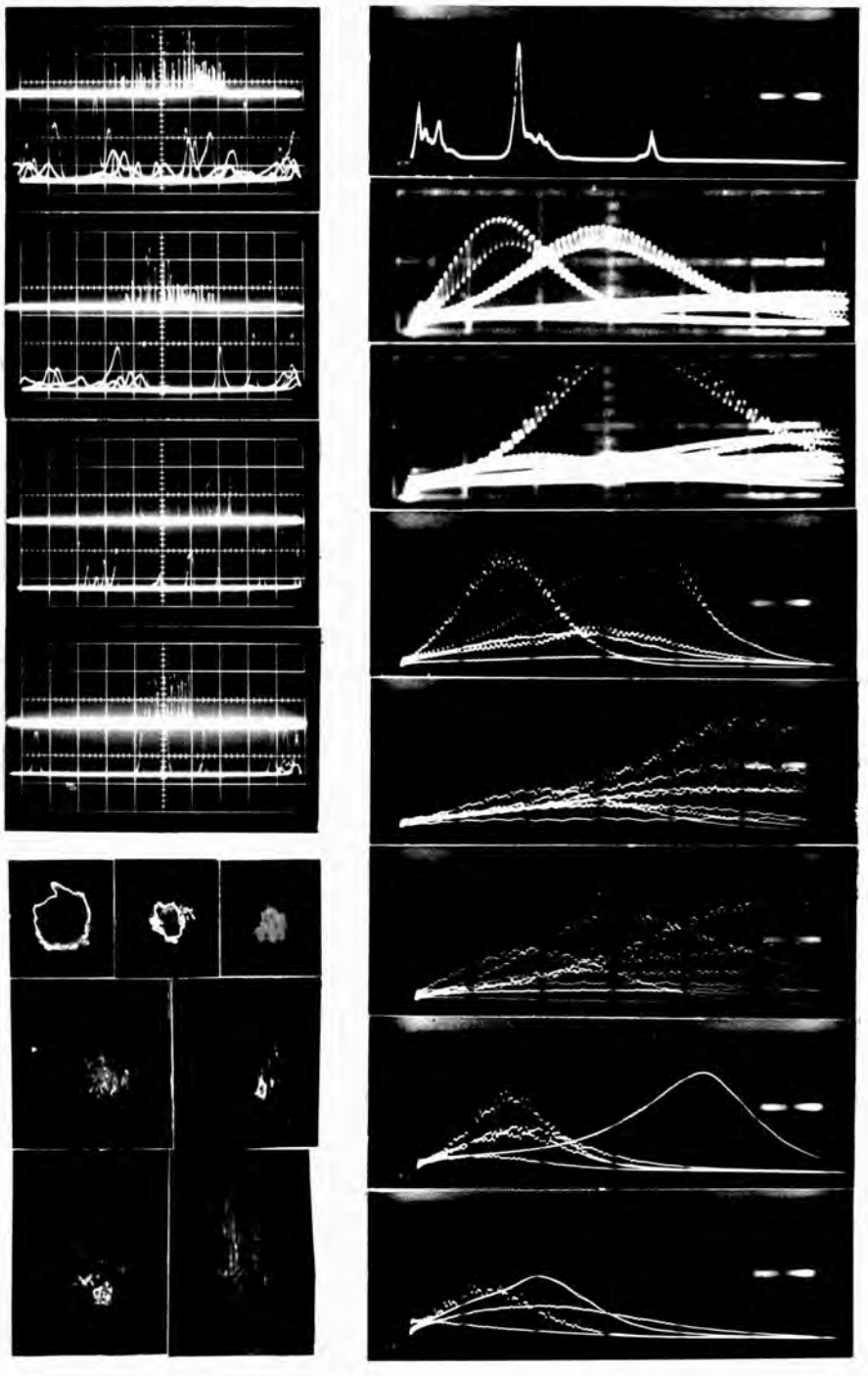

effect is very likely to be explained by the mechanism of Key et al[19] in terms of non-linear optics. When both liquid and glass are pumped, strong Q-switching is observed. We know from experience that when the glass laser is pumped with no liquid cell in the cavity, self-Q-switching is very seldom observed. We therefore conclude that the only effect which the pumped glass rod had on the system was simply to increase the cavity gain. It follows, therefore, that the same result should be obtainable with a longer liquid column. Experiment 1 indicates that more self-Q-switching is observed when the liquid alone is pumped harder.

The above experiments have shown that self-Q-switching in liquid columns is more likely the greater the cavity energy and the greater the cavity gain. They indicate that the mechanism of the process is likely to be a combination of the process suggested by Selden and that proposed by Key et al. In either event, the primary cause of the induced phase grating would seem to be the spatially periodic deposition of heat energy.

Fig.6.9 shows some of the beam burn patterns which were obtained for different delay times between firing the two lasers in the arrangement of Fig.6.6. It is interesting to notice the big distortion in the liquid laser when it is fired approximately 600-700 μs before firing the glass laser. This means that after laser operation (which is approximately 300 μs) the liquid medium continues to change its optical properties due to heating by the pumping radiation. It can be seen however, that when both liquid and glass are pumped simultaneously, uniform beam profiles are obtained.

CHAPTER VII

EXPERIMENTAL STUDY OF THE ACTIVELY Q-SWITCHED LIQUID LASER SYSTEM $Nd^{+3} : POCl_3 : ZrCl_4$

In this chapter the performance of the first actively Q-switched liquid laser is described[41].

7.1 THE EXPERIMENTAL ARRANGEMENT

The experimental arrangement is shown in Fig.7.1. The liquid laser head (Fig.5.2) was placed between two plane parallel reflectors. The capacitor bank consisted of two 200 μF condensers (section 5.1) which were charged up to 1.6 kV. The light pumping pulse is shown in Fig.5.4(a). A calcite prism was used as the polarizer and the system was Q-switched by removing the quarter-wave voltage of 4.1 kV applied to a KD*P Pockels cell (section 5.6) When the Pockels cell voltage is on, the polarized light from the prism changes its direction of polarization by 90° after traversing the Pockels cell twice, and is then reflected out of the cavity from the prism interface. When the population inversion in the active medium builds up to a value much higher than the threshold value, the Pockels cell voltage is switched off and the energy stored in the active medium is discharged in a very short time (section 2.2). The switching-off time of the Pockels cell was of the order of 40 ns, achieved with a Mullard PL81 valve (section 5.6). It is shown in Fig.7.3. It was not necessary to design a switching-off system faster than this since it has been shown experimentally[126] that there is no advantage in switching in a time which is much shorter than the build-up time of the pulse. The Pockels cell could be switched off at different times during the pumping pulse with the aid of a delay box following the trigger unit.

The pulses were recorded on a Tektronix 519 oscilloscope, using the ITT F4000 (S1) photodiode (section 5.4). The output energy was measured with a TRG 107 cone calorimeter placed as shown in Fig.7.1. The build-up time of the giant pulse was measured to an accuracy of 10 ns by using the

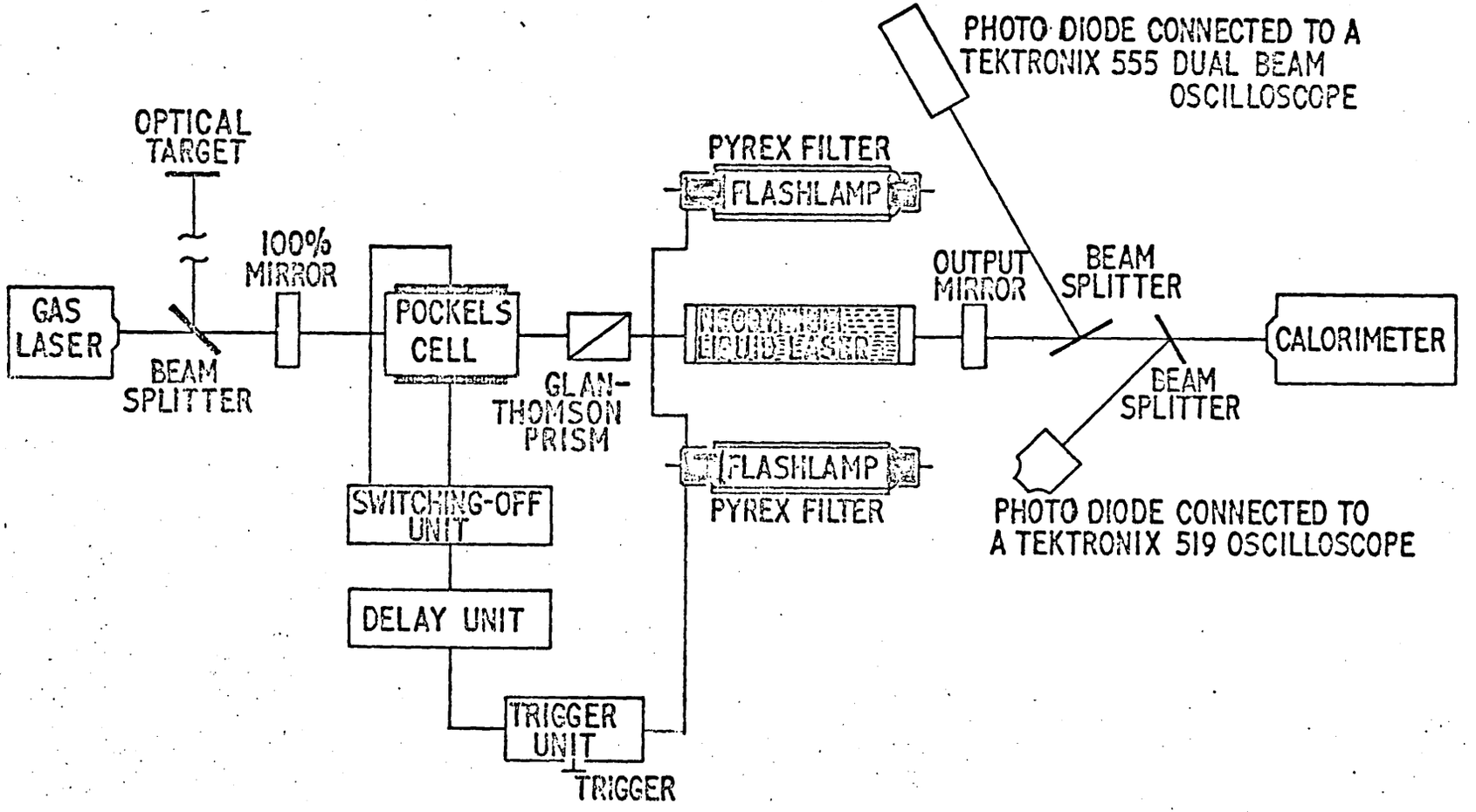

FIG. 7-1 INVESTIGATION OF THE DEVELOPMENT OF THE GIANT PULSE IN A NEODYMIUM LIQUID LASER

two beams of the Tektronix 555 oscilloscope simultaneously to record the decay of the Pockels cell and the photodiode response to the giant pulse. A typical oscillogram is shown in Fig.7.3.

The laser was fired at intervals of at least 15 minutes to avoid the distortion effects taking place in the liquid due to heating by the pumping radiation.

7.2 GIANT PULSE CHARACTERISTICS

Figure 7.2 shows a typical giant pulse from the $Nd^{+3} : POCl_3 : ZrCl_4$ system. Pulses as short as 13 ns with total energy of 0.7 J were recorded. The system was very reliable and its main characteristics were the high powers obtained ($\sim$ 50 MW) with small input energies (500 J).

Figure 7.4 shows the general behaviour of the giant pulse as a function of the pumping pulse for an output mirror reflectivity of 28%, an input energy of 512 J and a cavity length 57 cm. It can be seen from these graphs that the optimum giant pulse occurs when the Q-switching is delayed for 205 μs after triggering the flashtubes. This is longer than the time taken for the pumping pulse to attain its maximum intensity and is less than the fluorescense lifetime of the material ($\sim$ 300 μs). The curves shown in Fig.7.4 are self-consistent. In Chapter IX it is shown that this system has maximum gain at 205 μs after firing the flashlamps, i.e. that at this time the population inversion is maximum. The curves of Fig.7.4 are in good agreement with this result and with the results of section 2.2.2.

The dependence of the giant pulse on the output mirror reflectivity is shown in Fig.7.5. We note the agreement of these graphs with the theoretical considerations of Midwinter[40] on giant pulse formation (section 2.2.2), particularly that the optimum output mirror reflectivity is around 28%, and also the rapid build-up of the giant pulse with mirror reflectivities greater than 50%. Fig.7.6 shows the effect of the cavity

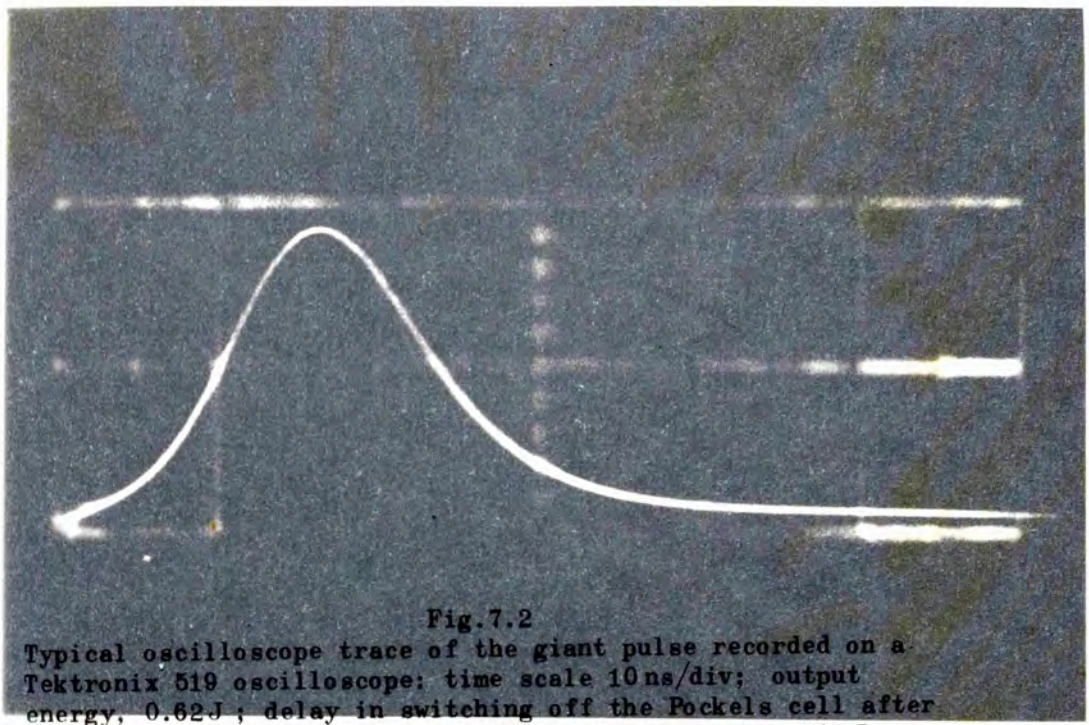

Fig.7.2
Typical oscilloscope trace of the giant pulse recorded on a Tektronix 519 oscilloscope: time scale 10 ns/div; output energy, 0.62 J ; delay in switching off the Pockels cell after triggering the flashlamps, 190 μs; input energy, 512 J .

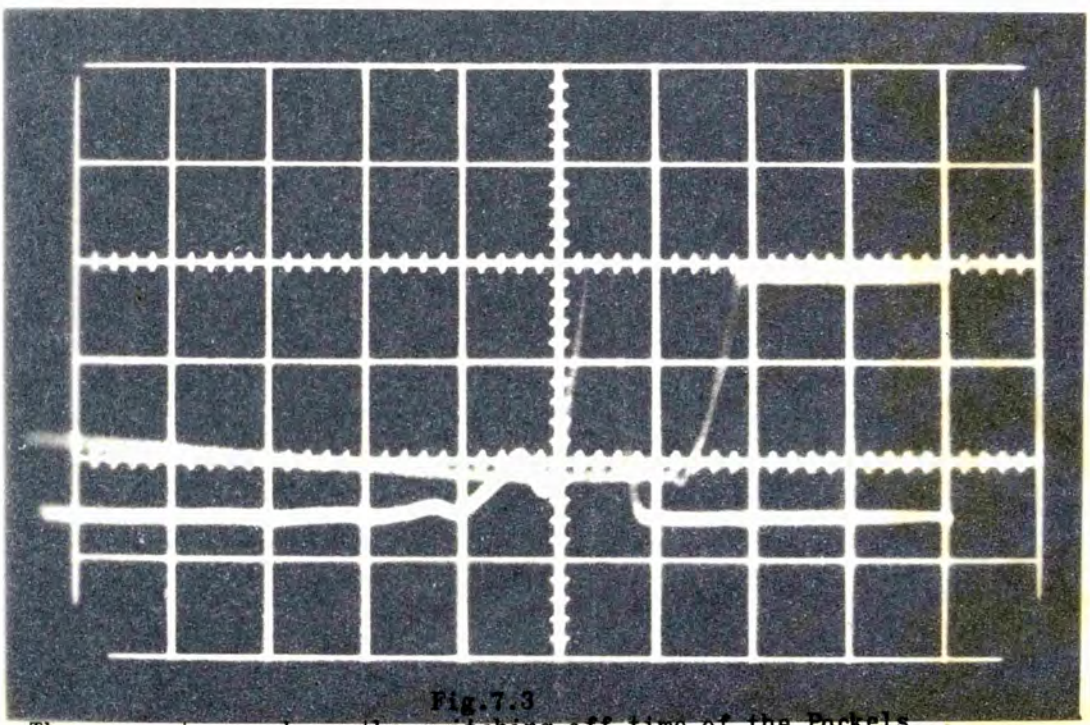

Fig.7.3
The upper trace shows the switching-off time of the Pockels cell to be approximately 40 ns. The lower trace shows the time it takes the giant pulse to appear. Both traces are on the same time base. Recordings from a Tektronix 555 oscilloscope. Time scale 100 ns/div

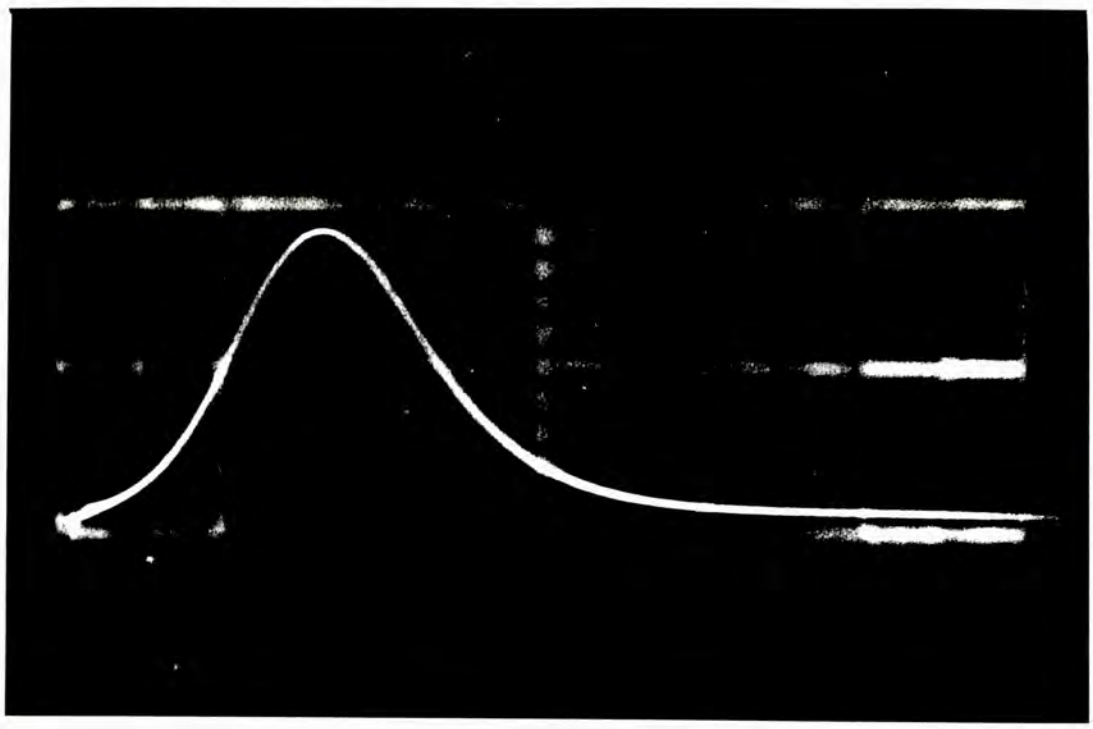

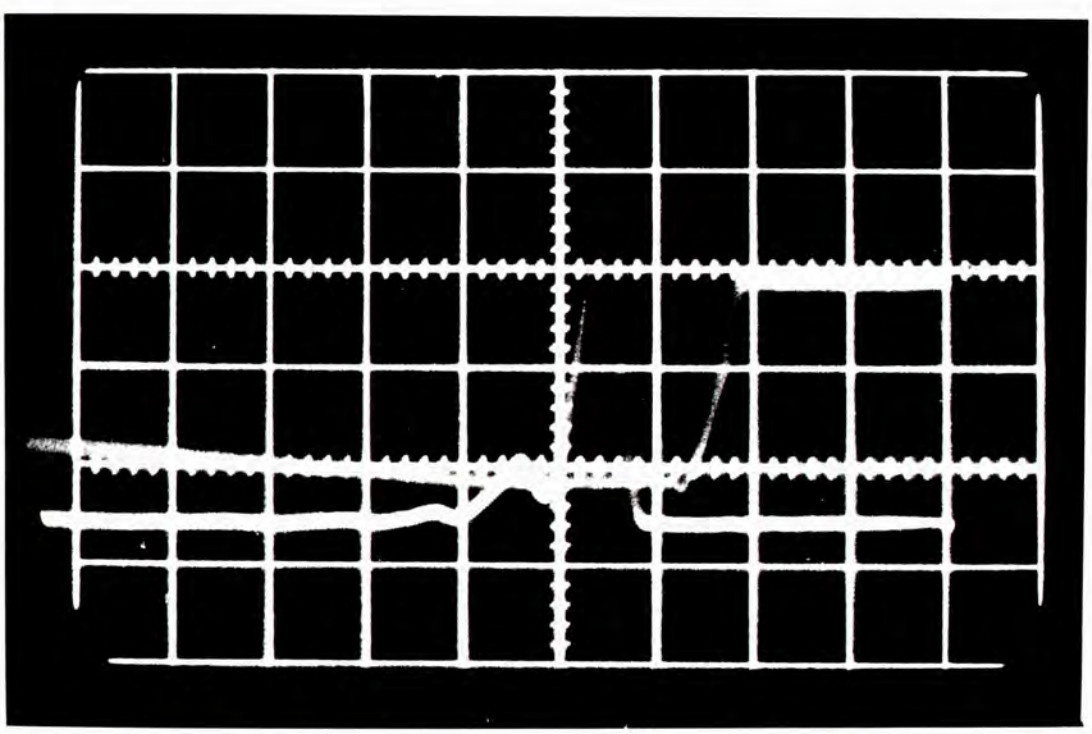

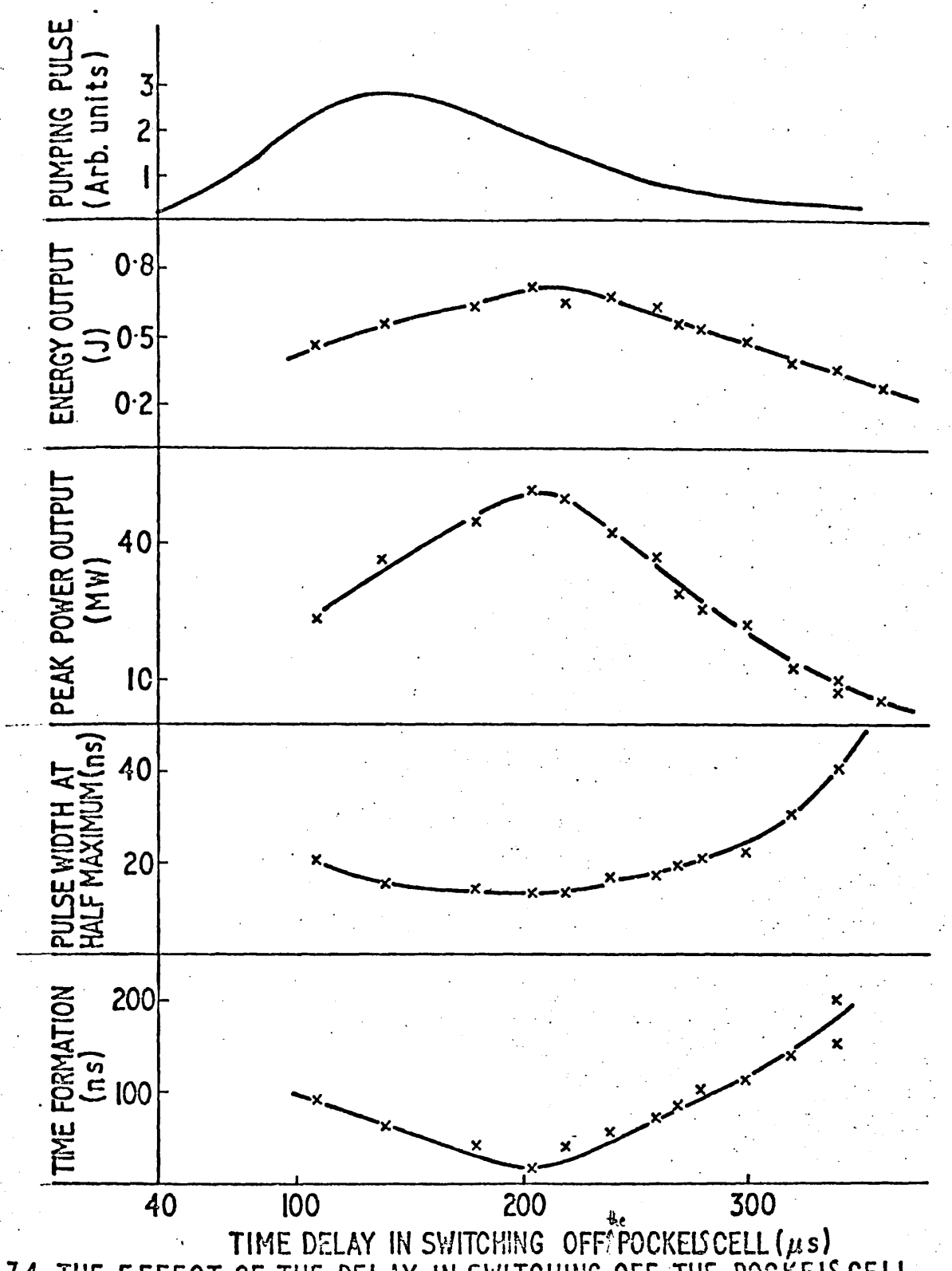

FIG 7·4 THE EFFECT OF THE DELAY IN SWITCHING OFF THE POCKELS CELL ON THE GIANT PULSE

CAVITY LENGTH 57cm
INPUT ENERGY 512 Joules
OUTPUT MIRROR REFLECTIVITY 28%

length on the giant pulse. The energy output of the giant pulse is seen to remain constant up to cavity lengths of 110 cm. For greater cavity lengths the resonator was unstable and the output energy dropped considerably. The output power was diminishing constantly due to the increasing pulse width with increasing cavity length. The results on Figs.7.5 and 7.6 are in agreement with the comments made on equation (2.19) in section 2.2.2. The points drawn on all graphs are averages of many measurements taken from the same arrangement. In Figs.7.4, 7.5 and 7.6 pulse width measurements were made to an accuracy of ±2%; all other ordinates to ±10%.

The most serious problems arising in the operation and further development of this kind of laser are the distortion effects in the active medium due to heating by the pumping radiation. For long delays in switching off the Pockels cell (over 300 μs) the beam cross-section showed discernible effects due to thermal distortion. Good filtering of the pumping light from UV radiation and the cavity design are therefore more important in the engineering of this kind of laser than in other lasers. Filtering of the pumping light with yellow Corning 3555 tubes instead of pyrex tubes, showed some improvement in the performance of the laser. The dependence of the giant pulse on the input energy was not investigated, because even with such low pumping energies (~512 J) the high output powers produced localized damage in the calcite prism. At these pumping energies, and for delays less than 300 μs in switching off the Pockels cell, the distortion effects were negligible. Uniform beam cross-sections were recorded on developed unexposed polaroid film. A typical beam cross-section is shown in Fig.7.7 at a magnification of 5.3. Note that the main beam is contained within a well defined circle, thermal distortion effects being noticeable at its perimeter. The divergence of the beam was estimated to be approximately 2 mrad.

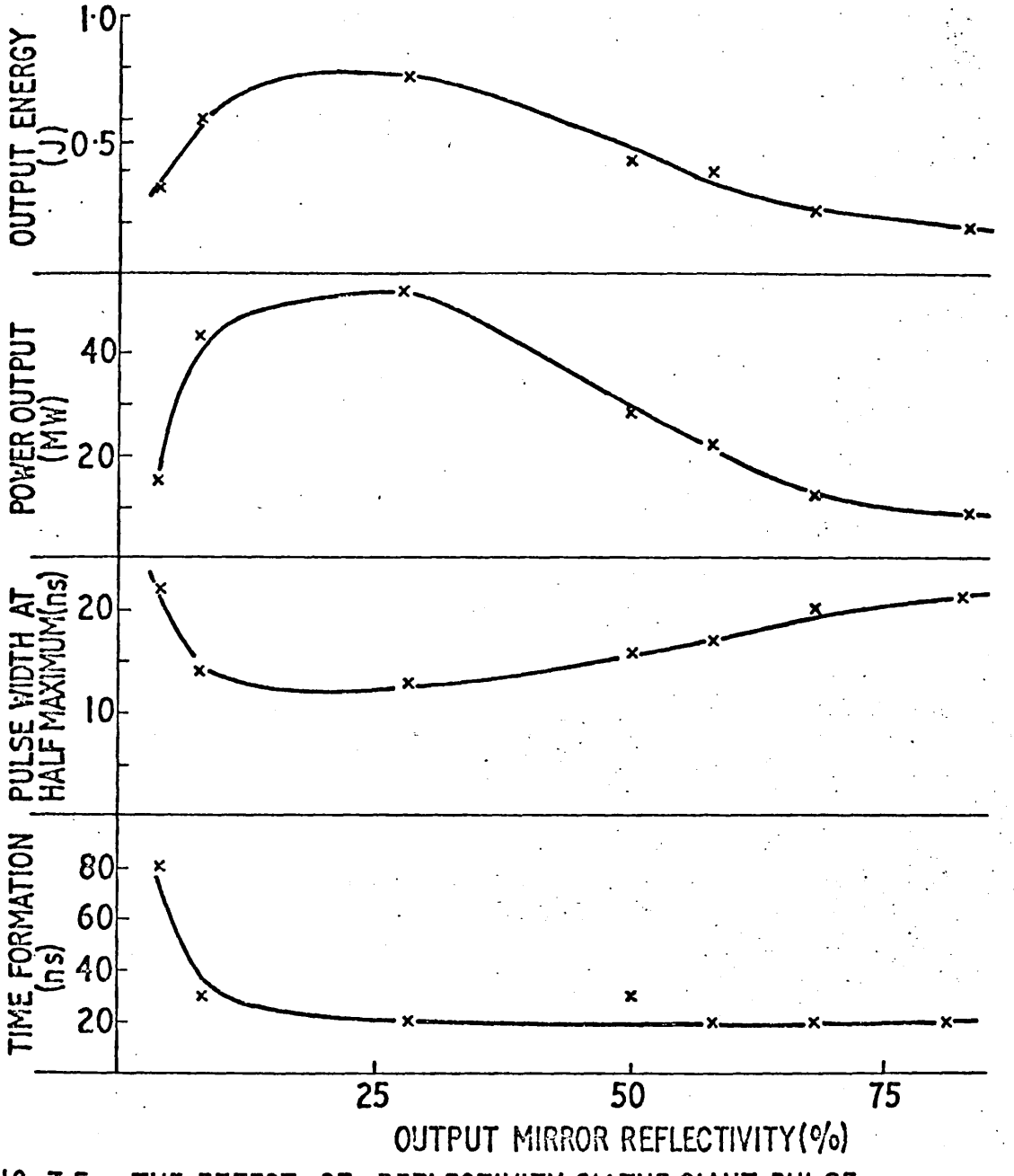

FIG. 7·5 THE EFFECT OF REFLECTIVITY ON THE GIANT PULSE
CAVITY LENGTH 57 cm
INPUT ENERGY 512 Joules
TIME DELAY IN SWITCHING OFF THE POCKEL CELL 210 μs

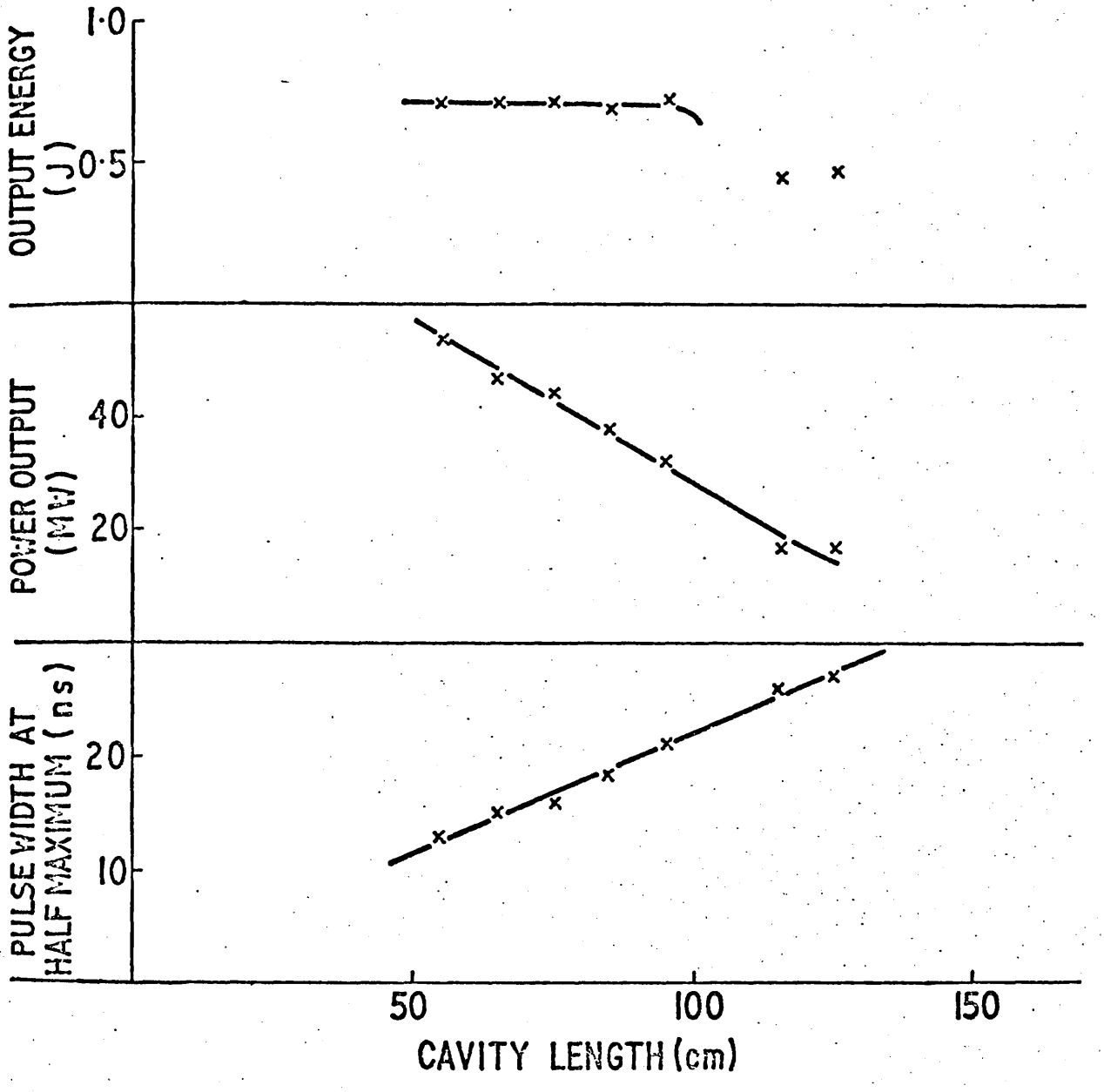

FIG. 7·6 THE EFFECT OF THE CAVITY LENGTH ON THE GIANT PULSE
INPUT ENERGY 512 Joules
OUTPUT MIRROR REFLECTIVITY 28%
TIME DELAY IN SWITCHING OFF THE POCKEL CELL 210μs

Fig.7.7
Typical beam burn pattern recorded on developed unexposed (Polaroid) film. Time delay in switching off the Pockels cell 200 μs; pumping energy 512 J; distance from the output mirror 90 cm; magnification ~5.3; estimated divergence 2 mrad

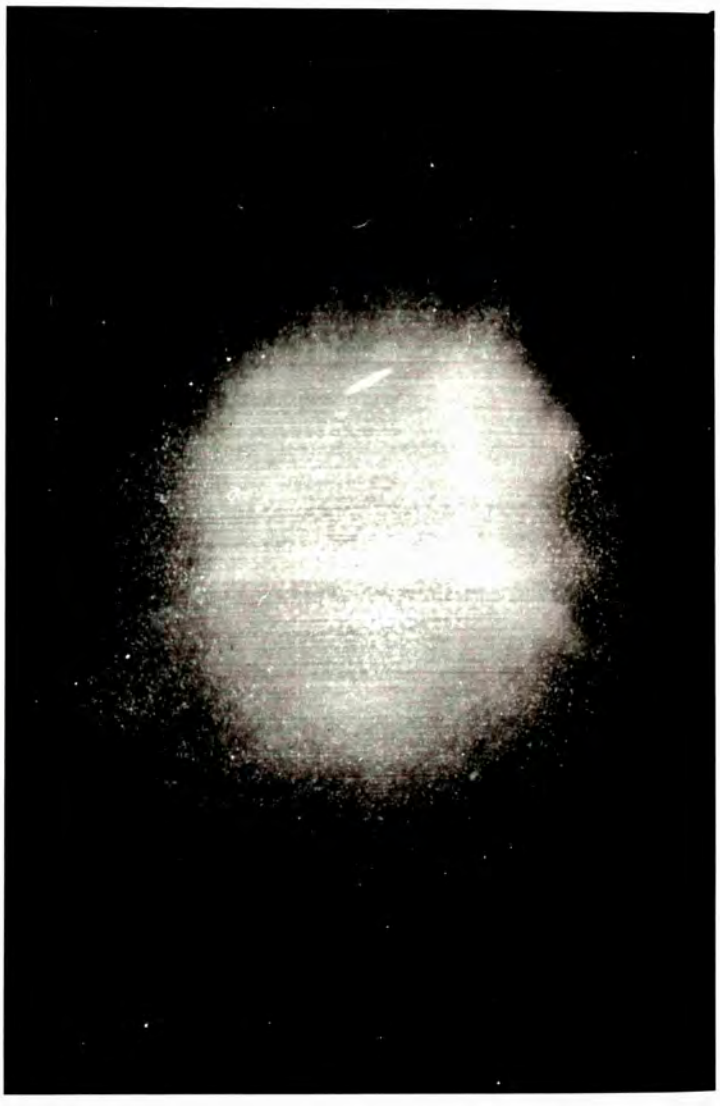

7.3 CONCLUDING REMARKS ON THE PERFORMANCE OF THE Q-SWITCHED SYSTEM

The results described above are in good agreement with the theoretical considerations described in section 2.2.2. The experiments have demonstrated certain important characteristics of the liquid laser when operated as a Q-switched oscillator: the pulses obtained are considerably shorter than those from glass lasers (full width at half the maximum ~25 ns) and $CaWO_4$ [126] lasers (full width at half the maximum ~18 ns) and are comparable to those from YAG lasers. Output powers of 50 MW have been obtained with input energies of 500 J (see Figs.7.4, 7.5, 7.6). Powers of this order of magnitude with such low input energies make the neodymium liquid laser at least as efficient as YAG and glass lasers. The performance of this laser in the 1 J output pulse region is superior to that of YAG and glass lasers.

Two important assets to this system are the uniformity of the pulses in the time dependent regime (oscillogram of Fig.6.2) and the uniform cross-sections of the beams (Fig.6.7). The system was very reliable and the results were reproducible at will. The performance of the system at higher input energies would be affected by the thermal distortion taking place in the active medium. In future designs uniform illumination of the liquid medium and good filtering of the pumping radiation should be the two main problems to overcome.

In view of the results described in this chapter, the liquid laser $Nd^{+3} : POCl_3 : ZrCl_4$ emerges as a serious competitor for laser applications where high output powers with small input energies are desired.

CHAPTER VIII

MODE-LOCKING OF THE Nd-GLASS AND THE Nd-LIQUID LASERS

In this chapter certain aspects of the mode-locking of Nd-glass and Nd-liquid lasers will be described. The original aim of the experiments involving the Nd-glass laser was the construction of a reliable mode-locked system for use in the experiments of Chapter IX. In the course of this investigation several interesting observations were made.

8.1 A MODE-LOCKED Nd-GLASS LASER SYSTEM

In section 6.1 it was shown that the introduction of a meniscus lens in the cavity strongly influences the relaxation oscillations of the neodymium laser. Everett[127] first showed that the introduction of a 2m.f.l. meniscus lens in the cavity of a mode-locked neodymium laser increases the reliability of mode-locking. An arrangement similar to that of Everett has been constructed, the main differences being the use of two flashlamps on either side of a clad rod and the introduction into the cavity of an aperture stop equal to the rod diameter.

Let us first describe the complete system. The oscillator head, shown in Fig.5.3, was placed between two plane parallel reflectors with reflectivities of 100% and 66%. The cavity was 1 m long. The capacitor bank consisted of two 400 μF condensers (section 5.1) which were discharged through the two xenon flashlamps giving the optical pumping pulse shown in Fig.5.4(b). A Laser Associates parallel-faced, 12 mm thick, output mirror was used, which had a hard coating in order to prevent damage due to the high powers of the picosecond pulses. The mode-locking dye cell was the Eastman model 6088 (1 mm path) antireflection-coated, which was placed next to the output mirror at the Brewster angle. The meniscus lens, 2 m.f.l., was placed at a distance of 2 cm from the 100% mirror, and an aperture equal to the diameter of the laser rod was placed between the

laser head and the output mirror. The arrangement was aligned, using a He-Ne gas laser. The system is shown in Fig.8.1

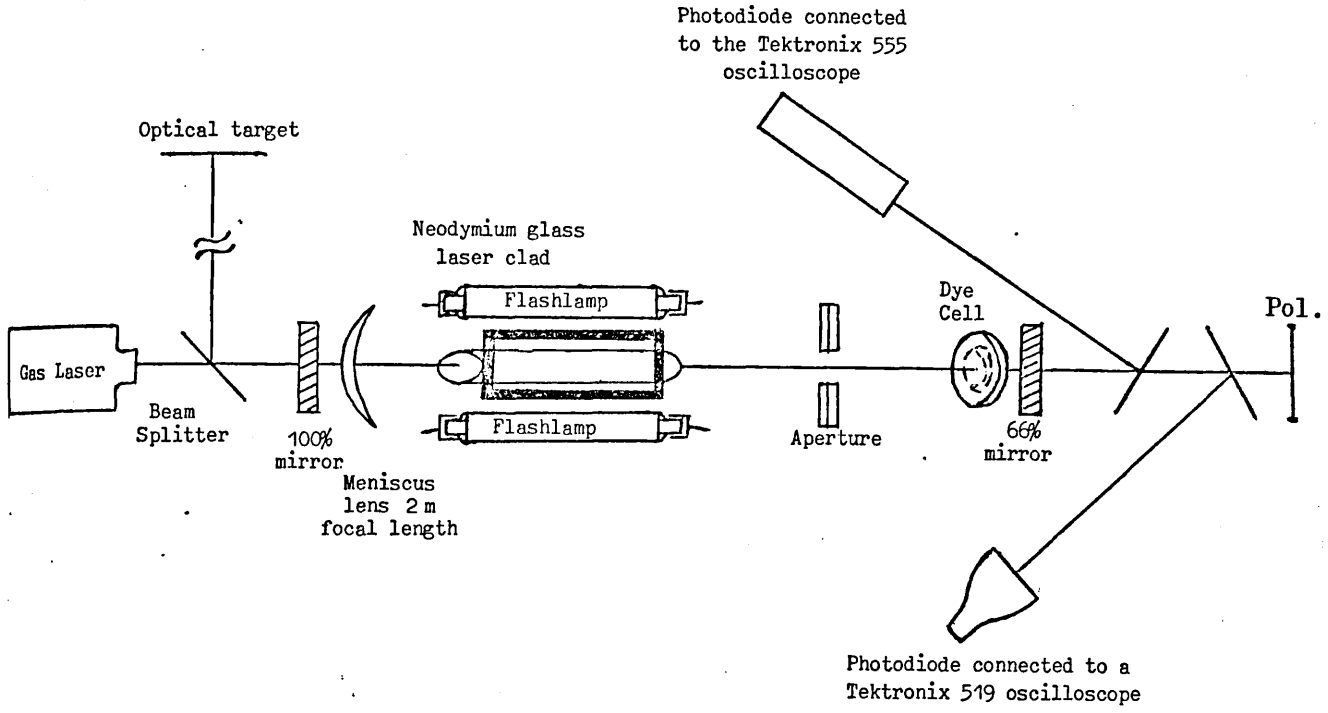

Fig.8.1
The mode-locked Nd-glass laser system

The performance of this system will be described below. For a given system the factors affecting the mode-locking are the dye concentration, the pumping level, the optical perfection of the laser rod, the alignment of the optical system and the optical qualities of the components of the system.

It was found that the dye concentration and the pumping level were critical in the production of good mode-locked trains, (see section 8.2). The mode-locking dye solution, Eastman 9740, was diluted in chlorobenzene and the optimum concentration was found to be 13:2. The optimum pumping was found to be 1.75 kV and was critical to within ± 0.05 kV for the above dye concentration. Under these conditions very good mode-locked trains with energies between 30 and 80 mJ were readily obtainable. Figs.8.2(a,b) show two examples of the mode-locked trains obtained. The pulses were measured by the two photon fluorescence technique to have a time duration

of $\sim 5\times10^{-12}$ s (section 9.4). Two photon fluorescence experiments will be described in the next chapter. The beam profiles are shown at the right of each picture (slightly enlarged) at a distance of 170 cm. Only one mode-locked train was produced in each firing, and it was emitted at a specific time after firing the flashlamps. This time was approximately 230 μs, and is shown in Fig.8.2(d). The divergence of the beam was estimated to be less that 2 mrad. The small divergence is characteristic of the newly developed Schott 55 glass laser. The recordings on Figs.8.2 (a,b,c) were made with a Tektronix 519 oscilloscope. Fig.8.2(c) shows the recording of mode-locked pulses on a very fast timescale (2 ns/div). The rise time of the oscilloscope-photodiode arrangement is seen to be approximately 0.4 ns (section 5.4). Mode-locked trains as described above were reproducible up to thirty times in succession before any deterioration in the quality of the beams could be observed. The results of Fig.8.2 could be reproduced at will. This system was used in the experiments of Chapter IX.

The trains shown in Figs.8.2(a,b) last for approximately 60 to 80 ns. The pulses are separated by the double transit time of the cavity and their duration is approximately 5 ps (section 9.4). Each of the pulses shown on the oscillograms (a) and (b) of Fig.8.2 consist of a series of smaller pulses separated by the double transit time of the thickness of the output mirror. These result from interference between the two faces of the mirror (section 2.3.3). The ratio of the peak power of the picosecond pulses to the background noise has recently been the subject of much controversy. Harrach et al[125] have recently reported that the picosecond pulses carry 15 to 20% of the energy of the mode-locked train from a Nd-glass laser. On the other hand Auston[128], using a method based on measuring the correlation functions, reported that the energy carried by the background intensity is only 5% of the whole train. The ratio of the peak power of

Fig.8.2
Mode-locked trains from the Nd-glass laser

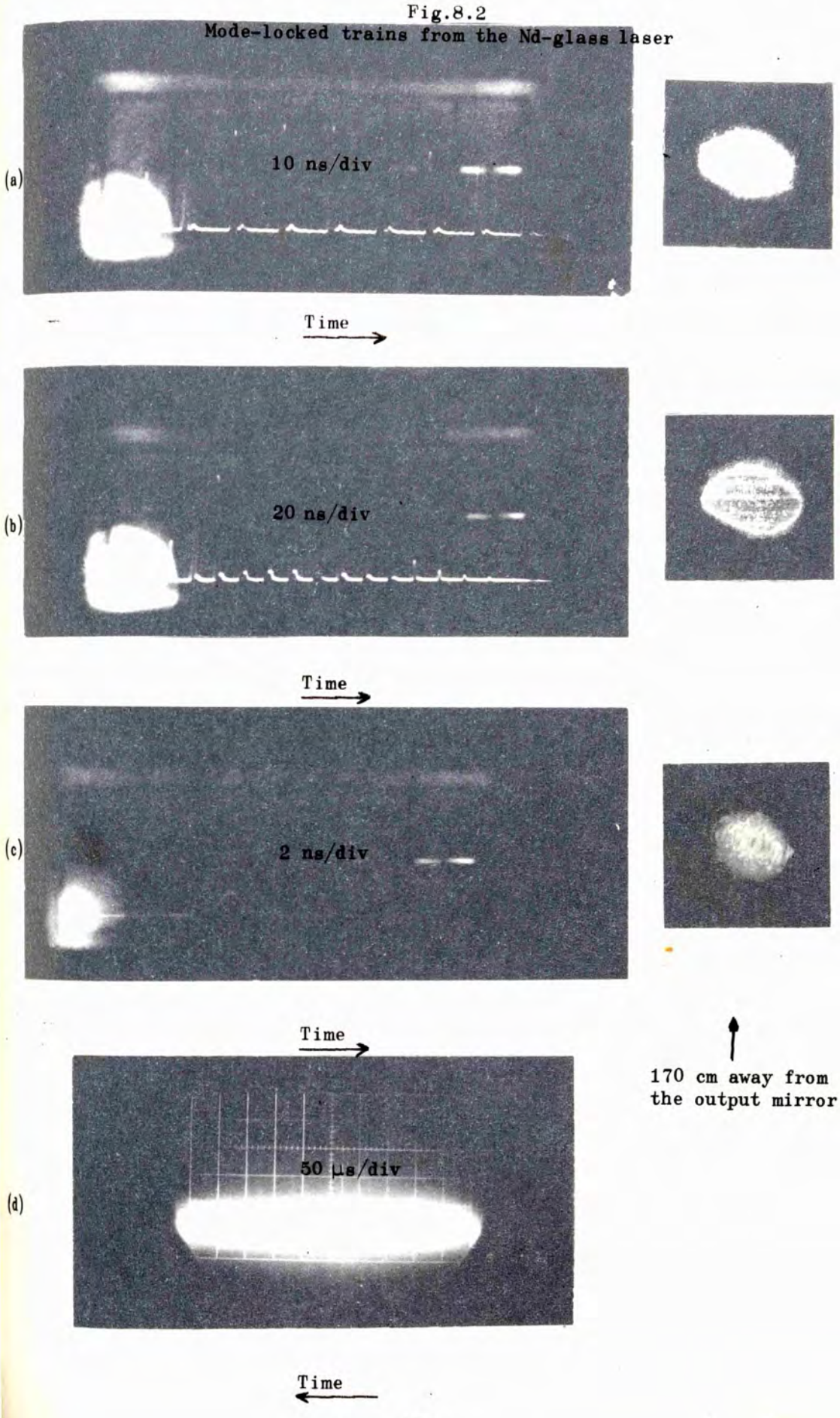

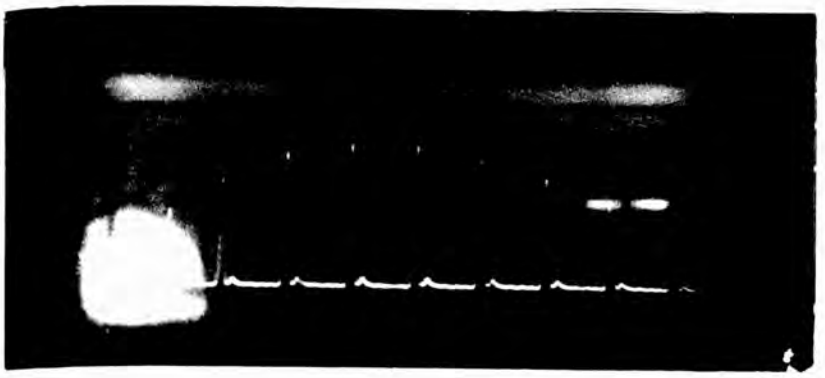

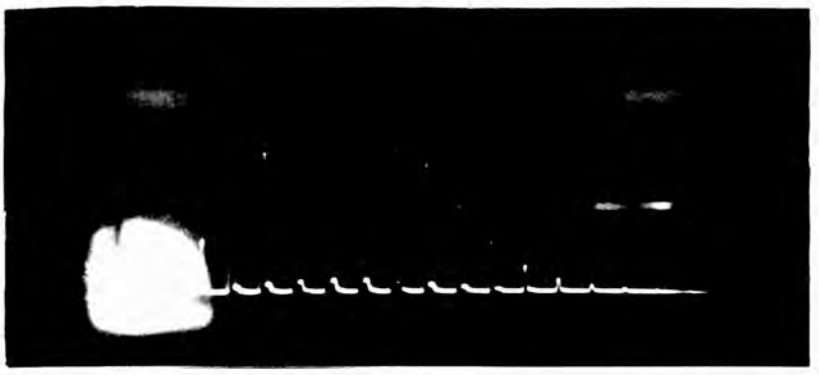

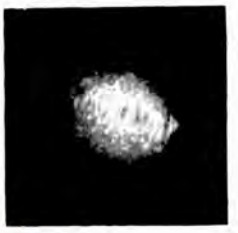

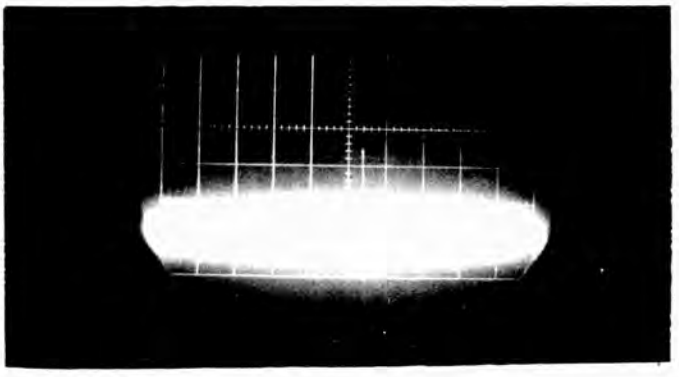

the picosecond pulses to the background noise power was only 10^{-4}. Several other authors have reported ratios lying between the two values mentioned above. Most of these suggest that, contrary to the earlier measurements, most of the energy is carried within the picosecond pulses.

Fig.8.3 shows typical spectra of the mode-locked laser taken with the image converter arrangement shown in Fig.5.6 , and a Monospek 1000 grating scanning spectrometer. The spectra cover a range of approximately 25-30 Å but the main power is contained within the central 10 Å . They are centred at 10580 Å which is the right wavelength as it can be seen from the fluorescence curve in Fig.4.4. The results concerning the spectra are in good agreement with the more detailed results of Von der Linde et al [58,59].

8.2 CHARACTERISTICS OF THE PASSIVELY MODE-LOCKED Nd-GLASS LASER

In section 8.1 a reliable mode-locked laser and its output characteristics have been described. Several problems arising under mode-locked conditions have been investigated and the results are described in this section.

(1) The position of the dye cell in the cavity. As pointed out in section 2.3.2, the position of the dye cell in the cavity affects the coupling of the modes. Fig.8.4(a) shows a mode-locked train obtained when the dye cell was placed in the centre of the cavity (L/2). In this case two pulses exist in the cavity which are bouncing back and forth between the reflectors and they meet at the centre of the cell. It can be seen from this picture that the two pulses do not necessarily have the same power, though generally they have comparable powers. Fig.8.4(b) shows a mode-locked train obtained when the dye cell was placed at L/3 . In this case three pulses are circulating in the cavity, and two of them always meet at the centre of the cell. The results of Fig.8.4(a) were

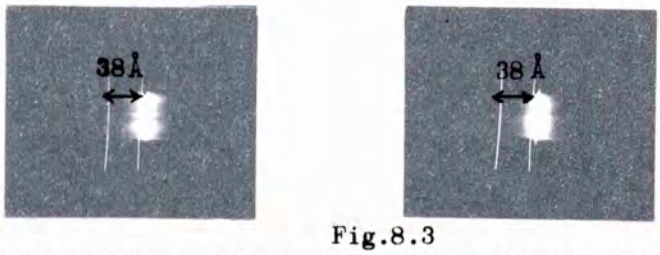

Fig.8.3
Spectra of the mode-locked Nd-glass laser. The two lines correspond to 10570 Å (right) and 10532 Å (left).

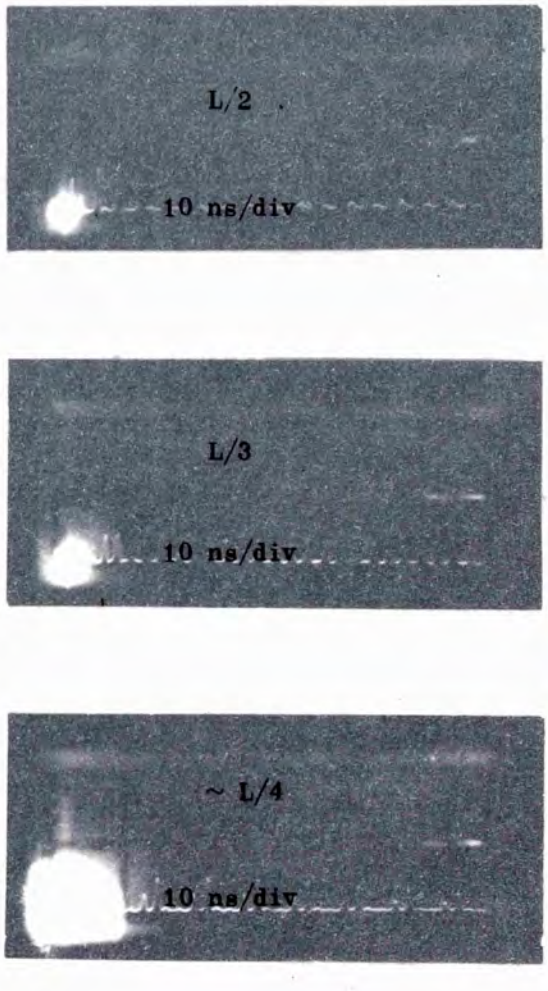

Fig.8.4
Mode-locking pictures for different positions of the dye cell in the cavity.

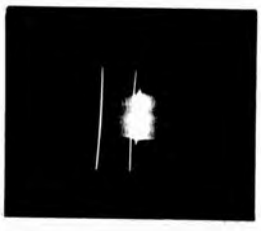

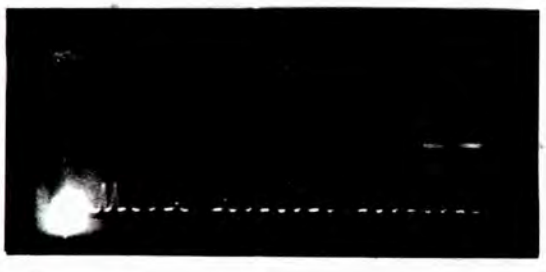

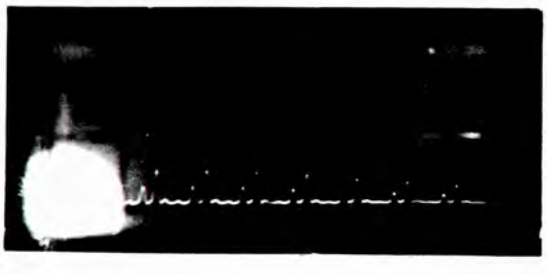

easily reproducible, whilst those of Fig.8.4(b) showed less consistency. These results are in very good agreement with the theoretical description given in section 2.3.2. The oscillogram on Fig.8.4(c) shows a mode-locked train obtained when the dye cell was placed approximately at L/4. The results were not readily reproducible for this arrangement. In general, however, it was found that whenever two pulses were observed, the pulse spacings were related to the transit time between the distances x_1, x_2 and $L = x_1 + x_2$ where x_1, x_2 are the distances of the two mirrors from the dye cell. Looking at these observations from the practical point of view, their generation can easily be visualized if we consider that at the moment of the bleaching of the dye, two pulses (the travelling pulses of light approach[129]) are crossing the dye travelling in opposite directions. Under these conditions the second pulse will originate from fluctuations in the cavity, at the moment when the first pulse bleaches the dye. The pulse crossing points will therefore alternate between the points x_1 and $L - x_1$. In the case of three pulses in the cavity (dye cell at $x_1 = L/3$) two successive pulses will be meeting at these points.

Finally it must be stressed that mode-locking was most easily achieved when the dye cell was at one end of the cavity (section 8.1). In fact it can easily be seen from equation (2.31) that in this case ξ reaches its highest possible value, and it can be shown that the time it takes for the phase to reach locking condition is a minimum[52].

(2) The dye concentration. It was found that the dye concentration was not very critical. Good mode-locking could be achieved with concentrations ranging from 8:1 to 6:1. Generally the stronger the dye concentration the higher the output powers produced and the higher the pumping powers needed to produce mode-locking. For concentrations higher than

6:1, the laser was not reliable and for the majority of the cases the patterns obtained showed filamentary action. This could be explained by assuming that filaments are formed in the dye at the points where the original fluctuation radiation is stronger, whilst at the other points it is not strong enough to bleach the dye. It is expected that the same situation would arise for longer dye cells and lower dye concentrations. However, this has been a subject of much controversy and has not been tackled experimentally in the present work. It was also found that the higher the concentration, the earlier the mode-locked pulse was emitted from the time of firing the flashlamps.

(3) The pumping level. It was found that for a particular dye concentration the pumping level was critical (section 8.1). This strong dependence is due to two main factors. First, that the gain of the active medium at the time of bleaching must have a certain value and the reason for this was given in section 2.3.2; secondly, the refractive gradient effects set in the rod by the pumping radiation, greatly influence the mode-locking (see below).

(4) Aperture in the cavity. It was found that for a normal dye concentration (13:2) and pumping level (1.75 kV), the beam divergence was smaller when an aperture equal to the diameter of the laser rod was introduced in the cavity (Fig.8.1).

(5) Transverse modes and filamentary action during mode-locking. As pointed out in section 1.1 the physical state of the laser medium at the time of emission greatly affects the development of the modes. Refractive index gradients due to heating by the pumping radiation are one of the main causes for the production of transverse modes. As described above the time of emission depends on the pumping level and the dye concentration. The emission will be governed by the refractive

index distribution in the laser rod, self-focusing in the laser rod, or by the filamentary processes in the dye. Now let us consider the beam cross-sections which will be produced under different conditions.

The production of pure transverse modes was easily achieved with the present system by pumping the rod with higher powers. Fig.8.5(d) shows two typical examples of the pure transverse modes obtained. The two flashlamps were to the left and right of each picture. The most straightforward interpretation is that when the pulse train was generated, the transverse mode structure was determined by the degree of thermal distortion existing in the rod at that moment. Fig.8.5(c) shows the near and far field patterns when higher than normal dye concentration was used. This structure is characteristic of confocal resonators[131] with Fresnel number $\gg 1$ (section 1.1).

Figs.8.5(e,f) show mode structures having x,y symmetry. In solid state lasers these may be due to polarization effects occurring during pumping, or to crystal defects in the active medium.

In glasses and crystals the laser emission under Q-switched or mode-locked operation can occur in thin filaments. These result from the interaction of the intense laser beam propagating through the glass rod with the glass, producing a variation in the index of refraction. Filamentary action affects the time and spectral structure of the mode-locked pulses (section 2.3.4). There exist two likely focusing mechanisms, thermal focusing due to optical absorption and the electrostrictive focusing[132].

For thermal focusing the change of index of refraction of the glass with temperature consists of two terms, one corresponding to the change of the index at constant volume and the other corresponding to the thermal expansion and dilution of density. Heating is due to the absorption of

(a)

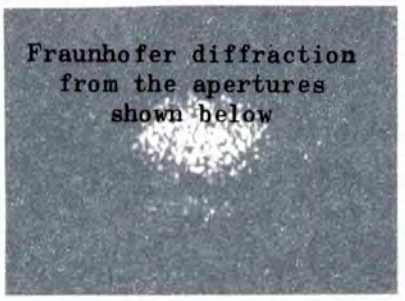

Form and distribution
of the apertures

Fraunhofer diffraction pattern from an irregular distribution of 56 identical and similarly situated apertures in a plane screen. (Reproduced from Born and Wolf 'Principles of Optics' Fig.8.15)

(b)

(e)

(c)

(f)

(d)

Pure transverse modes. 170 cm away from the output mirror

Transverse modes having x-y symmetry

Fig.8.5
Filamentary action and transverse modes
from the mode-locked Nd-glass laser

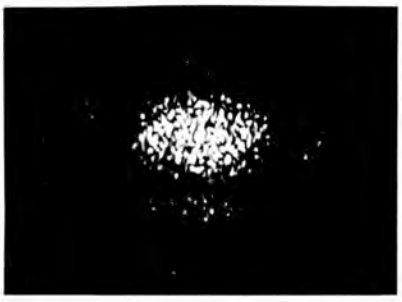

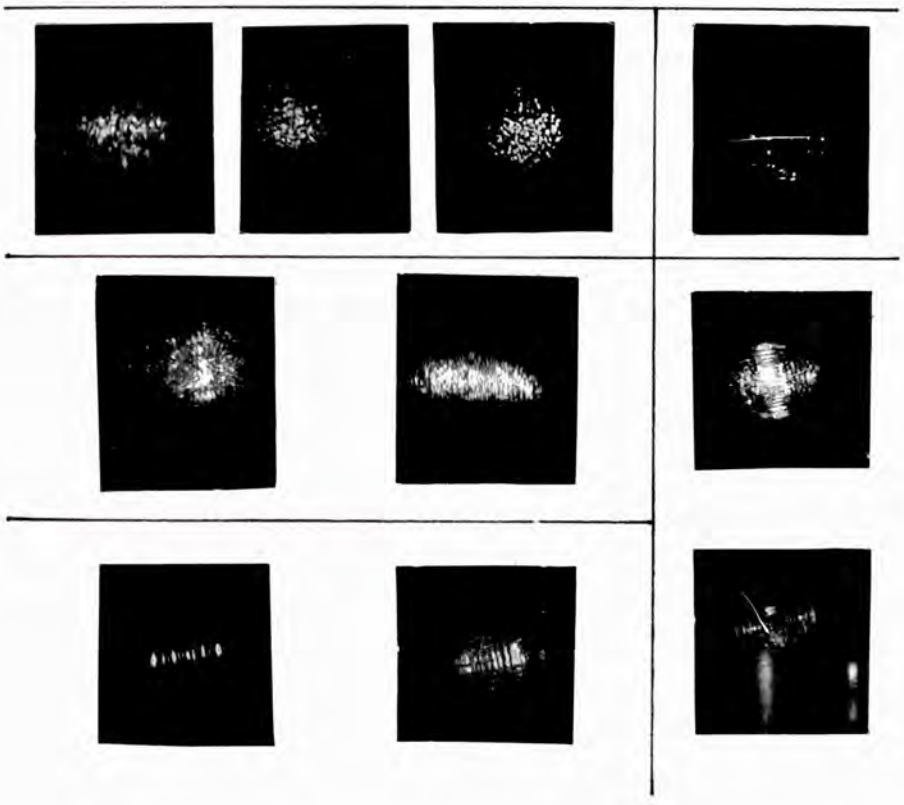

the beam as it passes through the glass, and it can be assumed that the time this occurs is so short that thermal conduction can be neglected. For a glass having an absorption of 0.1 percent/cm, a change in the index of refraction occurs of 10^{-9} per J/cm^2 [132]. In times short compared to the acoustic relaxation time, this energy dependent index of refraction change can give rise to focusing and the subsequent production of filamentary action.

Changes in the index of refraction can occur by the presence of strong electric fields interacting with the glass through electrostriction (section 2.4). For most laser glasses the electrostrictive focusing-threshold power is lower than the thermal-focusing threshold for short pulses. For very short pulses, acoustic relaxation does not take place before electrostrictive focusing occurs.

When the power density of the radiation in the filament reaches a certain threshold value, the self-focusing occurring will cause enormous increases in the energy density that will lead to damage of the laser material [133]. Repeated firings do not induce further deterioration except to produce additional tracks across the laser rod.

Figure 8.6(c) shows filamentary tracks produced in the laser rod due to filamentary action, under mode-locked conditions. The number of tracks kept increasing with increasing number of firings. The tracks shown resulted after approximately 700 firings, after which the laser rod had to be replaced. It is interesting to note that the damage was much more severe on the part of the rod nearest the output mirror. This was due to the fact that the powers of the picosecond pulses were always higher in this part of the rod due to the gain of the medium. Figs.8.6(a,b) show the two faces of the rod, and it can easily be seen that the damage on the end nearest the output mirror is much more severe than the damage on the end nearer to the 100% mirror.

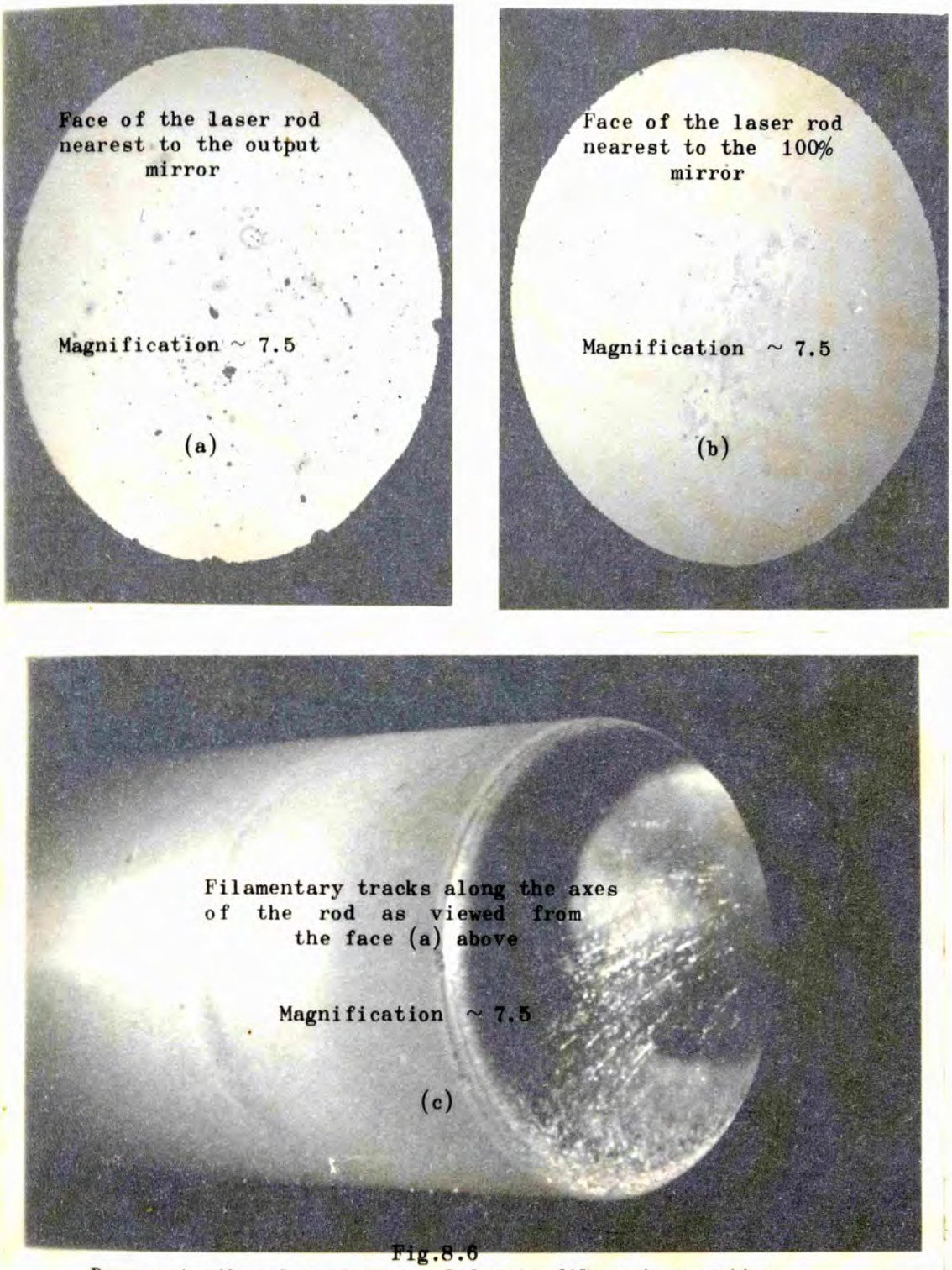

Fig.8.6
Damage to the glass laser rod due to filamentary action under mode-locked conditions. Number of firings ~ 700.

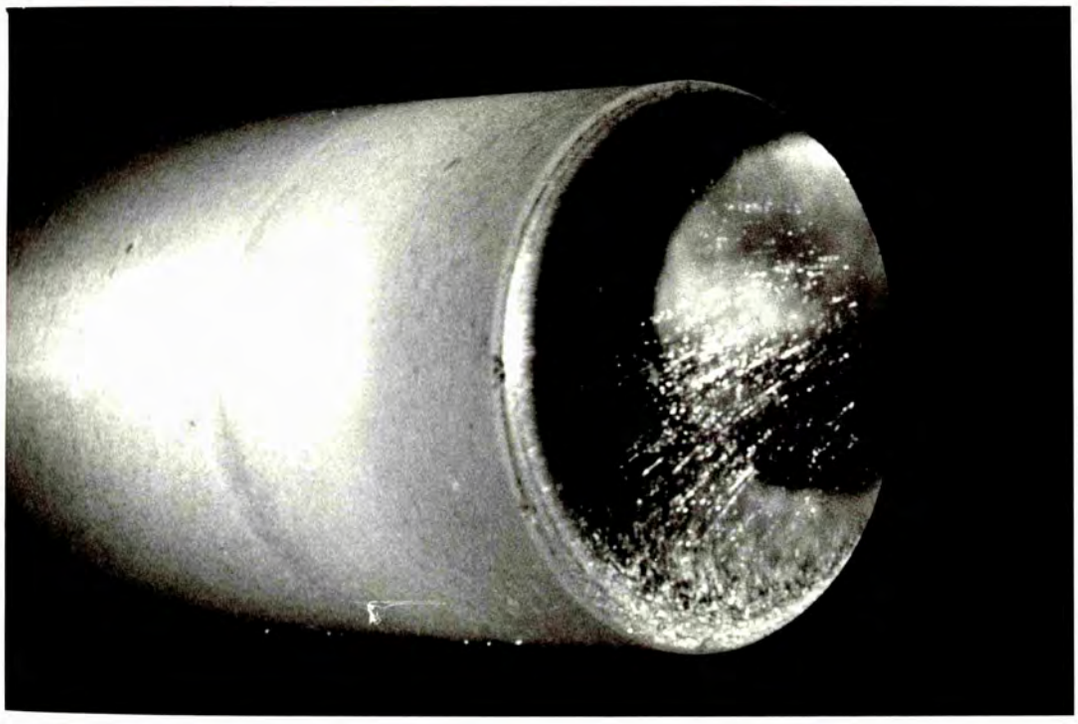

Now let us examine the far field patterns of the mode-locked laser when filamentary action takes place. Typical examples are shown in Fig. 8.5(b). In Fig.8.5(a) the Fraunhofer diffraction pattern from an irregular distribution of identical and similarly situated apertures is shown. The lower part of the picture shows the apertures. This figure is reproduced from Born and Wolf 'Principles of Optics'[134]. We now note the similarity of this pattern with the far field patterns of Fig.8.5(c). When filamentary action takes place in the laser, the output beam can be considered as emerging from a number of irregularly spaced apertures similar to those shown in Fig.8.5(a). These interfere to produce the Fraunhofer diffraction patterns shown in Fig.8.5(b).

The particular glass from which the laser rod is made has a damage threshold. For a given pulse length the damage threshold is defined on the minimum energy density of the laser beam at which a visible breakdown occurs in the glass. For pulses having duration of a few nansoeconds it has been found that the damage threshold for Schott glass is in the range of $10 \sim 30$ J/cm^2. On the picosecond scale the damage is usually caused by filamentary action as described above and the threshold is approximately 1GW. The damage thresholds for glasses set a severe problem in the development of high power glass oscillators and amplifiers[135].

8.3 MODE-LOCKING OF THE $Nd^{+3} : POCl_3 : ZrCl_4$ SYSTEM

An arrangement similar to that used for the glass laser, (section 8.1) was constructed for mode-locking the liquid laser. The liquid laser head was placed between two plane parallel reflectors with reflectivities of 100% and 55%. The cavity length was approximately 1 m long. The capacitor bank consisted of two 200μF condensers (section 5.1) which were discharged through the two xenon flashlamps giving the optical pumping pulse shown in Fig.5.4(a).

Several problems arose during the operation of this system because of the parallel faces of the laser cell (section 2.3.4). In order to avoid the reflections from the cell windows, the laser cell was slightly tilted to the laser axis. In this way mode-locked trains with period $\frac{2L}{c}$ were regularly observed and two typical oscillograms are shown in Figs. 8.8(a,b). The beam patterns to the right of each picture show beam profiles at a distance of 70 cm from the output mirror. It was found that the optimum dye concentration was 11/2 which is much higher than the concentration needed for the glass. Fig.8.8(c) shows the time it takes for the mode-locked train to be emitted after firing the flashlamps, approximately 240 μs. The optimum voltage on the capacitors was 1.6 kV. The energies of the mode-locked output ranged from 5 to 15 mJ. Fig.8.8(d) shows the mode-locked output when the dye cell was placed at L/2.

In Fig.8.7 two pictures showing the spectra of the mode-locked output are shown. It can be seen that they are much narrower (7 - 10 Å) than the spectra of the glass laser shown in Fig.8.3. This is most probably due to mode-selection by the parallel faces of the laser cell[71].

Although a complete investigation of the mode-locking of the liquid laser would require a Brewster-ended cell[136,138], attention should be paid to some of the observations made with the system described here. It was shown in section 6.1 that the introduction of a meniscus lens in the cavity of a liquid laser does not introduce any significant change in the relaxation oscillations. Here it was found that the meniscus lens did not produce any more reliable mode-locking or affect the beam patterns. Transverse modes were never observed; the beam patterns always had a uniform circular shape similar to those shown in Figs.8.8(a,b). This is attributed to the state of the liquid at the time of emission. As it will be shown in Chapter IX thermal motions have taken place in the liquid by this time, due to heating by the pumping radiation, and no local refractive

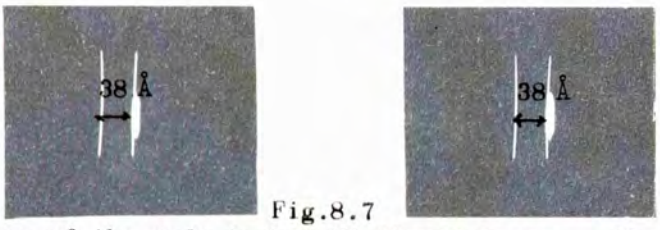

Fig.8.7
Spectra of the mode-locked Nd-liquid laser. The two lines correspond to 10520 Å (right) and 10482 Å (left)

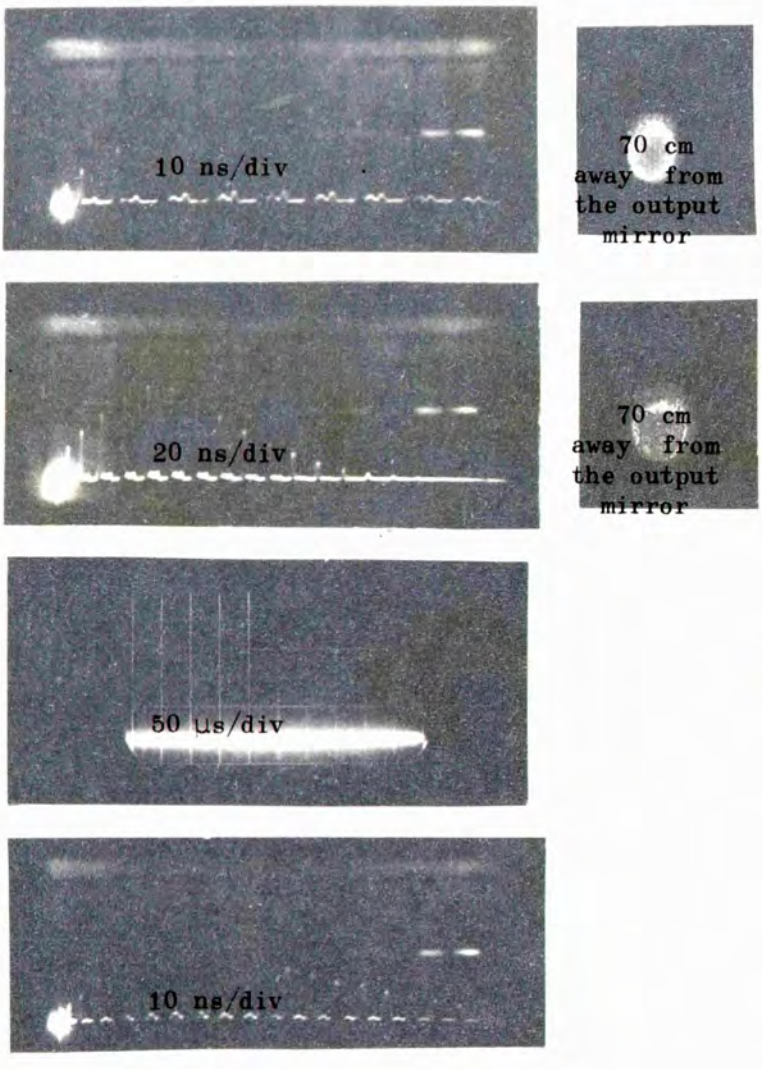

Fig.8.8
Mode-locking of the $Nd^{+3} : POCl_3 : ZrCl_4$ liquid laser

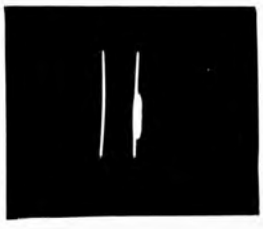

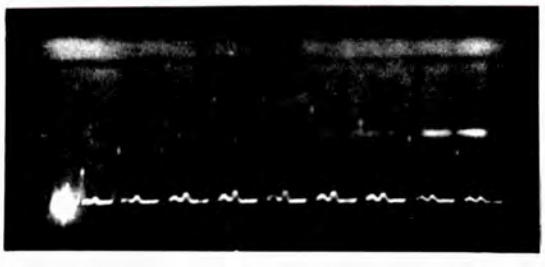

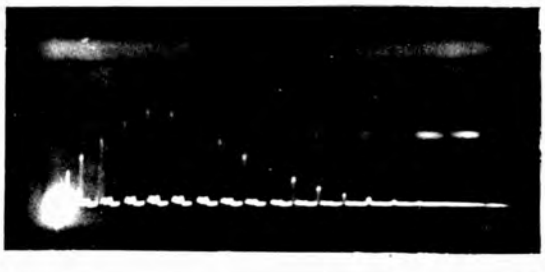

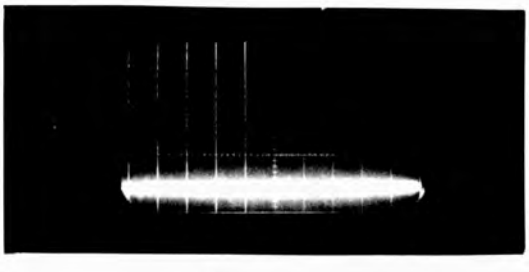

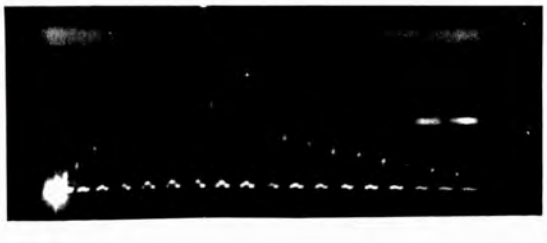

index variation exists in the active medium. The modes are scrambled together and no transverse mode structure is observed. It is to be noted that when a very small liquid laser system was mode-locked transverse modes were observed[8]. This was due to the fact that the heating by the pumping radiation produced local variations in the refractive index, but it was not strong enough to produce thermal motions because of the size of the system.

8.4 GENERAL COMMENTS

In sections 8.1 and 8.2 above, experimental details for the construction and performance of a reliable mode-locked Nd-glass laser have been given. In section 8.3 several practical problems which arise in the mode-locking of the liquid laser have been pointed out. The duration of the mode-locked pulses was measured by the two photon fluorescence method to be approximately 5 ps. It was difficult, however, to perform TPF experiments accurately because of the low powers of the mode-locked pulses.

Finally no Raman scattering could be observed from the mode-locked liquid laser system. This was due to the low powers of the pulses ($\sim$ 0.1 GW). As pointed out in section 4.5 the threshold power for stimulated Raman scattering in $POCl_3$ is approximately 0.15 GW. Thus for the powers obtained from the liquid laser there was not sufficient conversion into Raman frequencies.

Stimulated Raman scattering from mode-locked liquid lasers, twice as long as the one used here, has been observed[137,138] at a wavelength of 11105 Å (488 cm^{-1} shift). The peak powers obtained from these systems were approximately 1 GW.

CHAPTER IX

AMPLIFICATION OF MODE-LOCKED TRAINS WITH A LIQUID LASER AMPLIFIER $Nd^{+3} : POCl_3 : ZrCl_4$

9.1 INTRODUCTION

In this chapter the performance of the $Nd^{+3} : POCl_3 : ZrCl_4$ liquid system as an amplifier is described. Picosecond pulses of measured width 5×10^{-12} s generated by an Nd-glass oscillator were used as the input signals. Serious limitations on the observed gain are imposed by the fact that there is a mis-match between the spectrum of the input signals and the amplifier linewidth. The spectrum of the input signals is centred at 1.058 μm (Fig.8.3); the linewidth of the amplifier is centred at 1.052 μm (Fig.4.4). Several parameters of the liquid laser medium are measured directly (gain, stimulated emission cross-section, passive loss), and the problems associated with the operation of this system are described. Saturation effects occurring in light amplifiers (Chapter III) were observed when mode-locked trains with total energy more than approximately 50 mJ were used. The high intrinsic gains obtained, together with the ability of the active medium to be circulated and the fact that the active medium is free from damage problems, make the $Nd^{+3} : POCl_3 : ZrCl_4$ system a serious competitor in the field of high power amplifier development. An assessment of the results is given at the end of this chapter.

9.2 EXPERIMENTAL ARRANGEMENT AND METHOD OF MEASURING THE GAIN

The experimental arrangement is shown in Fig.9.1. A reliable mode-locked Nd-glass oscillator was constructed as described in section 8.1. Mode-locked trains with energies between 30 and 80 mJ were readily obtainable. The first two pictures at the top of Fig.9.16 show typical beam cross-sections at a distance 1.9 m from the output mirror. The divergence was estimated to be less than 2 mrad (section 8.1). The third

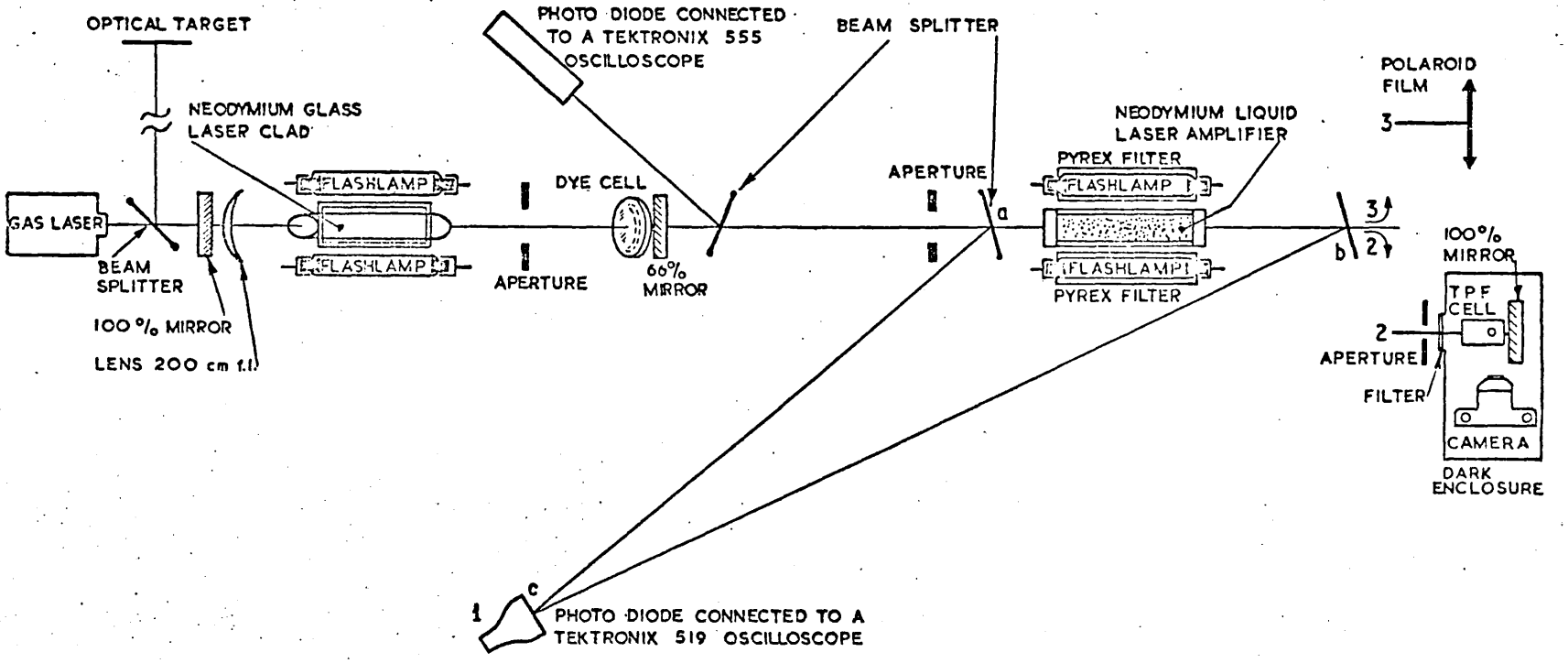

Fig.9.1 AMPLIFICATION OF MODE-LOCKED PULSES WITH A NEODYMIUM LIQUID LASER AMPLIFIER

1. measurement of gain
2. measurement of pulse width
3. observation of beam burn patterns on developed unexposed (Polaroid) film

picture at the top of Fig.9.16 shows the central part of the beam cross - section equal to the amplifier diameter which was selected for amplification by the aperture shown in Fig.9.1. The output characteristics of the mode-locked oscillator were reproducible up to thirty times in succession before any deterioration in the quality of the beams could be observed.

The amplifier head (Fig.5.2) was placed 2 m away from the output mirror of the oscillator and the whole arrangement was aligned with a He-Ne gas laser placed behind the oscillator. The time between triggering the oscillator and the amplifier was controlled with a delay box following the trigger unit. A beam splitter-photodiode arrangement at the exit of the oscillator recorded the time at which the mode-locked train was emitted after firing the oscillator. This was recorded on a Tektronix 555 oscilloscope. Since the relative time between firing the oscillator and the amplifier was known from the delay box, the time at which the mode-locked train passed through the amplifier after firing the flashlamps was readily obtained. An aperture was placed in front of the amplifier to select a beam cross-section equal to the internal diameter of the amplifier.

Energy measurements were made with the TRG 107 cone calorimeter connected to a microvoltmeter (section 5.1). Two photon fluorescence (TPF) measurements were performed with a cell 48 mm long and 25 mm wide containing Rhodamine 6G diluted in acetone. The TPF profile was recorded on HP 4 film using an Exackta VX1000 camera equipped with a Biotar f 1.5/75 mm lens. The arrangement was placed in a dark enclosure with a red filter window to avoid light from the amplifier flashlamps.

The photodiode-oscilloscope arrangement described in section 5.4 was used to record the two interpenetrating mode-locked trains of the experiment. The input and output signals were reflected on to the

photodiode connected to the Tektronix 519 oscilloscope with the aid of two beam splitters a and b placed before and after the amplifier so that the E-vector of the main beam was perpendicular to the plane of incidence (Fig.9.1).

The arrangement was fired at intervals of at least 15 min to avoid the distortion effects taking place in the liquid due to heating by the pumping radiation.

The method employed in measuring the gain of the liquid amplifier involved the recording of two interpenetrating mode-locked trains. The beam splitters a and b (Fig.9.1) were placed in the main beam with angles of incidence $28^{\circ}\ 54' \pm 30'$ and $13^{\circ}\ 40' \pm 30'$ respectively, the E-vector being perpendicular to the plane of incidence. The reflection coefficients for these angles were calculated to be $R_{N_1} = 0.117 \pm 2.8\%$ and $R_{N_2} = 0.089 \pm 2.4\%$ respectively, where the subscript N denotes an incident beam with the E-vector perpendicular to the plane of incidence. The optical path lengths were adjusted so that $ab + bc - ac < 2L$, where L is the length of the oscillator. In this way the input and output signals are recorded as two interpenetrating mode-locked trains with each output pulse directly following the input pulse.

The oscillator was first fired several times without firing the amplifier. The recorded mode-locked trains gave us the normalization of the amplifier-beam splitter arrangement allowing for the difference in the reflectivities of the two beam splitters, the reflections from the cell windows and the passive loss of the medium. All measurements taken when the amplifier was fired were normalized to this ratio to give the intrinsic gain of the amplifying medium.

The heights of the pulses on the oscilloscope were proportional to the energy of the pulses. The photodiode was calibrated against a calori-

meter for the angle of incidence of the first beam splitter. Calorimeter readings, however, involved errors of up to 20%. Thus only approximate values for the energies could be estimated.

It is important that a Brewster-ended oscillator is used so that the signals are only of one polarization (in this case the E-vector is normal to the plane of incidence). This keeps the ratio of the reflectivities of the two beam splitters constant for all measurements.

It can readily be seen that the change in the ratio of the reflectivities is insignificant even for large changes in polarization. If f is the fraction of the incident light with normal vibrations, the effective reflectivity of each beam splitter is

$$R(f,\delta_i) = f\ R_{N_i} + (1-f)\ R_{P_i} \qquad i = 1,2 \qquad \ldots\ (9.1)$$

where the subscripts N and P denote normal and parallel polarization to the plane of incidence respectively. For a particular angle this expression is linear in f as f changes from 0 to 1. Fig.9.2 shows the variation of the reflectivity with f for two different angles δ_1

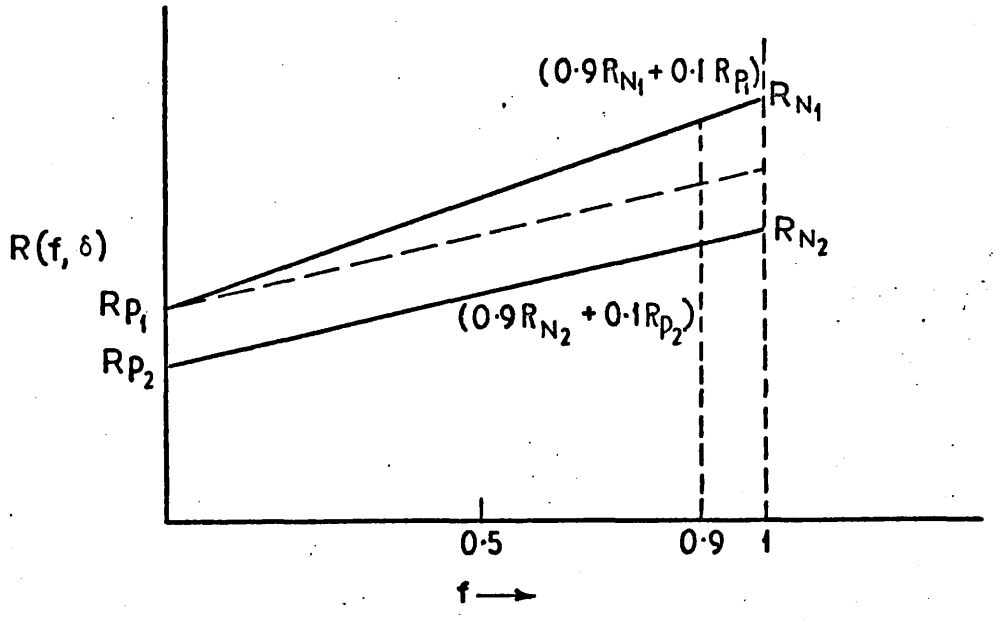

Fig.9.2
Variation of the reflectivity with polarization for two different angles δ_1 and δ_2. By drawing a line (broken) parallel to one of the lines it can be seen that the ratio of the reflectivities lies between the limits R_{P_1}/R_{P_2} and R_{N_1}/R_{N_2}.

and δ_2. Even if we assume that there is a change in polarization of 10% from normal polarization for different firings, then the ratio of the reflectivities will lie between the values R_{N_1}/R_{N_2} and

$$\frac{(0.9\ R_{N_1} + 0.1\ R_{P_1})}{(0.9\ R_{N_2} + 0.1\ R_{P_2})} .$$

For the particular angles used in the experiment these take the values 1.305 and 1.25 respectively, or a maximum change in the ratio of the reflectivities of 4%. In practice the error due to changes in polarization was much less than this since a Brewster-ended oscillator was used in these experiments. The normalization pictures showed that there was no change in the ratio of the reflectivities. All normalization pictures showed the same ratio for all the pulses. The only error in the measurements occurred in measuring the heights of the pulses.

The amplification of the profile of the mode-locked train is analogous to the amplification of a giant pulse of the same shape. Thus pulse sharpening effects are expected to occur (sections 3.2,3.3). A large amplification occurs in the leading pulses of the train. In the experiments described here it can be assumed that no significant changes in the population inversion occur due to the pumping radiation since the mode-locked trains were less than 70 ns long. After a certain amount of energy is passed through the amplifier, the gain is expected to deviate substantially from exponential form since the latter part of the amplifying medium is depleted more than the first part after each pulse passes through.

The accumulated input energy is the sum of the energies of all the input mode-locked pulses. The accumulated output energy is the sum of all the output mode-locked pulses. The instantaneous gain is the gain of a single pulse at any point along the train. Graphs can therefore be plotted showing the variation of the instantaneous gain with input and

output energy. The graphs are also analogous to graphs showing the output signal against time if a step function input signal is applied[87] as described in section 3.3.

The integrated gain is the ratio of the accumulated output energy to the accumulated input energy. This can be found from a graph of the accumulated input energy plotted against the accumulated output energy. The variation of the integrated gain with the input and output energies can then be plotted.

9.3 EXPERIMENTAL MEASUREMENT OF THE GAIN FOR SMALL INPUT PULSES

Figure 9.3 shows typical measurements of the gain of the liquid laser amplifier in the small-signal case; that is, when there is no drop in gain due to population depletion along the mode-locked train. Figs. 9.3(a,b) show the ratio of the photodiode signals when the amplifier is fired.

Figure 9.3(c) shows the normalization of the amplifier arrangement, that is, the photodiode signals when the amplifier is not pumped. A plot of all the ratios on a typical normalization picture is shown in Fig.9.4. The normalization procedure was carried out before any set of measurements was taken. In all cases it was found to be constant with a value of 0.58 ± 2%. Using the calculated reflection losses and the above normalization ratio the transmission loss of the unpumped liquid was estimated to be (0.5 ± 0.2)% per cm (Fig.9.4). This value is slightly higher than that reported by Brecher et al[105] (section 4.3). This slightly higher value may have its origins in the use of picosecond pulses for measuring the transmission losses and it is discussed in the final section of this chapter.

The intrinsic gain of the amplifier for a particular pumping energy and time delay after firing the flashlamps is found by dividing the ratio

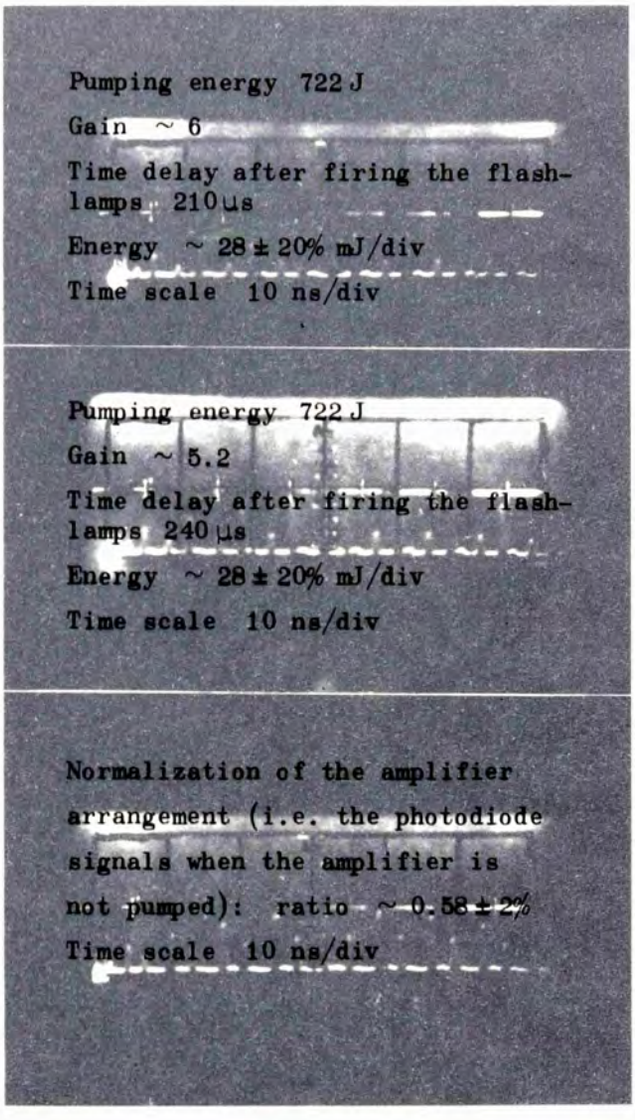

Fig.9.3
Amplification of mode-locked pulses with a liquid laser amplifier

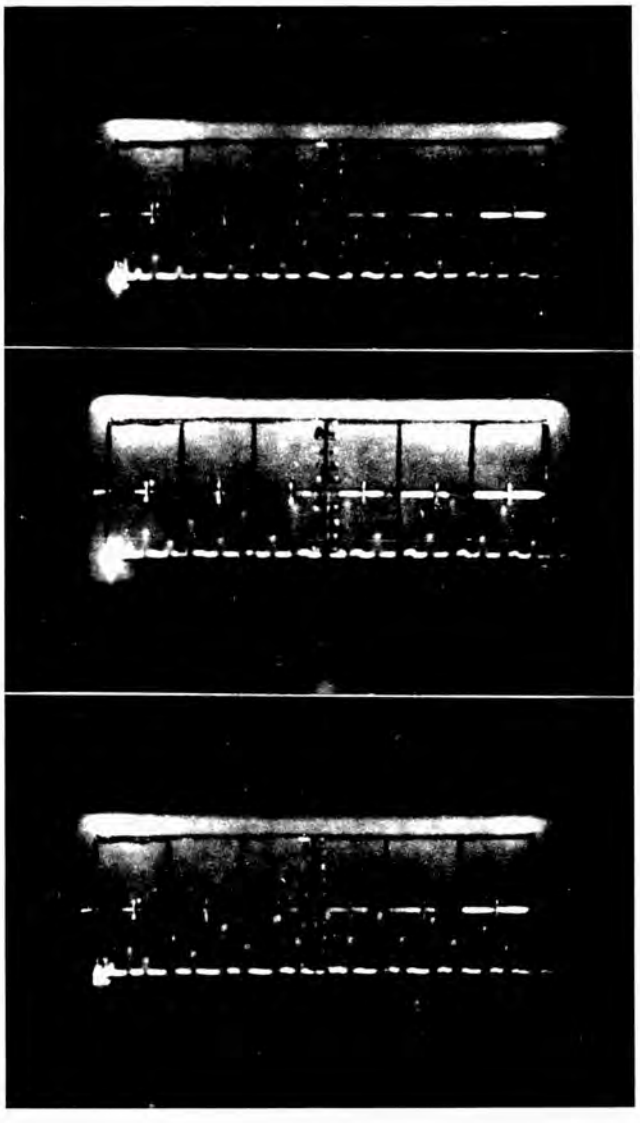

shown in any of the top two pictures of Fig.9.3 by the normalization shown in Fig.9.4. The experimental conditions for each picture in Fig. 9.3 are described in the captions. Gains of 9 were obtained in this way in the small-signal case.

Fig.9.5 shows the gain of the liquid laser amplifier as a function of the time delay after firing the flashlamps for three different pumping energies, 968J , 722J and 512J. All measurements taken lie near the curves shown. The points plotted represent a few typical measurements. The light pumping pulse is shown at the top of each curve. A point of practical interest is that the light pumping power is not exactly proportional to the electrical input energy. This is easily found by measuring the areas under the light pumping pulses of Fig.9.5, and comparing them to the corresponding electrical input energies shown on the figure. This may be due to a change in the electrical resistance of the flashlamps at higher voltages and subsequent improvement of the matching of the parameters of the electrical circuit.

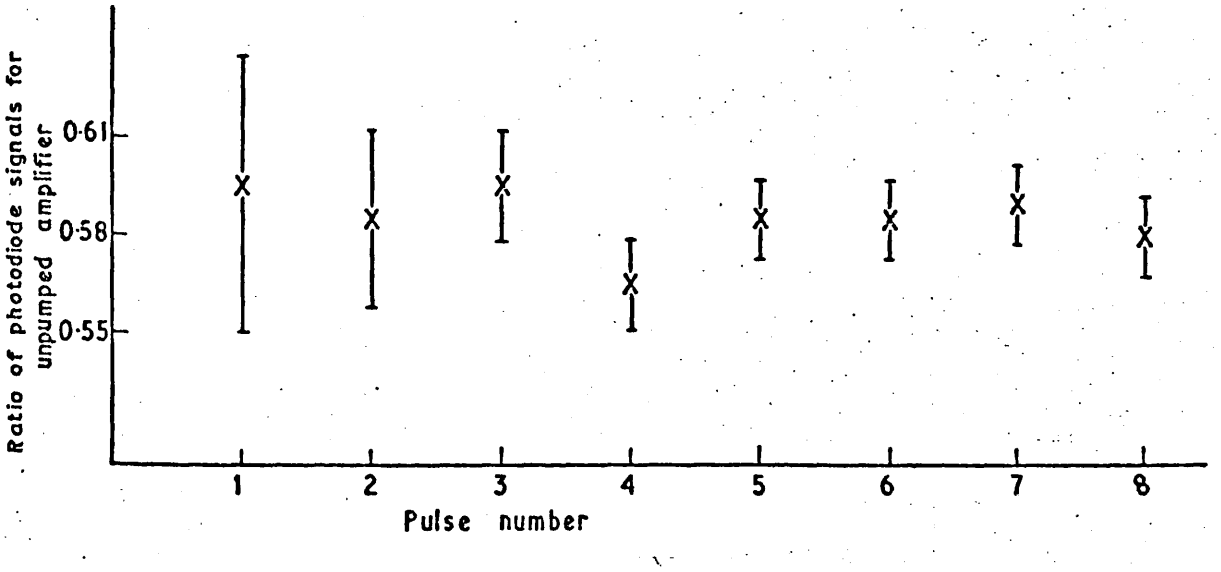

Fig.9.4
Measurement of the transmission losses of the liquid laser amplifier using a mode-locked pulse train.
Intrinsic transmission of the liquid laser=observed value(above)×(1.58±0.03).
Power of each mode-locked pulse ~ $(0.5-1) \times 10^9$ watts
Variation ~ 2%

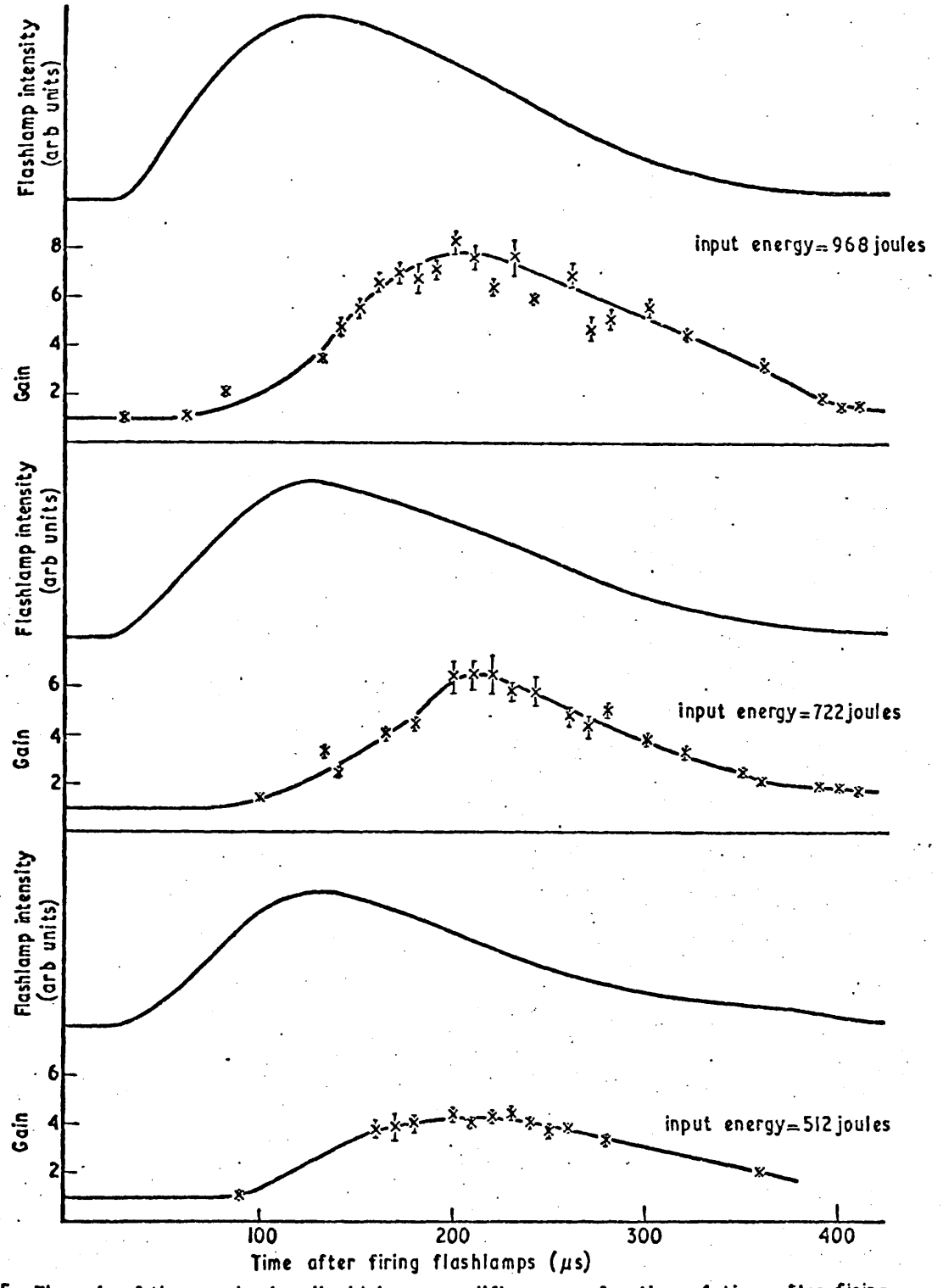

Fig. 9.5 The gain of the neodymium liquid laser amplifier as a function of time after firing the flashlamps for three different pumping energies. The flashlamp intensity in each case is shown at the top of each picture

It can be seen that the maximum gain occurs 205 μs after firing the flashlamps. Note the agreement of this result with the results of Chapter VII, particularly Fig.7.4, when the system was used as a Q-switched oscillator. The time taken for the population inversion to reach a maximum is longer than the time taken for the pumping pulse to attain its maximum intensity, and is less than the fluorescence lifetime of the material (~300 μs). The results shown in Fig.9.5 show similar behaviour to the characteristics of Nd-glass amplifiers obtained with different experimental methods[139].

9.4 MEASUREMENT OF THE PULSE WIDTH

Delineation of the pulse width was made by a standard two photon fluorescence method as shown in Fig.9.1. The pulses were reflected back on themselves using a 100% mirror (section 2.3.3) and the separation of the two photon fluorescence bands was equal to the effective thickness of the output mirror of the oscillator 60 ps. The measurements indicated pulse widths of 5 ps. Typical TPF pictures obtained are shown in Fig.9.6. It can easily be seen from the pictures on this figure that the left-hand side band is weaker than the first band. This could arise as a result of the energy loss occurring in the previous bands.

The contrast ratio of the TPF bands to the background intensity was measured by attaching a strip of neutral density filter of known contrast ratio, to the side of the TPF cell at the point where the first TPF band occurs. Typical TPF pictures taken in this way are shown in Figs.9.6(b,d). Since the contrast ratio of the filter is known, the contrast ratio of the TPF band to the background intensity is readily obtainable from microdensitometer traces of the picture. Fig.9.8 shows a microdensitometer trace of the TPF picture 9.6(d). The step defines a contrast ratio of 2.2. The contrast ratio for the pulse is seen to be 1.7. This value is in good agreement with the values reported by Bradley et al[130], who

(a)

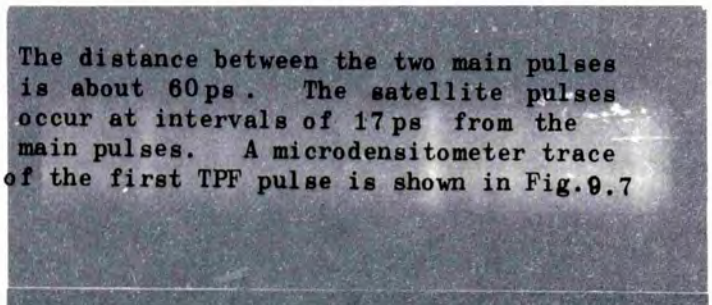

(b)

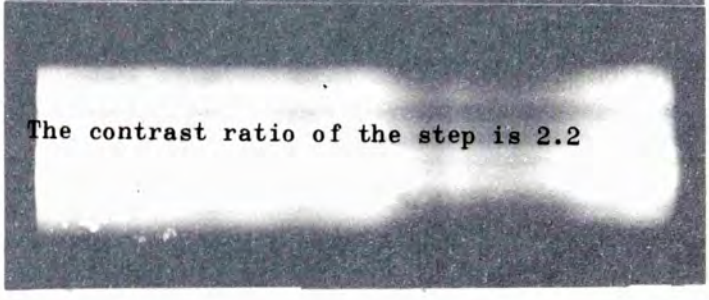

(c)

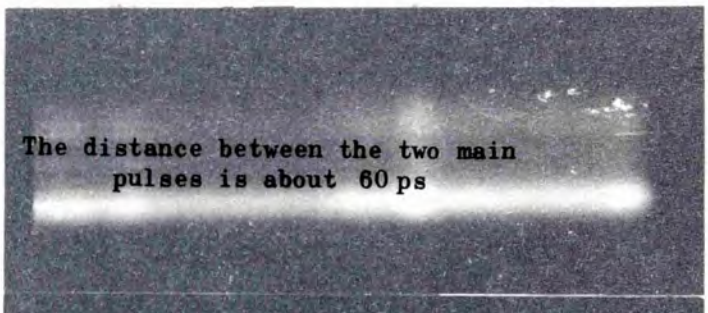

(d)

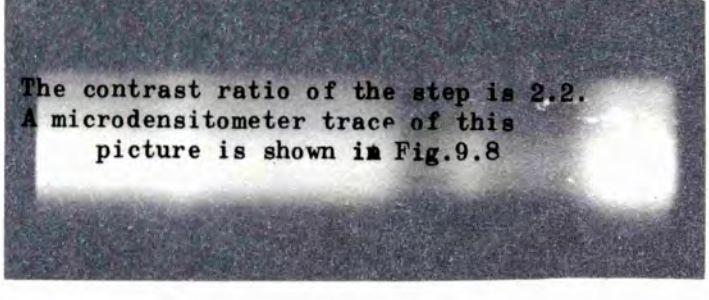

Fig.9.6
Two photon fluorescence pictures. The 100% mirror is to the right of each picture

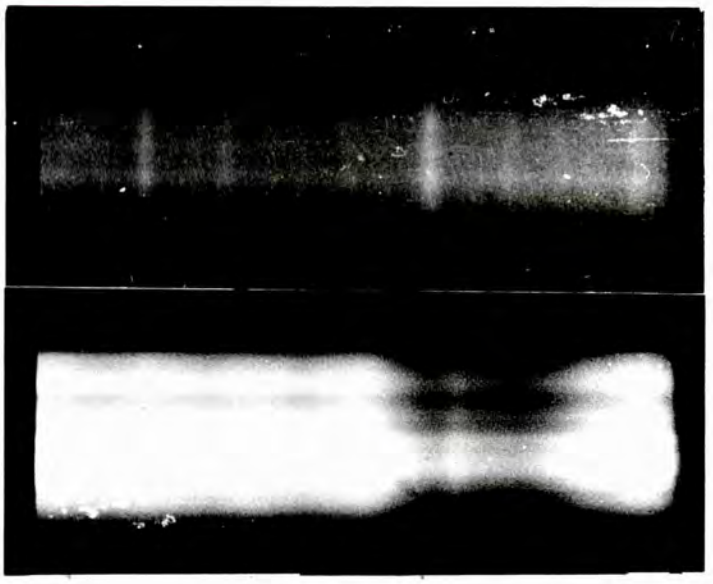

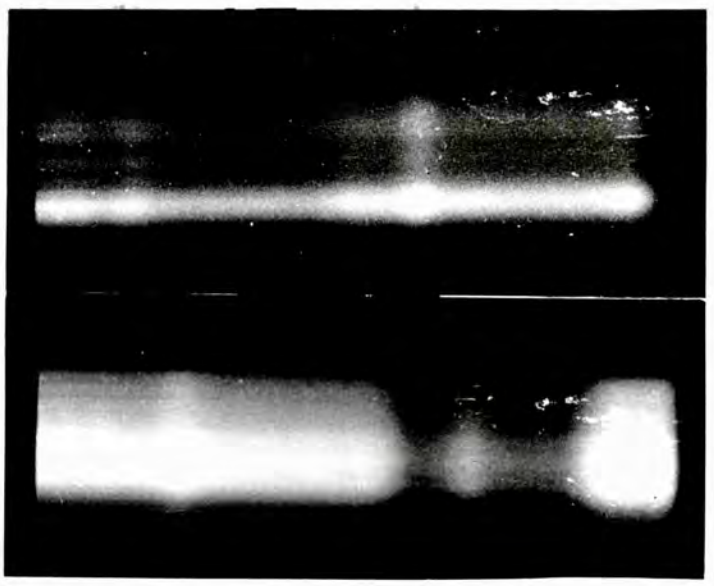

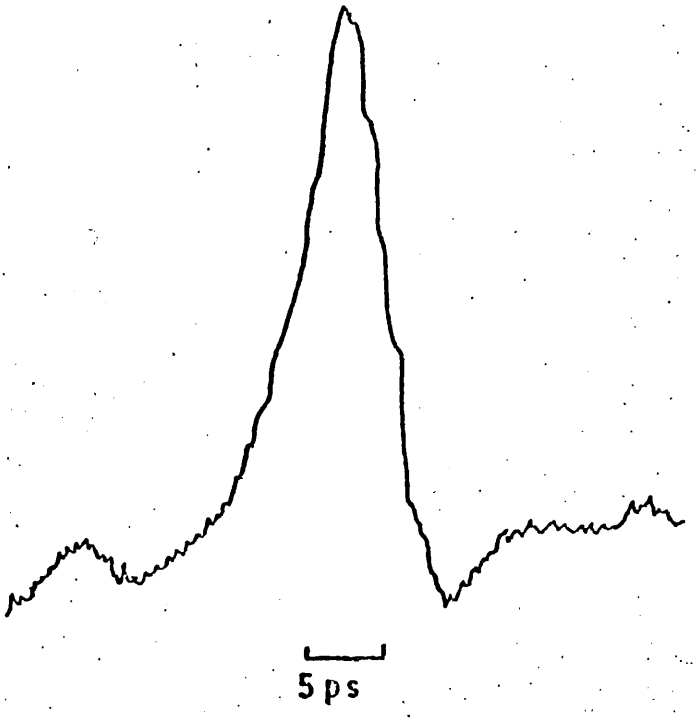

Fig.9.7
Microdensitometer trace of the first TPF pulse
in Fig.9.6(a); half width ~ 5 ps

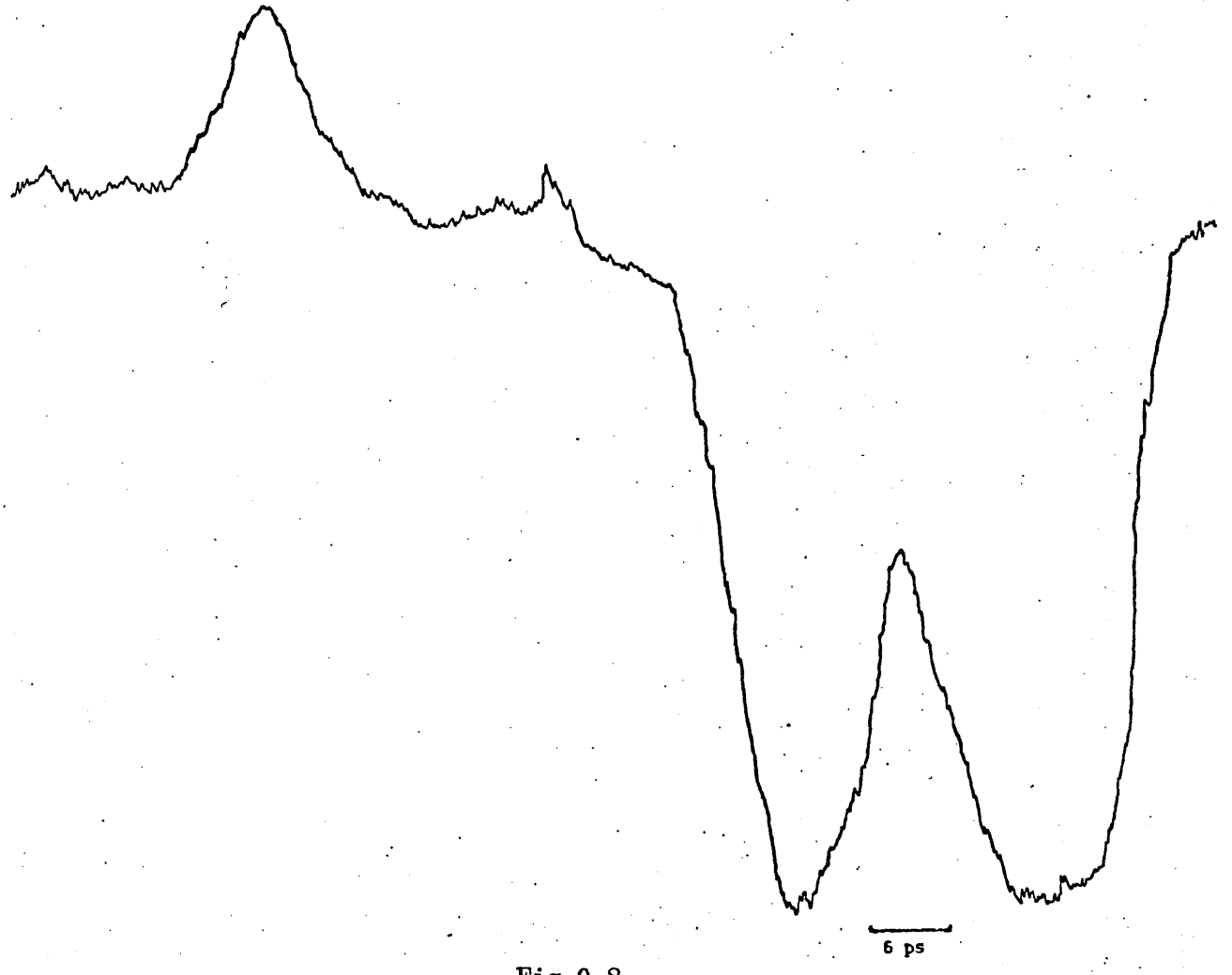

Fig.9.8
Microdensitometer trace of the TPF picture of Fig.9.6(d).
The step defines a contrast ratio of 2.2.

have also shown that the contrast ratio is much higher when the triangular method is used for two photon fluorescence measurements, instead of the direct reflection off a mirror. The significantly different values observed for the contrast ratios in the two cases were attributed to the pulses containing random fluctuations on a picosecond timescale.

A microdensitometer trace of the first pulse of Fig.9.6(a) is shown in Fig.9.7. The TPF measurements indicated that the pulses used for amplification had powers of approximately 10^9 W. Consequently the amplified pulses had powers of approximately 8×10^9 W.

It is important to note the weak satellite pulses on either side of the main pulses in Fig.9.6(a). These are symmetric about the main pulses and occur at intervals of 17 ps. Similar pulses were reported by Giordmain et al[55]. A theory which accounts for the origin of these pulses was derived in section 2.3.3. Note the agreement of the theoretical results with the experimental results of Fig.9.6(a). The first pair of satellite pulses have approximately 1/8 the intensity of the main pulse.

At times the satellite pulses had intensities comparable to the main TPF pulses. In these cases the contrast ratio was lower than that reported above for good TPF pictures. For some of the pictures multiple pulses occurred at regularly spaced intervals. Some typical examples of these pulses are shown in Fig.9.9. In general however, the TPF measurements made in this section are in good agreement with the results described in references 51, 55 and 130.

9.5 THE INPUT-OUTPUT CHARACTERISTICS OF THE LIQUID AMPLIFIER

When the energy content of the mode-locked trains was high, population depletion effects could be observed. Three pictures showing population inversion depletion effects are shown in Fig.9.10 for three different initial population inversions. The experimental conditions for each

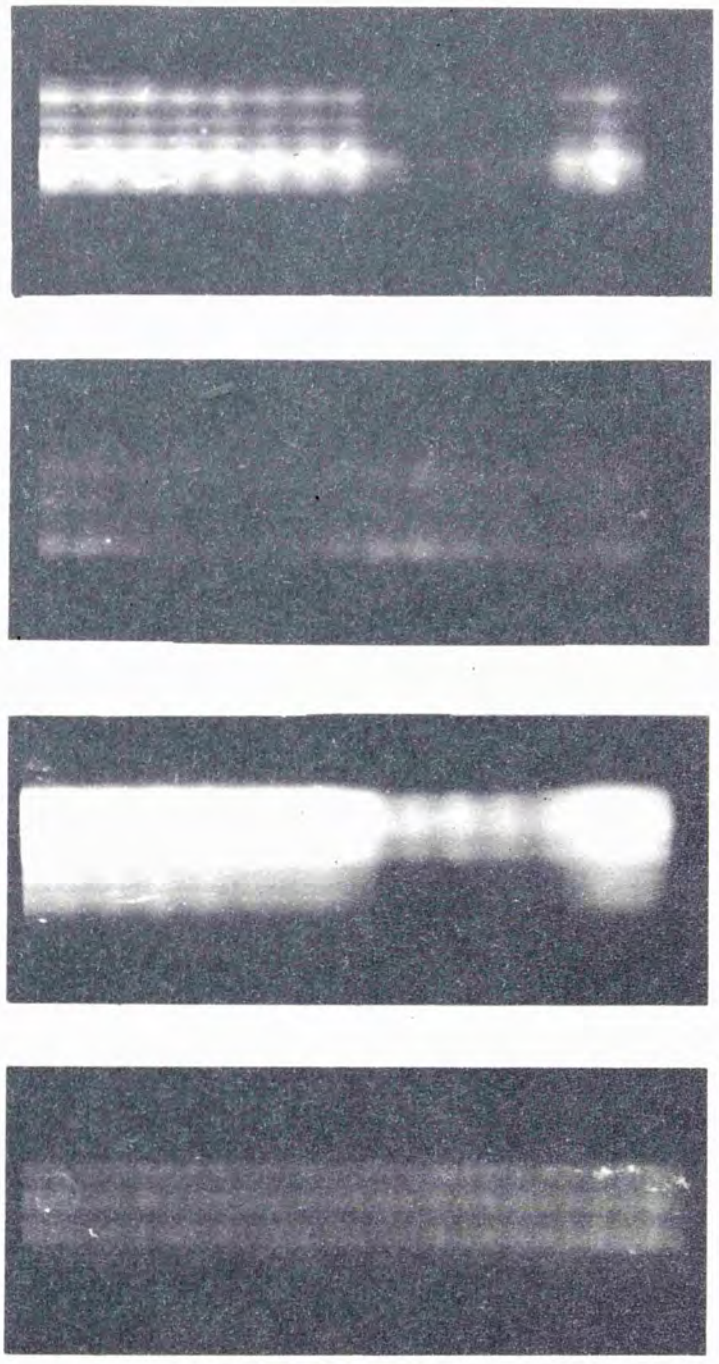

Fig.9.9
Multiple two photon fluorescence patterns attributed to strong frequency modulation within the picosecond pulses

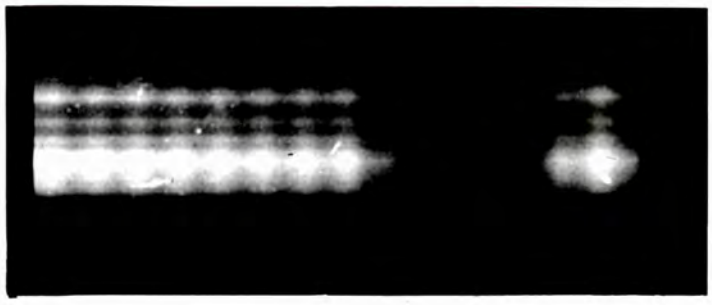

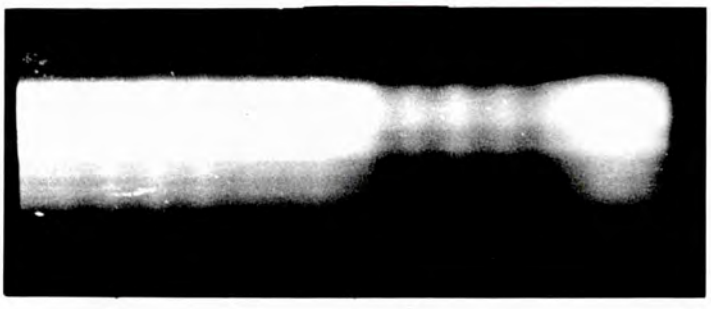

picture are described in the caption. The normalization for all three pictures is 0.58 ± 2%. It can readily be seen that the gain of the amplifier starts at a high value and falls as the successive pulses pass through it. This non linear behaviour depends on the population depletion brought about by the energy requirements of previously amplified pulses. It can be assumed that the contribution of the pumping pulse to the population inversion during the passage of the mode-locked train through the amplifier can be neglected. Population depletion effects were readily observable when energies greater than 50 mJ passed through the amplifier. Results similar to those shown in Fig.9.10 enabled the investigation of pulse sharpening and gain saturation effects in the liquid laser. These are described below.

The gain of the amplifier depends on the population inversion at any instant. Hence the small-signal gain depends on the energy of the previous signals which have passed through the amplifier. It is therefore meaningful to plot the instantaneous gain - that is the ratio of the signal of an output pulse to the corresponding input pulse - against the sum total of the energies of all the input pulses previous to the one under consideration. The graphs in Fig.9.11 show the fall of the instantaneous gain with accumulated input energy for four different initial population inversions. The results plotted here are in good agreement with the theoretical considerations of section 3.2, and in particular note that the fall is steeper for high initial gains and it smooths out for small gains. Also note the similarity of these graphs with the results of reference 87 where a step function input signal was applied.

Figure 9.12 shows the variation of the instantaneous gain with accumulated output energy for the same experimental conditions as in Fig.9.11. The results are similar to those for the accumulated input energy.

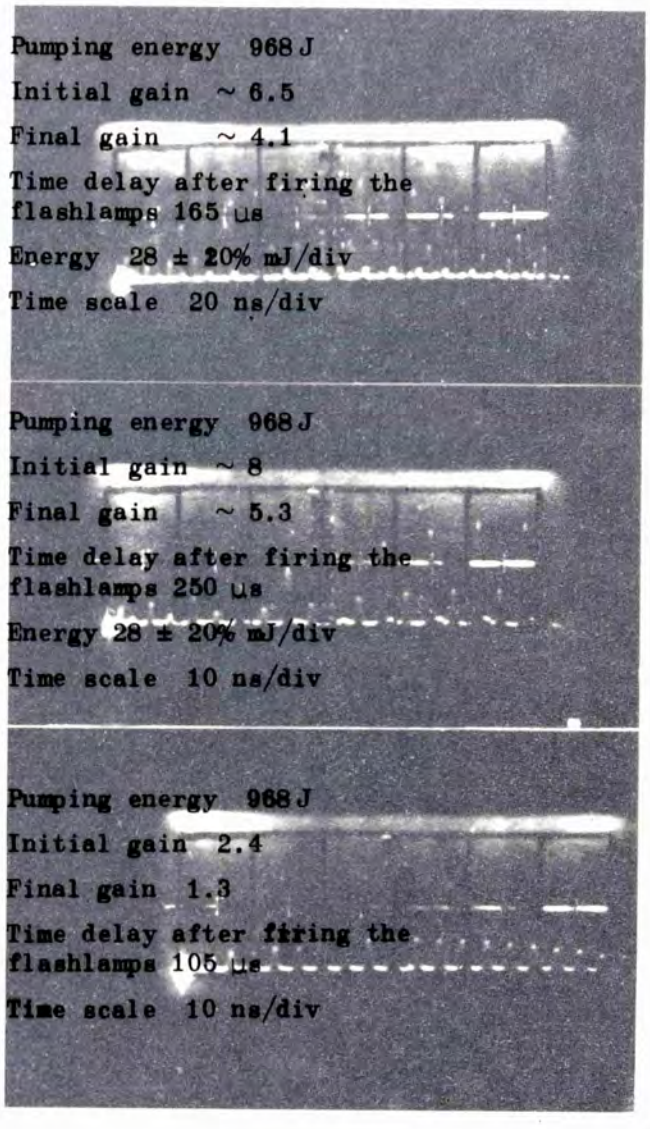

Fig.9.10
The depletion of the population inversion for three different initial population inversions. The normalization for all three pictures is 0.58 ± 2%

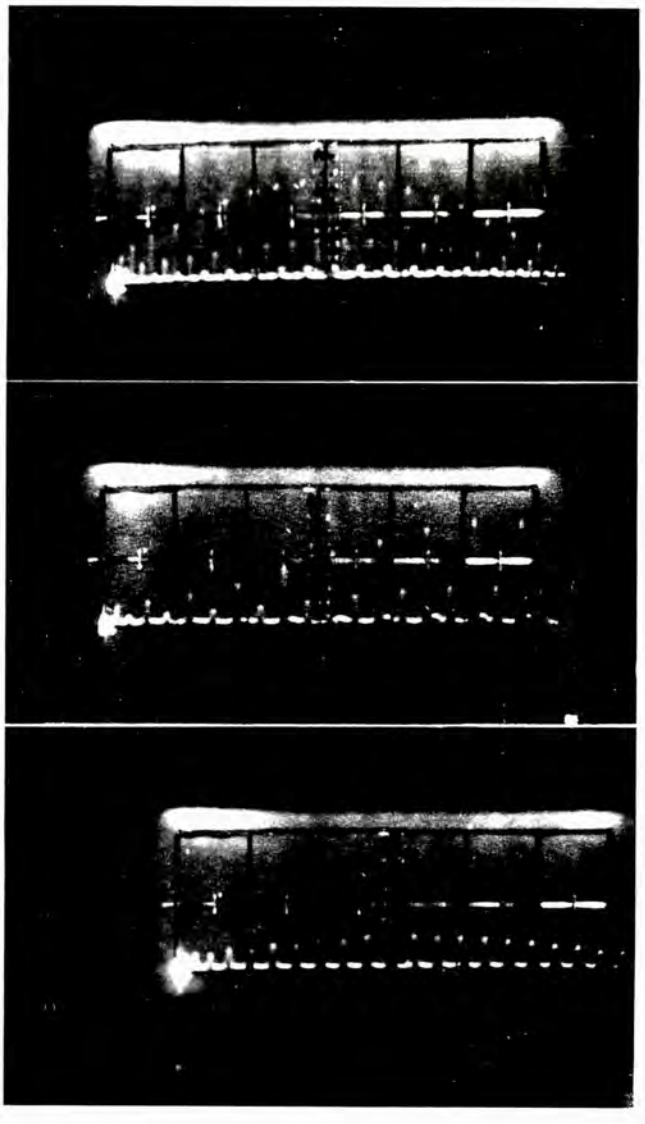

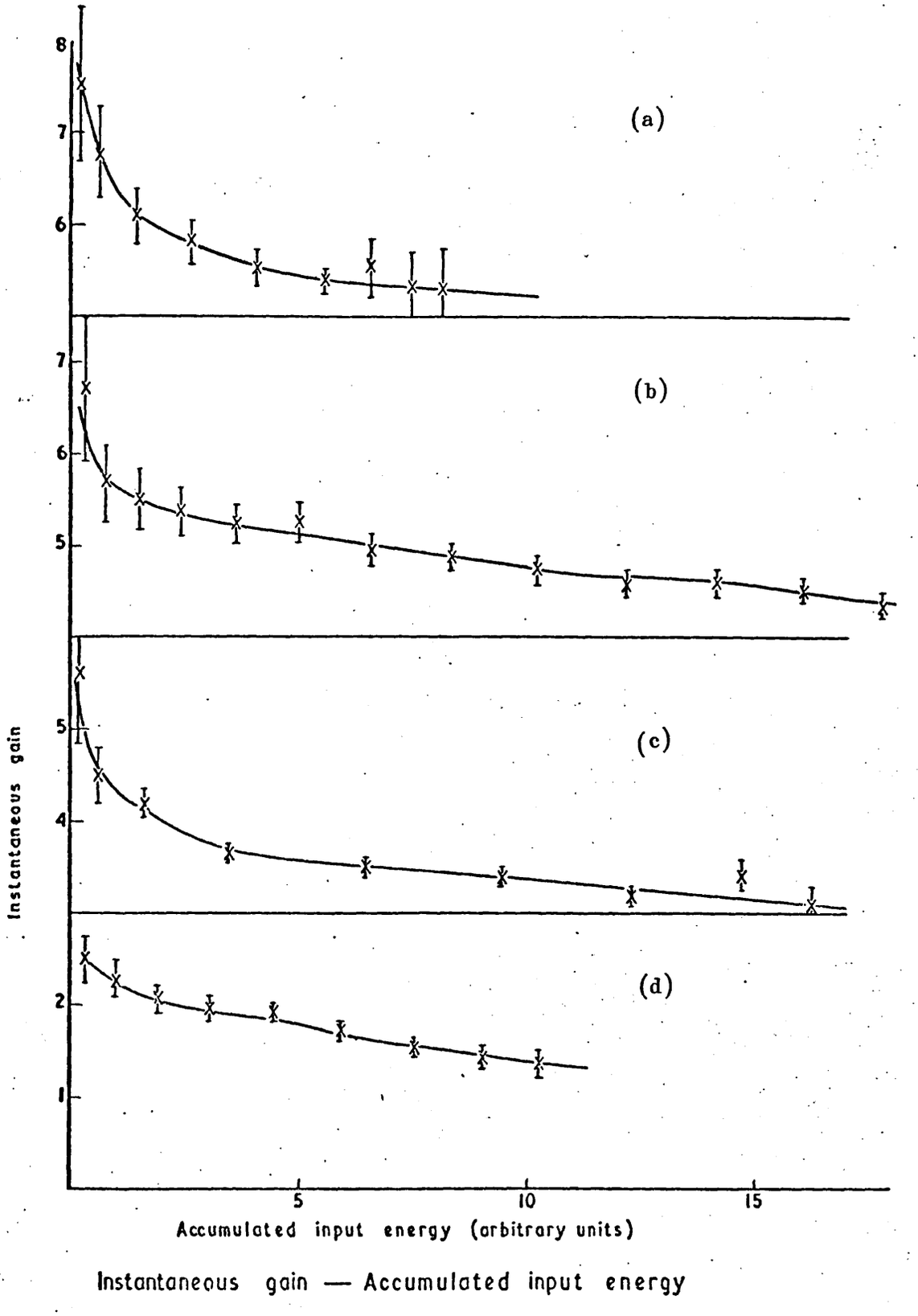

Fig.9.11

The instantaneous gain plotted against the accumulated input energy for four different initial population inversions. The second graph corresponds to the first picture in Fig.9.10.The true values of the energy are the units shown multiplied by a factor 7 ± 20%mJ. (a) flashlamp input energy 968J : time delay after firing the flashlamps 250μs . (b) 968J; 165 μs; (c) 968J ; 260μs. (d) 968J ; 105μs .

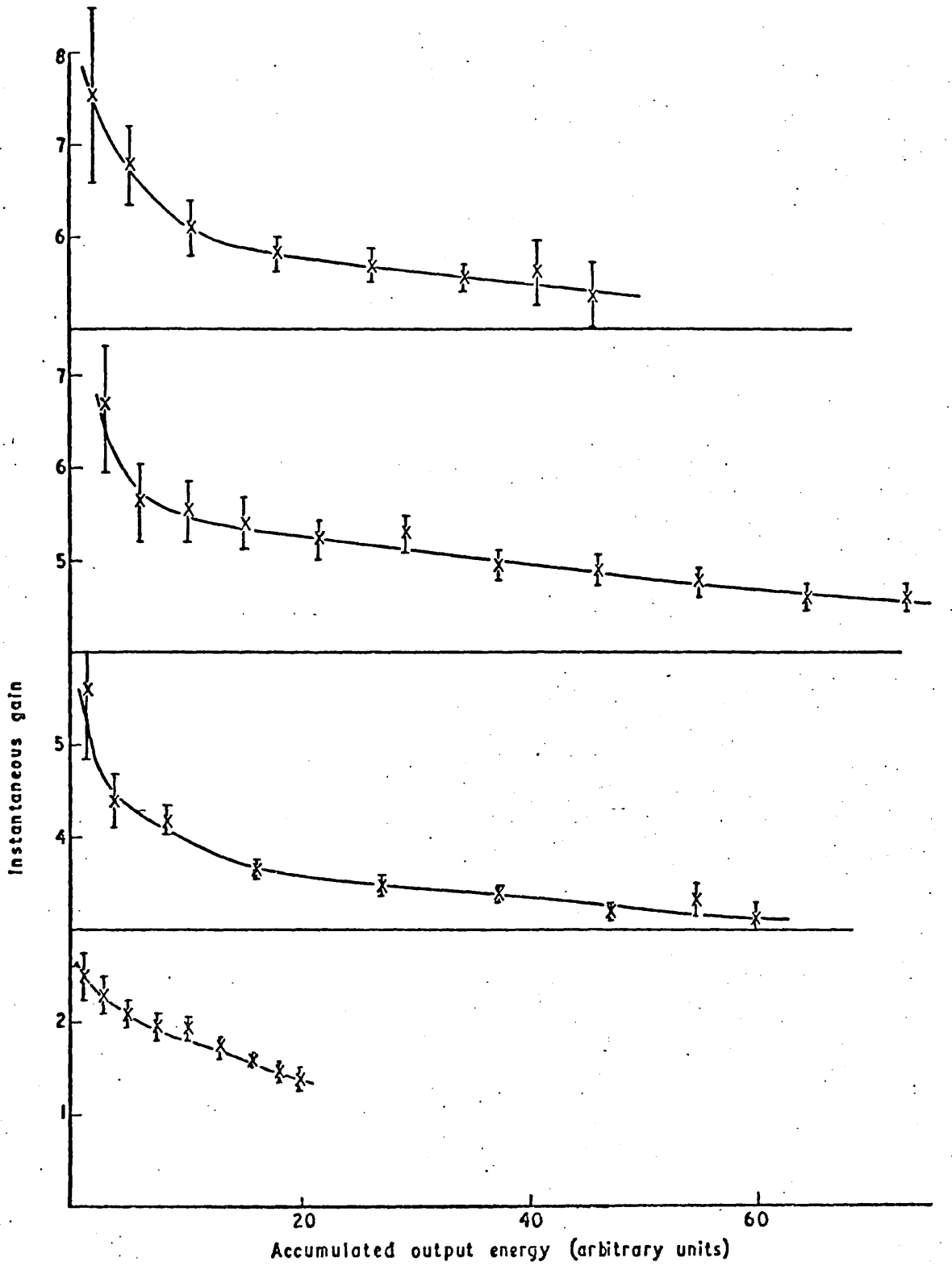

Instantaneous gain — Accumulated output energy

Fig.9.12
The instantaneous gain plotted against the accumulated output energy for the same experimental conditions as in Fig. 9.11. The true values of the energy are the units shown multiplied by a factor 7 ± 20% mJ

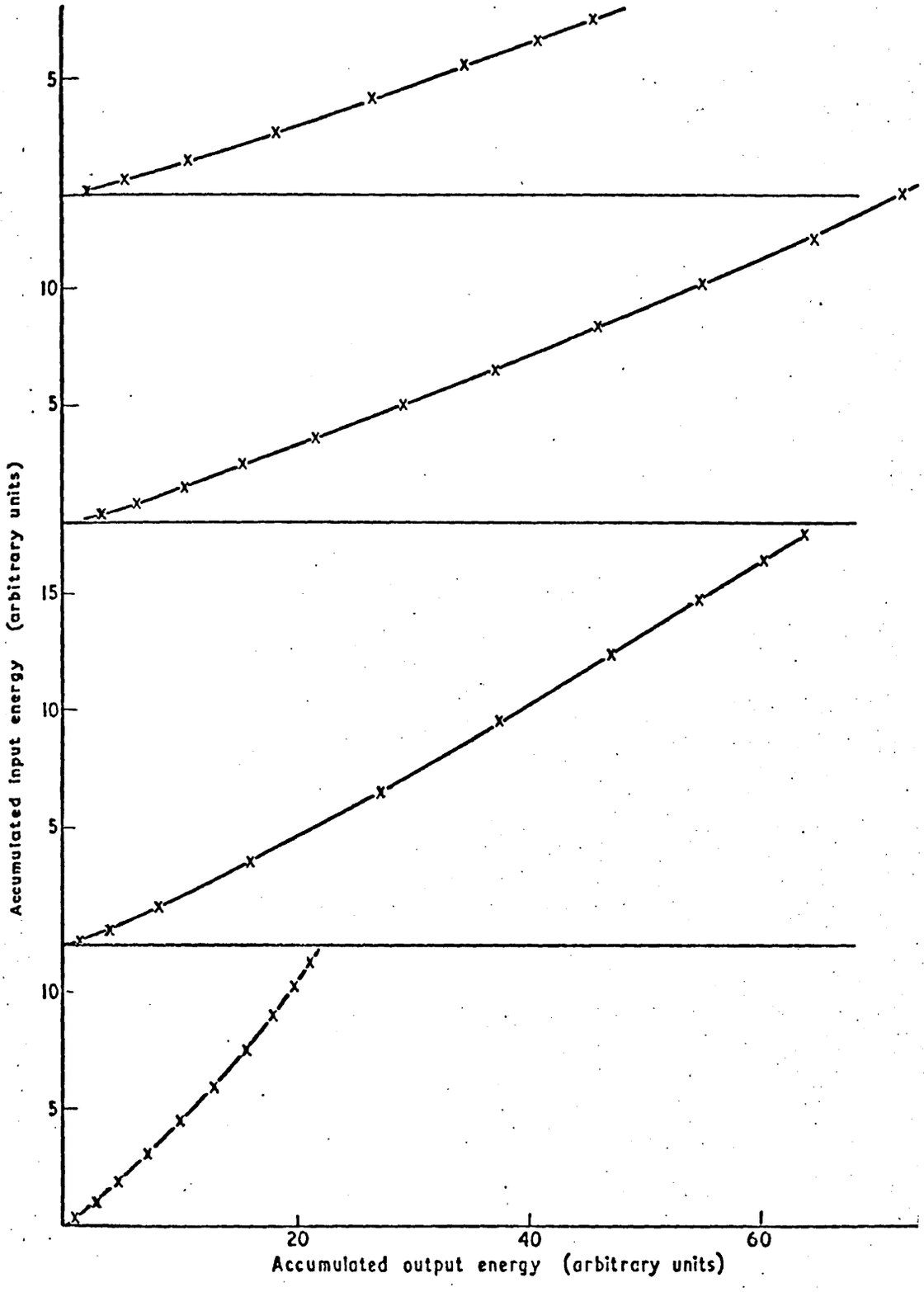

Fig.9.13
Graphs of the accumulated input energy against the accumulated output energy for the same experimental data as in Figs.9.11 and 9.12. The true values of the energy are the units shown multiplied by a factor 7 ± 20% mJ

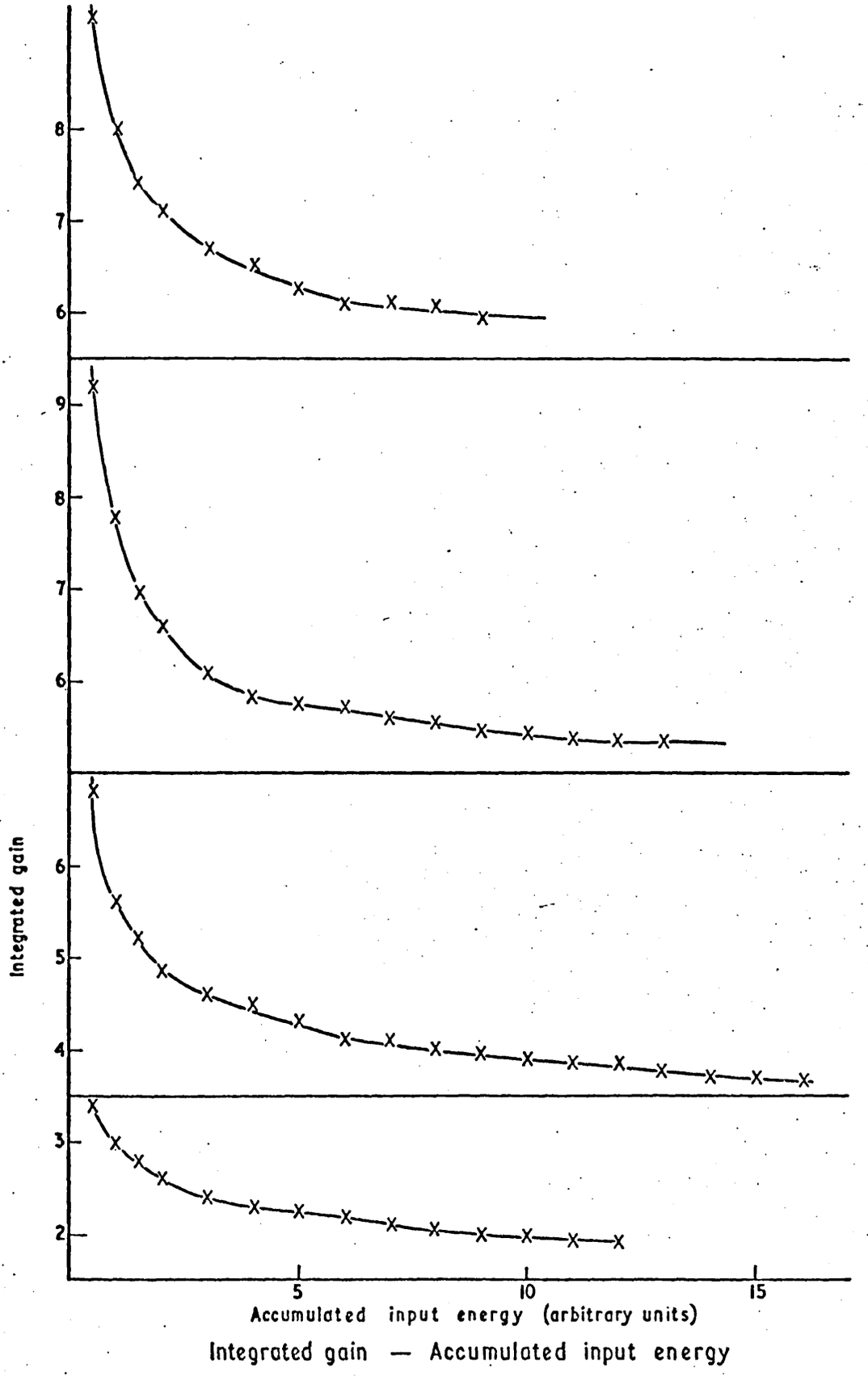

Fig.9.14
Graphs showing the variation of the integrated gain with the accumulated input energy. The data were taken from Fig.9.13

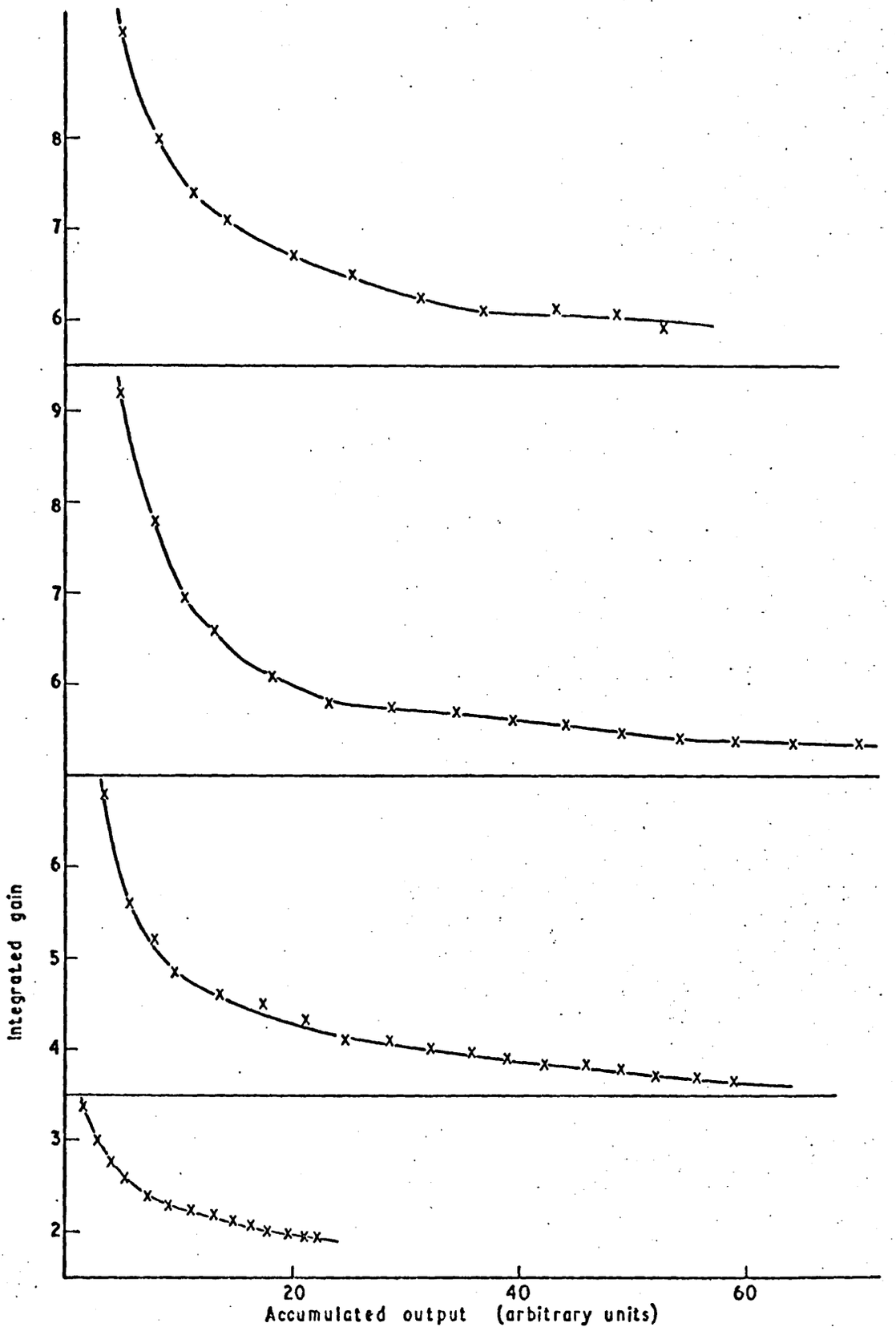

Integrated gain - Accumulated output energy

Fig.9.15
Graphs showing the variation of the integrated gain with the accumulated output energy. The data were taken from Fig.9.13

Figure 9.13 shows graphs of the accumulated input energy plotted against the accumulated output energy for the same experimental data as in Figs.9.11 and 9.12. From these graphs the integrated gain for different output and input energies was calculated. The integrated gain calculated from Fig.9.13 is plotted against the input and output energies in Figs.9.14 and 9.15 respectively. Note the agreement of these results with the theoretical results of Schulz-Dubois[82]. The curves shown in Fig.9.14 show similar characteristics to curves obtained from Nd-glass lasers[139] using different experimental methods. The second graph in each of these figures corresponds to the first picture in Fig.9.10.

The energy units plotted in these graphs are arbitrary. The true energy values in mJ are obtained by multiplying by a factor 7 ± 20%, obtained by calibrating the beam splitters with a calorimeter (the large error in this factor is due to the inaccuracy of the calorimeter measurements).

An approximate value for the stimulated emission cross-section of the liquid laser can be obtained from Figs.9.11 and 9.13. Consider the four level amplifier equation derived in section 3.1

$$\frac{dE}{dx} = h\nu\ \Delta N_1\left\{1 - \exp\left\{1 - \frac{\sigma_{(\nu)}E}{h\nu}\right)\right\} - \alpha E \qquad \ldots (9.2)$$

where $E(J\ cm^{-2})$ is the input energy, x is the distance along the amplifier axis, α is the loss per centimetre, $\sigma_{(\nu)}$ is the stimulated emission cross-section, and ΔN_1 is the population inversion per cm^3. Since the energies used are of the order $10^{-3}J$ and the quantum energy $h\nu = 1.88\times10^{-19}J$ we can write equation (9.2) for the small-signal gain as

$$\frac{dE}{dx} = (\Delta N_1\sigma_{(\nu)} - \alpha)E\ .$$

Integrating over the entire length ℓ of the amplifier and assuming that ΔN_1 is uniform along the length, we obtain

$$\ell n\, G_1 = \left(\Delta N_1\, \sigma_{(\nu)} - \alpha\right) \ell$$

where G_1 is the gain for a small signal. If G_2 is the small-signal gain corresponding to the population inversion ΔN_2 which is left after the passage of the first pulse through the amplifier, then

$$\ell n \left(\frac{G_1}{G_2}\right) = \left(\Delta N_1 - \Delta N_2\right) \sigma_{(\nu)} \ell \,.$$

If a pulse of energy W_{in} emerges from the amplifier with energy W_{out}, then $W_{out} - W_{in} = V(\Delta N_1 - \Delta N_2)\, h\nu$, where V is the volume of the amplifying medium. From the last two equations it follows that

$$\sigma_{(\nu)} = \frac{h\nu\, A\, \ell n(G_1/G_2)}{W_{out} - W_{in}} \qquad \ldots (9.3)$$

where A is approximately equal to the geometrical cross-section of the amplifier ($0.385\ cm^2$).

The gain for small input signals can be found from Fig.9.11. The gains of successive small signals with energies of 21×10^{-3} J each were found from this figure. The corresponding output energies were obtained from Fig.9.13. The stimulated emission cross-section was calculated from formula 9.3. The values obtained ranged from 2.8 to 5.2×10^{-20} cm^2 with most values lying around 4.2×10^{-20} cm^2 ± 40%. This is the stimulated emission cross-section at a wavelength of 10580 Å. To find the cross-section at the centre of the amplifier linewidth, we must multiply by a factor 1.8, which is the ratio of the amplitude of the centre of the fluorescence line profile to that at the part of the profile corresponding to the experiment (Fig.4.4). The stimulated emission cross-section is thus 7.5×10^{-20} cm^2 ± 40%. The large error in this estimate arises from the factor $\ell n \frac{G_1}{G_2}$ and the error in the energy calibration factor. Parts of the graphs where the errors in the gain measurements were small were chosen for these calculations, and these parts gave the most consistent results. The results obtained from the second graph in Fig.9.11 were the

most consistent, and those from the last graph the least consistent.

The values of the stimulated emission cross-section calculated above are in good agreement with the values recently reported[112,141] by other workers using standard methods.

9.6 THERMAL DISTORTION EFFECTS IN THE LIQUID AMPLIFIER

In section 1.1 and 1.5 it was pointed out that changes occurring in the refractive index of the active medium during laser operation can affect the performance of the laser. In liquid media the distortion effects due to heating by the pumping radiation are more severe than in solid state lasers because the thermal expansivity of liquids is much greater than that of solids.

In the experiments described here the far-field beam patterns at a distance of 0.7 m from the amplifier output were recorded on developed unexposed (Polaroid) film. Patterns were obtained corresponding to various times up to 410 μs after firing the flashlamps. The third picture at the top of Figs.9.16 and 9.17 shows the beam cross-section going into the amplifier. Typical beam cross-sections coming out of the amplifier are shown in these figures for three different pumping energies, 968 J, 722 J and 512 J. The beam patterns initially change towards vertically elongated shapes because the flashlamps are placed in a horizontal plane on either side of the amplifier. It can be seen that thermal distortion is less severe for lower pumping levels. It is clear from these patterns that thermal density distributions are established in the liquid due to heating by the pumping radiation. These density distributions probably also account for the large number of spikes around each beam pattern. It is important to notice that at the time of maximum gain the output beam is very much distorted. The geometry of the amplifier head and the elimination of UV radiation thus appear to be the most serious problems in the

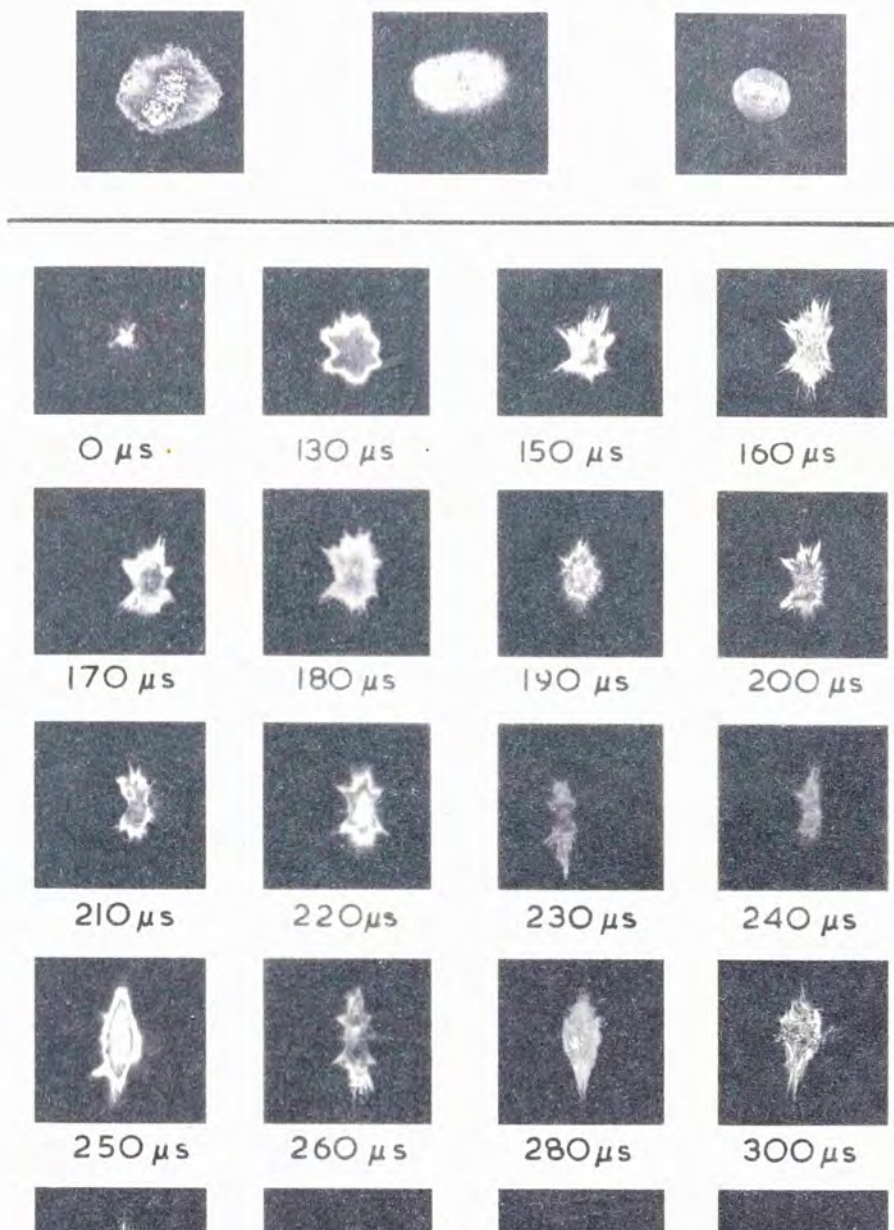

Fig.9.16
Beam patterns obtained on developed unexposed (Polaroid) film. The top three pictures represent the oscillator beam cross-section at a distance of 1.9 m from the output mirror. The third of these is the cross-section of the centre of the beam, equal to the diameter of the amplifier, selected for amplification by the 7.5 mm aperture shown in Fig.9.1. The rest of the pictures are beam patterns recorded at a distance of 0.7 m from the exit of the amplifier for different times after firing the flashlamps. The pumping energy was 968 J.

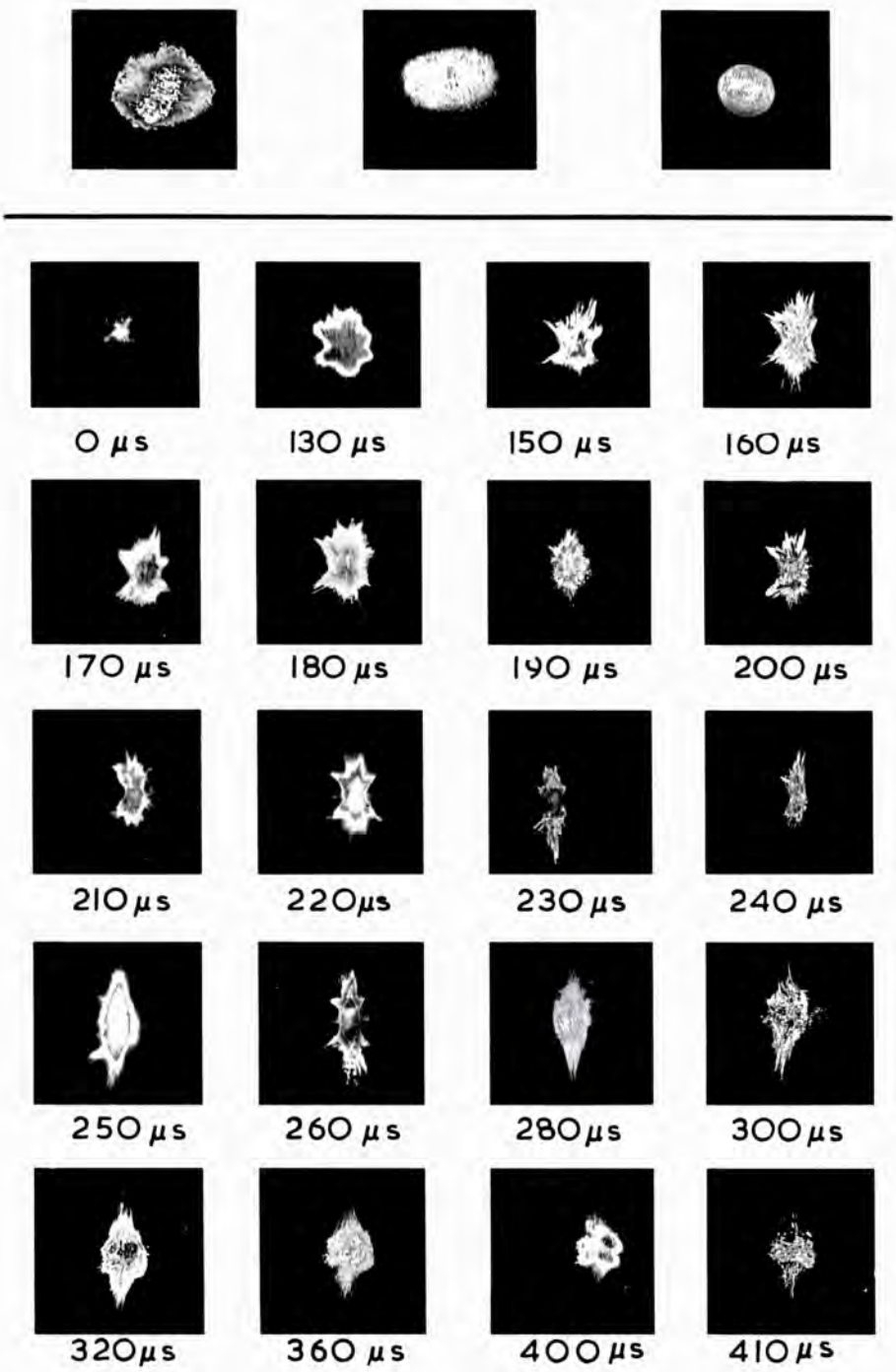
0 μs
130 μs
150 μs
160 μs
170 μs
180 μs
190 μs
200 μs
210 μs
220μs
230 μs
240 μs
250 μs
260 μs
280μs
300μs
320μs
360 μs
400 μs
410 μs

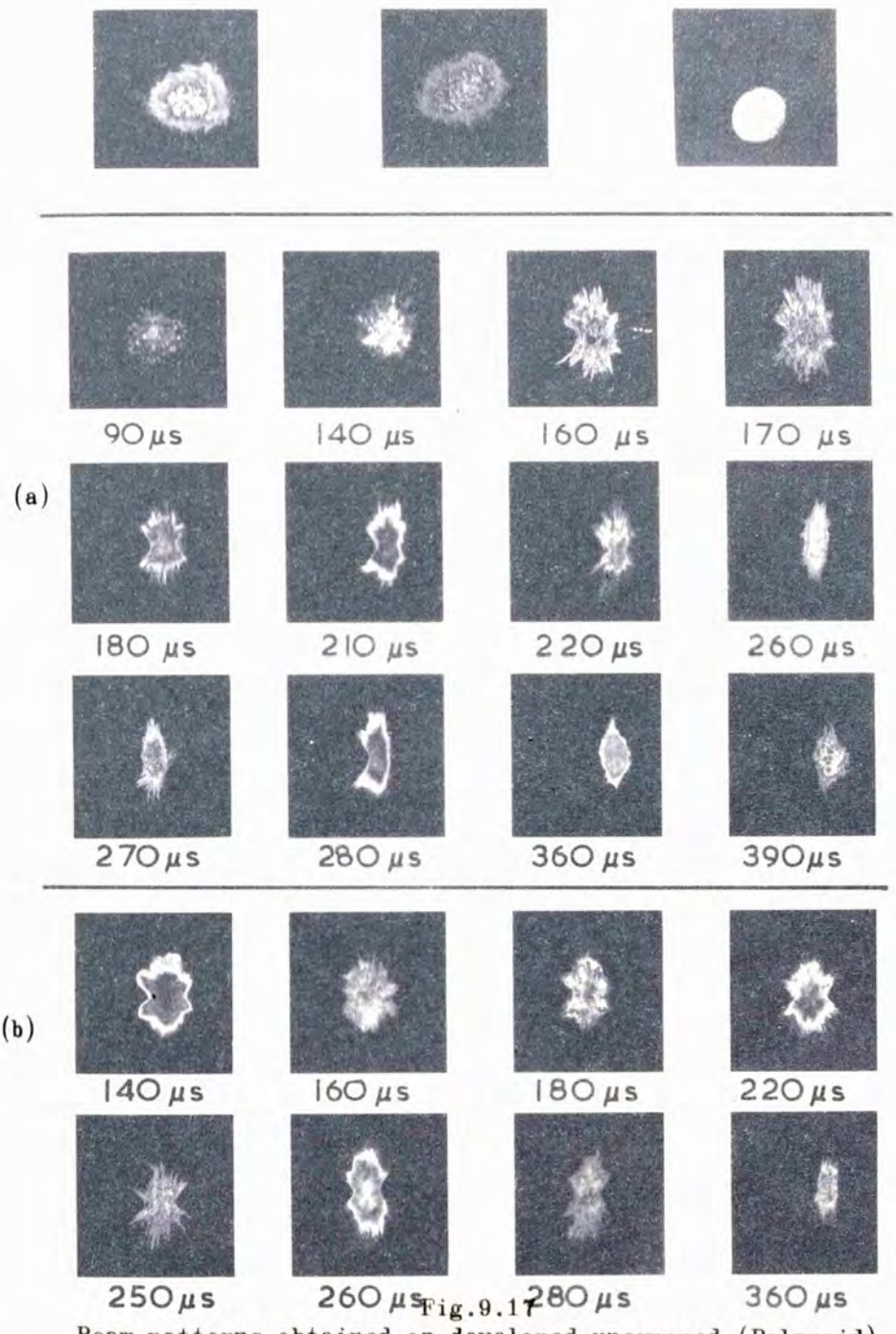

Fig.9.17

Beam patterns obtained on developed unexposed (Polaroid) film, similar to those in Fig.9.16, for two lower pumping energies: (a) 722 J ; (b) 512 J. It can be seen that the distortion is less for the beam patterns shown in (b) because of the lower pumping energy .

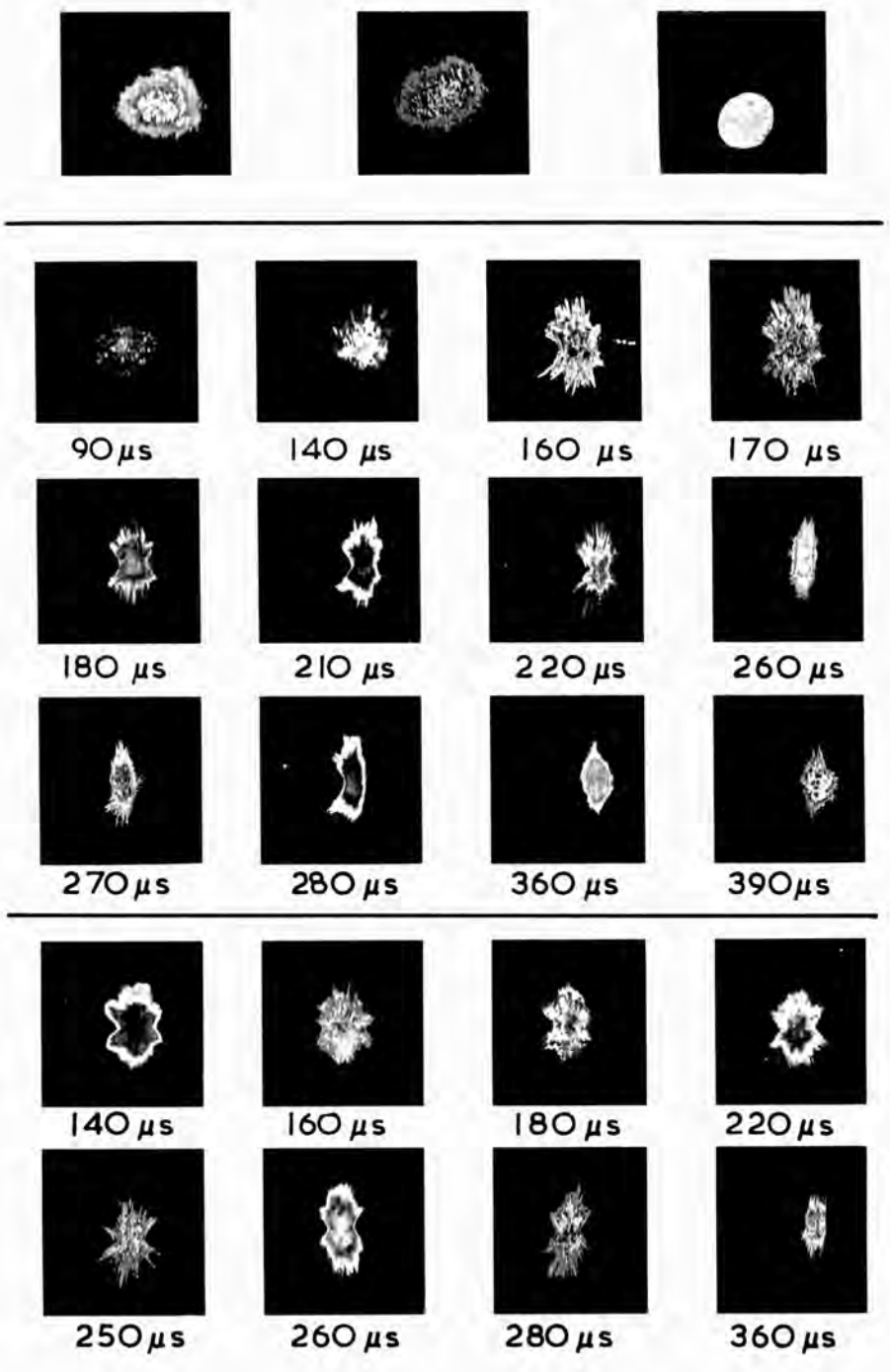
90 μs
140 μs
160 μs
170 μs
180 μs
210 μs
220 μs
260 μs
270 μs
280 μs
360 μs
390 μs
140 μs
160 μs
180 μs
220 μs
250 μs
260 μs
280 μs
360 μs

design of high-power liquid amplifiers. The patterns in Figs.9.16 and 9.17 suggest that an experiment with a small continuous gas laser beam passing through the amplifier when fired, in conjunction with a streak camera-image converter arrangement, would provide useful information about changes in the amplifying medium during pumping.

9.7 CONCLUDING REMARKS ON THE PERFORMANCE OF THE LIQUID LASER AMPLIFIER

In this chapter the behaviour of the neodymium liquid laser ($Nd^{+3} : POCl_3 : ZrCl_4$) as a high power amplifier has been investigated with short light pulses of duration 5 ps as the input signals. Some remarks on the amplification of picosecond pulses and certain points arising from the results described above are of interest and are briefly discussed below.

In section 9.3 the transmission loss of the unpumped amplifier was measured to be $(0.5 \pm 0.2)\%$ per cm, which is slightly higher than that reported by Brecher et al[105]. The powers used were approximately of the order of 1 GW. It is interesting to note that at these power levels two photon absorption processes may occur in neodymium systems and these will reduce the transmission of the medium[140]. This may well account for the slightly higher transmission losses observed.

Let us now consider the rate of change of the population inversion in the amplifier. For a four level system this can be written as

$$\frac{d\Delta N(t)}{dt} = \frac{P(t)}{h\nu_\ell} - \frac{\Delta N(t)}{\tau} \qquad \ldots (9.4)$$

where $\Delta N(t)$ is the population inversion at a time t after firing the flashlamps, $P(t)$ is the pumping rate of ions into level 2 in watts and τ is the lifetime of level 2; ν_ℓ is the frequency of the homogeneous line within the inhomogeneous linewidth corresponding to the signal frequency (2.836×10^{14} s^{-1}). In the above equation cross-relaxation effects

from other parts of the inhomogeneous linewidth have been omitted. This is reasonable in view of the fact that cross-relaxation rates are of the order of 10^5 s^{-1} and the mode-locked trains last for only a few dozen nanoseconds. Super-radiance effects have also been omitted. Note that the above equation is the same as equation (2.3) for a laser oscillator, where the stimulated emission term has been omitted. Multiplying the above equation by an integrating factor and solving for $\Delta N(t)$ we get

$$\Delta N(t) = \frac{e^{-t/\tau}}{h\nu_{\ell}} \int_{o}^{t} P(t)\ e^{t/\tau}\ dt \qquad \ldots (9.5)$$

the small-signal gain being given by

$$G(t) = e^{\Delta N(t)\ \sigma_{(\nu)}\ \ell} \qquad \ldots (9.6)$$

where $\sigma_{(\nu)}$ is the stimulated emission cross-section (4.2×10^{-20} cm^2) at the amplifying wavelength (calculated above) and the lumped losses have been omitted. It can readily be seen from equation (9.5) that for a fixed shape of the pumping rate (shape of the pumping pulse) the maximum of $\Delta N(t)$ and therefore the gain $G(t)$ occurs at a fixed time depending on the value of τ. The shape of $P(t)$ is shown in Fig.9.5 at the top of each gain curve. Values were taken from these curves and equation (9.5) was evaluated with the aid of a computer for several values of τ. The values of τ and P which would make the calculated curves for the gain $G(t)$ agree with the experimental gain curves of Fig.9.5, were found to be $\tau = 140\,\mu s$ and $P_{max} = 7.8 \times 10^3$ watts, 6.7×10^3 watts and 5.7×10^3 watts for the three graphs respectively. The calculated curves using these values are shown in Fig.9.18. The curves are a close fit to the experimental curves of Fig.9.5.

From the above discussion we see that the effective lifetime of level 2 is only $140\,\mu s$ instead of the $300\,\mu s$ as described in Chapters IV and VI. This is mainly due to the fact that fluorescence resulting from

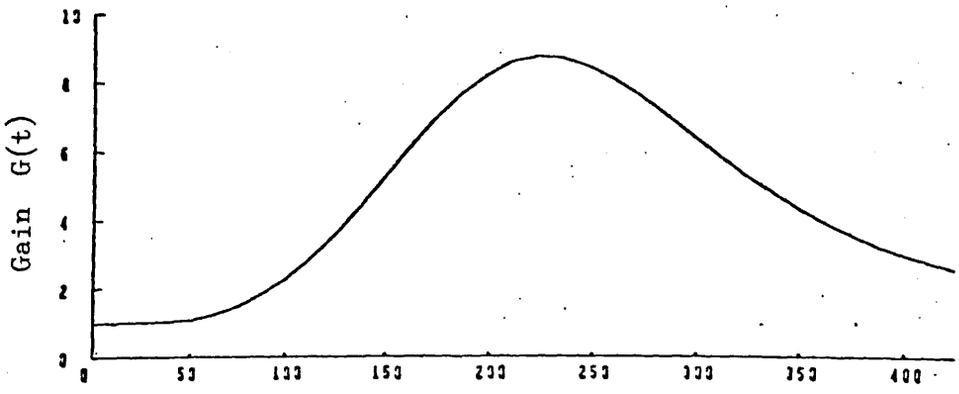

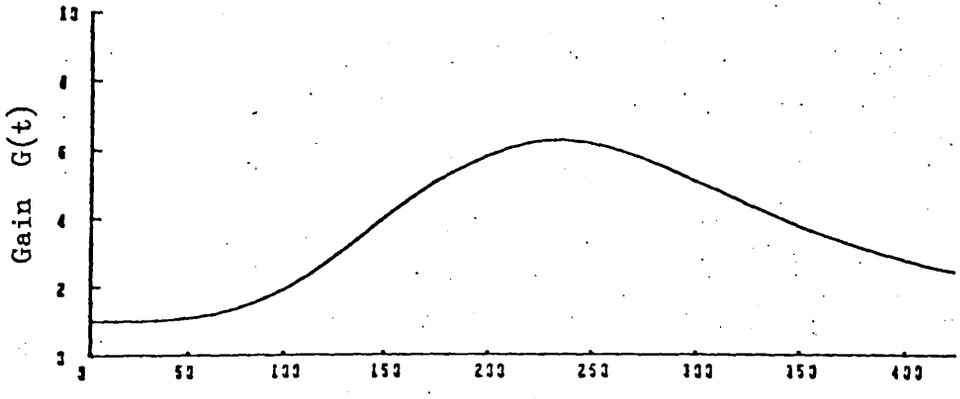

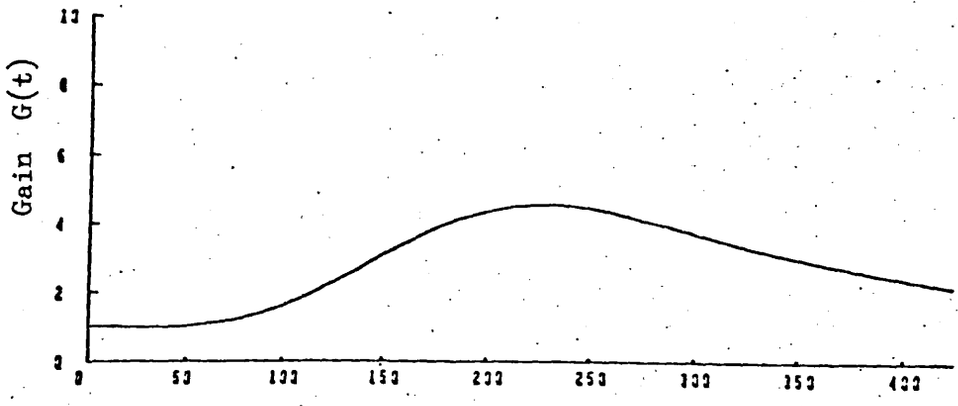

Fig.9.18
Calculated curves of the gain of the amplifier as a function of time after firing the flashlamps (compare them with Fig.9.5)

level 2 occurs in bands outside the one corresponding to the 1.052 μ transition (see Figs.4.1 and 4.4, and also section 4.4). This deviation however may also be partly the result of either of the following two processes. Stimulated transitions take place from the upper level of the laser transition to higher energy levels of the neodymium ion scheme (Fig.4.1) due to the pumping radiation. Secondly, at the powers used in the present experiments, two photon absorption processes can occur which lower the gain of the amplifier[140]. A third possibility is that self-quenching occurs which lowers the fluorescence lifetime. All these processes can occur simultaneously, thus diminishing the value of the fluorescence lifetime. The lifetime of level 1, decaying to the ground state, is of no consequence since this has been shown to be less than 5 ns [141]. It must be pointed out that the lifetime of level 2 found here is not the same as the t_2 value measured in section 6.2; t_2 is the spontaneous lifetime of level 2 for a $2 \rightarrow 1$ transition (section 2.1), whilst τ is the total lifetime of level 2, related to t_2 by

$$\frac{1}{\tau} = \frac{1}{t_2} + \frac{1}{t_q} \qquad \ldots (9.7)$$

where $1/t_q$ is the total transition rate for all the other processes. Note that the value of t_2 (240 μs) calculated in section 6.2, and the value of τ (140 μs) are consistent with equation (9.7). The above considerations are at the present being investigated in more detail.

Finally it should be pointed out that after approximately 1500 firings there was no deterioration in the performance or the physical quality of the liquid amplifier in which pulses up to eight times as powerful as those generated in the oscillator were amplified. It is interesting to recall here, the results of Chapter VIII, when the glass laser rod was badly damaged after approximately 700 firings (Fig.8.6).

To summarize the results of this chapter. Short pulses of light have been used to investigate the amplifying properties of the Nd^{+3} : $POCl_3$: $ZrCl_4$. Certain important characteristics of the amplification processes have been demonstrated, and the results confirm the theoretical predictions of Schulz-Dubois[32] (section 3.2). It was also shown that thermal distortion due to heating by the pumping radiation presents a serious problem in the operation of this kind of laser amplifier. The high gains obtained - although there was a mis-match between the amplifier linewidth and the oscillator signals - suggest that liquid amplifiers are more useful than crystal or glass lasers for high power amplification because the liquid is free of damage problems and can be recirculated.

CHAPTER X

FREQUENCY SHIFT EFFECTS IN WIDE-BAND AMPLIFIERS

10.1 LINEWIDTH PROBLEMS

In sections 1.5 and 3.4 certain aspects of linewidth problems were described. As pointed out before, the results discussed in Chapter IX were affected by the mis-match between the spectra of the input signals and the centre of the amplifying linewidth. In this chapter the results of several experiments designed to investigate the consequences of this mis-match are discussed.

The amplification of light signals by a material in an inverted state depends on the gain profile of the amplifying medium and the spectrum of the incoming signal. The fundamental light amplification processes suggest that if a Lorentzian (or Gaussian) shaped narrow spectrum signal is amplified by a wide linewidth amplifier whose centre does not coincide with that of the signal, frequency shifts occur during the amplification process. Here a direct experimental observation of a frequency shift occurring during the amplification of a narrow spectrum signal by an amplifier of wide linewidth is reported. The effect of this shift on the power gain of the amplifier is also investigated experimentally and theoretically. The ability of trivalent neodymium to serve as the active ion in different host materials provide the necessary experimental conditions because the spectra of the different systems do not coincide exactly (Fig.4.4).

Let us consider the situation with the aid of Fig.10.1. This diagram is only an illustration, but the values for the wavelengths and the shape of the amplifier linewidth are the true values corresponding to the experimental conditions. It is obvious from this diagram that the wing of the input signal nearer the centre of the amplifier linewidth will be amplified more and the spectrum of the amplified signal will be shifted

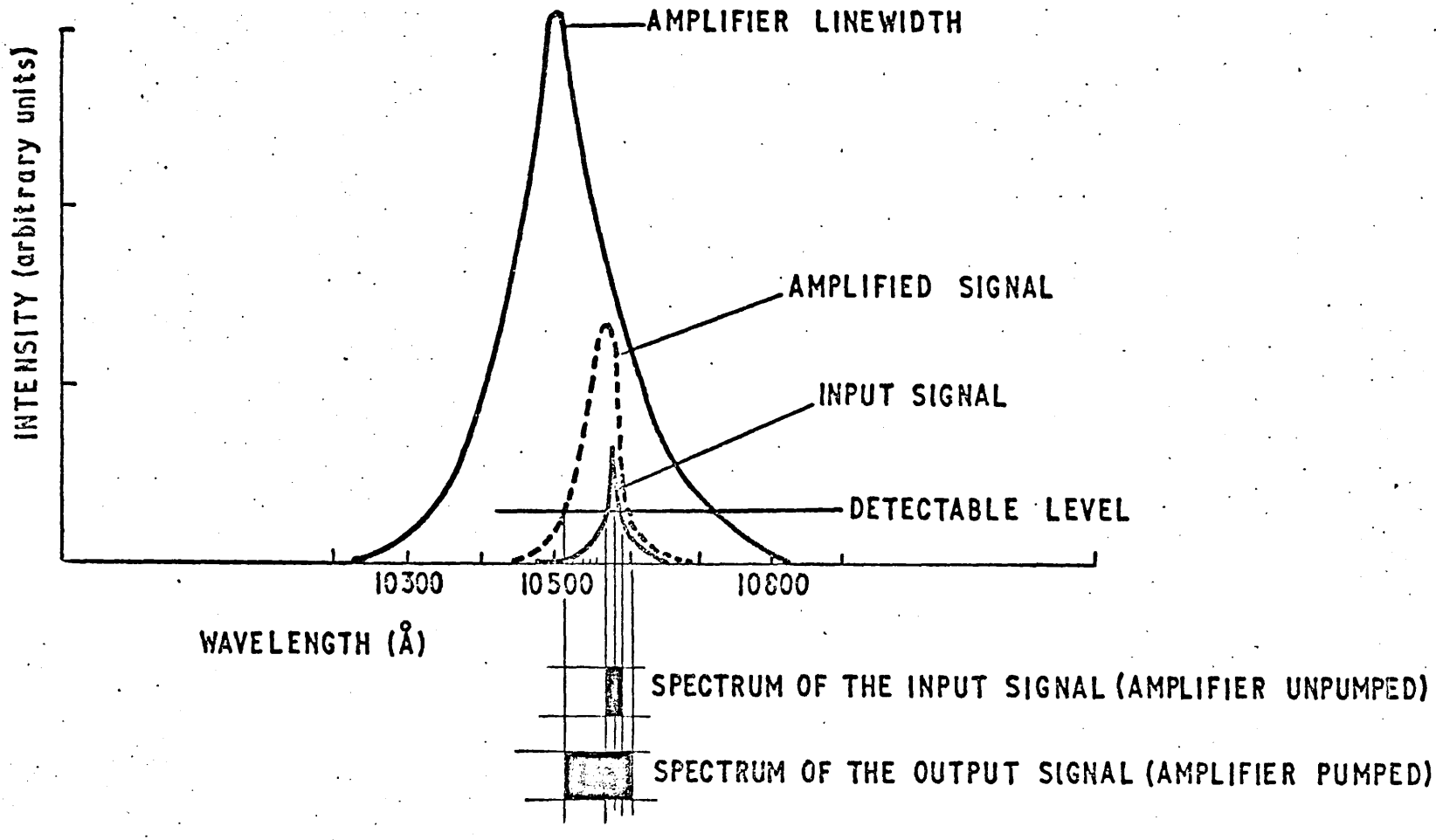

Fig.10.1

AMPLIFICATION OF A NARROW SPECTRUM SIGNAL WHOSE CENTRE DOES NOT COINCIDE WITH THE CENTRE OF THE LINEWIDTH OF THE AMPLIFIER

(schematic)

towards the centre of the linewidth as shown; exaggerated for clarity. (For the true shape of the amplified signal see Fig.10.6 later.) The expected spectra of the input and output signals are shown at the bottom of the figure and are defined by the vertical lines. In this section the physical picture of the situation was established. In the following sections experimental and theoretical results on the subject are presented.

10.2 EXPERIMENTAL OBSERVATION OF A FREQUENCY SHIFT DURING THE AMPLIFICATION OF A NARROW SPECTRUM SIGNAL

The experimental arrangement is shown in Fig.10.2. The input signals consisted of mode-locked trains from the Brewster-ended Nd-glass LGN 55 oscillator described in section 8.1. Oscillograms of the mode-locked trains were recorded using an oscilloscope 519, with the aid of the beam splitter shown in Fig.8.2. The amplifier head was the one shown in Fig.5.2. The linewidth of the amplifying medium ($Nd^{+3} : POCl_3 : ZrCl_4$) is 150 Å at half the maximum with the centre of the line lying at 10522 Å (see Figs.4.4 and 10.6).

The spectra of the signals were taken with a Monospek 1000 grating scanning spectrometer with the photocathode of the camera-image converter arrangement described in section 5.5 placed in the plane of the exit slit (the exit slit was previously removed). In order to avoid damaging the replica grating with the high powers of the picosecond pulses, only part of the output beam was reflected into the spectrometer. The exit of the amplifier was imaged at unit magnification onto the input slit of the spectrometer using a 35 cm focal length lens. A calibrating lamp was used to check the accuracy of the recording system, and it was found that the spectrometer-image converter arrangement was accurate to ± 0.5 Å.

The experimental results are shown in Fig.10.3. The two lines correspond to 10532 Å (left) and 10570 Å (right). The input signals were first recorded without firing the amplifier, and spectra ranging from 5 to

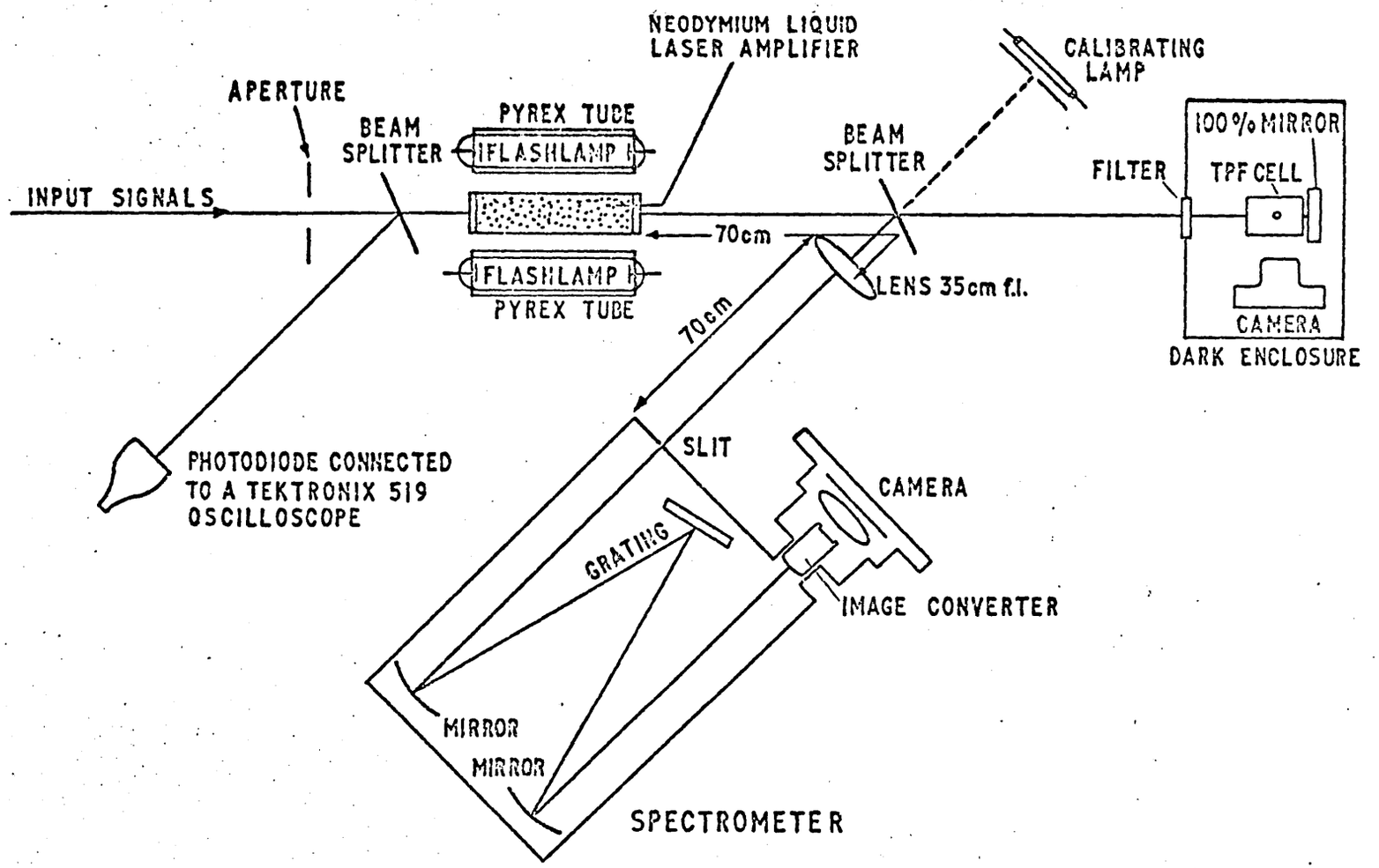

Fig.10.2

AMPLIFICATION OF MODE-LOCKED PULSES WHOSE SPECTRUM DOES NOT COINCIDE WITH THE CENTRE OF THE AMPLIFIER LINEWIDTH.

EXPERIMENTAL ARRANGEMENT

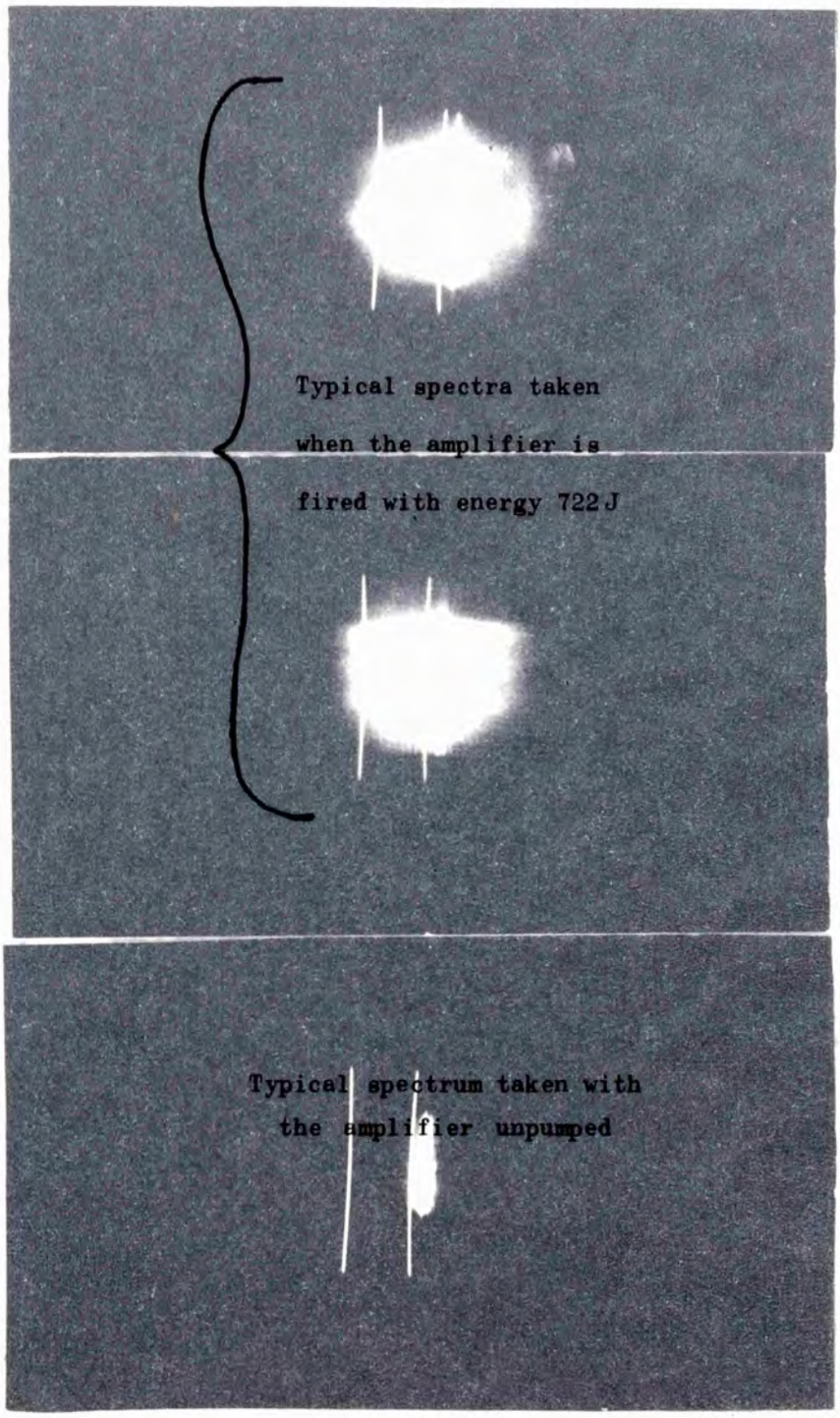

Fig.10.3
Experimental results showing the frequency shift occurring during the amplification of narrow spectrum signals whose spectrum does not coincide with the centre of the amplifier linewidth. The two lines correspond to 10532 Å (left) and 10570 Å (right) for all pictures.

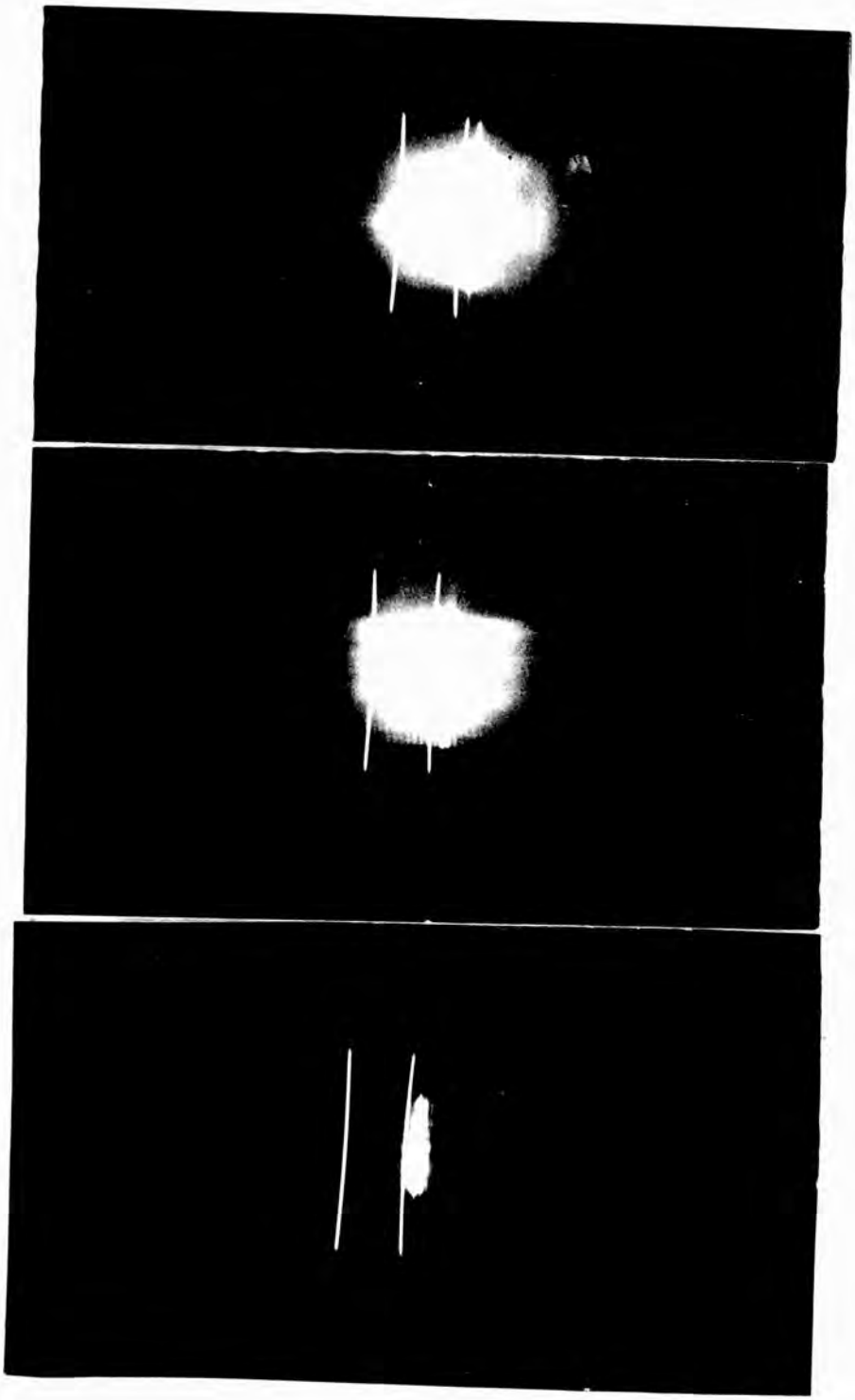

20 Å wide were obtained, each centred at 10580 Å (see Figs.4.4 and 8.3). The spectra of the mode-locked pulses from an Nd-glass laser were shown to be largely Lorentzian [58] with half-width ~5 Å (see section 2.3.3).

When the amplifier was fired the resulting spectrum was asymmetrical about the centre of the input signals. It was shifted towards the centre of the amplifier linewidth and the pictures (Fig.10.3) show that the asymmetry is approximately 27 Å. The gain of the amplifier at the time of transmission of the pulses was approximately 6 (Fig.9.5(b)). It is important to note that the shift never reaches the centre of the amplifier linewidth; this limits the gain obtained from the liquid. The results described here suggest that the potentialities of the liquid as a high power amplifier are much better than implied by the experiments of Chapter IX.

The experimental results of Fig.10.3 are similar to the expected spectra shown below the graphs of Fig.10.1 (compare these results with the calculated results of Fig.10.6 later).

Proper calibration of the film to record the intensity distributions of the spectral shifts, and measurements of the gain and energy of the input pulses, should allow important parameters of the cross-relaxation mechanisms in the liquid laser to be calculated by this method. The effect of this shift on the power gain of the amplifier is investigated in the next section and a simple theoretical analysis of the results is given in section 10.4.

10.3 THE EFFECT OF THE FREQUENCY SHIFT ON THE POWER GAIN OF THE LASER AMPLIFIER

In this section the effect of the frequency shift described above on the power gain of the amplifier is investigated. As it can be seen from Fig.10.3, the spectrum of the output signal is no longer the same as that of the input signal. It is asymmetric about the original centre of

the input signal and has a frequency shift towards the centre of the amplifier linewidth.

If the signal with the new spectrum is now sent back through the amplifier, and the signal is small so that no population depletion effects occur, the gain in the reverse direction will be greater than in the forward direction because of the better matching between the amplifier linewidth and the signal spectrum. In effect this could be considered as the amplification of the signal through an amplifier of twice the length, the gain in the latter parts being greater as a result of the frequency shift introduced in the signal spectrum by the earlier parts of the amplifier.

The input signals consisted of mode-locked pulse trains from the Brewster-ended Nd-glass LGN 55 oscillator described in section 8.1, and the energies of the input mode-locked trains ranged from 20 to 40 mJ, approximately 3 mJ per mode-locked pulse. The amplifying medium was the $Nd^{+3} : POCl_3 : ZrCl_4$ liquid system, and the amplifier head is shown in Fig.5.2. The spectral characteristics of the input signals and the amplifier linewidth were described in the previous section.

Figure 10.4 shows the experimental arrangement used for measuring the forward and backward gain of the amplifier. Beam splitters were placed at the entrance and exit of the amplifier, with a 62% dielectric mirror placed behind the second beam splitter to reflect part of the output pulse back through the amplifier. A 100% dielectric mirror was used in conjunction with the first beam splitter to record the input signals as shown in the figure. The distance between the first beam splitter and the 62% mirror was arranged to be less than the single transit time of the oscillator so that the forward and backward amplification of a mode-locked pulse was completed before the next pulse reached the amplifier. An aperture 6.5 mm in diameter was placed in front of the amplifier in order to select the central

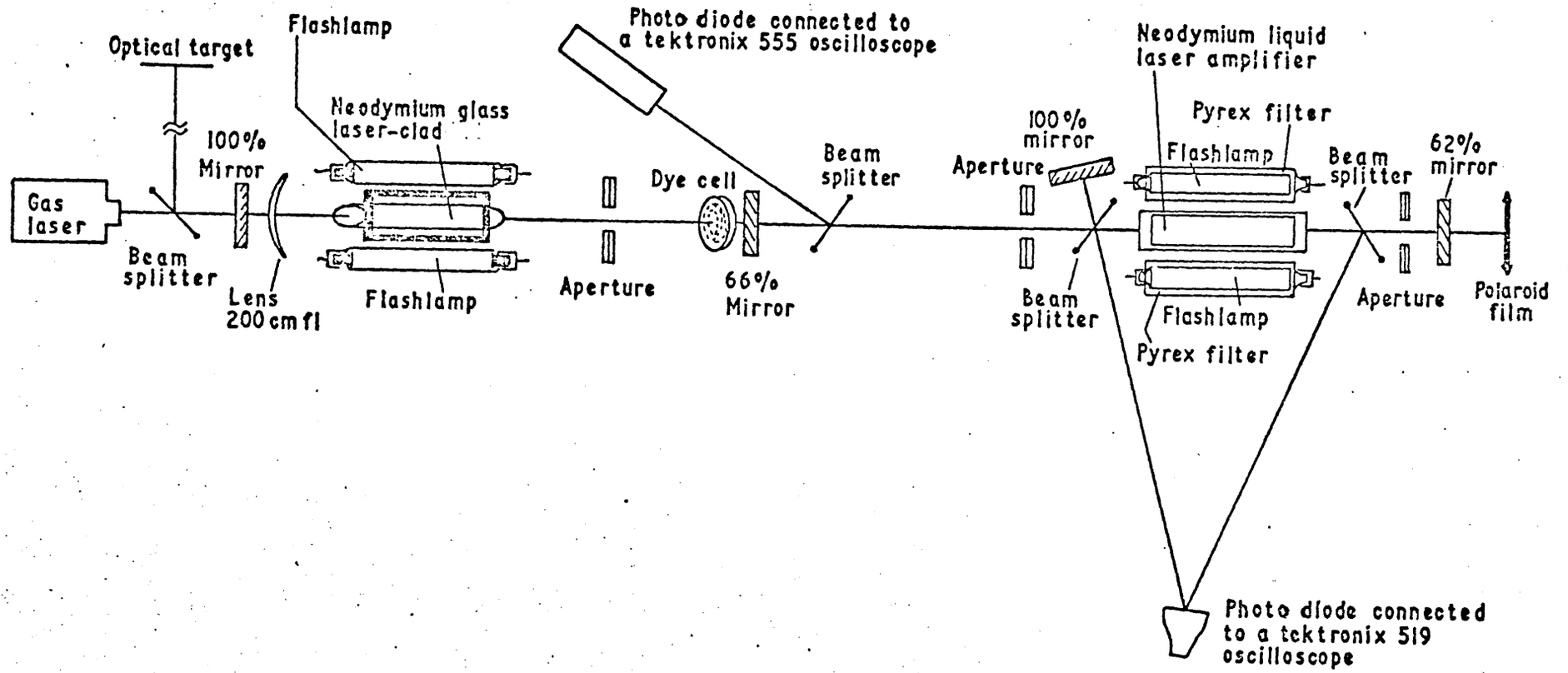

Fig.10.4
Experimental arrangement for the measurement of the forward and backward gain of the $Nd^{+3} : POCl_3 : ZrCl_4$ system using mode-locked pulses from a Nd-glass oscillator

part of the mode-locked beam for amplification. The pulses were recorded with the fast ITT F 4000 photodiode described in section 5.4, connected to a Tektronix 519 oscilloscope. The short rise time of the photodiode (section 8.1) enabled the recordings of three interpenetrating mode-locked trains as described below.

First the mode-locked pulse trains were passed through the unpumped amplifier. The input signal A was recorded with the first beam splitter and the 100% mirror, the output signal B was recorded with the second beam splitter, and the returned signal C was recorded with the first beam splitter. Thus three interpenetrating mode-locked trains were recorded, the ratios B/A and C/B taking account of all the losses in the system for the forward and backward passes due to the difference in the reflectivity of the two beam splitters, the reflection from the cell windows, the passive loss of the medium, the 62% mirror and the diffraction losses. Several firings were taken with the amplifier unpumped. An example is shown in the last picture of Fig.10.5 (an asymmetric mode-locked train was chosen here in order to show the consistency of the ratios whatever the input signal). This is a normalization picture analogous to those described in section 9.3. The ratios B/A and C/B were then calculated for all the pictures taken. For the pictures of Fig.10.5 the ratios are $B/A \simeq 0.64 \pm 2.5\%$ and $C/B = 0.26 \pm 4.5\%$.

More filters were then used to attenuate the photodiode signals, and the amplifier was pumped. The recordings A' for the input signal, B' for the output signal and C' for the returned signal were taken. The ratios B'/A' and C'/B', for the forward and backward passes respectively were calculated. Typical examples are shown in the top two pictures of Fig.10.5. The ratios

$$G_F = \frac{B'/A'}{B/A} \quad \text{and} \quad G_B = \frac{C'/B'}{C/B}$$

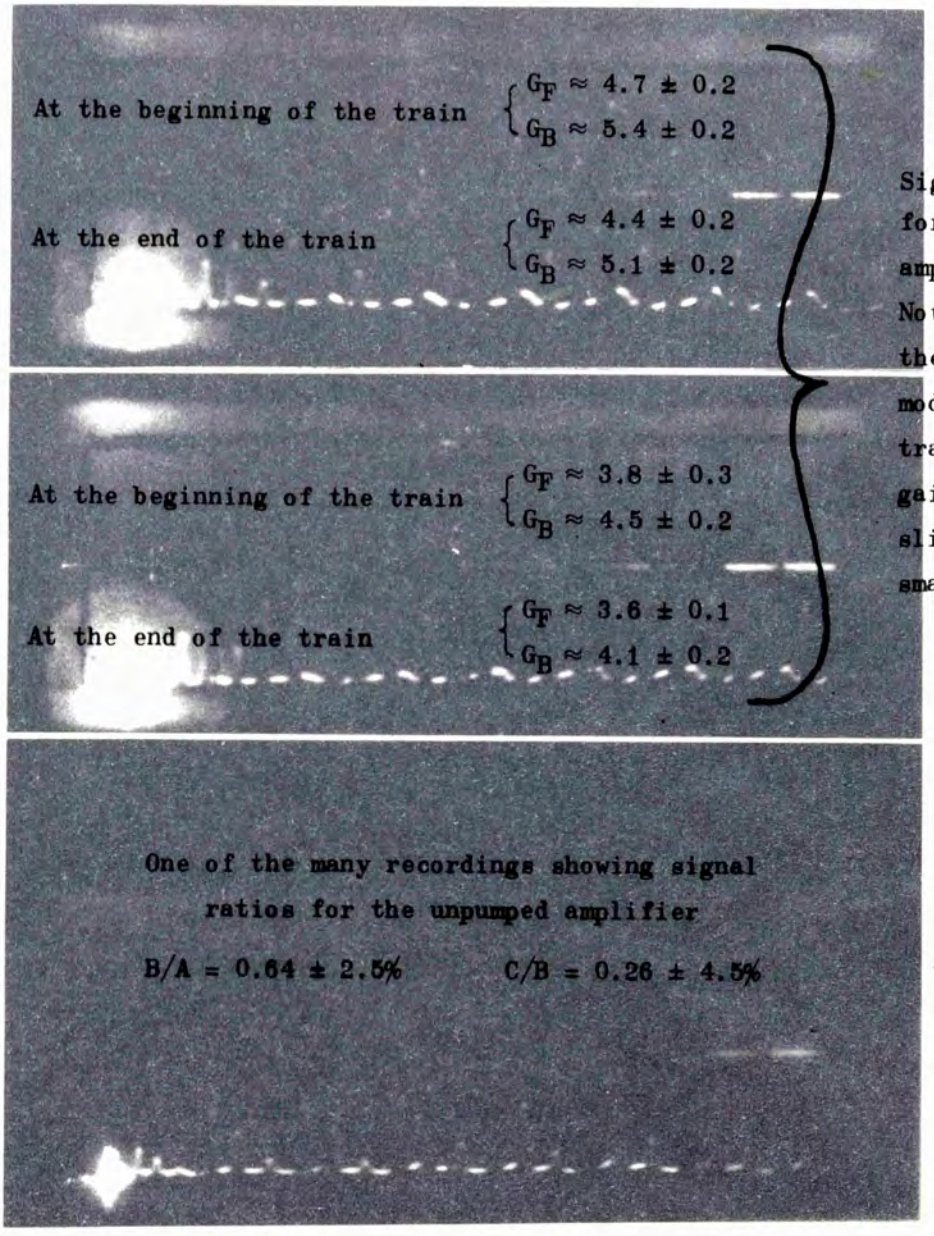

Fig.10.5
Measurement of the forward and backward gain of the liquid amplifier

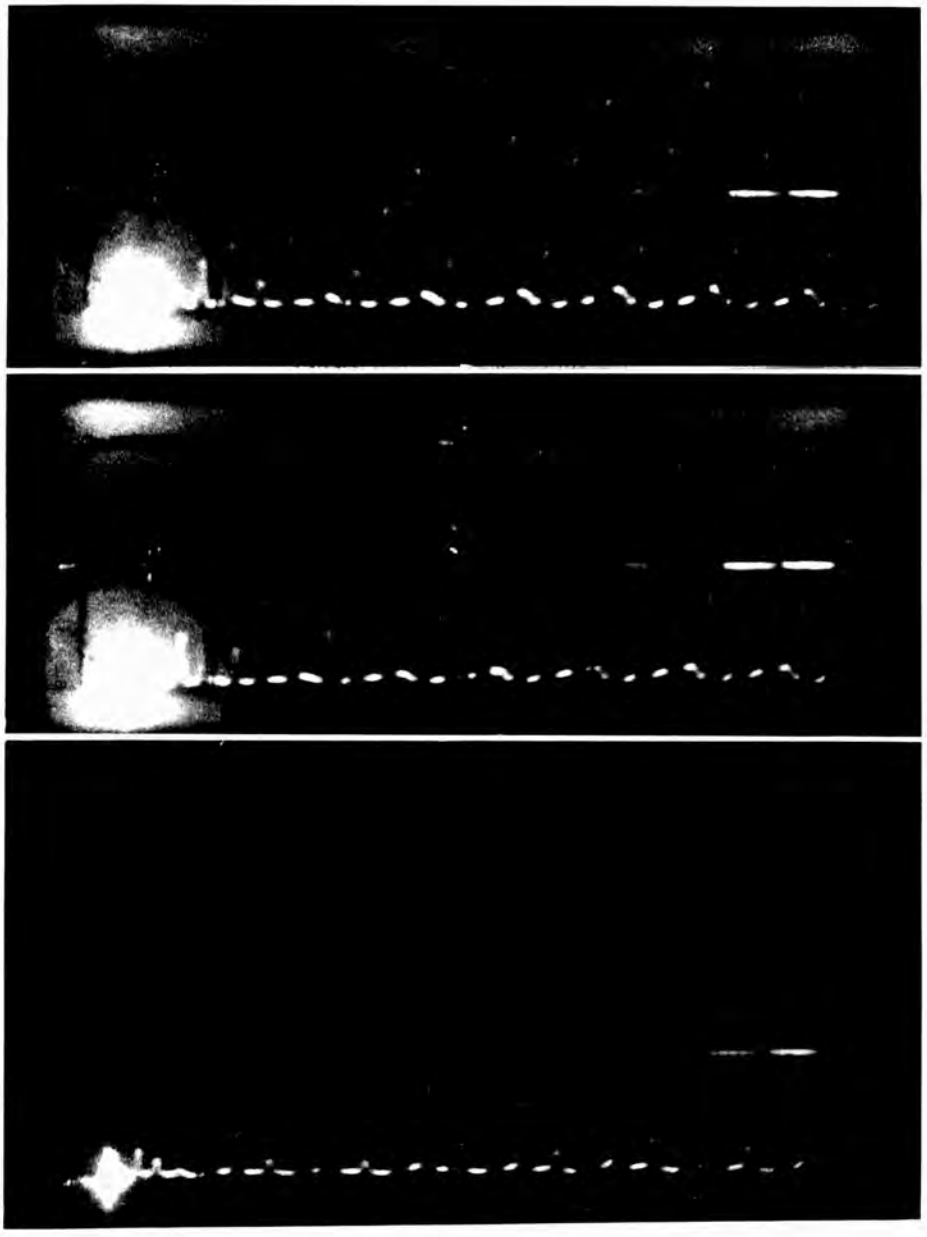

give the gain of the medium in the forward and backward directions respectively. This method of measuring the gain is analogous to the one described in section 9.3 for measuring the gain of the amplifier. Details on the method of recording were given in that particular section. This method of measuring the gain of the amplifier is very accurate as it eliminates the effect of all the losses in the system, the measured gain being the intrinsic gain of the medium. The consistency of the ratios B/A and C/B for the unpumped amplifier is an indication of the accuracy of the results.

With input energies of 512J the backward gain G_B was found always to be greater than the forward gain G_F for each mode-locked pulse. Fig.10.5 shows two sets of observations of this kind. For forward gains of 4 ± 0.2 the backward gains were found to be 4.7 ± 0.2. This results from the shift in the spectrum of the mode-locked pulses as they travel through the amplifier. The wing of the signal spectrum lying nearer the centre of the amplifier linewidth is amplified more than the other. On the way back there is better matching between the spectrum of the mode-locked pulses and the gain profile. Since the pulses are small we can assume that there is no change in the population inversion for successive pulses, therefore the gain in the backward direction is bigger. It can be seen from Fig.10.5 that there is a slight change in gain for pulses at the beginning and end of the train. This is due to small saturation effects. For higher pumping energies the experiment could not be performed because of the severe thermal distortion in the liquid amplifier (section 9.6).

Let us now summarize the results of this section. Mode-locked pulses generated by an Nd-glass laser have been amplified in the forward and reverse directions by an $Nd^{+3} : POCl_3 : ZrCl_4$ liquid laser. The gain in the reverse direction was found to be greater than the gain in the

forward direction. This was attributed to the frequency shift introduced in the spectrum of the mode-locked pulses during the first passage through the amplifier, which was described in section 10.2. In the following section a simple theoretical analysis is given which accounts for the effects observed in sections 10.2 and 10.3.

10.4 THEORETICAL CONSIDERATIONS

Considering equations (3.6a) for the small signal case and negligible lump losses, and introducing the spectral dependence of the quantities I, ΔN and σ, we can write the amplifier equation for the spectral intensity:

$$\frac{dI(\nu)}{dx} = I(\nu)\, K(\nu) \qquad \ldots (10.1)$$

where $I(\nu)$ is the intensity of the incident radiation is Joules/s cm^2 per unit frequency range, the total power density I at any point x along the amplifier length being

$$I = \int_0^\infty I(\nu)\, d\nu \quad \text{watts cm}^{-2}$$

$K(\nu)$ may be defined as the convolution of $\sigma(\nu)$ and $\Delta N(\nu)$

$$K(\nu) = \sigma(\nu) \otimes \Delta N(\nu) = \int_0^\infty \sigma(\nu - \nu')\, \Delta N(\nu')\, d\nu'$$

where $\sigma(\nu)$ is the ionic cross-section in cm^2 (section 3.4) centred at a frequency ν' and is assumed constant throughout the amplifier linewidth; $\Delta N(\nu')$ is the total inversion density in ions cm^{-3} per unit frequency range. In effect $K(\nu)$ is the factor governing the fluorescence line of the amplifier in cm^{-1}. Thus $K(\nu)$ can be assumed to have approximately the shape of the fluorescence line of the amplifier.

For an amplifier of length ℓ equation (10.1) becomes

$$I_{out}(\nu) = I_{in}(\nu)\, \exp K(\nu)\ell\,. \qquad \ldots (10.2)$$

Using equation (10.2) and denoting the forward and backward passes with the subscripts 1 and 2 respectively, the forward gain is given by

$$G_F = \frac{I_{1_{out}}}{I_{1_{in}}} = \frac{\int_0^\infty I_{1_{in}}(\nu) \exp K(\nu)\ell \, d\nu}{\int_0^\infty I_{1_{in}}(\nu) \, d\nu} \qquad \ldots (10.3)$$

The backward spectral input intensity is $I_{2_{in}}(\nu) = R\, I_{1_{out}}(\nu)$ where R is the reflectivity of the mirror at the back of the amplifier (62% in this case). Then

$$I_{2_{out}}(\nu) = I_{2_{in}}(\nu) \exp K(\nu)\ell = R\, I_{1_{in}}(\nu) \exp 2\, K(\nu)\ell$$

The backward gain (assuming no change in the population inversion during the passage of the forward pulse) is thus given by

$$G_B = \frac{I_{2_{out}}}{I_{2_{in}}} = \frac{\int_0^\infty I_{1_{in}}(\nu) \exp 2K(\nu)\ell \, d\nu}{\int_0^\infty I_{1_{in}}(\nu) \exp K(\nu)\ell \, d\nu} = \frac{\int_0^\infty I_{1_{in}}(\nu) \exp 2\, K(\nu)\ell \, d\nu}{G_F \int_0^\infty I_{1_{in}}(\nu) \, d\nu} \qquad \ldots (10.4)$$

Comparing equations (10.3) and (10.4) we see that the forward and backward gains are not the same. It can also be seen from equation (10.4) that the product of the gains $G_B G_F$ is the same as the gain of an amplifier of length 2ℓ, the gain at each part of the amplifier depending on the spectrum of the propagating pulse at that point.

Since we are considering a narrow signal the amplifier equation (10.2) for a small pulse without any frequency shift gives us $\ell n \frac{I_{out}}{I_{in}} = K_s \ell$ where K_s is the value of K at the signal frequency 2.836×10^{14} Hz. The forward gains measured ranged from 3.5 to 4.5. Assuming the small signal gain to be 4.25 at the signal frequency, an approximate value for $K_s \sim 0.094$ cm^{-1} is calculated (ℓ = 15.3 cm). From the fluorescence line (broken line in Fig.10.6) the value $K_0 \sim 0.2$ cm^{-1} at the centre of the

amplifier line 2.856×10^{14} Hz is calculated. Using $K_o \sim 0.2$ cm^{-1} and the fluorescence line of Fig.10.6, the integrals of equations (10.3) and (10.4) were evaluated with the aid of a computer.

The shape of the input signals was assumed to be Lorentzian

$$I_{1_{in}}(\nu) = I_o \frac{1}{1 + \left(\frac{\nu - \nu_s}{\frac{\Delta\nu_s}{2}} \right)^2}$$

with half width $\Delta\nu_s = 0.002 \times 10^{14}$ Hz (equivalent to 7.5Å). This is a very reasonable assumption in agreement with the results of reference (58) and the results of section 8.1. Using a value $K_o \sim 0.2$ cm^{-1} and finding the values of K for different ν from Fig.10.6, the integrals

$$a = \int_0^\infty \frac{1}{1 + \left(\frac{\nu - \nu_s}{\frac{\Delta\nu_s}{2}} \right)^2} \, d\nu \quad ,$$

$$b = \int_0^\infty \frac{1}{1 + \left(\frac{\nu - \nu_s}{\frac{\Delta\nu_s}{2}} \right)^2} \exp K(\nu)\ell \, d\nu \quad ,$$

$$c = \int_0^\infty \frac{1}{1 + \left(\frac{\nu - \nu_s}{\frac{\Delta\nu_s}{2}} \right)^2} \exp 2K(\nu)\ell \, d\nu \quad ,$$

have been evaluated.

These integrals were plotted by a computer against the frequency ν and the graphs are shown in Fig.10.6. From equations (10.3) and (10.4) the ratios b/a and c/b of the areas under the graphs correspond to the forward and backward gains respectively. The computed values are

$$b/a = G_F = 4.4 \qquad c/b = G_B = 5.1 \; .$$

These are in very good agreement with the experimental results described

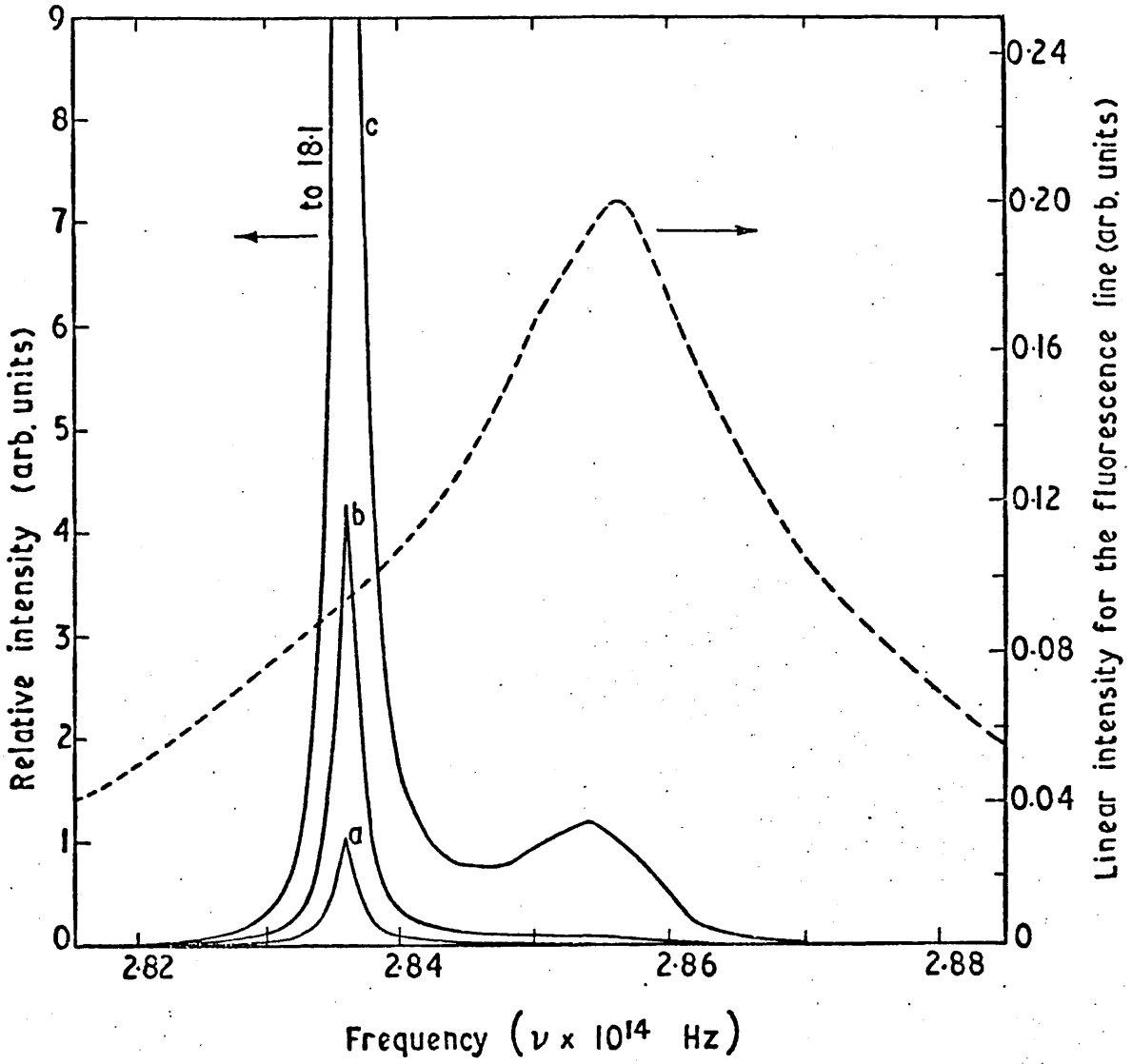

Fig.10.6

The fluorescence line of the $Nd^{+3} : POCl_3 : ZrCl_4$ system is shown by the broken line.
Computer plot of (a) the input, (b) the output and (c) the returned pulse spectra.
The ratios of the areas under the curves correspond to the forward and backward gains. These were evaluated by the computer to be $G_F = b/a = 4.4$ and $G_B = c/b = 5.1$ which are in good agreement with the experimental results of Fig.10.4. Note the shifts towards the centre of the fluorescence linewidth.

in section 10.3. It is interesting to note the agreement of the calculated spectral shift shown in b with the experimental results of Fig.10.3 It can also be seen from the graphs of Fig.10.6 that the effect of the shift becomes greater with increasing number of passes.

10.5 COMMENTS ON THE OBSERVATIONS AND THE RESULTS

The experimental and theoretical results described in the last three sections demonstrate some fundamental characteristics of the amplification process. They show directly the effect of frequency shifts on the power gain in a travelling wave amplifier. As has been pointed out in section 3.4, if the pulse width is short compared with the cross-relaxation time from different parts of the inhomogeneous line width, most of the available energy in the amplifier remains untapped. Thus in the case of high power amplification (nanosecond and picosecond pulses) with neodymium lasers the spectra of the input pulses should be made as wide as possible in order that the interaction of the signals with the atomic medium takes place over a wide range of wavelengths. In the latter case more of the available energy under the inhomogeneous linewidth will be extracted.

The agreement of the experimental results of section 10.3 with the simple theory of section 10.4, which assumes a Lorentzian shape of half width between 5 and 10 Å for the mode-locked pulses, argues strongly for the conclusion that the pulses are indeed a close approximation to Lorentzian shape, in confirmation of the results in references 58 and 59.

CONCLUSIONS

In this thesis I have tried to carry out a definitive series of experiments in order to marshal together all the important data concerning inorganic liquid lasers. The work is largely original, in fact only the parts which relate to the actual formation of the liquid itself and the construction of the glass oscillator have been derived from other sources. It should be pointed out that the work described here represents the only active research in the field of liquid lasers in this country. This introduced several difficulties during the course of the investigation, since most of the apparatus had to be devised and constructed without any knowledge of the experimental consequences. Four other groups working in this field are in countries abroad - U S A, Germany, Japan and the Soviet Union - and they have taken completely different lines of investigation. The information conveyed here together with that conveyed by the latter groups, is at the present moment drawing the attention of many scientific laboratories around the world as to the potentialities of the inorganic liquid laser $Nd^{+3} : POCl_3 : ZrCl_4$.

The thesis itself has been arranged so as to provide a complete reference to the properties and capabilities of the inorganic liquid laser and at the same time to describe and explain those aspects of laser physics related to the observed phenomena and laser operations. The apparatus and experimental techniques used have been described in detail in order to provide the basic information for the future experimenter in the field.

Although the experimental results and the new observations made are summarized in the relevant sections and their importance in laser operation and design is pointed out there, it would be appropriate to mention briefly the main results here:

(i) In the Q-switched operation of the liquid laser output powers of 50 MW have been obtained with input energies of 500 J. The uniformity of the pulses, the uniform cross-section, the short pulse width and the high powers obtained from this system with input energies of 500 J make the liquid laser at least as efficient as YAG and glass lasers. The performance of this system in the 1 J output pulse region is superior to that of YAG and glass lasers.

(ii) As a high power amplifier, using picosecond pulses of duration $\sim 5 \times 10^{-12}$ s and powers of approximately 1 GW, the $Nd^{+3}:POCl_3:ZrCl_4$ system (155 mm long and 7.5 mm in diameter) has produced gains of 9. This performance is quite remarkable in view of the mis-match between the spectrum of the input signals and the amplifier linewidth.

(iii) Thermal distortion due to heating by the pumping radiation has been shown to be an important problem in the design and performance of this kind of laser.

(iv) Experiments have been carried out to explore the mechanism of self-Q-switching in the liquid laser. These have shown that the effect is due to a phase grating formed by the spatially periodic deposition of heat energy.

(v) Frequency shifts occurring in wide band amplifiers have been observed and their effect on the power gain of the amplifier has been investigated. A simple theoretical explanation of the effect was given.

(vi) Several parameters of the liquid laser have been measured directly: stimulated emission cross-section $\sim 7.5 \times 10^{-20}$ cm^2 ± 40%; transmission loss using picosecond pulses $\sim(0.5 \pm 0.2)\%$ per cm; effective lifetime of level 2 $\sim$140 μs; dynamic loss of the liquid laser oscillator $\sim$2% per cm.

(vii) A simple theoretical explanation for the occurrence of satellite pulses on the two photon fluorescence pictures was given. These were also observed experimentally.

Several other observations were also made.

The present results indicate that the neodymium liquid laser is a serious competitor in the field of high power laser applications. The ability of the active medium to be circulated, the absence of damage problems and the low cost of production are three inherent advantages over other kinds of lasers.

In view of the results of this thesis the next steps to be taken in the further development of liquid lasers should be the construction of larger systems and the investigation of the limitations on the performance of the laser imposed by non-linear optical processes. In addition to this, the extraction of as much energy as possible from the energy stored under the inhomogeneous linewidth of the amplifier, should be a matter of considerable importance.

REFERENCES

1. SCHALOW, A.L. and TOWNES C.H., Phys. Rev., 112, 1940 (1958).

2. STATZ, H. and deMARS, G., In 'Quantum Electronics', p.530 Columbia University Press (1960).

3. TANG, C.L., STATZ, H. and deMARS, G., J. Appl. Phys., 34, 2289 (1963).

4. CASPERSON, L.W. and YARIV, A., IEEE J. Quantum Electron., QE-8, 69 (1972).

5. MAGYAR, G., Opto-Electron., 2, 68 (1970).

6. SOTSKII, B.A. and GONSHARENKO, A.M., Opt. Spectrosc., 19, 435 (1965).

7. KOROBKIN, V.V., LEONTOVICH, A.M., POPOVA, M.V. and SHCHELEY, M.Ya., Soviet Phys. - JETP, 26, 10 (1968).

8. SELDEN A.C., Opt. Commun., 5, 62 (1972).

9. ANDREOU, D., SELDEN A.C. and LITTLE V.I. J. Phys. D: Appl. Phys., 5, 1405 (1972).

10. FOX, A.G. and LI T., In 'Advances in Quantum Electronics', p.308 ed. J. Singer, Columbia University Press (1961).

11. VAINSHTEIN, L.A., Sovier Phys. - JETP, 17, 709 (1963).

12. LENGYEL B.A., 'Introduction to Laser Physics', Wiley, New York (1966).

13. ROSS D., 'Lasers, Light Amplifiers and Modulation', (AP) Academic Press (1969).

14. YARIV, A. and GORDON, J.P., Proc. IEEE, 51, 4 (1963).

15. CABEZAS, A.Y. and TREAT, R.P., J. Appl. Phys., 37, 3556 (1966).

16. WINSTON, H. and GUDMUNDSEN, R.A., Appl. Opt., 3, 143 (1964).

17. HELLER, A., Physics Today, 20, 34 (1967).

18. KATZENSTEIN, J., MAGYAR, G. and SELDEN, A.C. Opto-Electron., 1, 13 (1969).

19. KEY, P.Y., HARRISON, R.G., LITTLE, V.I. and KATZENSTEIN, J., IEEE J. Quantum Electron., QE-6, 641 (1970).

20. SAMELSON, H., LEMPICKI, A. and BROPHY, V., J. Appl. Phys., 39, 4029 (1968).

21. LETOKHOV, V.S. and PAVLIK, B.D., Soviet Phys. - Tech. Phys., 13, 251 (1968).

22. SAMELSON, H., LEMPICKI, A. and BROPHY, V.A., IEEE J. Quantum Electron., QE-4, 849 (1968).

23. KOGELNIC, H., In 'Lasers', vol.1, p.295, ed. A. Levine, Edward Arnold Ltd., (1966).

24. MAITLAND, A. and DUNN, M.H., In 'Laser Physics', North Holland Publishing Co., (1969).

25. MILLER, S.E., Scientific American, 214, 19 (1966).

26. YARIV, A. In 'Quantum Electronics III', p.1055, ed. P. Grivet and N. Bloembergen, Columbia University Press (1964).

27. JOHNSON, L.F., J. Appl. Phys., 34, 897 (1963).

28. SNITZER, E., In 'Quantum Electronics III' p.999, ed. P. Grivet and N. Bloembergen, Columbia University Press (1964).

29. BALDWIN, G.D. and RIEDEL, E.P., J. Appl. Phys., 38, 2726 (1967).

30. MELAMED, N.T. and HIRAYAMA, C., Appl. Phys. Letters, 6, 43 (1965).

31. SNITZER, E. and WOODCOCK, R., IEEE J. Quantum Electron., QE-2, 627 (1966).

32. SNITZER, E. and YOUNG, C.G., In 'Lasers', vol.2, p.191, ed. A.K. Levine, Edward Arnold Ltd., (1968).

33. DEVLIN, G.E., McKENNA, J., MAY, A.D. and SCHALOW, A.L. Appl. Opt., 1, 11 (1962).

34. SAMELSON, H., KOCHER, R., WASZAK, T. and KELLNER, S., J. Appl. Phys., 41, 2459 (1970).

35. YARIV, A., Proc. IEEE, 51, 1723 (1963).

36. McCLUNG, F.J. and HELLWARTH, R.W., J. Appl. Phys., 33, 828 (1962).

37. WAGNER, W.G. and LENGYEL, B.A., J. Appl. Phys., 34, 2040 (1963).

38. MENAT, M., J. Appl. Phys., 36, 73 (1965).

39. VUYLSTEKE, A.A., J. Appl. Phys., 34, 1615 (1963).

40. MIDWINTER, J.E., Brit. J. Appl. Phys., 16, 1125 (1965).

41. ANDREOU, D., LITTLE, V.I., SELDEN, A.C. and KATZENSTEIN, J., J. Phys. D: Appl. Phys., 5, 59 (1972).

42. RATNER, A.M. and CHERNOV, V.S., Soviet Phys. - Tech. Phys., 13, 55 (1968).

43. LETOKHOV, V.S. and SUCHKOV, A.F., Soviet Phys - JETP, 23, 763 (1966).

44. SELDEN, A.C., J. Phys. D: Appl. Phys., 3, 1935 (1970).

45. HERCHER, M., Appl. Opt., 6, 947 (1967).

46. DARÉE, K. and PUELL, H., Z. Naturforsch, 25a, 909 (1970).

47. HEYNAU, H.A. and FOSTER, M.C., Laser Focus, p.20, August 1968.

48. KEY, M.H. and PRESTON, D.A., J. Phys. E : Scient. Instrum., 3, 932 (1970).

49. DiDOMINICO, M., J. Appl. Phys., 35, 2870 (1964).

50. SMITH, P.W., Proc. IEEE, 58, 1342 (1970).

51. DUGUAY, M.A., HANSEN, J.W. and SHAPIRO, S.L., IEEE J. Quantum Electron, 6, 725 (1970).

52. SACCHI, C.A., SONCINI, G. and SVELTO, O., Nuovo Cimento, 48, 58 (1967).

53. KUZNETSOVA, T.I., MALYSHEV, V.I. and MARKIN, A.S., Soviet Phys. - JETP, 25, 286 (1967).

54. BRADLEY, D.J., LIDDY, B. and SLEAT, W.E., Opt. Commun., 2, 391 (1971).

55. GIORDMAINE, J.A., RENTZEPIS, P.M., SHAPIRO, S.L. and WECHT, K.W., Appl. Phys. Letters, 11, 216 (1967).

56. AKHMANOV, S.A. and CHIRKIN, A.S., Opto-Electron., 3, 111 (1971).

57. BRADLEY, D.J., NEW, G.H.C. and CAUGHEY, S.J., Phys. Letters, 30A, 78 (1969).

58. VON DER LINDE, D., BERNECKER, O. and KAISER, W., Opt. Commun., 2, 149 (1970).

59. VON DER LINDE, D., IEEE J. Quantum Electron., QE-8, 328 (1972).

60. STUART, R.D., 'An Introduction to Fourier Analysis', p.107, Methuen, London (1961).

61. MAGYAR, G. and SELDEN, A.C., Appl. Opt., 9, 2040 (1970).

62. KOROBKIN, V.V., MALYUTIN, A.A and PROKHOROV, A.M., Soviet Phys. - JETP Letters, 12, 150 (1970).

63. KOROBKIN, V.V., MALYUTIN, A.A. and SHCHELEV, M.Ya., Soviet Phys - JETP Letters, 11, 103 (1970).

64. LETOKHOV, V.S., Soviet Phys. - JETP, 27, 746 (1968).

65. ECKARDT, R.C., LEE, C.H. and BRADFORD, J.N., Appl. Phys. Letters, 19, 420 (1971).

66. KUIZENGA, D.J. and SIEGMAN, A.E., IEEE J. Quantum Electron., QE-6, 709 (1970).

67. HARRACH, R. and KACHEN, G., J. Appl. Phys., 39, 2482 (1968).

68. KLAUDER, J.R., DUGUAY, M.A., GIORDMAINE, J.A. and SHAPIRO, S.L., Appl. Phys. Letters, 13 174 (1968).

69. MALYSHEV, B.I., MASALOV, A.V. and SYCHEV, A.A., Soviet Phys.-JETP, 32, 27 (1972).

70. PICARD, R.H. and SCHWEITZER, P., Phys. Rev. A., 1, 1803 (1970).

71. KACHEN, G.I. and KYSILKA, J.O., IEEE J. Quantum Electron., QE-6, 84 (1970).

72. KEY, P.Y. and HARRISON, R.G., Phys. Rev. A., 5, 1839 (1972).

73. DENARIEZ, M. and BRET, G., Phys. Rev., 171, 160 (1968).

74. LANDAU, L.D. and LIFSHITZ, E.M. In 'Electrodynamics of Continuous Media', p.387, Pergamon Press (1960).

75. WIGGINS, T.A., WICK, R.V., FOLTZ, N.D., CHO, C.W. and RANK, D.H., J. Opt. Soc. Am., 57, 661 (1967).

76. HARRISON, R.G., KEY, P.Y. and LITTLE, V.I., To be published in Proc. Royal Society.

77. FOLTZ, N.D., CHO, C.W., RANK, D.H. and WIGGINS, T.A., Phys. Rev., 165, 396 (1968).

78. ALFANO, R.R., LEMPICKI, A. and SHAPIRO, S.L., IEEE J. Quantum Electron., QE-7, 416 (1971).

79. AVIZONIS, P.V. and GROTBECK, R.L., J. Appl. Phys., 37, 687 (1966).

80. CABEZAS, A.Y., McALLISTER, G.L. and NG, W.K., J. Appl. Phys., 38, 3487 (1967).

81. FILL, E.E. and FINCKENSTEIN, K.G.V., IEEE J. Qauntum Electron., QE-8, 24 (1972).

82. SCHULZ-DuBOIS, E.O., Bell Syst. Tech. J., 43, 625 (1964).

83. KRYUKOV, P.G. and LETOKHOV, V.S., Soviet Phys. - Uspekhi, 12, 641 (1970).

84. BASOV, N.G., AMBARTSUMYAN, R.V., ZUEV, V.J., KRYUKOV, P.G. and LETOKHOV, V.S., Soviet Phys. - JETP, 23, 16 (1966).

85. LETOKHOV, V.S., Soviet Phys. - Tech. Phys., 13, 644 (1968).

86. EILBECK, J.C. and BULLOUGH, R.K., J. Phys. A., 5, 820 (1972).

87. YOSHIDA, K., SASAKI, T., WAKI, M., YAMANAKA, T., KANG, H. and YAMANAKA, C., Japan J. Appl. Phys., 10, 1643 (1971).

88. MICHON, M., IEEE J. Quantum Electron., QE-2, 612 (1966).

89. MICHON, M., ERNEST, J., DUMANCHIN, R., HANUS, J. and RAYNAUD, S. Phys. Letters, 19, 217 (1965).

90. DUMANCHIN, R., FARCY, J.C., MICHON, M. and VINCENT, P., IEEE J. Quantum Electron., QE-7, 53 (1971).

91. BELAN, V.R., BRISKINA, Ch.M., CRICOR'YANTS, V.V. and ZHABOTINSKII, M.E. Soviet Phys.-JETP, 30, 627 (1970).

92. GRIGOR'YANTS, V.V., Soviet Phys.-JETP, 31, 853 (1970).

93. WINSTON, H. and GUDMUNDSEN, R.A., Appl. Opt., 3, 143 (1964).

94. LEMPICKI, A. and SAMELSON, H., Phys. Letters, 4, 133 (1963).

95. SOROKIN, P.P. and LANKARD, J.R., IBM J. Research Develop., 10, 162 (1966).

96. HELLER, A., Appl. Phys. Letters, 9, 106 (1966).

97. LEMPICKI, A., and HELLER, A., Appl. Phys. Letters, 9, 108 (1966).

98. SOROKIN, P.P., LANKARD, J.R., MORUZZI, V.L. and HAMMOND, E.C., J. Chem. Phys., 48, 4726 (1968).

99. BASS, M., DEUTSCH, T.F. and WEBER, M.J., In 'Lasers', vol.3, p.269, Marcel Dekker (1971).

100. HUTCHINSON, C.H. and MAGNUM, B.W., J. Chem. Phys., 32, 1261 (1960).

101. CALLAGHER, P.K., J. Chem. Phys., 43, 1742 (1965).

102. HELLER, A., J. Am. Chem. Soc., 88, 2058 (1966).

103. WHITTAKER, B., Nature, 228, 157 (1970).

104. HAAS, Y. and STEIN, G., J. Phys. Chem., 75, 3677 (1971).

105. BRECHER, C., FRENCH, K., WATSON, W. and MILLER, D., J. Appl. Phys., 41, 4578 (1970).

106. SHEPHERD, T.M., Nature, 216, 1200 (1967).

107. G.T. & E. Report 'High-Energy Pulsed Liquid Laser', Contract N00014-68-C-0110, No. TR 70-826.10, January (1970).

108. DEUTSCHBEIN O.K. and PAUTRAT, C.C., IEEE J. Quantum Electron., QE-4, 48 (1968).

109. HELLER, A. and BROPHY, V., J. Appl. Phys., 39, 4086 (1968).

110. ANDREOU, D., FENEMORE, K., KATZENSTEIN, J., SELDEN, A.C. and WARD, S. UKAEA Culham Laboratory Report No. CLM-R119 (1972).

111. SAMELSON, H., HELLER, A. and BRECHER, C., J. Opt. Soc. Am., 58, 1054 (1968).

112. COLLIER, F., GIRARD, G., MICHON, M. and POCHOLLE, J.P., IEEE J. Quantum Electron., QE-7, 519 (1971).

113. ALFANO, R.R. and SHAPIRO, S.L., Opt. Commun., 2, 90 (1970).

114. LANG, R.S., BAUMHACKER, H. and FILL, E.E., Phys. Lett., 32A, 433 (1970).

115. WATSON, W., REICH, S., LEMPICKI, A. and LECH, J., IEEE J. Quantum Electron., QE-4, 842 (1968).

116. G.T. & E. Report 'High-Energy Pulsed Liquid Laser', Contract N00014-68-C-0110, No.70-826.12, July (1970).

117. MALYSHEV, B.N., KARNAUKH, N.P., PARAMONOVA, N.A. and KULIKOVSKII, B.N. Soviet J. Quantum Electron., 1, 103 (1971).

118. ANAN'YEV, Yu.A., BUZHINSKIY, L.M., VANYUKOV, M.P., DAUENGAUER, E.F. and SHOROKHOV, O.A., Soviet J. Opt. Tech., 35, 561 (1968).

119. LANG, K.R. and BARNES, F.S., J. Appl. Phys., 35, 107 (1964).

120. EDWARDS, J.G., Opto-electron., 1, 1 (1969).

121. TOLANSKY, S., 'An Introduction to Interferometry', p.197, Longmans (1962).

122. SALKOVA, E.N., SOSKIN, M.S. and POGORETSKY, P.P., Ukran. Physical J. 15, 824 (1970).

123. SELDEN, A.C., Opt. Commun., (in press) (1972).

124. ANDREOU, D. and LITTLE, V.I., J. Phys. D. : Appl. Phys., (in press) (1973).

125. HARRACH, R.J., MacVICAR, T.D., KACHEN, G.I. and STEINMETZ, L.L., Opt. Commun., 5, 175 (1972).

126. NEWBERY, A.R., Brit. J. Appl. Phys. (J. Phys. D.)., 1, 1849 (1968).

127. EVERETT, P.N., Rev. Scient. Instrum., 41, 1495 (1970).

128. AUSTON, D.H., Appl. Phys. Letts., 18, 249 (1971).

129. GARMIRE, E.M. and YARIV, A., IEEE J. Quantum Electron., QE-3, 222 (1967).

130. BRADLEY, D.J., NEW, G.H.C. and CAUGHEY, S.J., Phys. Letters, 32A, 313 (1970).

131. POLANYI, T.G., and WATSON, W.R., J. Appl. Phys., 34, 553 (1963).

132. QUELLE, F.W., In 'Damage in Laser Glass', p.110. (obtainable from The American Soc. Testing Materials (ASTM), Publication 469 (1969).

133. DAVIT, J., In 'Damage in Laser Glass', p.100 (obtainable from The American Soc. Testing Materials (ASTM) Publication 469 (1969).

134. BORN, M. and WOLF, E., 'Principles of Optics', p.399, Pergamon Press (1959).

135. FELDMAN, A., WAYLER, R. and HOROWITZ, D., NBS Technical Note 565, p.41 (1971).

136. SAMELSON, H. and LEMPICKI, A., J. Appl. Phys., 39, 6115 (1968).

137. LANG, R.S., BAUMHACKER, H. and FILL, E.E., Phys. Letters, 32A, 43 (1970).

138. ALFANO, R.R. and SHAPIRO, S.L., Opt. Commun., 2, 90 (1970).

139. TITTEL, K.F. and CHERNOCH, J.P., Proc. IEEE 53, 82 (1965).

140. PENZKOFER, A. and KAISER, W., Appl. Phys. Letters, 21, 427 (1972).

141. HONGYO, M., SASAKI, T., NAGAO, Y., UEDA, K. and YAMANAKA, C., IEEE J. Quantum Electron., QE-8, 192 (1972).

APPENDIX

DEFINITIONS OF SYMBOLS USED IN THE TEXT

SECTION 1.1

$\Gamma_{12}(\tau)$ is the correlation function describing the average fluctuation between two points 1 and 2 in space and within a time interval τ

$I(\vec{r},t)$ is a complex, random and analytic function corresponding to the amplitude of the wave in the classical representation.

X and Y are the real and imaginary parts of $I(\vec{r},t)$

τ is the coherence time

ν is the frequency of the light signal

$\Delta\nu$ is the band-width of the light signal

$\Gamma_{11}(\tau)$ is the auto-correlation function

$\Gamma_{12}(0)$ is the spatial correlation function

$\vec{r}$ denotes the position coordinate

t denotes the time

$*$ denotes the complex conjugate

$\langle\ \rangle$ denotes the ensemble average

$2d$ is the limiting diameter of the aperture in the resonator

λ is the wavelength of the radiation

θ is the diffraction angle

L is the length of the resonator

N is the Fresnel number

$\mathfrak{I}$ is the intensity of the radiation

SECTION 1.2

$W(\nu)$ is the induced transition rate

ν is the frequency of the radiation

$A = 1/\tau$ is the spontaneous transition rate

$I_\nu d\nu$ is the energy flux (watts/cm^2) due to frequencies between ν and $\nu + d\nu$

$g(\nu)$ is the atomic lineshape function

$p(\nu)$ is the radiation density per unit frequency interval

$\Delta\nu$ is the full width at half the maximum

ν_0 is the frequency at the centre of the distribution

$I(\nu,x)$ is the value of $I_0(\nu)$ at a distance x along the amplifier

$k(\nu)$ is the absorption coefficient of the medium

$\sigma(\nu)$ is the stimulated atomic cross-section of the active medium

N_1, N_2 are the population densities of levels 1 and 2 in ions/cm^3

g_1, g_2 are the multiplicities of levels 1 and 2

B is the Einstein stimulated emission coefficient.

SECTION 1.3

I is the energy density of radiation

c is the velocity of light

W induced transition rate

h is Planck's constant

ν is the frequency of the radiation

t_p is the lifetime of a photon in the cavity

L is the length of the cavity

γ is the total loss per pass

Q is the quality factor of the cavity

g_1, g_2 are the multiplicities of levels 1 and 2

τ is the fluorescence lifetime of level 2

N_1, N_2 are the population densities of levels 1 and 2

ΔN_T is the population inversion at threshold per unit volume

V is the volume of the active material

$\Delta\nu$ is the full width at half the maximum of the fluorescence line

P_{min} minimum power which must be expended to maintain ΔN_T atoms in level 2.

SECTION 1.5

ℓ is the length of the active medium

n is the refractive index of the active medium

λ is the wavelength of the laser radiation

c is the velocity of light

L is the length of the cavity

L_1', L_2' are the radii of the cavity mirrors

SECTION 2.1

Φ is the number of photons per unit volume in the cavity

N_2 is the inverted population per unit volume

t_p is the photon lifetime in the cavity

$\tau = \frac{1}{A\mu}$ is the lifetime of level 2, A being the spontaneous emission rate for a 2 → 1 transition and μ taking account of all the other processes depleting the population inversion such as spontaneous emission in other lines and non-radiative transitions.

f is the fraction of spontaneously emitted light coupled into the aperture of the clad rod

n_1 is the refractive index of the core

n_c is the refractive index of the cladding

P_i is the pumping power

$N'_2 = \frac{P_i}{A\mu}$ is the inversion that would exist had there been no laser radiation in the cavity

p_m is the density of the modes

$B' = \frac{1}{\tau p_m}$ is the stimulated emission coefficient

F is the cross relaxation rate and it is proportional to the departure of the population inversion from equilibrium

$$P'_i = P_i \left(1 + \frac{F}{A\mu}\right)$$

$$\mu' = \left(\mu + \frac{F}{A}\right)$$

N_o is the steady state value of N_2 obtainable from equation (2.2) by putting $dN_2/dt = 0$

Φ_o is the steady state value of Φ obtainable from equation (2.1) by putting $d\Phi/dt = 0$

$n'(t)$ is a term representing small oscillations about N_o

$i(t)$ is a term representing small oscillations about Φ_o

r_1 is the radius of the active medium

r_2 outer radius of the laser cell (cladding)

W is the induced transition rate

N_1 is the population of level 1 per unit volume

t_1 is the lifetime of atoms in level 1

t_2 is the spontaneous lifetime of level 2 for a 2→1 transition

R_1, R_2 represent the number of atoms per unit volume per second pumped into levels 1 and 2 respectively

R'_2 is the effective pumping rate of level 2

h is Planck's constant

ν is the frequency of oscillation

V is the volume of the active medium

ΔN_T is the population inversion at threshold

P_c is the rate of stimulated emission into the cavity

P is the electrical input power to the lamp

$h\nu_p$ is the average energy per photon in the absorption bands

ε_1 is the conversion efficiency of the electrical power into useful light in the pump bands

$\varepsilon_2 \frac{\nu_p}{\nu}$ is the efficiency with which photons are coupled into the active medium

ϵ_3 is the quantum efficiency with which the medium utilizes the photons

$q = \epsilon_1 \epsilon_2 \epsilon_3 \frac{\nu}{\nu_p}$ is the material efficiency factor

P_T is the threshold power

P_{out} is the output power

T is the transmission of the output mirror

α is the passive loss of the laser material per cm

ℓ is the length of the active medium

E_{out} is the output energy from the laser

E is the electrical input energy

E_T is the threshold energy

R is the output mirror reflectivity

σ is the stimulated emission cross section of the laser

c is the velocity of light

t_{laser} time during which the laser is operating

$\zeta = \frac{q\, t_2}{h\nu V}$

SECTION 2.2.2

Φ is the photon density in the cavity

ΔN is the population inversion per unit volume

k is the amplification coefficient and it is proportional to the population inversion

k_o is the absorption coefficient of the unexcited material

N_o is the number of active ions per unit volume

ℓ is the length of the laser material

L is the optical distance between the reflectors

$n = \frac{\Delta N}{N_o}$

$\varphi = \frac{\Phi}{N_o}$

t_p is the photon lifetime in the cavity

γ is the total loss per pass

c is the velocity of light

n_m is the inversion at the peak of the pulse

n_i is the initial value of n, immediately after switching

n_f is the final value of n, after the pulse is emitted

t_m is the time it takes the pulse to reach its maximum

φ_i is the initial photon density immediately after switching

φ_m is the photon density in the cavity corresponding to the peak of the pulse

φ_f is the final photon density, after the pulse is emitted

V is the volume of the active material

γ_c represents the losses due to coupling to the output

γ_i represents all the other losses except those accounted for by γ_c

P_{out} is the output power

SECTION 2.3.1

φ is the fixed phase difference between modes

$E(t)$ is the time dependent electric field at any point

ω_o is the centre frequency of oscillation

$\Delta\omega$ is the frequency difference between two successive resonances

$\Delta f = \frac{\Delta\omega}{2\pi}$

t is the time

L is the cavity length

c is the velocity of light

$2N+1$ is the number of modes

E_o is the amplitude of the electric field of each mode

$A(t)$ is the amplitude of the distribution resulting from the interaction of modes

T is the round trip time of the cavity

$\Delta\nu$ is the total oscillating bandwidth

$\Delta\tau = \frac{1}{\Delta\nu}$ is the pulse width

I_p is the peak power radiated

SECTION 2.3.2

$E_m(\vec{r},t)$ is the electric field of the m^{th} cavity mode

$A_m(t)$ is the amplitude of the m^{th} cavity mode

$U_m(\vec{r})$ is the space dependent part of the mode function

ω_m is the frequency of the m^{th} cavity mode

$\theta_m(t)$ is the quantity describing the evolution of the phase of the field

Δ is the factor accounting for the gain of the active medium and the losses of the cavity, but not the loss due to the saturable absorber

Δ_a is the factor accounting for the losses due to the saturable absorber

C_1, C_2 are constants

T_1 is the relaxation time of the saturable absorber

μ is the electric dipole moment of the absorber

ξ is a parameter characterizing the mode overlap in the dye cell and is defined in the text

$\hbar = \frac{h}{2\pi}$ is Planck's constant

$\Delta\omega$ is the difference frequency between adjacent modes

V is the volume of the resonator

x is the distance along the resonator axis

x_0 is the coordinate of the centre of the dye cell

L is the length of the resonator

c is the velocity of light.

SECTION 2.3.3

$F(\tau)$ is the fluorescence density from the TPF dye cell

TPF stands for 'Two Photon Fluorescence'

τ is twice the light transit time from the mirror to the point under consideration

$\Gamma^{(2)}(\tau)$ is the second order correlation function and characterizes the overlapping of the pulses

$I(t)$ is the intensity of the light beam at time t

$F(\omega)$ denotes the frequency spectrum of the pulses

$H(\omega)$ defines the form of the amplitude modulated function

$G'(t)$ is the waveform of the time dependent amplitude

$G(t)$ is the Fourier transform of unmodulated spectrum $F(\omega)$

ω is the frequency of the radiation

τ' is the time displacement of the subsidiary waveforms

a is the amplitude modulation of the frequency spectrum

$p = \frac{1}{4} a^2$

$I_1(t)$ is the intensity of the radiation corresponding to $G^2(t)$

SECTION 2.4

P is the non-linear polarization

$\chi_1, \chi_2, \chi_3 \ldots$ denote the first, second, third ... order polarizabilities

E is the electric field

SECTION 3.1

τ is the duration of the light pulse.

$E(x)$ is the energy of the pulse as a function of position x along the amplifier length, in $J\ cm^{-2}$

x is the point under consideration along the amplifier length

ℓ is the amplifier length

$I(x,t)$ is the photon flux at a point x along the amplifier length and at time t, in photons/s cm^2

δx is the thickness of a slab at a distance x along the amplifier length

$\Delta N(x,t)$ is the population inversion per cm^3 at a distance x along the amplifier and at time t

α represents the lumped losses per cm

σ is the stimulated emission cross-section of the amplifying medium

ΔN is the population inversion per cm^3 before any stimulated emission occurs

ν is the frequency of the input pulse

h is Planck's constant

SECTION 3.2

α represents the lumped losses per cm

$I(x,t)$ is the photon flux at a point x along the amplifier length and at time t, in photons/s cm^2

$\Delta N(x,t)$ is the population inversion per cm^3 at a distance x along the amplifier length and at time t

x is the point under consideration along the amplifier length

$I_o = \int_o^t I(t)dt = I(t)\ dt$ represents an input square pulse

$\Delta N = \int_o^x \Delta N(x)dx = \Delta N(x)x$ represents a uniform distribution of the population inversion along the amplifier length

σ is the stimulated emission cross-section of the amplifying medium

$G(x,t)$ is the saturation parameter at a point x along the amplifier and at time t

$S(x,t)$ is the saturation parameter at a point x along the amplifier and at time t

$G(x,0)$ initial value of the gain at a point x

SECTION 9.2

R is the effective reflectivity of the beam splitter

f is the fraction of the incident light with normal vibrations

R_N is the reflectivity of the beam splitter for light having normal polarization to the plane of incidence

R_p is the reflectivity of the beam splitter for light having parallel polarization to the plane of incidence

δ is the angle of incidence on to the beam splitter

SECTION 9.5

E is the input energy in J cm^{-2}

x is the distance along the amplifier axis

α is the loss coefficient per cm

$\sigma_{(\nu)}$ is the stimulated emission cross-section

ΔN_1 is the population inversion per cm^3

ν is the frequency of the amplified signal

h is Planck's constant

ℓ is the amplifier length

G_1 is the gain of a small input signal

ΔN_2 is the population inversion per cm^3 which is left in the amplifier after the passage of the first pulse

V is the volume of the amplifying medium

W_{in} is the input energy to the amplifier

W_{out} is the output energy from the amplifier

G_2 is the small-signal gain corresponding to the population inversion ΔN_2

A is the geometrical cross-section of the amplifier

SECTION 9.7

$\Delta N(t)$ is the population inversion at or time t after firing the flashlamps

P(t) is the pumping rate of ions into level 2 in watts

ν_ℓ is the signal frequency

τ is the total lifetime of level 2

h is Planck's constant

G(t) is the small-signal gain

ℓ is the amplifier length

t_2 is the lifetime of level 2 for a 2→1 transition

$1/t_q$ is the total transition rate from level 2, excluding 2-1 transitions

SECTION 10.4

$I(\nu)$ is the spectral intensity of the radiation

x is the distance along the amplifier length

ν denotes the frequency

$\sigma(\nu)$ is the stimulated emission cross-section in cm^2

$\Delta N(\nu)$	is the total inversion density in ions/cm^3 per unit frequency interval
$K(\nu)$	is the convolution of $\sigma(\nu)$ and $\Delta N(\nu)$ and has the shape of the fluorescence line
ℓ	is the length of the amplifier
I	is the total power density at a point along the amplifier (watts cm^{-2})
$I_{out}(\nu)$	is the output spectral intensity
$I_{in}(\nu)$	is the input spectral intensity
R	is the reflectivity of the mirror at the back of the amplifier
G_F	is the gain of the amplifier in the forward direction
G_B	is the gain of the amplifier in the backward direction
K_s	is the value of K at the signal frequency
K_o	is the value of K at the centre of the fluorescence line
ν_s	represents the signal frequency

ACKNOWLEDGEMENTS

I would like to acknowledge the guidance and able supervision of Dr V.I. Little during the course of this work, and to thank him for his constant encouragement. I also wish to thank Dr A.C. Selden whose interest and discussions on the subject have helped towards the more precise statement of the results, and Dr P.Y. Key for many stimulating discussions on non-linear optics and mode-locking.

I am grateful to Royal Holloway College for a financial award to carry out this work and to the UKAEA for the opportunity to use the extensive facilities of Culham Laboratory. The work was carried out under an agreement between the latter two Institutions, and my thanks go to Drs T.K. Allen and J. Katzenstein who were principally involved in making this research project a reality. My appreciation goes to Mr S. Ward for his expert technical assistance and Mrs I. Godwin for typing the manuscript, though many others deserve my thanks.

Finally my appreciation and thanks to my parents without whose support and encouragement I would have not had an academic career.

PUBLICATIONS

(*Reprinted from Nature, Vol.* 238, *No.* 5361, *pp.* 216–217.
July 28, 1972)

Observation of a Frequency Shift during the Amplification of a Narrow Spectrum Light Signal

THE amplification of light signals by a material in an inverted state depends on the gain profile of the amplifying medium and the spectrum of the incoming signal. The fundamental light amplification processes suggest that if a Gaussian (or Lorentzian) shaped narrow spectrum signal is amplified by a wide linewidth amplifier whose line centre does not coincide with that of the signal, frequency shifts occur during the amplification process. In this letter we report a direct experimental observation of a frequency shift occurring during the amplification of a narrow spectrum signal by an amplifier of wide linewidth. The ability of trivalent neodymium to serve as the active ion in different host materials provided us with the necessary experimental conditions because the spectra of the different systems do not coincide exactly.

The experimental arrangement is shown in Fig. 1. The input signals consist of mode-locked pulse trains from an

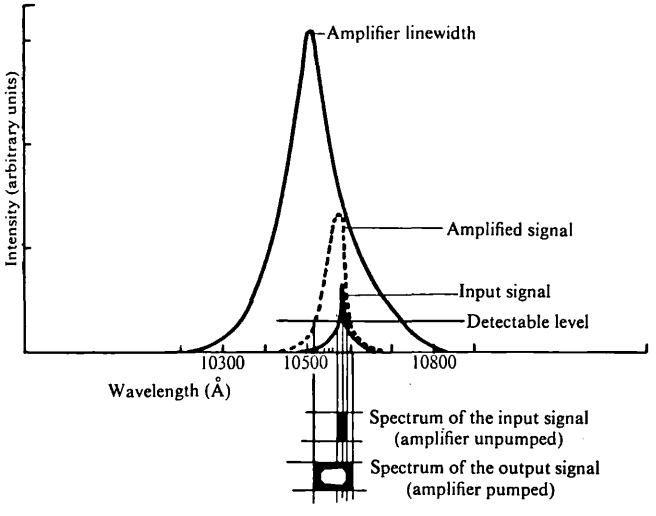

Fig. 2 Schematic diagram demonstrating the amplification results of Fig. 3.

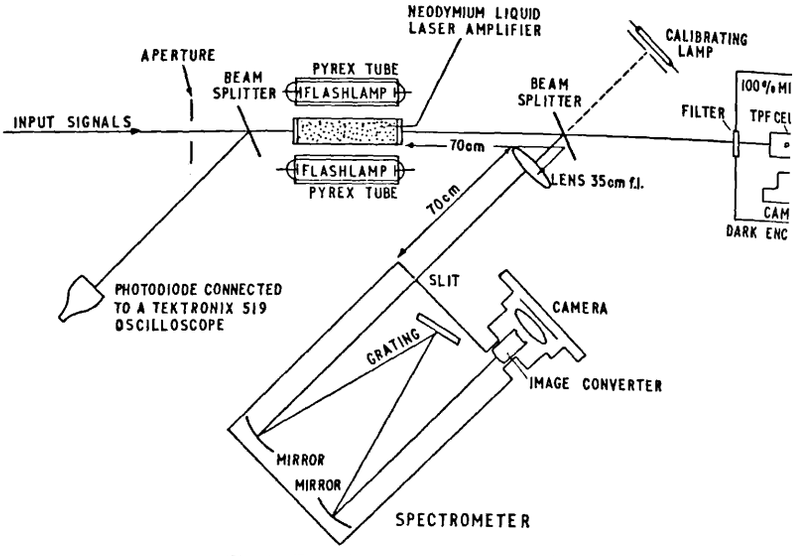

Fig. 1 Experimental arrangement for recording the spectra of the amplified signals.

Nd-glass LGN 55 oscillator. These pulses have a time duration of approximately 5 ps. The energies of the input signals used ranged from 30 to 80 mJ, and the amplifying medium was an $Nd^{3+}:POCl_3:Z_rCl_4$ liquid system contained in a cell 155 mm long and 7.5 mm in diameter. It was pumped with a double flashlamp arrangement with 'Pyrex' tubes around each flashlamp to eliminate UV radiation. The linewidth of this system is 200 Å at half maximum[1] (Fig. 2), with the centre of the line at 10,520 Å.

The spectra of the signals were taken with a Monospek 1000 grating scanning spectrometer with a Mullard 6929-1 (S1) image converter tube placed in the plane of the exit slit. In order to avoid damaging the replica grating with the high powers of the picosecond pulses, only part of the output beam was reflected into the spectrometer. The exit of the amplifier was imaged at unit magnification onto the input slit of the spectrometer using a 35 cm focal length lens. We used a calibrating lamp to check the accuracy of the recording system, and found that the spectrometer-image converter arrangement is accurate to ± 0.5 Å.

The experimental results are shown in Fig. 3. The two lines correspond to 10,532 Å (left) and 10,570 Å (right). The input signals were first recorded without firing the amplifier, and spectra ranging from 5 to 20 Å wide were obtained, each

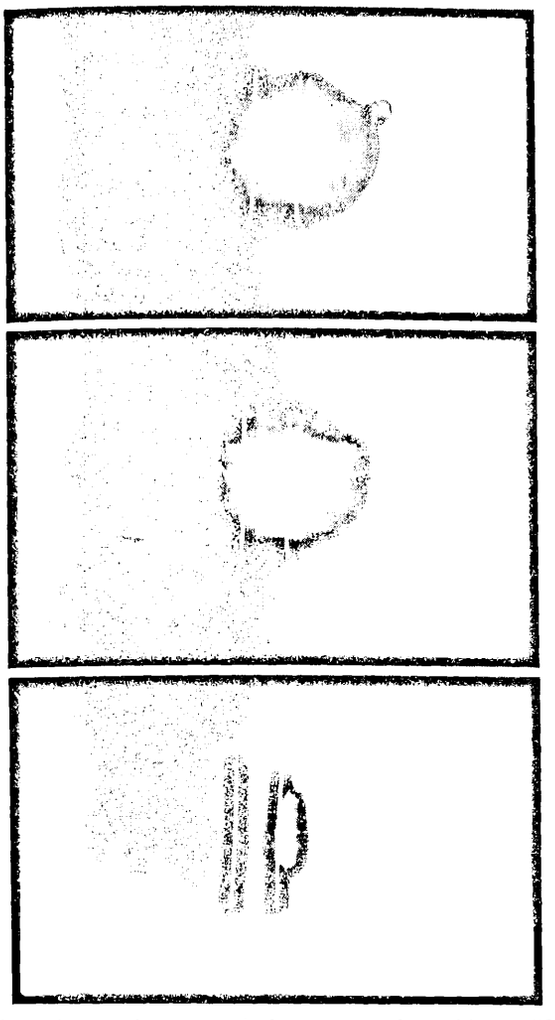

Fig. 3 Lower picture: typical spectrum taken with amplifier unpumped. The lines shown are 10,532 Å (left) and 10,570 Å (right). Top two pictures: typical spectra when the amplifier is fired with energy 722 J. The two lines correspond to the same wavelengths as in the lower picture.

centred at 10,580 Å. The spectra of the mode-locked pulses from an Nd-glass laser were shown to be largely Gaussian[2] with half width ~5 Å.

When the amplifier is fired the resulting spectrum is asymmetrical about the centre of the input signals. It is shifted

towards the centre of the amplifier linewidth and the pictures (Fig. 3) show that the asymmetry is approximately 27 Å. The gain of the amplifier at the time of transmission of the pulses was approximately 6. It is important that the shift never reaches the centre of the amplifier linewidth; this limits the gain obtained from the liquid. In experiments performed with the liquid as an amplifier (refs. 1, 3 and our unpublished work) an Nd-glass oscillator was used. The results described here suggest that the potentialities of the liquid as an amplifier are much better than implied by those experiments.

A schematic demonstration of the amplification process is shown in Fig. 2. The predicted spectra, similar to those obtained in our experiment, are shown below the graphs and are defined by the vertical lines.

Proper calibration of the film to record the intensity distributions of the spectral shifts, and measurements of the gain and energy of the input pulses, will allow important parameters of the cross-relaxation mechanisms in the liquid laser to be calculated by this method. Attempts to evaluate the effects of the spectral mismatch on the gain of the amplifier are now being made.

We thank Dr A. C. Selden for discussions and Mr. S. Ward for technical assistance. The experimental work was performed at the Culham Laboratory, UKAEA.

D. ANDREOU
V. I. LITTLE

Department of Physics,
Royal Holloway College,
University of London,
Englefield Green, Surrey

Received April 11, 1972.

[1] Samelson, H., Kocher, R., Waszak, T., and Kellner, S., *J. Appl. Phys.*, **41**, 2459 (1970).
[2] Von Der Linde, D., Bernecker, O., and Kaiser, W., *Opt. Commun.*, **2**, 149 (1970).
[3] Selden, A. C., *Eighth International Conference on Microwaves and Optical Generators and Amplification* (North-Holland, Amsterdam, 1970).

Printed in Great Britain by Flarepath Printers Ltd., St. Albans, Herts.

(Reprinted from Nature, Vol. 225, No. 5239, pp. 1239-1240, March 28, 1970)

Frequency Mixing in the Scattering of Light by Harmonically Bound Electrons

CLASSICAL electrodynamics predicts harmonic generation[1-3] and frequency mixing[4] in the scattering of light by free electrons. Quantum theory confirms these results[3-7]. Several authors (for example, refs. 8 and 9) have used the classical anharmonic oscillator model to give a qualitative account of non-linear phenomena in dielectrics. In the absence of an anharmonic restoring force, non-linear effects, up to the lowest order in external electric field, are in general quite small[10]. Calculations[11] stress this point in the case of second harmonic generation in the scattering of light. Here we extend these calculations to study the scattering of light when the incident beam contains two frequencies. As expected, we find that the combination frequencies also exist in the scattered radiation besides the fundamentals and their harmonics, and that the non-linear cross-sections become large for resonant denominators. Further, a proper choice of the two incident frequencies can yield an appreciable increase in the non-linear scattering cross-sections even without any precise resonance.

The equation of motion of the electron bound by a restoring force $m\omega_0^2\,\mathbf{z}$ when the incident electromagnetic beam contains two frequencies ω_a with wave vectors $\mathbf{k}_a$ $(a=1, 2)$ can be written as

$$v_0[\ddot{\mathbf{z}}+v^2(\ddot{\mathbf{z}}\cdot\dot{\mathbf{z}})\,\dot{\mathbf{z}}]+\omega_0^2\mathbf{z} = (e/m)\sum_a\{\mathbf{E}_a+[\dot{\mathbf{z}},\mathbf{H}_a]\}\cos(\omega_a t-\mathbf{k}_a\cdot\mathbf{z}+\delta_a) \quad (1)$$

where $\mathbf{z}$ is the position of the electron, δ_a are constants and $v_0=(1-\dot{\mathbf{z}}^2)^{-1/2}$.

This equation can be solved by making a perturbation expansion in power of E_a ($|\mathbf{E}_a|=|\mathbf{H}_a|=E_a$). The radiation field can then be evaluated by a method described in detail in ref. 1. It contains a complete spectrum of combination frequencies as well as the fundamentals and their harmonics. If terms are retained up to the third order in the amplitude of the two incident frequencies, scattering cross-sections are produced which correspond to sum and beat frequencies, along with those for fundamentals and their harmonics. Explicit expressions for the total cross-sections for scattering into ω_1, $2\omega_1$ and $\omega_1+\omega_2$ are given by

$$\sigma\omega_1=(I_1/I_0)\sigma_T\omega_1^4\,g_1^2\,[1+(1/20)\,g_1^2\,g_1\,\omega_1^4\,(10\,g_{1+1}-g_1+15\omega_1^2\,g_1^2)+(1/40)\,g_2^2\,\omega_2^2\,\{10\omega_1^2\,g_1\,(g_{1+2}+g_{1-2})+10\omega_1\omega_2\,g_2\,(g_{1+2}-g_{1-2})-\omega_1^2\,g_2^2+30\,\omega_1^2\,\omega_2^2\,g_1\,g_2^2\}] \quad (2a)$$

$$\sigma_2\omega_1 = (32\pi e^2/5m^2)\ (I_1^2/I_0)\ \sigma_T\ \omega_1^6\ g_1^2\ (5g_{1+1}^2 + g_1^2) \quad (2b)$$

$$\sigma\omega_1 + \omega_2 = (2\pi e^2/5m^2)\ (I_1 I_2/I_0)\sigma_T(\omega_1+\omega_2)^4 \times [5(\omega_1\, g_1 + \omega_2\, g_2)^2\, g_{1+2}^2 + (\omega_1+\omega_2)^2\, g_1^2\, g_2^2] \quad (2c)$$

where

$$g_{a\pm b} = (\omega_0^2 - \omega^2_{a\pm b})^{-1}, \quad q_a = e\,E_a/m\,\omega_a,$$

$\sigma_T = (8\pi/3) r_0^2$ is the Thomson scattering cross-section, $I_a = E_a^2/8\pi$ is the intensity of the components of the incident wave, and $I_0 = I_1 + I_2$.

Total cross-sections for scattering into ω_2, $2\omega_2$ and $\omega_1 - \omega_2$ can be obtained from those for ω_1, $2\omega_1$ and $\omega_1 + \omega_2$ respectively by interchanging the suffixes 1 and 2 in the first two cases and changing the sign of ω_2 in the third. In evaluating cross-sections for the fundamental frequency we have excluded the case $\omega_1 = \omega_2$, for its inclusion would unnecessarily complicate the calculations.

We may note that the expressions for $\sigma\omega_1 \pm \omega_2$ obtained here agree in the limit $\omega_0/\omega_a \to 0$ with those given by Fried and Frank[7] and do not agree with those given by Prakash and Vachaspati[4]. Expression 2c, however, is consistent with 2b, as can be seen by putting $\omega_1 = \omega_2$.

Expression 2b is in general quite small, except for resonant denominators (see equation 7d of ref. 11). The same is true for 2c, and for the intensity dependent part of expression 2a. It may, however, be noted that the cross-section for the fundamental frequency, ω_1, depends not only on ω_1 but also on ω_2. The change in the cross-section of the fundamental frequency due to the presence of ω_2 is easily obtained from the expression under the curly bracket in 2a. It is determined by the relative positions of ω_1, ω_2 and ω_0 in addition to the intensity of ω_2. Simple numerical analysis shows that this change is too small to be detectable when neither ω_1 nor ω_2 ($\sim\omega_1$) is in resonance with ω_0. When $\omega_1 \gg \omega_2$, ω_0 an interesting situation arises. It is clear that the cross-section for sum and difference frequencies should in this case be added to that of the fundamental. The total increase in $\sigma\omega_1$, denoted by $\Delta\sigma\omega_1$, can then be seen to be $\sim (3\pi/5)\ (e^2/m^2c^3) I_2\ \sigma_T\ \omega_1^2\ g_2^2 \sim 1{\cdot}4 \times 10^{-3} \times (\lambda_2^3/\lambda_1 d)^2 I_2\ \sigma_T$, $\lambda = 2\pi c/\omega$, if ω_0 and ω_2 are of the same order and $d (= \lambda_0 \sim \lambda_2)$ is expressed in Å. It can further be seen that $\Delta\sigma\omega_1$ is larger than $\sigma_2\omega_1$ or $\sigma\omega_{1\pm}\omega_2$ ($\omega_1 \sim \omega_2$) for a large d.

The expression for $\Delta\sigma\omega_1$ given above suggests that the non-linear increase in scattering could become large. This could happen also for those incident frequencies that are far away from the resonance frequency of the scattering body which consists of harmonically bound electrons. As an illustration we consider a simple experiment consisting of the scattering of two incident light beams, one of which is ruby laser light ($\lambda_2 \sim 7 \times 10^{-5}$ cm, $I_2 \sim 10^7$ W/cm^2, say), by sodium vapour ($\lambda_0 \sim 6 \times 10^{-5}$ cm, $d \sim 10^3$ Å). For this case we find the non-linear increase in scattering to be $\Delta\sigma\omega_1 \sim 1{\cdot}7 \times 10^{-20} \times \lambda_1^{-2}\ \sigma_T$, which is appreciable for high frequencies and seems to be experimentally detectable for λ_1 in the X-ray region. Instead of sodium vapour as

scatterer and ruby laser light as one of the incident beams, one can choose other scatterers and incident frequencies. With the advent of dye lasers one can have a fairly intense coherent radiation over a wide range of frequencies. This would allow for a suitable selection of λ_2, and hence of d, for a given λ_0, keeping in view the availability of I_2 and λ_1.

We thank Professor E. H. Hutten for his interest in this work, and the Royal Holloway College and the Science Research Council for their financial support.

D. Andreou
L. M. Bali

Department of Physics,
Royal Holloway College,
University of London,
Englefield Green,
Surrey.

Received November 25, 1969; revised January 20, 1970.

[1] Vachaspati, *Phys. Rev.*, **128**, 664 (1962); **130**, 2598 (E) (1963).
[2] Vachaspati, and Punhani, S. L., *Proc. Nat. Inst. Sci. Ind.* (*A*), **29**, 129 (1963).
[3] Brown, L. S., and Kibble, T. W. B., *Phys. Rev.*, **133**, A705 (1964).
[4] Prakash, H., and Vachaspati, *Nuovo Cimento*, **53B**, 24, 34 (1968).
[5] Fried, Z., *Nuovo Cimento*, **22**, 1303 (1961).
[6] Prakash, H., and Vachaspati, *Ind. J. Pure Appl. Phys.*, **5**, 21 (1967).
[7] Fried, Z., and Frank, W. M., *Nuovo Cimento*, **27**, 218 (1963).
[8] Bloembergen, N., *Non-linear Optics* (Benjamin, New York, 1965).
[9] Garret, C. G. B., and Robinson, F. N. J., *J. Quant. Electron.*, QE-2, 328 (1966).
[10] Adler, E., *Phys. Rev.*, **134**, A728 (1964).
[11] Bali, L. M., and Dutt, J., *Nuovo Cimento*, **35**, 805 (1965).

J. Phys. D: Appl. Phys., Vol. 5, 1972. Printed in Great Britain

The output characteristics of a Q-switched liquid laser system, Nd^{3+} : $POCl_3$: $ZrCl_4$

D ANDREOU†, V I LITTLE†,
A C SELDEN‡ and J KATZENSTEIN‡
† Royal Holloway College, University of London, Englefield Green, Surrey
‡ UKAEA, Culham Laboratory, Abingdon, Berks

MS received 10 August 1971

Abstract. Output powers of 50 MW have been obtained from an actively Q-switched Nd^{3+} : $POCl_3$: $ZrCl_4$ liquid laser with input energies of 500 J. Powers of this order of magnitude with such low input energies make the neodymium liquid laser at least as efficient as YAG and glass lasers. The performance of this laser in the 1 J output pulse region is superior to that of YAG and glass lasers. The output characteristics of this laser were studied as a function of the pumping pulse, the cavity mirror reflectivity and the cavity length.

1. Introduction

In the past two years liquid neodymium lasers with performances comparable to those of YAG and glass lasers have been developed (Samelson *et al* 1970). Several authors have reported passive Q-switching and mode-locking of liquid lasers based on $SeOCl_2$ (Samelson and Lempicki 1968) and $POCl_3$ (Alfano and Shapiro 1970). Active Q-switching for a liquid laser based on $SeOCl_2$ was recently reported (Lang 1970). The pulses described, however, were fluctuating and input energies required to produce powers of the order of 50 MW were excessively high (2·0 kJ). In this paper we describe the performance of an actively Q-switched Nd^{3+} : $POCl_3$: $ZrCl_4$ liquid laser. Smooth output pulses with full width at half maximum of 13–14 ns were obtained. The system was very reliable and its main characteristics are the high powers obtained ($\sim$50 MW) with small input energies ($\sim$500 J). The neodymium liquid laser thus emerges as a serious competitor for laser applications where high output powers with small input energies are desired.

The development of the giant pulse in this laser was investigated as a function of the pumping pulse, the output mirror reflectivity and the cavity length. The results are compared with the theoretical consideration on giant pulse formation of Midwinter (1965).

2. Apparatus

The experimental arrangement is shown in figure 1. The laser cell containing the active medium was 15·5 cm long and had an internal diameter of 0·75 cm. The active medium was Nd^{3+} : $POCl_3$: $ZrCl_4$, of concentration $1{\cdot}8 \times 10^{20}$ cm^{-3} and fluorescence lifetime 330 μs. Chemically this medium is highly active and should not be allowed to come into

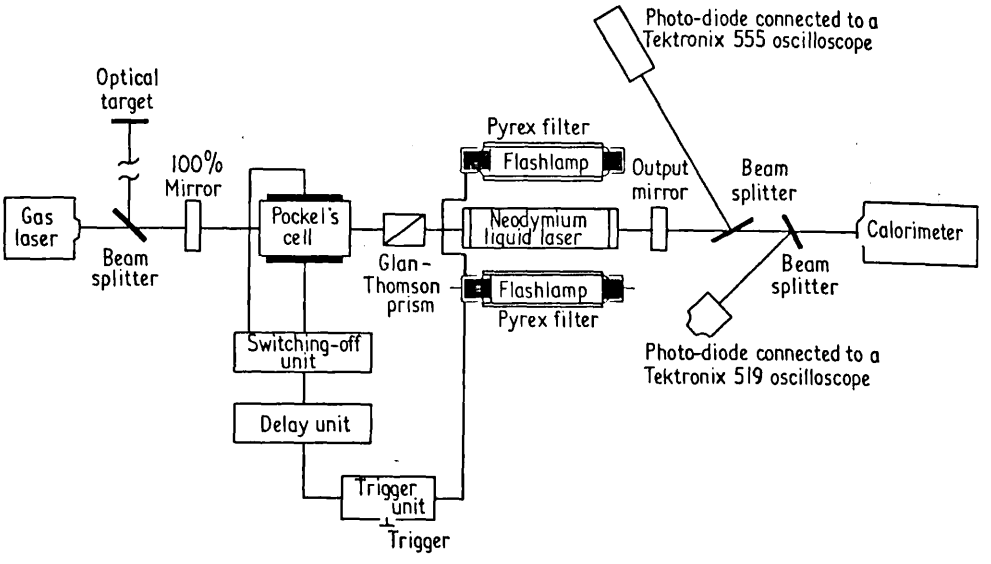

Figure 1. The experimental arrangement used to study the output characteristics of the actively Q-switched Nd^{3+} : $POCl_3$: $ZrCl_4$ laser.

contact with the atmosphere; its properties are described by Samelson *et al* (1970). Two linear xenon flashlamps were placed on either side of the laser cell and the whole arrangement was wrapped with a polished silver reflector. It was found in setting up the laser head that a silver reflector was much more efficient for pumping than an aluminium reflector. Pyrex tubes were used round the flashtubes to filter the UV radiation. The capacitor bank consisted of two 200 μF condensers which were charged up to 1·6 kV. The light pulse from the flashlamps is shown in figure 3.

A calcite prism was used as the polarizer and the system was Q-switched by removing the quarter-wave voltage of 4·1 kV applied to a KDP Pockels cell. The switching-off time was of the order of 40 ns, achieved with a Mullard PL 81 valve. The Pockels cell could be switched off at different times during the pumping pulse with the aid of a delay box following the trigger unit.

The pulses were recorded on a Tektronix 519 oscilloscope, using an ITT F4000 (S1) photodiode. The output energy was measured with a TRG 107 cone calorimeter connected to a microvoltmeter. The build-up time of the giant pulse was measured to an accuracy of 10 ns by using the two beams of the Tektronix 555 simultaneously to record the decay of the Pockels cell and the photodiode response to the giant pulse.

The laser was fired at intervals of at least 15 min to avoid the distortion effects taking place in the liquid due to heating by the pumping radiation.

3. Results

Figure 2 shows a typical giant pulse from the Nd^{3+} : $POCl_3$: $ZrCl_4$ system. Pulses as short as 13 ns with a total energy of 0·7 J were recorded. The switching-off time of the Pockels cell was approximately 40 ns.

Figure 3 shows the general behaviour of the giant pulse as a function of the pumping pulse for an output mirror reflectivity of 28%, an input energy of 512 J and a cavity

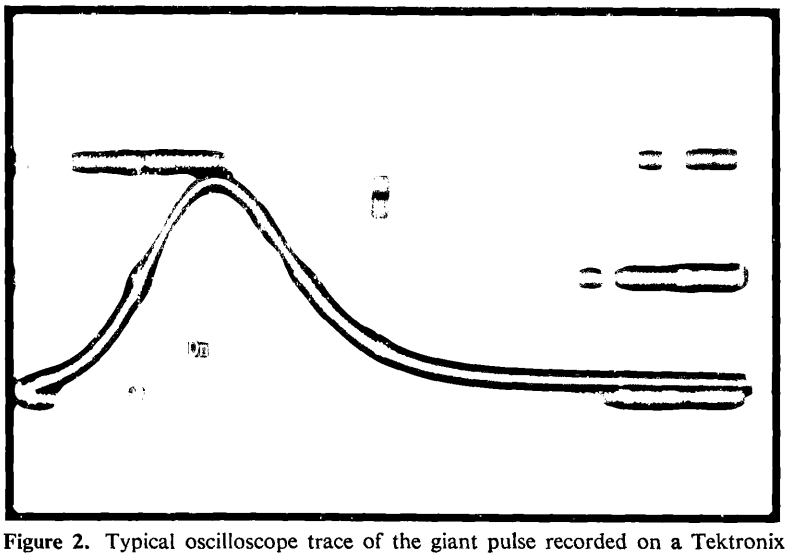

Figure 2. Typical oscilloscope trace of the giant pulse recorded on a Tektronix 519 oscilloscope: time scale, 10 ns/div.; output energy, 0·62 J; delay in switching off the Pockels cell after triggering the flashlamps, 190 μs; input energy, 512 J.

length 57 cm. It can be seen from these graphs that the optimum giant pulse occurs when the Q-switching is delayed for 205 μs after triggering the flashtubes. This is longer than the time taken for the pumping pulse to attain its maximum intensity and is less than the fluorescence lifetime of the material. The curves shown in figure 4 are self-consistent. From amplifier experiments which we have performed in this laboratory

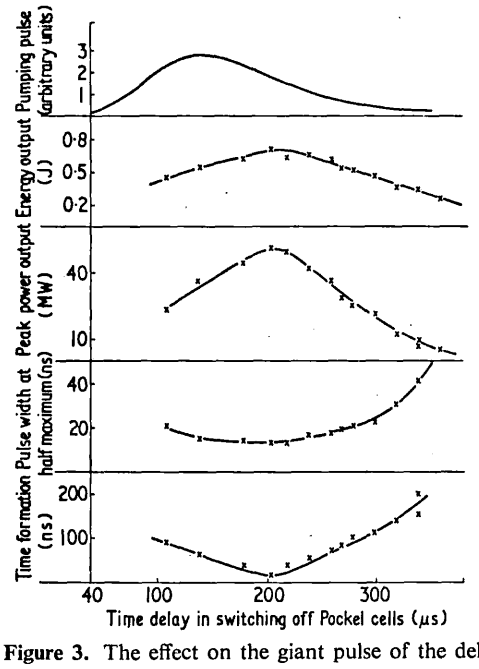

Figure 3. The effect on the giant pulse of the delay in switching off the Pockels cell: cavity length, 57 cm; input energy, 512 J; output mirror reflectivity, 28%; pulse width measurements to ±2%; all other ordinates to ±10%.

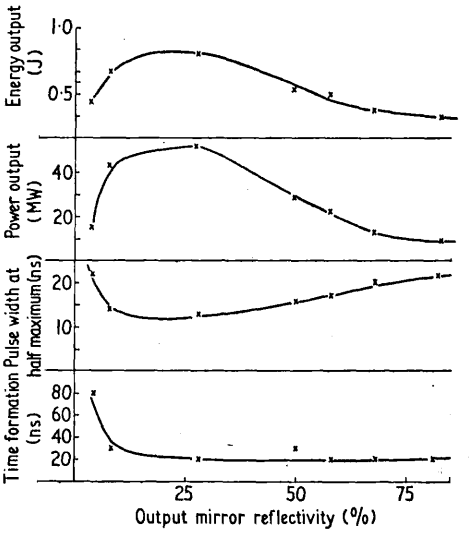

Figure 4. The effect on the giant pulse of the output mirror reflectivity: cavity length, 57 cm; input energy 512 J; time delay in switching off the Pockels cell, 210 μs; pulse width measurements to ±2%; all other ordinates to ±10%.

with the same arrangement, we have found that this system has maximum gain at 205 μs after firing the flashtubes. This result is in good agreement with the curves of figure 4.

The dependence of the giant pulse on the output mirror reflectivity is shown in figure 4. We note the agreement of these graphs with the theoretical considerations of Midwinter on giant pulse formation, particularly that the optimum output mirror reflectivity is around 28%; also, the rapid build-up of the giant pulse was found to remain constant for cavity lengths up to 110 cm. For greater cavity lengths the resonator became unstable and the output energy dropped considerably. The output power was diminishing constantly due to the increasing pulse width with increasing cavity length. The points drawn on the graphs in figures 3 and 4 are averages of many measurements taken from the same arrangement.

The most serious problems arising in the operation and further development of this kind of laser are the distortion effects in the active medium due to heating by the pumping radiation. For long delays in switching off the Pockels cell (over 300 μs) the beam cross sections showed discernible effects due to thermal distortion. Good filtering of the pumping light from UV radiation and the cavity design are therefore more important in the engineering of this kind of laser than in other lasers. Filtering of the pumping light with yellow Corning 3555 tubes instead of Pyrex tubes showed some improvement in the performance of the laser.

We did not investigate the dependence of the giant pulse on the input energy, because even with such low pumping energies (~ 500 J) the high output powers produced localized damage in the calcite prism.

4. Conclusions

The behaviour of an actively Q-switched neodymium liquid laser (Nd^{3+} : $POCl_3$: $ZrCl_4$) has been found to confirm the theoretical predictions of Midwinter. The present work

demonstrates certain important characteristics of the liquid laser: the pulses obtained are considerably shorter than those from glass lasers and $CaWO_4$ lasers and are comparable to those from YAG lasers.

Acknowledgments

The authors wish to thank Mr S Ward for his expert technical assistance.

This paper includes work carried out under a CVD contract and is published by permission of the Ministry of Defence (Navy Department). The work was carried out at Culham Laboratory, UKAEA, Abingdon, Berks.

References

Alfano R R and Shapiro S L 1970 *Opt. Commun.* **2** 90–2
Lang R S 1970 *Z. Naturf.* **25a** 1534–5
Midwinter J E 1965 *Br. J. appl. Phys.* **16** 1125–33
Samelson H, Kocher R, Waszak T and Kellner S 1970 *J. appl. Phys.* **41** 2459–69
Samelson H and Lempicki A 1968 *J. appl. Phys.* **39** 6115–6

J. Phys. D: Appl. Phys., Vol. 5, 1972. Printed in Great Britain.

Amplification of mode-locked trains with a liquid laser amplifier, Nd^{3+} : $POCl_3$: $ZrCl_4$

D ANDREOU†, A C SELDEN† and V I LITTLE
Royal Holloway College, University of London, Englefield Green, Surrey, TW20 0EX

MS received 30 March 1972

Abstract. The performance of the Nd^{3+} : $POCl_3$: $ZrCl_4$ system as a laser amplifier is investigated using mode-locked pulse trains as the input signals. These have energies of 30 to 80 mJ, and they consist of pulses of width approximately 5×10^{-12} s. Gains of 9 have been obtained from a system 155 mm long and 7·5 mm in diameter with input energies of 1 kJ. The high gains obtained make the Nd^{3+} : $POCl_3$: $ZrCl_4$ system a serious competitor in the field of high-power amplifier development in view of its advantages over other kinds of systems, namely that the active medium can be circulated and is free of damage problems. Beam patterns obtained show that the most serious problem in this kind of amplifier is thermal distortion due to heating by the pumping radiation. Experimental curves showing the gain, input and output characteristics of the amplifier are presented. They are in good agreement with the theoretical curves of Schulz-Dubois and show similar behaviour to the characteristics of Nd-glass amplifiers obtained with different experimental methods.

1. Introduction

The advent of the neodymium liquid laser with its high intrinsic gain has drawn attention to the possibility of developing high-power liquid amplifiers. The performance of liquid lasers as oscillators has been extensively studied for the different modes of operation: free running (Samelson *et al* 1970); passive Q-switching and mode-locking (Alfano and Shapiro 1970); and active Q-switching (Andreou *et al* 1972). The performance of the Nd^{3+} : $SeOCl_2$: $SnCl_4$ system as an amplifier was investigated in the small-signal case (Samelson *et al* 1970). Amplification of mode-locked pulses with a liquid amplifier Nd^{3+} : $POCl_3$: $SnCl_4$ was recently reported and gains of 3 were obtained (Selden 1970).

In this paper we describe the performance of an Nd^{3+} : $POCl_3$: $ZrCl_4$ liquid laser amplifier using picosecond pulses of measured width 5×10^{-12} s as the input signals. Gains of 9 were obtained from a system 155 mm long and 7·5 mm in diameter with input energies of 1 kJ. Serious limitations on the observed gain are imposed by the fact that there is a mismatch between the spectrum of the input signals and the amplifier linewidth. The spectrum of the input signals is centred at 1·058 μm; the linewidth of the amplifier is centred at 1·052 μm. The beam patterns obtained suggest that thermal motions may be taking place in the amplifier due to heating by the pumping radiation. The method employed here enables us to plot curves describing the gain, input and output

† Attached to Culham Laboratory, UKAEA, Abingdon, Berks.

characteristics of the amplifier. Saturation effects were observed when mode-locked trains with total energy more than approximately 50 mJ were used. The results are in good agreement with the theoretical curves of Schulz-Dubois (1964) on the gain characteristics of amplifiers. The system also shows characteristics similar to Nd-glass amplifiers (Tittel and Chernoch 1965, Yoshoda and Yamanaka 1971). The high intrinsic gains obtained, together with the ability of the active medium to be circulated and the fact that the active medium is free from damage problems, make the $Nd^{3+} : POCl_3 : ZrCl_4$ system a serious competitor in the field of high-power amplifier development.

2. Apparatus

The experimental arrangement is shown in figure 1. Special attention was taken in constructing a reliable mode-locked Nd-glass oscillator using an arrangement similar

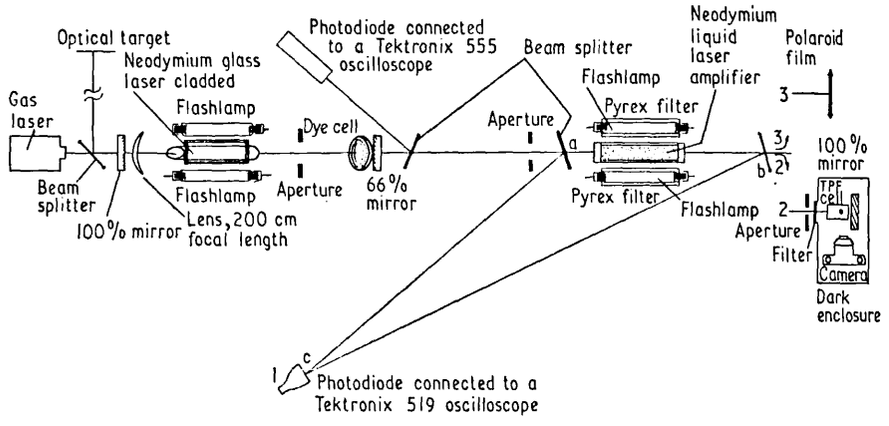

Figure 1. The experimental arrangement used to study the characteristics of the liquid laser amplifier system $Nd^{3+} : POCl_3 : ZrCl_4$—1. Measurement of gain; 2. Measurement of pulse width; 3. Observation of beam burn patterns on developed unexposed (Polaroid) film.

to that of Everett (1970) as shown in figure 1. The oscillator head consisted of a Brewster-ended Nd^{3+}-glass rod LGN 55 150 mm long and 9·5 mm in diameter with nominal 5% doping, pumped by a pair of linear xenon flashlamps, one placed on either side of the rod. The whole arrangement was wrapped with a polished silver reflector. The capacitor bank consisted of two 400 μF condensers which were discharged through the flashlamps giving an optical pumping pulse of approximate duration 550 μs at a third of its peak value. The cavity was 1 m long and consisted of two dielectric mirrors with reflectivities of 100% and 66%. A Laser Associates parallel-faced, 12 mm thick, output mirror was used, which had a hard coating in order to prevent damage due to the high powers of the picosecond pulses. The mode-locking dye cell was the Eastman model 6088 (1 mm path) antireflection-coated, which was placed next to the output mirror. The mode-locking dye solution, Eastman 9740, was diluted in chlorobenzene at a concentration of 13 : 2. A 2 m focal length meniscus lens was placed 20 mm from the 100% mirror. An aperture equal to the diameter of the laser rod was used in the cavity as shown. Mode-locked trains with energies between 30 and 80 mJ were readily obtainable. Only

one mode-locked train was produced in each firing, and it was emitted at a specific time after firing the flashlamps for a particular dye concentration and pumping energy. The first two pictures at the top of figure 7 (Plate) show typical beam cross sections at a distance 1·9 m from the output mirror. The divergence was estimated to be less than 2 mrad. The third picture at the top of figure 7 shows the central part of the beam cross section equal to the amplifier diameter which is selected for amplification by the aperture shown in figure 1. Mode-locked trains as described above were reproducible up to thirty times in succession before any deterioration in the quality of the beams could be observed.

The amplifier consisted of liquid laser solution contained in a silica cell 155 mm long and with an internal diameter of 7·5 mm. The active medium was Nd^{3+} : $POCl_3$: $ZrCl_4$ of concentration $1{\cdot}8 \times 10^{20}$ cm^{-3} and fluorescence lifetime 330 μs. Its properties are described by Samelson *et al* (1970). Two linear xenon flashlamps were placed one either side of the laser cell and the whole arrangement was wrapped with a polished silver reflector. Pyrex tubes were used round the flashlamps to filter UV radiation. The capacitor bank consisted of two 200 μF condensers, and light pulses from the flashlamps are shown in figure 5 for three different pumping energies, 968 J, 722 J and 512 J. The whole arrangement was placed in a Perspex box for safety purposes against accidental breakage of the laser cell.

Since the experiment required the recording of two interpenetrating mode-locked trains a fast detector was needed. The pulses were recorded on a Tektronix 519 oscilloscope using an ITT F4000 (Si) photodiode. A special holder was constructed for the photodiode according to the design of Edwards (1969) to give short response time. The rise time of the oscilloscope–diode arrangement was measured to be 0·4 ns. Diffusers, consisting of 3 mm thick discs of sintered PTFE, were mounted in front of the attenuating filters on the photodiodes to avoid damage to the photocathodes, and to avoid any transmission nonlinearity caused by fine structure in the laser beam profile. Sintered PTFE is ideal for this purpose because it is granular and is highly transmissive in the near-infrared, out to wavelengths of 3·7 μm.

Energy measurements were made with a TRG 107 cone calorimeter connected to a microvoltmeter. Two-photon fluorescence (TPF) measurements were performed with a cell 48 mm long and 25 mm wide containing Rhodamine 6G diluted in acetone. The TPF profile was recorded on HP4 film using an Exakta VX 1000 camera equipped with a Biotar *f* 1·5/75 mm lens. The arrangement was placed in a dark enclosure with a red filter window to avoid light from the amplifier flashlamps.

The oscillator–amplifier arrangement is shown in figure 1. The amplifier was placed 2 m away from the output mirror of the oscillator and the whole arrangement was aligned with an He–Ne gas laser placed behind the oscillator. The time between triggering the oscillator and amplifier was controlled with a delay box following the trigger unit. A beam splitter–photodiode arrangement at the exit of the oscillator recorded the time at which the mode-locked train was emitted after firing the oscillator. This was recorded on a Tektronix 555 oscilloscope. Since the relative time between firing the oscillator and the amplifier was known from the delay box, the time at which the mode-locked train passed through the amplifier after firing the flashlamps was readily obtained. An aperture was placed in front of the amplifier to select a beam cross section equal to the internal diameter of the amplifier.

The input and output signals were reflected on to the photodiode connected to the 519 Tektronix oscilloscope with the aid of two beam splitters A and B placed before and after the amplifier so that the ***E***-vector of the main beam was perpendicular to the plane of incidence.

The arrangement was fired at intervals of at least 15 min to avoid the distortion effects taking place in the liquid due to heating by the pumping radiation.

3. Method

The beam splitters A and B were placed in the main beam with angles of incidence $28° 54' \pm 30'$ and $13° 40' \pm 30'$ respectively, the *E*-vector being perpendicular to the plane of incidence. The reflection coefficients for these angles are calculated to be $R_{N_1} = 0{\cdot}117 \pm 2{\cdot}8\%$ and $R_{N_2} = 0{\cdot}089 \pm 2{\cdot}4\%$ respectively, where the subscript N denotes an incident beam with the *E*-vector perpendicular to the plane of incidence. The optical path lengths were adjusted so that $AB + BC - AC < 2L$, where L is the length of the oscillator. In this way the input and output signals are recorded as two interpenetrating mode-locked trains with each output pulse directly following the input pulse.

The oscillator was first fired several times without firing the amplifier. The recorded mode-locked trains gave us the normalization of our amplifier–beam splitter arrangement allowing for the difference in the reflectivities of the two beam splitters, the reflections from the cell windows and the passive loss of the medium. All measurements taken when the amplifier was fired were normalized to this ratio to give the intrinsic gain of the amplifying medium.

The heights of the pulses on the oscilloscope were proportional to the energy of the pulses. The photodiode was calibrated against a calorimeter for the angle of incidence of the first beam splitter. Calorimeter readings, however, involved errors of up to 20%. Thus only approximate values for the energies could be estimated.

It is important that a Brewster-ended oscillator is used so that the signals are only of one polarization (in this case the *E*-vector is normal to the plane of incidence). This keeps the ratio of the reflectivities of the two beam splitters constant for all measurements.

It can readily be seen that the change in the ratio of the reflectivities is insignificant even for large changes in polarization. If f is the fraction of the incident light with normal vibrations, the effective reflectivity of each beam splitter is

$$R(f, \delta_i) = f R_{N_i} + (1 - f) R_{P_i} \qquad i = 1, 2 \tag{1}$$

where the subscripts N and P denote normal and parallel polarization to the plane of incidence respectively. For a particular angle this relation is linear in f as f changes from 0 to 1. Figure 2 shows the variation of the reflectivity with f for two different angles δ_1 and δ_2. Even if we assume that there is a change in polarization of 10% from normal polarization for different firings then the ratio of the reflectivities will lie between the values R_{N_1}/R_{N_2} and $(0{\cdot}9R_{N_1} + 0{\cdot}1R_{P_1})/(0{\cdot}9R_{N_2} + 0{\cdot}1R_{P_2})$. For the particular angles used in the experiment these take the values 1·305 and 1·25 respectively or a maximum change in the ratio of the reflectivities of 4%. In practice the error due to changes in polarization was much less than this since a Brewster-ended oscillator was used in these experiments. The normalization pictures showed that there was no change in the ratio of the reflectivities. All normalization pictures showed the same ratio for all the pulses. The only error in the measurements occurred in measuring the heights of the pulses.

The amplification of the profile of the mode-locked train is analogous to the amplification of a giant pulse of the same shape. Thus pulse-sharpening effects are expected to occur. A large amplification occurs in the leading pulses of the train. In the experiments described here it can be assumed that no significant changes in the population inversion occur due to the pumping radiation since our mode-locked trains are less

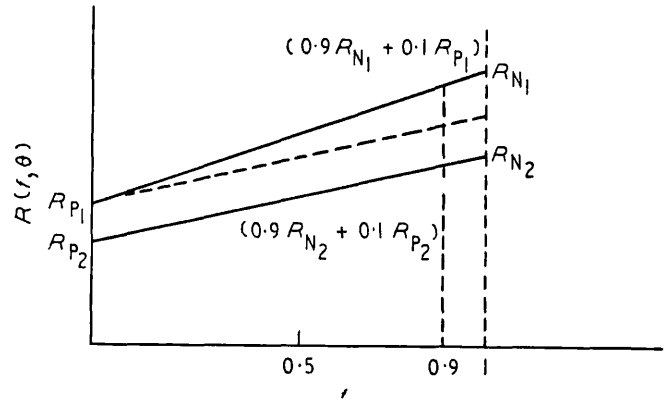

Figure 2. Variation of the reflectivity with polarization for two different angles δ_1 and δ_2. By drawing a line (broken) parallel to one of the lines it can be seen that the ratio of the reflectivities lies between the limits R_{P_1}/R_{P_2} and R_{N_1}/R_{N_2}.

than 70 ns long. After a certain amount of energy is passed through the amplifier, the gain is expected to deviate substantially from exponential form since the latter part of the amplifying medium is depleted more than the first part after each pulse passes through.

The accumulated input energy is the sum of the energies of all the input mode-locked pulses. The accumulated output energy is the sum of all the output mode-locked pulses. The instantaneous gain is the gain of a single pulse at any point along the train. We can thus plot graphs showing the variation of the instantaneous gain with input and output energy. The graphs are also analogous to graphs showing the output signal against time if a step function input signal is applied (Yoshoda and Yamanaka 1971).

The integrated gain is the ratio of the accumulated output energy to the accumulated input energy. This can be found from a graph of the accumulated input energy plotted against the accumulated output energy. The variation of the integrated gain with the input and output energies can then be plotted.

4. Results

Figure 3 (plate) shows typical measurements of the gain of the liquid laser amplifier in the small-signal case; that is, when there is no drop in gain due to population depletion along the mode-locked train. Figures 3(*a*) and (*b*) show the ratio of the photodiode signals when the amplifier is fired. Figure 3(*c*) shows the normalization of the amplifier arrangement—that is, the photodiode signals when the amplifier is not pumped. A plot of all the ratios on a typical normalization picture is shown in figure 4. The normalization procedure was carried out before any set of measurements was taken. In all cases it was found to be constant with a value of $0{\cdot}58 \pm 2\%$. Using the calculated reflection losses and the above normalization ratio the transmission loss of the unpumped liquid was estimated to be $0{\cdot}5 \pm 0{\cdot}2\%$/cm. This value is in agreement with the values given by Brecher *et al* (1970). The intrinsic gain of the amplifier for a particular pumping energy and time delay after firing the flashlamps is found by dividing the ratio shown in any of the top two pictures by the normalization. The experimental conditions for each picture in figure 3 are described in the caption. Gains of 9 were obtained in this way in the small-signal case.

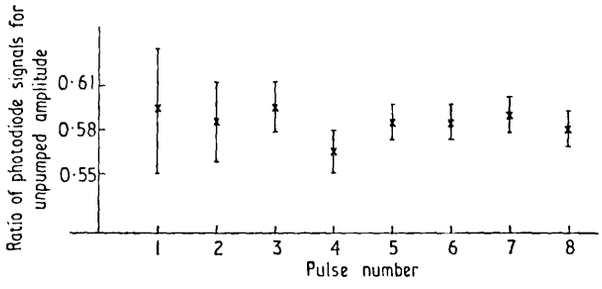

Figure 4. All the ratios for a typical normalization picture; variation ~2%.

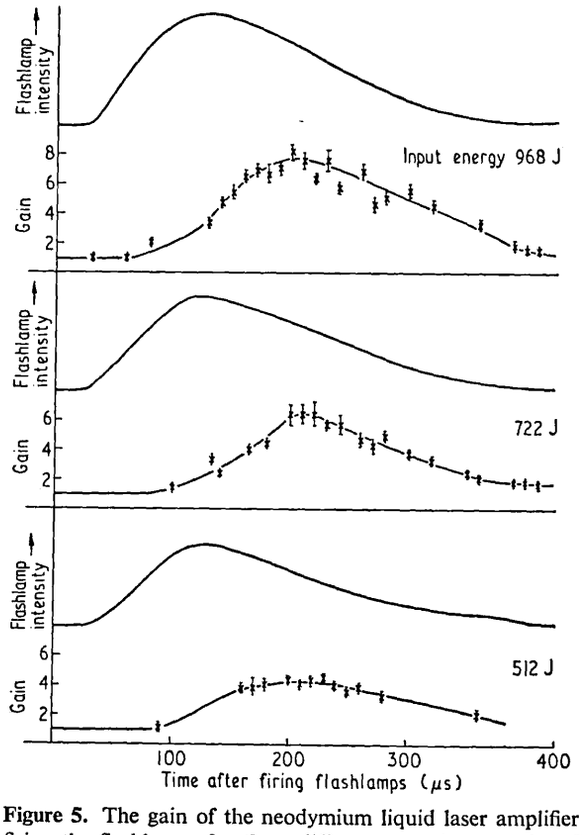

Figure 5. The gain of the neodymium liquid laser amplifier as function of time after firing the flashlamps for three different pumping energies. The flashlamp intensity in each case is shown at the top of each curve.

Figure 5 shows the gain of the liquid laser amplifier as a function of the time delay after firing the flashlamps for three different pumping energies, 968 J, 722 J and 512 J. All measurements taken lie near the curves shown. The points plotted represent a few typical measurements. The light-pumping pulse is shown at the top of each curve. It can be seen that the maximum gain occurs 205 μs after firing the flashlamps. Note the agreement of this result with our previous results when the system was used as a Q-switched oscillator (Andreou *et al* 1972). The time taken for population inversion to reach a maximum is longer than the time taken for the pumping pulse to attain its maximum intensity and is less than the fluorescence lifetime of the material (330 μs).

The results shown in figure 5 show similar characteristics to Nd-glass amplifiers (Tittel and Chernoch 1965).

Three pictures showing population inversion depletion effects are shown in figure 6 for three different initial population inversions. The experimental conditions for each picture are described in the caption. The normalization for all three pictures is $0{\cdot}58 \pm 2\%$. It can readily be seen that the gain of the amplifier starts at a high value and falls as the successive pulses pass through it. This nonlinear behaviour depends on the population depletion brought about by the energy requirements of previously amplified pulses. It can be assumed that the contribution of the pumping pulse to the population inversion during the passage of the mode-locked train through the amplifier can be neglected. Population depletion effects were readily observable when energies greater than 50 mJ passed through the amplifier. Results similar to those shown in figure 6 enabled us to investigate pulse sharpening and gain saturation effects in the liquid laser.

The far-field beam patterns at a distance of 0·7 m from the amplifier output were recorded on developed unexposed (Polaroid) film. Patterns were obtained corresponding to various times up to 410 μs after firing the flashlamps. The third picture at the top of figure 7 (plate) shows the beam cross section going into the amplifier. Typical beam cross sections coming out of the amplifier are shown in this figure for pumping energies of 968 J. The beam patterns initially change towards vertically elongated shapes because the flashlamps are placed in a horizontal plane on either side of the amplifier. It is clear from these patterns that thermal density distributions are established in the liquid due to heating by the pumping radiation. These density distributions probably also account for the large number of spikes around each beam pattern. It is important to notice that at the time of maximum gain the output beam is very much distorted. The geometry of the amplifier head and the elimination of UV radiation thus appear to be the most serious problems in the design of high-power liquid amplifiers. For lower pumping energies the distortion effects were not very serious and for energies of approximately 500 J the beam patterns retained a nearly circular shape. The patterns in figure 7 suggest that an experiment with a small continuous gas laser beam passing through the amplifier when fired, in conjunction with a streak camera–image converter arrangement, would provide useful information about changes in the amplifying medium during pumping.

Delineation of the pulse width was made by a standard two-photon fluorescence method as shown in figure 1. The measurements indicated pulse widths of 5 ps. A typical TPF picture is shown in figure 8 (plate). The separation of the two bands shown is equal to the effective thickness of the output mirror of the oscillator 60 ps. It can easily be seen from this picture that the left-hand side is weaker than the first band. This could arise as a result of the energy loss occurring in the previous bands. A microdensitometer trace of the first pulse is shown in figure 9. These measurements indicate that the pulses used for amplification had powers of approximately 10^9 W. Consequently the amplified pulses had powers of approximately 8×10^9 W. It is important to note the weak satellite pulses on either side of the main pulses. These are symmetric about the main pulses and occur at intervals of 17 ps. At times these pulses had intensities comparable to the main TPF pulses. Similar pulses were reported by Giordmaine *et al* (1967), who assumed that they arise from reflections at elements within the resonator though no precise explanation was given. In our oscillator the only elements with reflections parallel to the main beam were those from the two mirrors. Our TPF measurements are in good agreement with the measurements reported by Giordmaine *et al* in their paper (but see Duguay *et al* 1970).

The gain of the amplifier depends on the population inversion at any instant. Hence

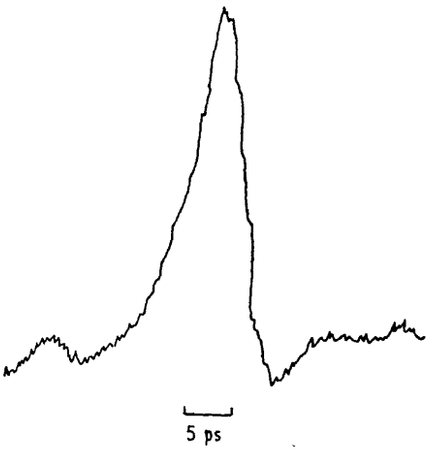

Figure 9. Microdensitometer trace of the first TPF pulse in figure 8; halfwidth ~5 ps.

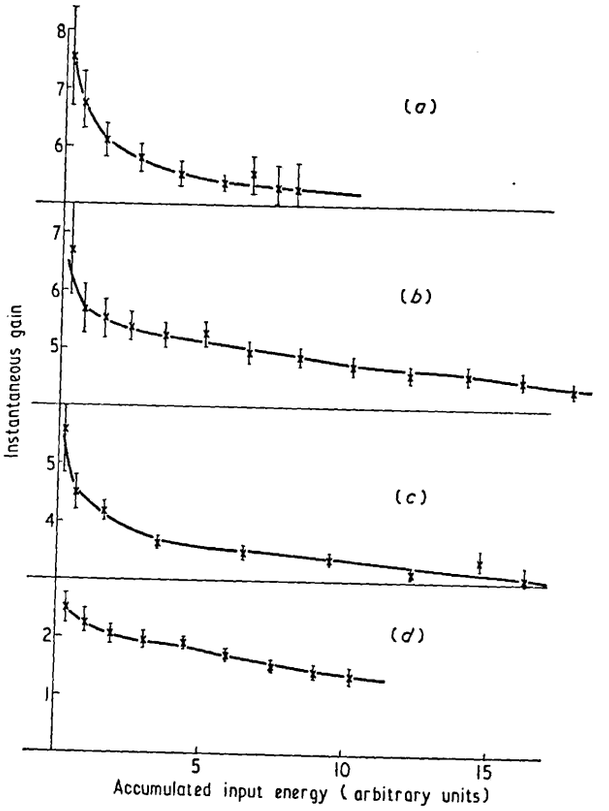

Figure 10. The instantaneous gain plotted against the accumulated input energy for four different initial population inversions. The second graph corresponds to the first picture in figure 6. The true values of the energy are the units shown multiplied by a factor $7 \pm 20\%$ mJ. (*a*) flashlamp input energy 968 J; time delay after firing the flashlamps 250 μs. (*b*) 968 J; 165 μs. (*c*) 968 J; 260 μs. (*d*) 968 J; 105 μs.

the small-signal gain depends on the energy of the previous signals which have passed through the amplifier. It is therefore meaningful to plot the instantaneous gain—that is, the ratio of the signal of an output pulse to the corresponding input pulse—against the sum total of the energies of all the input pulses previous to the one under consideration. The graphs in figure 10 show the fall of the instantaneous gain with accumulated input energy for four different initial population inversions. Note that the fall is steeper for high initial gains and it smooths out for small gains. The results plotted here are in

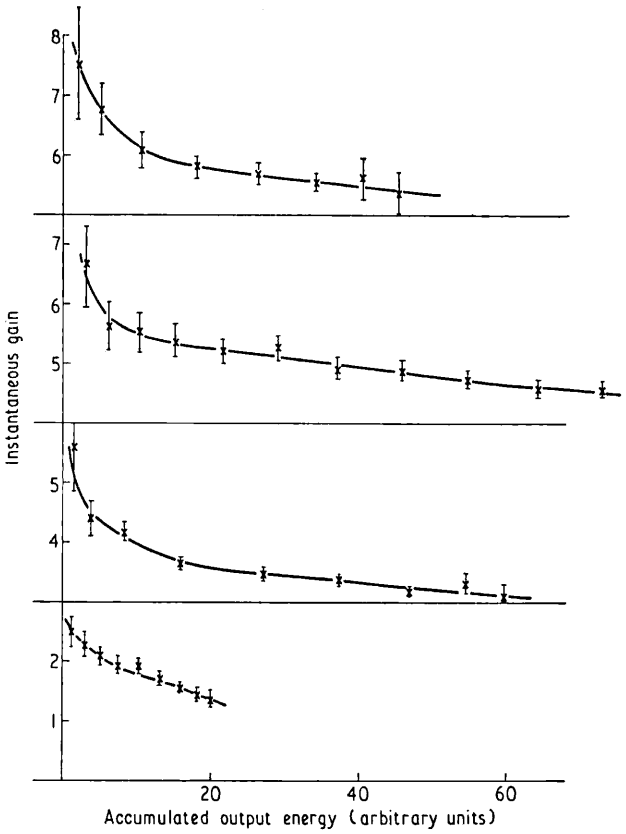

Figure 11. The instantaneous gain plotted against the accumulated output energy for the same pictures as in figure 10. The true values of the energy are the units shown multiplied by a factor $7 \pm 20\%$ mJ.

very good agreement with the theoretical considerations of Schulz-Dubois (1965). Note the similarity of these graphs with the results of Yoshoda and Yamanaka (1971), where a step function input signal was applied.

Figure 11 shows the variation of the instantaneous gain with accumulated output energy for the same experimental conditions as in figure 10. The results are similar to those for the accumulated input energy.

Figure 12 shows graphs of the accumulated input energy plotted against the accumulated output energy for the same experimental data as in figures 10 and 11. From these graphs the integrated gain for different output and input energies was calculated. The integrated gain calculated from figure 12 is plotted against the input and output energies in figures 13 and 14 respectively. Again note the agreement of these results with the

theoretical results of Schulz-Dubois. The curves shown in figure 13 show similar characteristics to curves obtained from Nd-glass lasers (Tittel and Chernoch 1965). The graphs in figures 10–14 are all plotted for the same data. The second graph in each of these figures corresponds to the first picture in figure 6.

The energy units plotted in these graphs are arbitrary. The true energy values in mJ are obtained by multiplying by a factor $7 \pm 20\%$, obtained by calibrating the beam splitters with a calorimeter (the large error in this factor is due to the inaccuracy of the calorimeter measurements).

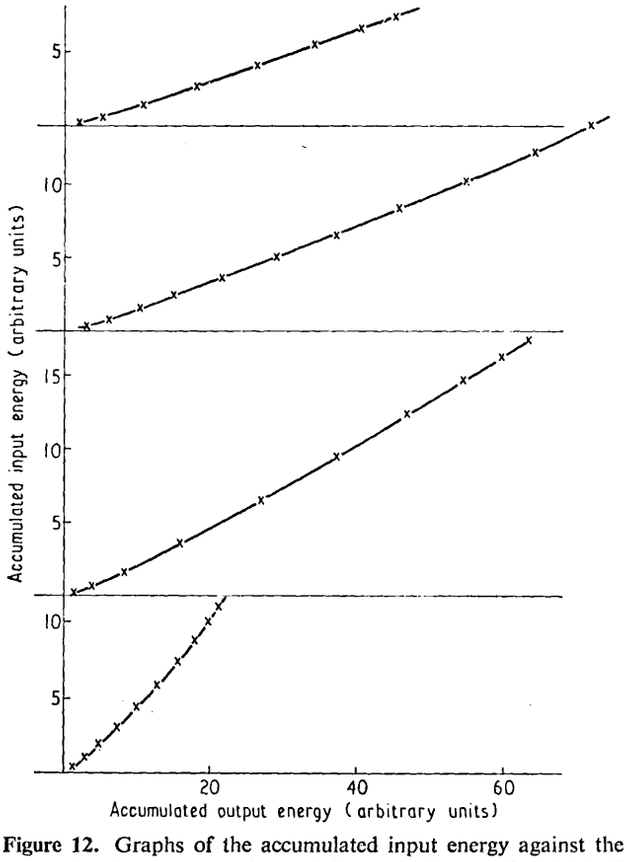

Figure 12. Graphs of the accumulated input energy against the accumulated output energy for the same experimental data as in figures 10 and 11. The true values of the energy are the units shown multiplied by a factor $7 \pm 20\%$ mJ.

An approximate value for the stimulated emission cross section for this material can be obtained from figures 10 and 12. The four-level amplifier equation is

$$\frac{dE}{dx} = h\nu N_1 \left\{1 - \exp\left(-\frac{\sigma_{(\nu)} E}{h\nu}\right)\right\} - \alpha E \tag{2}$$

where E (J cm^{-2}) is the input energy, x is the distance along the amplifier axis, α is the loss per centimetre, $\sigma_{(\nu)}$ is the stimulated emission cross section, and N_1 is the population inversion per cm^3. Since the energies used are of the order 10^{-3} J and the quantum

energy $h\nu = 1{\cdot}88 \times 10^{-19}$ J, we can write equation (2) for the small-signal gain as

$$\frac{dE}{dx} = (N_1\sigma_{(\nu)} - \alpha)\, E.$$

Integrating over the entire length L of the amplifier and assuming that N_1 is uniform along the length, we obtain

$$\lg G_1 = (N_1\sigma_{(\nu)} - \alpha)\, L$$

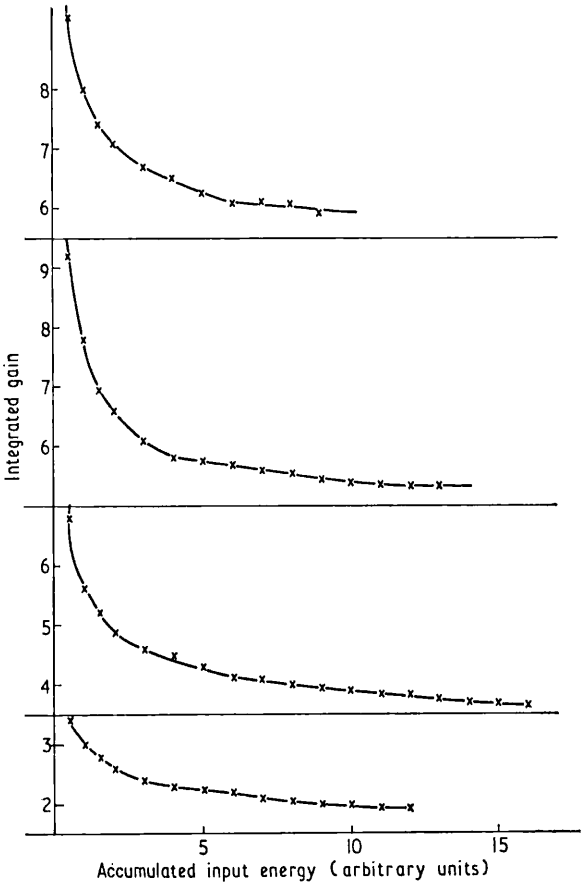

Figure 13. Graphs showing the variation of the integrated gain with the accumulated input energy. The data were taken from figure 12.

where G_1 is the gain for a small signal. If G_2 is the small-signal gain corresponding to the population inversion N_2 which is left after the passage of the first pulse through the amplifier, then

$$\lg\left(\frac{G_1}{G_2}\right) = (N_1 - N_2)\,\sigma_{(\nu)} L.$$

If a pulse of energy W_{in} emerges from the amplifier with energy W_{out}, then $W_{\text{out}} - W_{\text{in}} = V(N_1 - N_2)\, h\nu$, where V is the volume of the amplifying medium. From the last two equations it follows that

$$\sigma_{(\nu)} = \frac{h\nu A \lg (G_1/G_2)}{W_{\text{out}} - W_{\text{in}}} \tag{3}$$

where A is approximately equal to the geometrical cross section of the amplifier (0·385 cm^2).

The gain for small input signals can be found from figure 10. The gains of successive small signals with energies of 21×10^{-3} J each were found from this figure. The corresponding output energies were obtained from figure 12. The stimulated emission cross section was calculated from formula (3). The values obtained ranged from 2·8 to

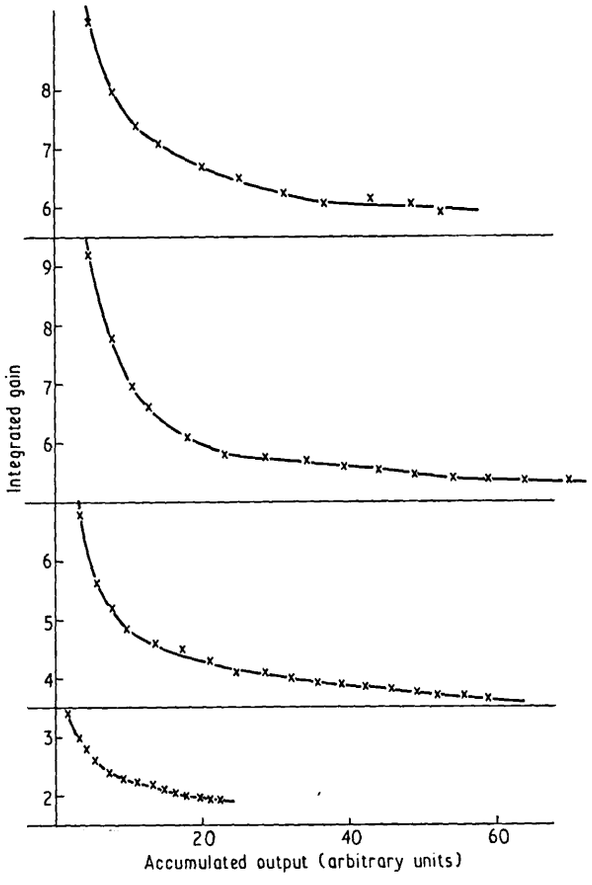

Figure 14. Graphs showing the variation of the integrated gain with the accumulated output energy. The data were taken from figure 12.

$5{\cdot}2 \times 10^{-20}$ cm^2 with most values lying around $4{\cdot}2 \times 10^{-20}$ cm$^2 \pm 40\%$. This is the stimulated emission cross section at a wavelength of 10 580 Å. To find the cross section at the centre of the amplifier linewidth, we must multiply by the factor 1·8, which is the ratio of the amplitude of the centre of the fluorescence line profile to that at the part of the profile corresponding to the experiment. The stimulated emission cross section is thus $7{\cdot}5 \times 10^{-20}$ cm$^2 \pm 40\%$. The large error in this estimate arises from the factor lg (G_1/G_2) and the error in the energy calibration factor. Parts of the graphs where the errors in the gain measurements were small were chosen for these calculations, and these parts gave the most consistent results. The results obtained from the second graph in figure 10 were the most consistent, and those from the last graph the least consistent.

It is interesting to remark that after approximately 700 firings the oscillator rod was badly damaged due to the high powers of the mode-locked pulses and had to be replaced. Photographs of the rod taken showed lines of bubbles parallel to the rod axis. These were concentrated at the end nearer the output mirror. Some of the bubbles were as much as $\frac{1}{2}$ mm diameter. Surface damage was also observed, the face nearer the output mirror being the most severely damaged. There was no deterioration in the performance or the physical quality of the liquid amplifier in which pulses up to eight times as powerful as those generated in the oscillator were amplified.

5. Conclusions

The behaviour of a neodymium liquid laser (Nd^{3+} : $POCl_3$: $ZrCl_4$) as an amplifier has been investigated with short light pulses of duration 5 ps as the input signals. Certain important characteristics of the amplification processes have been demonstrated, and the results confirm the theoretical predictions of Schulz-Dubois. It is also shown that thermal distortion due to the pumping radiation presents a serious problem in the operation of this kind of laser amplifier. The high gains obtained—although there was a mismatch between the amplifier linewidth and the oscillator signals—suggest that liquid amplifiers are more useful than crystal or glass lasers for high-power amplification because the liquid is free of damage problems and can be recirculated.

Acknowledgments

The authors wish to thank Mr S Ward for his expert technical assistance and Mr K Fenemore for workshop assistance. They also wish to thank Drs J Katzenstein and T K Allen for their interest in this work and for many useful discussions.

This paper includes work carried out under a joint contract with CVD and UKAEA and is published by permission of the Ministry of Defence (Navy Department). The work was carried out at Culham Laboratory, UKAEA, Abingdon, Berks.

References

Alfano R R and Shapiro S L 1970 *Opt. Commun.* **2** 90–2
Andreou D, Little V I, Selden A C and Katzenstein J 1972 *J. Phys.* D: *Appl. Phys.* **5** 59–63
Brecher C, French K, Watson W and Miller D 1970 *J. appl. Phys.* **41** 4578–81
Duguay M A, Hansen J W and Shapiro F L 1970 *IEEE J. Quantum Electron.* **QE-6** 725–43
Edwards J G 1969 *Opto-Electron.* **1** 1–8
Everett P N 1970 *Rev. sci. Instrum.* **41** 1495–500
Giordmaine J A, Rentzepis P M, Shapiro S L and Wecht K W 1967 *Appl. Phys. Lett.* **11** 216–8
Samelson H, Kocher R, Waszak T and Kellner S 1970 *J. appl. Phys.* **41** 2459–69
Schulz-Dubois E O 1964 *Bell Syst. tech. J.* **43** 625–58
Selden A C 1970 *Proc. 8th Int. Conf. on Microwaves and Optical Generation and Amplification, Amsterdam* (Deventer : Kluwer) section 21 pp 11–4
Tittel K F and Chernoch J P 1965 *Proc. IEEE* **53** 82–3
Yoshoda K and Yamanaka T 1971 *Jap. J. appl. Phys.* **10** 1643–4

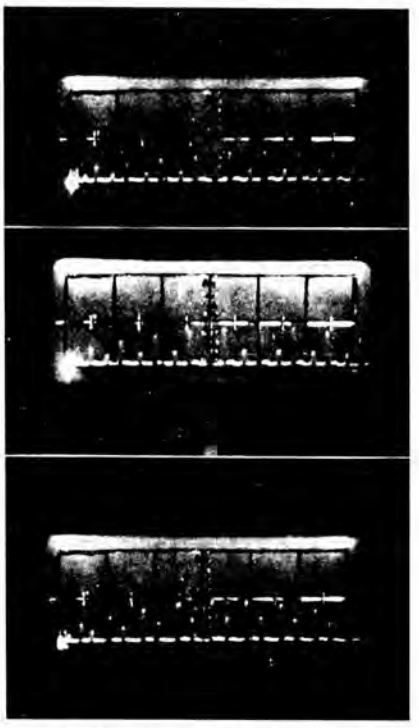

Figure 3. Amplification of mode-locked pulses with a liquid laser amplifier. (*a*) Pumping energy 722 J; gain ~6; time delay after firing the flashlamps 210 μs; energy ~28±20% mJ/div; time scale 10 ns/div. (*b*) 722 J; ~5·2; 240 μs; ~28±20% mJ/div; 10 ns/div. (*c*) Normalization of the amplifier arrangement (ie the photodiode signals when the amplifier is not pumped): ratio ~0·58±2%; time scale 10 ns/div.

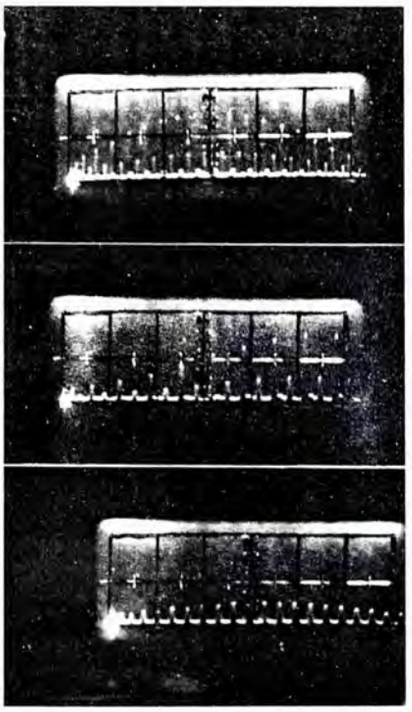

Figure 6. The depletion of the population inversion for three different initial population inversions. The normalization for all three pictures is $0{\cdot}58 \pm 2\%$. (*a*) Pumping energy 968 J; initial gain $\sim 6{\cdot}5$; final gain $\sim 4{\cdot}1$; time delay after firing the flashlamps 165 μs; energy $28 \pm 20\%$ mJ/div; time scale 20 ns/div. (*b*) 968 J; ~ 8; $\sim 5{\cdot}3$; 250 μs; $28 \pm 20\%$ mJ/div; 10 ns/div. (*c*) 968 J; $\sim 2{\cdot}4$; $\sim 1{\cdot}3$; 105 μs; $28 \pm 20\%$ mJ/div; 10 ns/div.

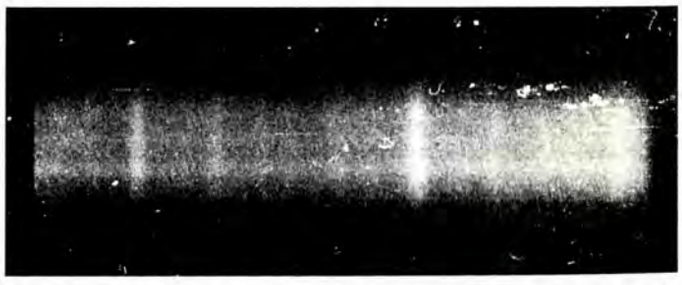

Figure 8. Typical TPF picture. The 100% mirror is to the right of the picture. The distance between the two main pulses is about 60 ps. The satellite pulses occur at intervals of 17 ps.

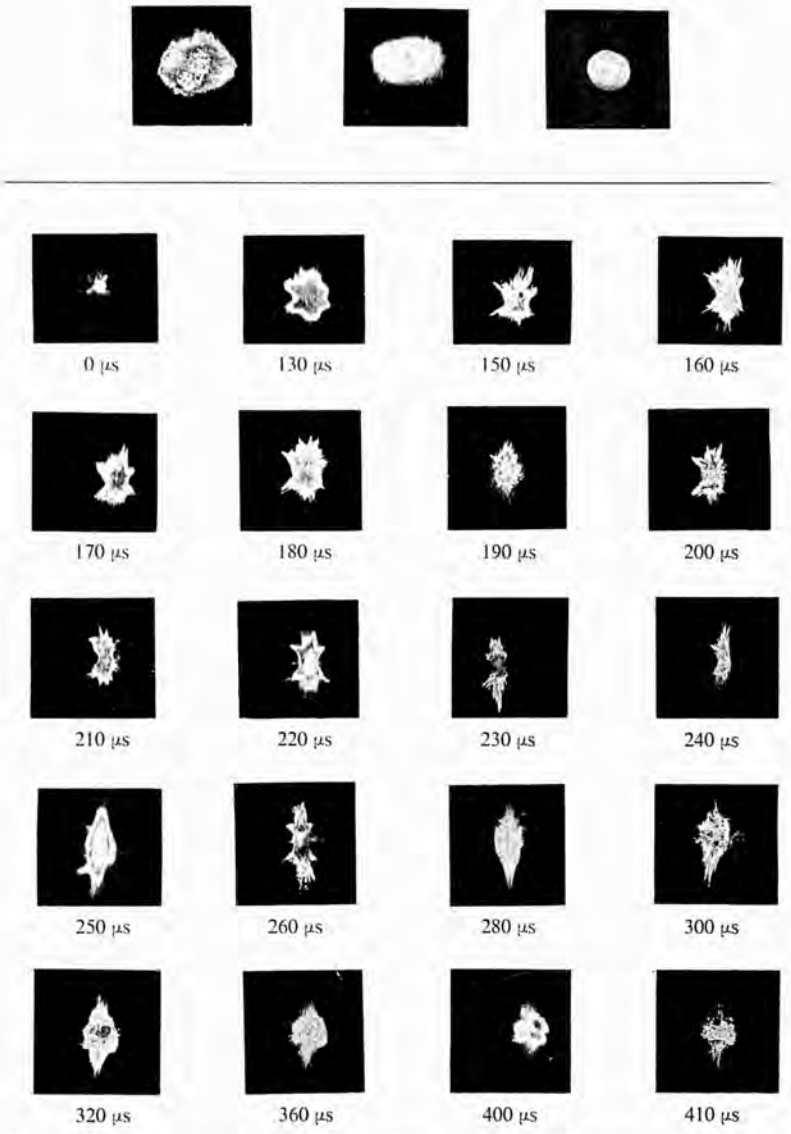

Figure 7. Beam patterns obtained on developed unexposed (Polaroid) film. The top three pictures represent the oscillator beam cross section at a distance of 1·9 m from the output mirror. The third of these is the cross section of the centre of the beam, equal to the diameter of the amplifier, selected for amplification by the 7·5 mm aperture shown in figure 1. The rest of the pictures are beam patterns recorded at a distance of 0·7 m from the exit of the amplifier for different times after firing the flashlamps.

D4171 Andreou & Little Paper

J. Phys. D: Appl. Phys., Vol. 6, 1973. Printed in Great Britain.

The spiking behaviour of a laser having combined liquid- and glass-active media

D Andreou† and V I Little
Department of Physics, Royal Holloway College, University of London, Egham Hill, Egham, Surrey, TW20 0EX

MS received 21 June 1972, in final form 25 October 1972

Abstract. Experiments have been carried out to explore the mechanism of the self-Q-switching behaviour of a liquid laser. An experimental arrangement was adopted in which a Nd-glass rod and a Nd-liquid column were contained in the same cavity. This arrangement enabled the overall gain in the cavity to be increased without changing the parameters controlling the state of the liquid. The results indicate that the self-Q-switching mechanism is likely to be thermal in character.

1. Introduction

The self-Q-switching behaviour of a liquid laser has lately been the subject of considerable discussion. One mechanism which has been proposed (Samelson *et al* 1968) involved the establishment of a phase grating from backward stimulated Brillouin scattering (SBS) within the liquid column. This would have altered the overall reflectivity in the cavity, and thereby have changed the cavity gain. However, if the mechanism had been due to SBS, there would have been an observable frequency shift in the back-scattered light. Alfano *et al* 1971 were unable to confirm this experimentally, and they concluded that the mechanism proposed by Key *et al* 1970, was therefore more likely to be true. In this mechanism, the phase grating was produced by the superposition of the forward and backward waves in the cavity. At the maxima of the standing wave, the refractive index of the liquid would be increased by one of a number of possible nonlinear optical processes. Two very obvious processes would be electrostriction and heating due to absorption. This kind of phase grating, because of its stationary nature, would not produce a Doppler shift in the reflected light, and would thus account for Samelson's observations.

Very recently, Selden (1972) has devised a mechanism for the production of a thermal grating which seems to account for most of the observed phenomena. In this mechanism, the fast nonradiative decay to the ground state of the lower level of the laser transition deposits thermal energy into the liquid.

Since the population of the lower level of the laser transition is determined by the stimulated emission process, the heat flow into the liquid from the fast transition of this level to the ground state also follows the stimulated emission process. The fast transitions which populate the upper laser level, however, are controlled by the pumping process, and the heat evolved in this process has no spatial correlation with the heat evolved in the

† Attached to Culham Laboratory, UKAEA, Abingdon, Berks.

lower transition. The latter heat is spatially deposited in the liquid with maxima corresponding to the maxima of the stimulated optical standing wave. The net effect is a density, and hence refractive-index, variation which gives rise to a phase grating. Selden shows that the reflectivity of this thermal grating is proportional to the cavity gain. Furthermore, he points out that owing to the much greater thermal expansivity of liquids over solids, the effect of this process in liquids is very much greater than the corresponding effect in solids. This accounts very simply for the fact that self-Q-switching phenomena are more readily observed in liquids than in solids.

In this paper we report four simple sets of experiments designed to measure the spiking behaviour of the following:

(i) A liquid laser, as a function of output mirror reflectivity.
(ii) A glass rod alone, using a cavity with a fixed reflectivity and a constant length.
(iii) The glass rod with the liquid laser column in the cavity unpumped.
(iv) The combined glass and liquid laser.

2. Experimental details and results

The liquid laser head consisted of a cell 15·5 cm long and 0·75 cm in diameter, containing Nd^{3+} : $POCl_3$: $ZrCl_4$ solution, pumped by a pair of xenon flashlamps. The whole arrangement was wrapped with a silver reflector. The light pumping pulse was approximately 150 μs long at half-maximum. A similar laser head was used for a Brewster-ended Nd-glass laser, 15 cm long and 0·9 cm diameter. The light-pumping pulse for the glass laser was approximately 350 μs at half-maximum. The fluorescence spectra of the liquid and glass lasers do not coincide exactly.

First the spiking behaviour of the Nd^{3+} : $POCl_3$: $ZrCl_4$ system was investigated as a function of the reflectivity product R_1R_2. The laser was placed between two plane-parallel reflectors, and output energies of 1·7 J with input energies of 650 J were obtained for a reflectivity product greater than 0·3. Irregular spiking was observed starting 130 μs after firing the flashlamps and lasting for 200 μs. The spiking had a duration of approximately 500 ns and a power of 10 KW. With a reflectivity product of 0·04, output energies of 0·9 J were obtained using input energies of 650 J. Fewer spikes were now observed, and amongst these were some of duration 100–200 ns and peak power of the order of 80 KW. A pause in spiking was usually observed following each high-power spike. This self-Q-switching behaviour is similar to that originally reported by Samelson *et al* (1968). The effect, however, was less marked in our experiments because of the lower energy and smaller size of our system.

The Nd-glass laser was placed in a cavity 100 cm long with fixed reflectivities of 100% and 50%. Output energies of 1·7 J and 2·5 J were obtained with input energies of 1000 J and 1600 J respectively. The threshold of the laser was 600 J. Spiking started 300 μs after firing the flashlamps and lasted for 400 μs. The spikes (see figure 1(*a*)) were approximately 700 ns long and had power approximately 5 to 10 KW.

The liquid laser was now introduced into the same cavity as the Nd-glass laser. With the liquid not pumped, the threshold of the glass laser increased to 900 J—that is, by a factor of 3/2 of its value—without the liquid laser cell in the cavity. This was attributed to the passive loss of the $POCl_3$ and the reflections from the cell windows, a total insertion loss of 30% per double pass. A few spikes with duration 150–250 ns and peak power 60–80 KW were regularly observed when the glass laser was pumped up to 1600 J.

Figure 1(*b*) shows the spiking behaviour of the Nd-glass laser with the liquid laser cell placed in the cavity unpumped. Thus the introduction of the Nd-liquid medium into the cavity of the Nd-glass laser produces a small *Q*-switching effect analogous to *Q*-switching by organic solvents, in accordance with the findings of Katzenstein *et al* (1969), who

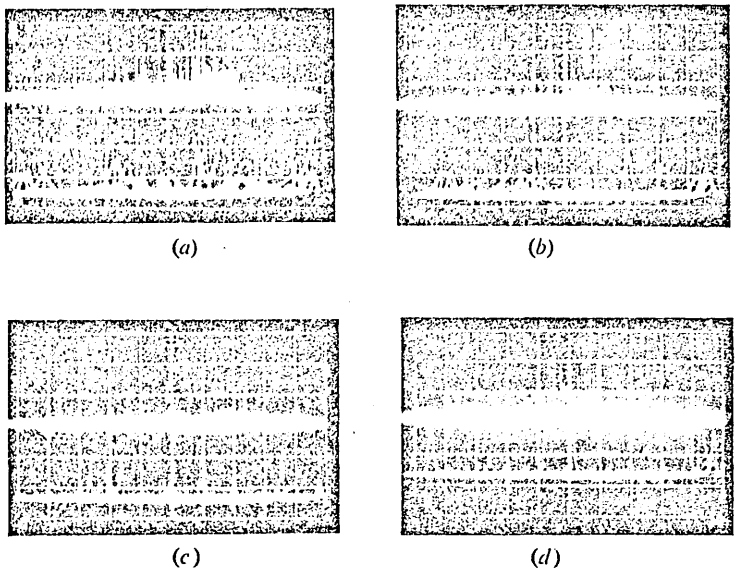

Figure 1. The spiking behaviour of (*a*) the Nd-glass laser, (*b*) the Nd-glass laser with the liquid laser in the cavity unpumped, (*c*) the laser with combined active media, (*d*) both lasers with a time delay of 150 μs between them. The top traces in each picture show parts of the top traces on an expanded scale (read from right to left).

	(*a*)	(*b*)	(*c*)	(*d*)
Pumping (J)	1600	1600	1000 500	1600 1000 (Liquid)
Top trace:				
Horiz. scale (μs/div)	100	100	100	100
Vert. scale (kW/div)	5	30	200	200
Lower trace:				
Horiz. scale (μs/div)	2	1	1	1

All pictures were recorded with a Tektronix 555 dual-beam oscilloscope.

pointed out that liquids which had very little absorption at the laser wavelength showed very small *Q*-switching effects. The $POCl_3$ solution falls into this category and behaves as expected.

The most interesting results were obtained when both lasers were simultaneously pumped in the same cavity. Spiking started approximately 90 μs after firing the flash-lamps and lasted for 150 μs. The oscillations consisted of powerful uniform pulses of approximately equal height as can be seen from figure 1(*c*) and (*d*). Short pulses of 20 ns FWHM and powers up to 1 MW were observed for every shot. These were recorded on a T519 oscilloscope. Typical oscillograms are shown in figure 2. Total output energies of 3·5 to 4 J were obtained.

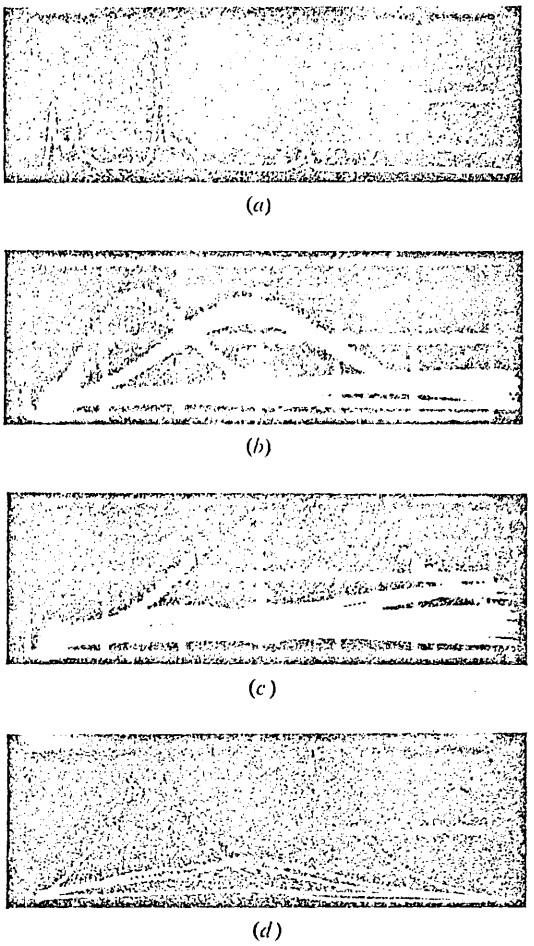

(a)

(b)

(c)

(d)

Figure 2. Typical oscillograms of the self-Q-switched pulses obtained on a Tektronix 519 oscilloscope. (*a*) Time scales: 1 μs/div. (*a*); 20 ns/div. (*b*, *c*, *d*). The modulation on the pulses is due to the subcavities formed by the cell windows and the cavity mirrors. Unmodulated pulses of the same pulse width were also obtained.

3. Discussion

Because of the limitations of our flashlamps we were not able to pump the system harder than the levels reported. We would draw attention, however, to the results of experiments 3 and 4. When the liquid was not pumped, the glass laser showed some signs of Q-switching. Clearly, the mechanism at work here cannot be that proposed by Selden, because the quantum energy of the stimulated radiation in the cavity is insufficient to raise the liquid laser to its upper laser transition level. Since Samelson *et al* (1968) have shown that SBS is not the operative mechanism either, this small effect is very likely to be explained by the mechanism of Key *et al* (1970) in terms of nonlinear optics. When both liquid and glass are pumped, strong Q-switching is observed. We know from experience that when the glass laser is pumped with no liquid cell in the cavity, self-Q-switching is very seldom observed. We therefore conclude that the only effect which the pumped glass rod had on the system was simply to increase the cavity gain. It follows, therefore, that the

same result should be obtainable with a longer liquid column. Experiment I indicates that more self-Q-switching is observed when the liquid alone is pumped harder.

We conclude therefore that self-Q-switching in liquid columns is more likely the greater the cavity energy and the greater the cavity gain. The mechanism of the process is likely to be a combination of the process suggested by Selden and that proposed by Key *et al.* In either event, the primary cause of the induced phase grating would seem to be the spatially periodic deposition of heat energy.

Acknowledgments

The authors would like to thank Dr A. C Selden for many useful discussions on the subject. This work was carried out at Culham Laboratory, UKAEA., Abingdon, Berks.

References

Alfano R R, Lempicki A and Shapiro S L 1971 *IEEE J. Quantum Electron.* QE-7 416
Katzenstein J, Magyar G and Selden A C 1969 *Optoelectron.* 1 13
Key P Y, Harrison R G, Little V I and Katzenstein J 1970 *IEEE J. Quantum Electron.* QE-6 641
Samelson H, Lempicki A and Brophy V A 1968 *IEEE J. Quantum Electron.* QE-4 849
Selden A *Optics Commun.* 1972 in the press

PROGRESS REPORT ON A 10 PPS Q-SWITCHED Nd:$POCl_3$–$ZrCl_4$ LIQUID LASER

April 1970 - December 1971

D. Andreou, K. Fenemore
J. Katzenstein, A. C. Selden, S. Ward

ABSTRACT

This Progress Report presents experimental results on the Q-switching parameters and energy scaling of the liquid laser, and information on the construction and preliminary operation of a 10 pps circulating system.

* Work carried out under a CVD contract, and published with the permission of the Ministry of Defence (Navy Department).

UKAEA Research Group,
Culham Laboratory,
Abingdon, Berks.
March, 1972.

SBN: 85311 008 5

CONTENTS

1. INTRODUCTION: DEVELOPMENT PHILOSOPHY

The raison d'etre of this work is the development of a small-scale repetitively pulsed Q-switched liquid laser for assessing the performance of a relatively new laser material compared with alternative media. At the beginning of the contract period the liquid properties and spectroscopic parameters were only known approximately, and no information was available on whether giant pulses could be produced by Q-switching the laser medium. It was decided therefore to divide the programme into two parts, one concerned with Q-switching behaviour, the other with development of a circulating system for 10 pps operation. No attempt would be made to scale the flow system until adequate data was available from Q-switching experiments, and sufficient experience gained of the construction and operation of an experimental circulating liquid laser. The development of the latter involved the selection of materials compatible with the corrosive solvent $POCl_3$-$ZrCl_4$, finding a leakproof mechanical pump for circulating this liquid, and constructing a dry sealed flow system of pipes and mechanical joints incorporating a suitable laser cell.

2. DESIGNING A Q-SWITCHED LIQUID LASER

We discuss first the scaling of a Q-switched laser with respect to efficient operation in the desired energy range. Experimental results are presented supporting the predicted parameters.

2.1 Cross-sections and energy scaling

For a specific loop gain, such as the laser threshold requirement, the total energy stored in the metastable state is proportional to the cross-sectional area of the laser element and inversely proportional to the stimulated emission cross-section. For two different media to have the same stored energy and the same gain, the ratio of their geometric cross-sections should therefore equal the ratio of their atomic cross-sections, other things being equal. Thus we have two simple scaling laws:

$$E_s = kA \qquad ..(1)$$

$$\frac{A_1}{A_2} = \frac{\sigma_1}{\sigma_2} \qquad ..(2)$$

where E_s is the total stored energy, A and σ are the geometric and atomic cross-sections respectively. Relation (1) is for a given gain, and (2) for the same gain and energy. The factor

$$k = \frac{hV}{\sigma} \log_e G \qquad ..(3)$$

where G is the single pass gain, corrected for the effects of cavity losses and non-uniform excitation, and hV is the photon energy.

The cross-sections for stimulated emission in Nd:YAG and $Nd:POCl_3-ZrCl_4$ are in the ratio $\sigma(YAG)/\sigma(POCl_3) \sim 10$. Therefore a Q-switched $Nd:POCl_3-ZrCl_4$ liquid laser of comparable energy to a 6.35 mm (¼ in) diameter YAG laser has a diameter $\sim \frac{6.35}{\sqrt{10}}$ mm i.e. approximately 2 mm.

For efficient release of the energy stored in a Q-switched laser, the initial inversion should be at least three times threshold [1]. The optimum mirror transmittance for peak power output lies in the range 50-80 per cent[2], requiring an initial gain $10 \geq G > 3$ prior to Q-switching.

Since $\frac{hV}{\sigma} \sim 2.5$ Joule cm^{-2} for $Nd:POCl_3-ZrCl_4$, a 2 mm diameter laser of this material with a single pass gain of $G = 5$ has a total stored energy $E_s \sim 125$ mJ. In a real laser the non-uniform gain and finite losses make the energy emitted in the Q-switched pulse less than E_s. To allow for this the diameter must be increased. In this way the estimated diameter of the liquid laser becomes ~3 mm for 100 mJ output.

2.2 Excitation

For efficient excitation of the active volume by optical pumping we require a laser diameter greater than the absorption length. The precise value is obtained from a convolution of the emission and absorption spectra of the lamp and laser respectively.

The $Nd:POCl_3-ZrCl_4$ solution has an average absorption length ~ 15 mm at the half intensity points of the absorption bands.

Thus a diameter of 2-3 mm, as indicated by energy scaling, makes the laser optically thin. Increasing the Nd ion concentration to improve the absorption efficiency is precluded by stoicheiometry, departure from equilibrium affecting the chemical stability of the laser solution. However, since the liquid consists of three components, namely the phosphorus oxychloride, the metallic chloride $ZrCl_4$, and a dissolved neodymium salt, chemical substitution of alternative compounds may make possible the addition of more Nd^{3+} ions or others to increase the excitation efficiency.

With regard to beam quality, i.e., mode structure and divergence, it is necessary to pump the laser volume uniformly by making an appropriate choice of lamp/reflector geometry. This can be critical with a liquid laser because the change of refractive index with temperature is some 50 times as great as that for solids. Bilateral symmetry, with a well polished non-focussing reflector and two lamps of equal brightness, enables low beam divergence and symmetric intensity profiles to be achieved. For perfect circular symmetry a rotationally symmetric reflector is required, e.g. a sphere or prolate spheroid [3] with lamp and laser mounted end-to-end on the axis of rotation.

2.3 Experimental results - small cells

Liquid laser Q-switching performance measured for several laser cells of different diamters and lengths provides a

comparison with predictions of scale size and output based on physical parameters (section 2.1, 2.2). The experimentally scaled diameter for 100 mJ pulses is 2.9 ± 0.2 mm for single pass gain G = 3.5 nett prior to Q-switching. This was determined from output energy and threshold measurements on Sylvania Nd:$POCl_3$-$ZrCl_4$ solution contained in plane-ended cylindrical silica or Pyrex cells of dimensions 8 mm dia x 6 ins long, 7 mm x 6 in, 5 mm x 6½ ins, 5 mm x 3½ ins, each pumped by a pair of straight flashlamps of appropriate size. The arrangement of the laser cell and lamps and the electro-optically Q-switched cavity is shown in Figure 1.

Divergence is largely dependent on the thermal gradients induced in the liquid by optical pumping. The two lamp geometry gives 4 milli-radian full angle containing at least 67% of the emitted energy. Pulse-widths down to 13 ns and peak powers up to 55 MW are observed with the 8 mm x 6 in cell.

A giant pulse profile and the switching behaviour are shown in Figure 2. An extensive examination of the parameters of this Q-switched system has been published[5].

Experimental measurement of pulse energy versus excitation energy yields a straight line graph of the form:

$$E_{out} = \mathcal{E}(E_{in} - E_{th})$$

from which the slope efficiency $\mathcal{E}$ and extrapolated threshold E_{th} (for zero Q-switched emission) are obtained. This linear relation makes scaling of the laser particularly simple. The

threshold determined from Q-switched pulse energy measurements agrees with that found by observing the initial appearance of spiking with the electro-optic elements remaining in the transmitting state. However, the ordinary spiking threshold with the Q-switching elements removed from the cavity shows a reduction by a factor of 1.5 to 2, depending on cavity length and the transmission of the output mirror. This has been traced to the Glan-Taylor polarising prism.

A comparison of spiking and giant pulse performance is shown in Fig. 3. The difference in threshold is clear, although the slope efficiencies are approximately the same. For a scaled 3 mm diameter laser, an input energy ~40 J is estimated for 100 mJ Q-switched output energy at the observed efficiency. With further development work on excitation and pulse generation this might be reduced to ~25 J. Further reduction in the energy requirement would follow from increased efficiency of the laser solution, which would put the miniature liquid laser on a comparable footing with Nd:YAG systems. For this reason a comprehensive approach to the chemistry of the system is envisaged as part of a continued programme, and appears in detail in the proposal submitted for 1972/73.

3. THE CIRCULATING SYSTEM

Liquid lasers can be cooled by flowing the laser medium through a heat exchanger and returning it to the laser cell. Thus they have an intrinsic advantage over solid lasers for

repetitive pulsing because heat can only be removed from the latter by conduction to the surface and transfer to a coolant flow, resulting in radial temperature gradients and thermal stresses which affect the quality of the laser beam. By ensuring turbulent flow in the liquid laser cell and controlling the wall temperature, radial temperature gradients can be avoided[4]. Beam quality becomes solely dependent on the distribution of optical pumping, which can be controlled independently (section 2.2), and the pulse repetition rate is only limited by the flow rate.

3.1 Description of the flow system

Because of the chemical activity of the neodymium:phosphorus oxychloride laser solution used in this work, a dry air-tight system of inert materials had to be developed for flowing this liquid. The system was largely constructed with PTFE joints and pipework, and contained the pump, laser flow cell and heat exchanger in a closed loop.

A filter was included to remove solid scattering particles from the liquid, since these degrade the laser performance. Figure 4 is an outline diagram of the fluid flow circuit. Also shown is the dry helium line for purging the system prior to filling, and for pressurising the supply vessel for filling the system. In addition, a second flow system for fluid cooling of the laser head(lamps, cell and reflector) is necessary, with a similar loop containing pump, heat exchanger and the laser head. This is included in the diagram, and indicates the

nature of two-component flow and the thermal coupling between them. The heat exchanger for the laser liquid consisted of nickel tubing arranged for parallel flow and immersed in a water cooling jacket. Nickel is resistant to phosphorus oxychloride and the unit was vacuum tested to ensure it was leak tight. Two views of the assembled laser liquid flow system are shown in Figure 5. The reservoir, and the pump and heat exchanger for the cooling fluid are not included.

3.2 The pump

In order to have a circulating liquid laser, a pump is required which is chemically inert in the presence of phosphorus oxychloride and which can provide the desired flow rate. Suitable materials are PTFE, glass and nickel. The flow rate depends on the pulse repetition rate and the requirement for turbulent flow, and is determined from the dimensions of the laser cell. For 10 pps operation and a cell 6 mm diameter by 6 inches long, the minimum rate for changing the liquid volume between pulses is 43 cc/sec. For turbulent flow the Reynolds number must exceed 3000. For the Nd:$POCl_3$-$ZrCl_4$ laser liquid, the density is 1.8 gm/cc and the viscosity 5 centipoise at 25°C, yielding a minimum flow velocity for turbulence of 140 cm/sec for diameter 6 mm, and a volume flow 40 cc/sec. The two requirements agree for this system and a minimum pump performance of ~50 cc/sec or 3 litre/min is indicated, working at a pressure head of a few feet to overcome pipe losses.

The laser liquid has a tendency to creep through fine crevices and lightly assembled joints, and to form a crystalline deposit and hydrogen chloride fumes on contact with moist air. For this reason any pump with rotating seals, round the drive shaft for example, tends to wear rapidly and eventually bind. An example of this type of failure is shown in Figure 6 for a glass loaded PTFE radial seal used on an early test with an all glass centrifugal pump. This was replaced by a PTFE bellows pump, gas driven with a double cylinder reciprocating action. The piston drive is isolated from the working fluid by the bellows and PTFE face seals. Auxiliary expansion bellows are fitted on the high pressure outlet side to reduce the pressure pulse in the liquid at the end of each stroke.

3.3 The laser head

The approach to efficient, uniform and symmetric optical pumping of the liquid laser has been discussed (section 2.2), and the need for well-mixed turbulent flow indicated (section 3). An outline of the cell is shown in Figure 7. The tube material is fused silica with a wall thickness 2 mm, bore diameter 6 mm and active length 153 mm (6 inches). The end windows are composite with solid nozzles extending into the inlet and outlet regions of fluid flow. They serve the dual purpose of diverting the flow into or from the straight centre section and completing the optical path through the main body of the laser medium. By coupling out to external mirrors and switching elements, a laser

cavity can be formed with the flowing liquid as the active medium. The arrangement is similar to the static cell experiment (Fig. 1).

For optical excitation of the circulating liquid laser a two lamp geometry with close-contoured reflector is employed for symmetry. To overcome some thermal distortion which was corrected by a meniscus lens on the static laser (Fig. 1), spectral selection of the flash lamp's emission is achieved using a gold coating on the reflector and yellow glass filters between the lamps and laser flow cell (Fig. 8). The combination of gold and yellow glass cuts off all wavelengths below 0.4 micron (4000 Å), with the result that only light covering the range of the Nd^{3+} ion absorption bands is incident on the laser liquid. The phosphorus oxychloride solvent is transparent from below 0.4 micron to ~5 microns wavelength. Therefore the only extraneous heating expected is that from radiationless Nd^{3+} transitions and by comparison with unfiltered excitation this is found to cause much less thermal distortion of the laser medium.

In operation the laser head is flooded with the cooling fluid, which is pumped through at an adequate rate for cooling the lamps when running at 10 pulses per second. The coolant thus also fulfils a secondary role as a temperature bath. Cylindrical sleeves are sealed to the ends of the laser cell by O-rings to preserve an optical path in air to the external mirrors.

3.4 Operation and results

3.4.1 Flow characteristics

When the circulating system was filled with laser liquid, some simple optical tests were first carried out to assess optical quality and particle scattering. By shining a helium-neon laser beam (λ 6328 Å) through the length of the liquid column and back again small variations in optical path can be observed by noting changes in the emergent beam pattern. A mirror behind the cell reflects the beam back and the image is diverted by a beam splitter onto a white card.

Distortion of the pattern takes the form of rippling with a frequency of a few Hertz, and a more disturbed motion at the end of a pump stroke. These effects are more pronounced at low flow rates and diminish as the pump speed is increased. At operating speeds the deflections fall below 1 milli-radian.

Scattering of light by the liquid has two causes; extrinsic, due to solid particles and impurities picked up from the system, and intrinsic due to the polymer form of the complex solvent. The latter contributes a minimum total scattering of order 0.3% cm^{-1} and cannot be removed. The former can by fine filters with ~5 micron pore size. If a helium neon laser beam is again shone through the length of the liquid column, angular fluctuations in the forward scattering due to fluid flow can be detected with a lens and pinhole arrangement. Choosing a big focal length lens and placing a metal foil with a small hole at the focus,

variations in transmitted intensity can be detected by a photomultiplier and related to angular variations from the dimensions. Using a 1 metre focal length and 0.5 mm hole determines an acceptance cone with 0.5 milli-radian full angle. Under these conditions 10% intensity fluctuation was observed with flow rate ~35 cc/sec, about 0.9 of the operational flow. For comparison, a glycerol-water mixture used earlier to test the pumping system showed a scattering intensity fluctuation of 0.2%. The pressure pulse at the end of each pump stroke could be seen as a sharp spike under these conditions, but was too small to show up on the laser liquid scattering measurement.

3.4.2 Laser operation

To power the laser, the pair of xenon flashlamps (Fig. 8) mounted in the laser head are connected to an identical pair of capacitor banks. Each bank contains a simple two-stage LC network impedance matched to the lamp. Each lamp is triggered by a 15 kV pulse from a hydrogen thyratron unit, resulting in the rapid discharge of energy stored at ~1.5 - 1.8 kV in the capacitors, and the emission of a nearly rectangular light pulse from the lamps with rise time 100 μs, plateau 250 μs, decay time 150 μs. At least 90% of the energy is emitted in 350 μs and 70% of this at constant intensity. The capacitor charging supply is rated at 4 kW and charging is completed in 30 ms. Operation of charging, firing and re-set for repeating the sequence is

electronically controlled. Single shot, burst and continuous running at 10 pps can each be selected. The burst mode has a pulse counter, which can be set to allow a number of consecutive firings from 2 to 8 pulses at 10 pps. Q-switching of the laser is accomplished by a pre-set delay which switches the Pockels cell voltage at any desired time during the lamp discharge. The sequence is:-

1. initiate charging
2. stop charging when set voltage reached
3. delay
4. signal to trigger lamps
5. delay
6. signal to Q-switch
7. reset.

The sequence is repeated at 0.1 second intervals until stopped either by the pulse counter for the burst mode or manually for continuous running.

3.4.3 Results

Two test fillings of the circulating laser system have been performed so far. For the first a slightly degraded solution used previously to test the centrifugal pump (section 3.2) was put into the system. The initial purpose was to assess the flow characteristics (section 3.4.1) and then to obtain preliminary results on laser action. However the solution performed well and appeared to have suffered little contamination so a full set

of laser measurements were obtained. No cooling was provided for the laser head at this stage, so operation was limited to the burst mode, with a maximum of 3 to 4 consecutive pulses determined by the energy loading of the flashlamps.

The threshold for normal spiking with a 62% reflecting output mirror was 35 J compared with a predicted value of 32 J scaled from measurements on a 5 mm diameter static laser cell. At 110 J input spiking lasted for 250 μs, i.e. for the duration of the flashlamp plateau (section 3.4.2). When Q-switched with a delay of 260 μs from the start of the lamp discharge, the beam pattern recorded on black Polaroid film contained a higher order transverse mode superimposed on an elliptical background, with overall divergence 5 milli-radian. Consecutive shots fired manually at intervals of a few seconds showed the same beam pattern with the laser liquid flowing at a low rate (~ $\frac{1}{5}$ operational flow). The observed slope efficiency for Q-swtiched pulse energy was 0.23%, $\frac{2}{3}$ the best value for static tests and a result of using a mirror transmission below the optimum (section 2.2) for laser output; 38% versus 56% for 0.37% static slope efficiency. A pulse energy of 200 mJ was obtained for 170 J input under these conditions.

With the pump running and the laser operating in bursts of 3 pulses at a rate of 10 pps, consecutive pulses were recorded with a fast photodiode and oscilloscope (ITT F4000/Tektronix 519). In each case the second and third pulses decreased in peak power

from the first, which was identical with the giant pulse generated in the stationary liquid with the pump off (Fig. 9 b,c,d). Only for manual firing at intervals of 10 seconds were the pulse shapes reproducible. The beam patterns, recorded on a rotating Polaroid target, were also repeated in this case. By varying the pumping speed and pulse repetition rate a recovery time ~2 seconds was deduced for the system. This was attributed to thermal relaxation of the laser, in the cell wall or the head, and supports the finding of General Telephone and Electronics Laboratories that thermal equilibrium must be achieved for reproducibility[4]. They immersed the entire laser head in a temperature stabilised water flow to do this. Because of the energetic reaction of phosphorus oxychloride with water, we used a non-reacting fluorocarbon oil to flood the laser head and by circulating it in a separate loop (Fig. 4) to cool the lamps achieved extended laser operation at 10 pps. This will now be described.

Modifications to the head required emptying the circulating system, followed by stripping, neutralising the remaining laser solution, and cleaning. After modification the system was reassembled and filled with fresh laser liquid and coolant in the appropriate flow loops (Fig.4). Repetitive flashing of the lamps showed no detectable variation in intensity at 10 pps, so bursts of laser spiking at this repetition rate were examined with both fluids circulating. Similar filamentary patterns for each pulse were recorded on a rotating Polaroid target.

Integrated signals representing the energy of each set of spikes showed shot-to-shot fluctuations, but the cooling fluid made possible extended operation at 10 pps. A run of 4 seconds representing 40 laser firings, contained 40 energy pulses, demonstrating that the thermal relaxation problem had been overcome.

To examine reproducibility of the Q-switched laser at 10 pps, the single pulse output was similarly integrated for each shot. Variations in the pulse energy, displayed as a series of signals on a slow sweep (Fig. 9 e,f,g) could thus be examined. By altering the pump speed it was demonstrated that the energy quickly fell to zero at low flow rates where the cell volume was not fully changed between shots, that at higher speed fluctuations without decay were present, and at sufficient flow velocity the fluctuations were significantly reduced (Fig. 9,e,f,g). Since some saturation of the photodiode was discovered after this run a quantitative estimate could not be made. Carbon precipitated by flash photolysis of the cooling oil prevented further work on the system. To avoid this problem the circulating laser is being modified to use an inert fluorochemical (probably 3M FC-75) as the cooling fluid, and Germisil lamps to reduce the UV emission.

A further effect of immersing the laser flow cell in the cooling fluid was the generation of Q-switched emission with nearly circular symmetry (Fig. 9a), indicating more uniform excitation of the liquid laser in this condition.

REFERENCES

1. W. G. Wagner, B. A. Lengyel, J. Appl. Phys. 34, 2040-2046(1963).

2. J. E. Midwinter, Brit. J. Appl. Phys. 16, 1125-1133(1965).

3. D. Röss, "Laser Lichtverstärker und Oszillatoren", p.465 ff. Publishers Akadem. Verlag, Frankfurt, 1966.

4. GTE Semi-annual technical summary report TR 71-826.2 (28 February 1971).

5. D. Andreou, V. I Little, A. C. Selden, J. Katzenstein; J. Phys. D: Appl.Phys. 5, 59-63 (1972).

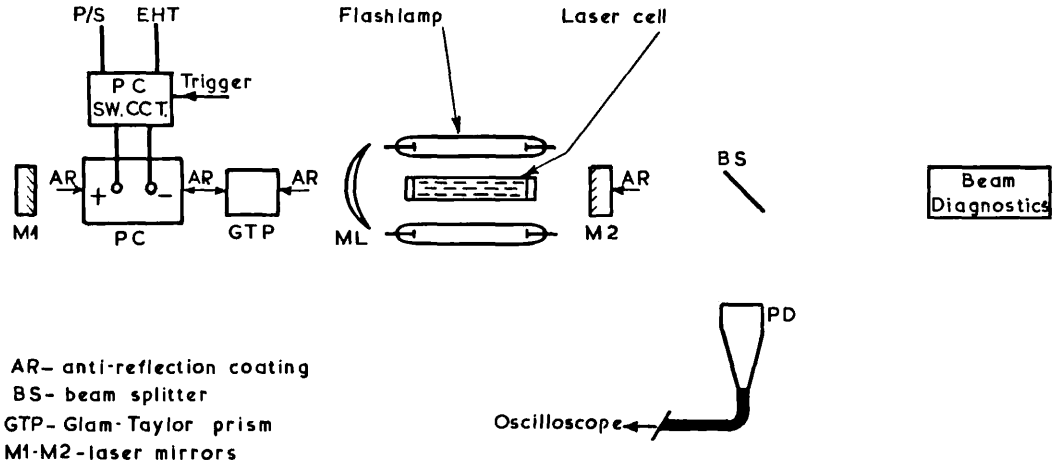

Fig.1 Arrangement of Q-switched liquid laser.

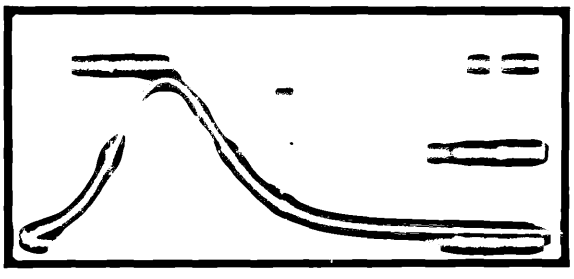

(a) Giant pulse profile 10 ns/cm 48 MW peak power.

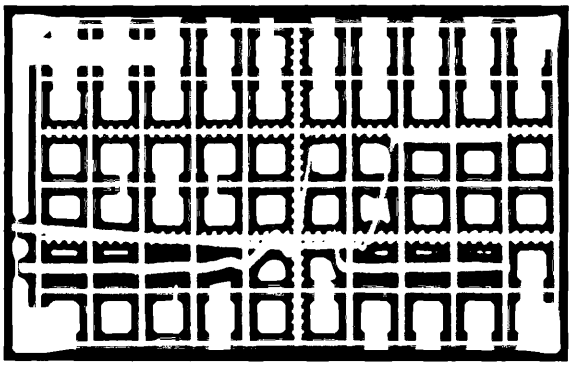

(b) Formative time delay 0.1 μs/cm.

Fig.2 Q-switching behaviour.

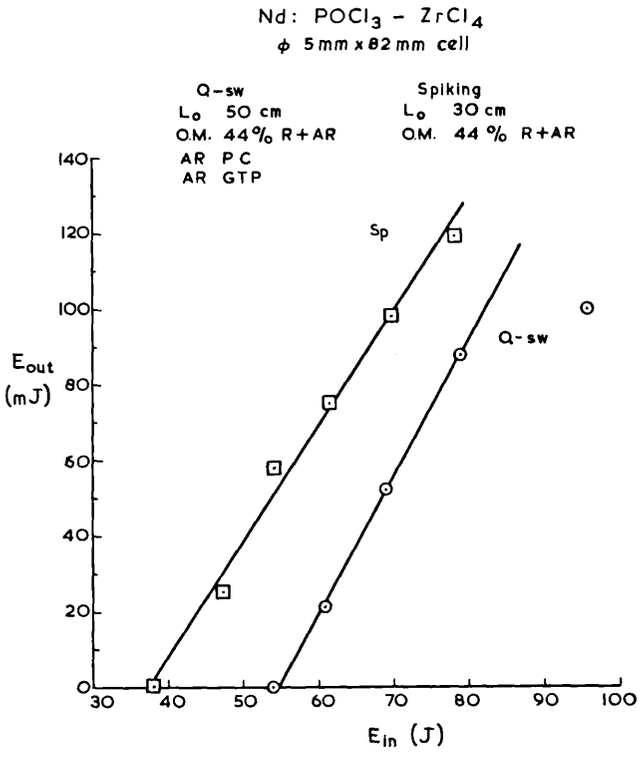

Fig.3 Liquid laser slope efficiency.

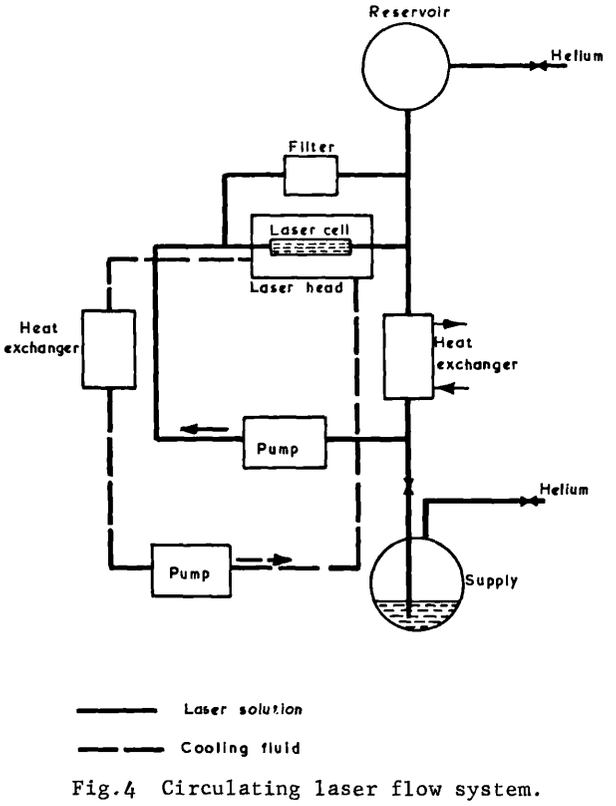

Fig.4 Circulating laser flow system.

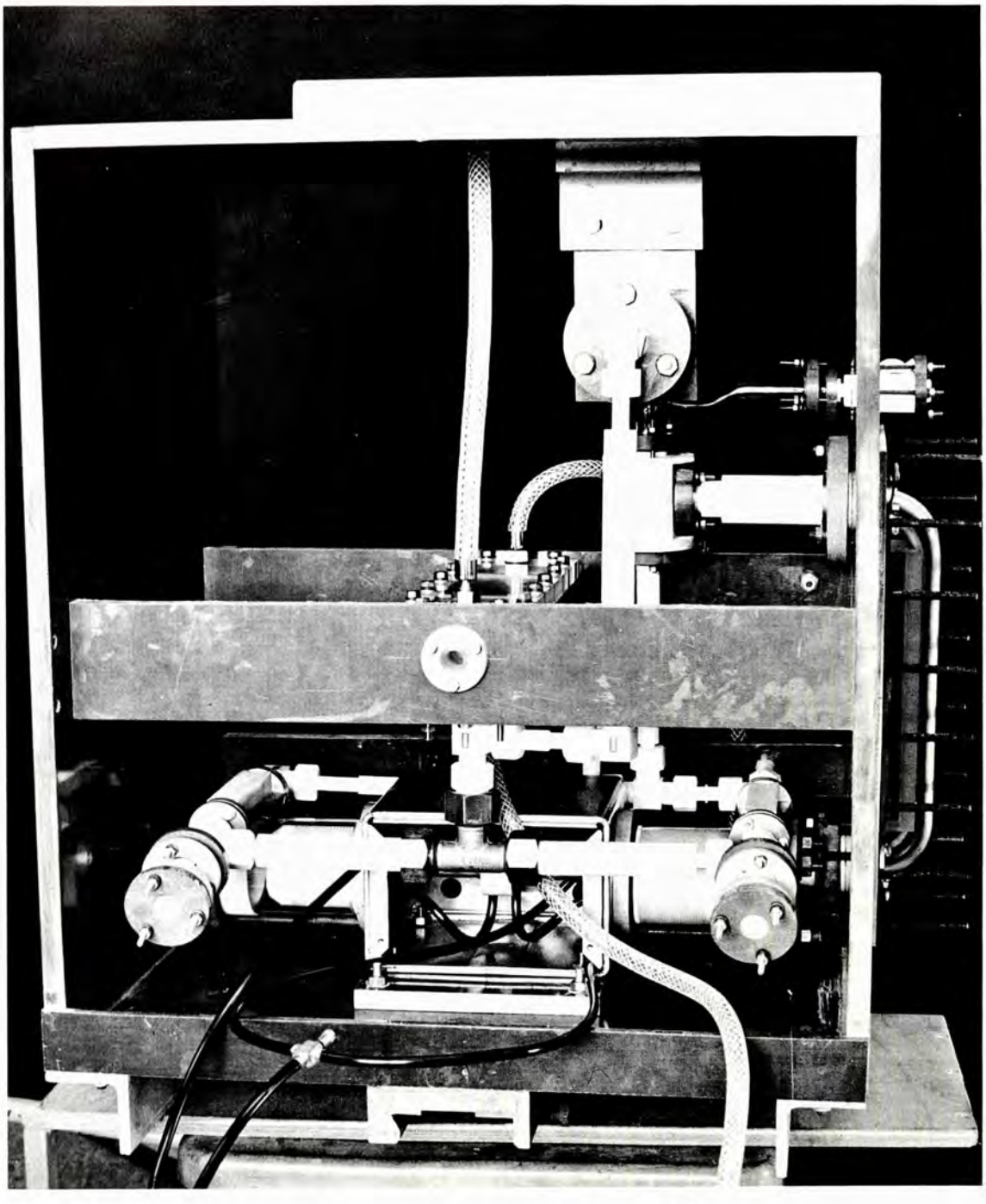

Fig.5 Assembled circulating system (i)

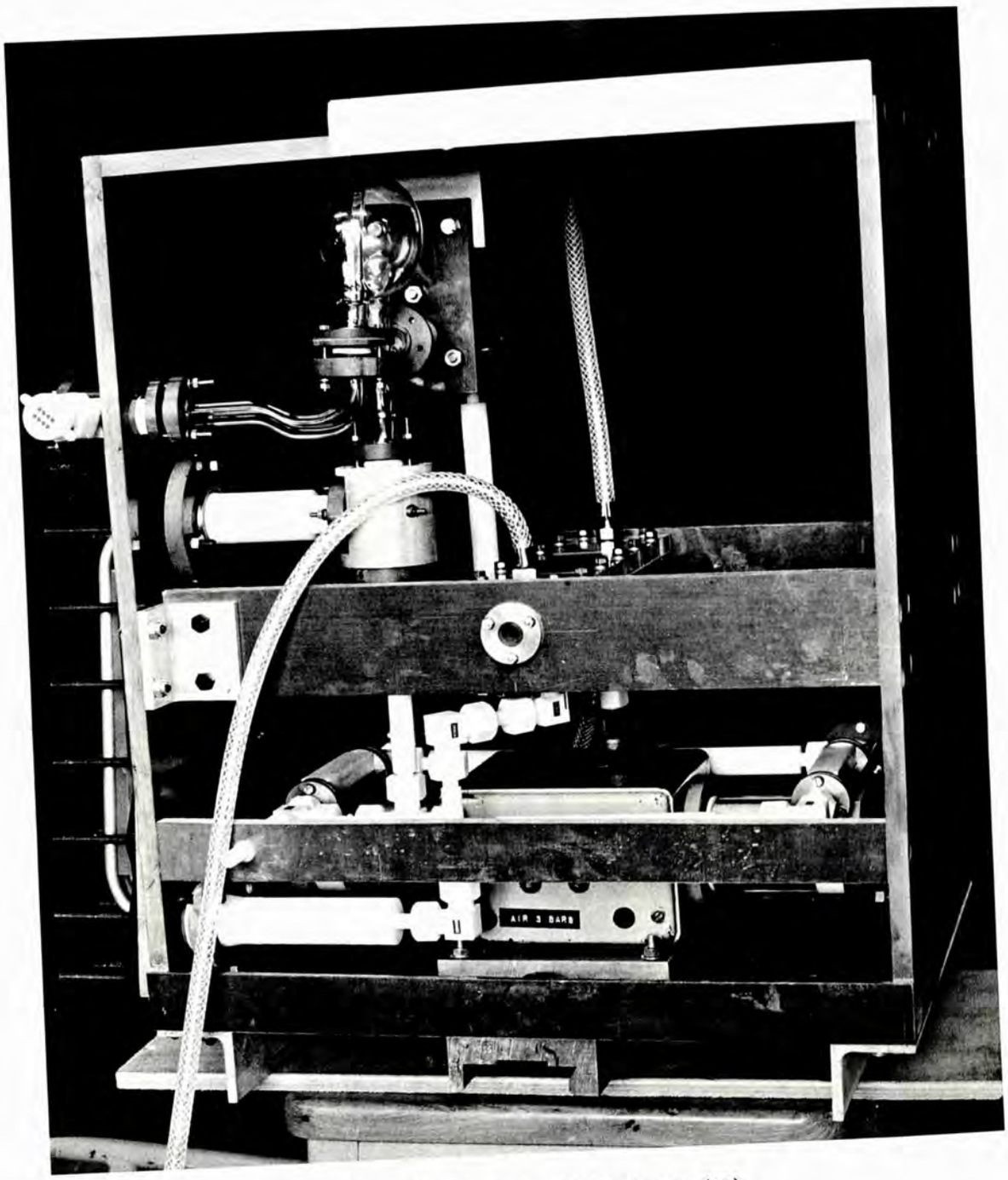

Fig.5 Assembled circulating system (ii)
CLM-R 119

Fig.6 Abraded PTFE radial seal.

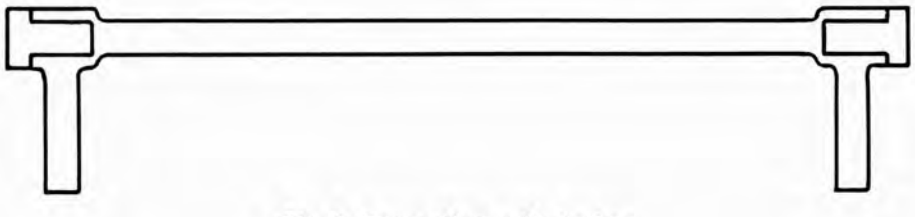

Fig.7 Laser flow cell design.

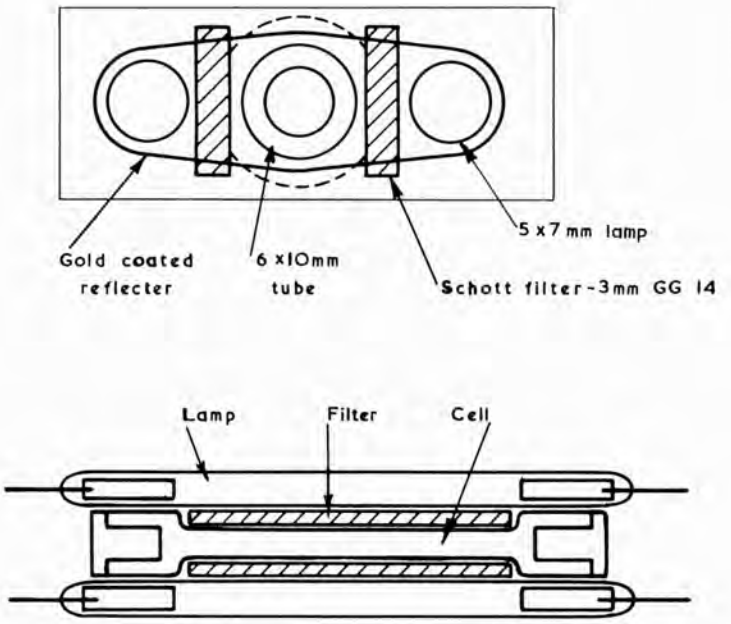

Fig.8 Laser head - disposition of lamps, filters and flow cell.

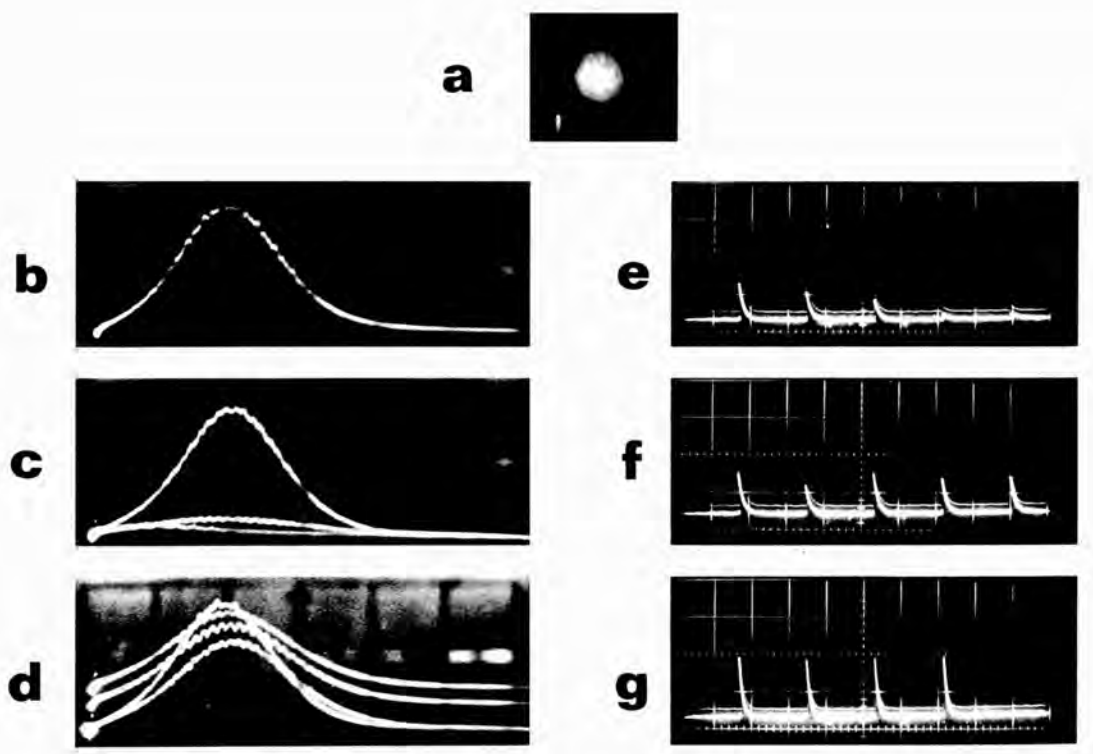

Fig.9 Repetitive Q-switching
(a) Beam pattern - static (b-d) No coolant. Pulse profiles, sweep 20 ns/cm
(b) Static (c) 3 pulses at 10 pps (d) 4 pulses at 10 second intervals
(e-g) 10 pps with coolant. Integrated pulses, sweep 0.05 sec/cm. Increasing flow rate